EXAMINATION OF PRIMARY EPITHELIAL CELLS UNDER NORMAL AND PATHOPHYSIOLOGICAL CONDITIONS

Ph.D. Thesis

Viktória Venglovecz

First Department of Medicine,
University of Szeged,
Szeged, Hungary

2008

TABLE OF CONTENTS

LIST OF ABBREVIATIONS

Arg	Arginine
Ach	Acetylcholine
AE	Cl^-/HCO_3^- exchanger
BAPTA-AM	1,2-bis(o-aminophenoxy)ethane-N,N,N',N'-tetraacetic acid
BCECF-AM	2.7-bis-(2-carboxyethyl)-5-(and-6-)carboxyfluorescein acetoxy-methyl ester
CACC	Calcium-activated chloride channel
$[Ca^{2+}]_i$	Intracellular calcium concentration
CDC	Chenodeoxycholate
CFTR	Cystic fibrosis transmembrane conductance regulator
DMSO	Dimethyl sulfoxide
ECL	Enterochromaffin-like cell
FBS	Fetal bovine serum
FURA 2-AM	5-Oxazolecarboxylic acid, 2-(6-(bis(carboxymethyl)amino)-5-(2-(2-(bis(carboxymethyl)amino)-5-methylphenoxy)ethoxy)-2-benzofuranyl)-5-oxazolecarboxylic acetoxymethyl ester
G17	Heptadecapeptide gastrin
Gas-KO	Gastrin null
GCDC	Glycochenodeoxycholate
HBSS	Hank's balanced salts solution
H_2DIDS	Dyhidro-4,4'-diisothiocyanostilbene-2,2'-disulfonic acid
HSP72	Heat shock protein 72
IκBs	Inhibitor of κB proteins
LCDC	Lacrimal gland ductal cell
NBC	Na^+/HCO_3^- cotransporter
NHE	Na^+/H^+ exchanger
NF-κB	Nuclear factor κB
OATP	Organic anion transporter protein
pH_i	Intracellular pH
PPDC	Primary pancreatic ductal cells
ROI	Region of interest

LIST OF FULL PAPERS CITED IN THE THESIS

I. Pagliocca A., Hegyi P., **Venglovecz V**., Rackstraw S.A., Khan Z., Wang T.C., Dimaline R., Varró A., Dockray G.J. Identification of ezrin as target of gastrin in immature gastric parietal cells. *J Physiol* (under revision). **IF: 4.407**

II. Tóth-Molnár E., **Venglovecz V**., Ózsvári B., Rakonczay Z. Jr., Varró A., Papp J.G., Tóth A., Lonovics J., Takács T., Ignáth I., Iványi B., Hegyi P. New experimental method to study acid/base transporters and their regulation in lacrimal gland ductal epithelia. *Invest Ophthalmol Vis Sci* 2007;**48**:3746-3755. **Please note:** the first two authors equally contributed to this work (mentioned in the article), therefore, both of them have to be regarded as first authors. **IF: 3.643**

III. Venglovecz V., Rakonczay Z. Jr., Ózsvári B., Takács T., Lonovics J., Varró A., Gray M.A., Argent B.E., Hegyi P. Effects of bile acids on pancreatic ductal bicarbonate secretion in guinea pig. *Gut* (under final revision). **IF: 9.02**

IV. Czakó L., Szabolcs A., Vajda Á., Csáti S., **Venglovecz V.**, Rakonczay Z. Jr., Hegyi P., Tiszlavicz L., Csont T., Pósa A., Berkó A., Varga Cs., Varga I.S., Boros I., Lonovics J. Hyperlipidemia induced by a cholesterol-rich diet aggravates necrotizing pancreatitis in rats. *Eur J Pharmacol* 2007;**572**:74-81. **IF: 2.477**

LIST OF FULL PAPERS RELATED TO THE SUBJECT OF THE THESIS

V. Hegyi P., Rakonczay Z., Farkas K., **Venglovecz V.**, Ózsvári B., Seidler U., Gray M.A., Argent B.E. Controversies in the role of SLC26 anion exchangers in pancreatic ductal bicarbonate secretion. *Pancreas*, 07-00649, (accepted). **IF: 2.12**

Number of full publications:	**5**
Cumulative impact factor:	**21.667**
Number of abstract publications:	**15**
Number of scientific presentations:	**16**

SUMMARY

Background & Aims. Epithelial cells play an important role in several processes, including protection, absorption or secretion. Secretory epithelia of exocrine glands are responsible for the transport of acid, base and electrolytes, therefore play an essential role in the regulation of the volume and ion composition of body fluids. Since most of the epithelial diseases result from incomplete fluid secretion or absorption, the exact knowledge of epithelial ion transport processes are of crucial importance. In most of the exocrine glands, the epithelial function and regulation is not completely understood. The **aim** of my work was to investigate the ion transport mechanisms of i) gastric parietal cells, ii) lacrimal intra/interlobular ducts and iii) pancreatic intra/interlobular ducts under normal [Annex No. I-II] and pathophysiological conditions [Annex No. III]. In addition, we investigated the role of hyperlipidemia in acute pancreatitis, with a particular emphasis on the expression of pancreatic heat shock protein 72 (HSP72) and inhibitor of κB proteins (IκBs) [Annex No. IV].

i) It is generally known that gastrin has a central role in the regulation of acid secretion by parietal cells. However, the role of gastrin in the maturation of parietal cell function is not fully understood.

ii) Similarly to the gastric gland, not much data is available concerning the regulatory mechansims of the lacrimal gland ductal cells (LGDC). Studies have been conducted that investigate the mixed fluid and protein secretion of isolated lacrimal acini, but no methods have been developed to characterize LGDC secretion.

iii) Nevertheless, the examination of the function of exocrine glands is very important not only under normal but pathophysiological conditions, since numerous protective mechanisms can only be investigated under abnormal conditions. One of the most common diseases which is related to exocrine glands is acute pancreatitis. Biliary reflux or hyperlipidemia are well known etiologic factors which are associated with acute pancreatitis or aggravate its course. However our knowledge concerning the protective mechanisms during acute pancreatitis is limited.

Methods. We performed our experiments on isolated primary epithelial cells.(see annex No. I-III) During the isolation process the epithelial cells retained their polarity and functional characteristics, thus they were suitable to study their transport properties. The activity of the ion transporters were investigated using a fluorescent dye BCECF to monitor intracellular pH (pH_i) by microfluorimetry. The intracellular calcium concentration ($[Ca^{2+}]_i$) was measured by FURA-2. In addition, we performed western blots to investigate the effect of hyperlipidemia

on the expression of pancreatic HSP72 and IκBs in rats with acute necrotizing pancreatitis. Acute pancreatitis was induced with 2x2 g/kg body weight of L-arginine (Arg) respectively, in normal and hyperlipidemic rats. (see annex No. IV.).

Results and Conclusions. i) In gastrin null mice (Gas-KO mice) acute gastrin stimulation (incubation for 1 hr *in vitro* with 1 nM heptadecapeptide gastrin (G17) did not restore H^+ pump activity in gastric parietal cells, however, prolonged exposure to gastrin (incubation for 24 hr in vitro with 1 nM G17, which we refer to as "priming") totally restored H^+ secretion. Our results suggest, that gastrin is a key factor in parietal cell maturation and is required for acid secretion.

ii) The next part of this thesis focuses on the basic transport mechanisms of the lacrimal gland ductal epithelia. In this study, we have developed a rapid method to isolate intact rabbit lacrimal gland ducts, which allowed us for the first time to perform real-time functional experiments on cleaned ducts. Our results showed that LGDC express functionally active Na^+/H^+ (NHEs), and Cl^-/HCO_3^- exchangers (AEs). Moreover, parasympathomimetic stimulation by carbachol stimulated the NHE and AE, via elevation of intracellular calcium concentration. These data combined with the novel isolation facilitated understanding of the regulation mechanisms of ductal cell secretion at cellular and molecular levels.

iii) In the pathophysiological studies, in connection with the defence mechanisms during biliary pancreatitis, we have shown that luminal administration of a low dose (0.1mM) of chenodeoxcholate (CDC) stimulated HCO_3^- secretion, while a high dose (1mM) of this bile acid, both from the luminal and basolateral membrane, inhibited HCO_3^- secretion. We have also shown that 1,2-bis(o-aminophenoxy)ethane-N,N,N',N'-tetraacetic acid (BAPTA-AM) blocked the stimulatory effect of low doses of CDC on HCO_3^- secretion, but did not modulate the inhibitory effect of high doses of CDC. Our hypothesis is that this stimulated HCO_3^- secretion by low concentration of CDC acts to protect the pancreas against toxic bile, whereas the inhibition of HCO_3^- secretion by high concentrations of bile acids may contribute to the progression of acute pancreatitis.

Finally, we have found that the pancreatic HSP72 expression during acute pancreatitis was not influenced by hyperlipidemia, however the level of IκB-α was significantly lower in pancreatitic rats on cholesterol enriched diet as compared with those on normal diet.

In summary in this thesis we tried to provide a better understanding of epithelial cell function under normal and pathophysiological conditions. Our results may open up the possibility to develop new strategies in the treatment of diseases.

1. INTRODUCTION

Normal epithelial ion transport is essential for the maintenance of healthy function of several exocrine glands. For example, in the pancreas it helps to wash out the digestive enzymes,[1] while the acid secretion by the stomach protects against infection by pathogenic micro-organisms.[2-3] The fluid secretory properties of exocrine glands are mainly due to the epithelial cells. The epithelial cells are usually organized into a branching ductal system, which form the structural frame of numerous glands, such as the pancreas[4] or the lacrimal gland.[5, 6] Due to this tubular arrangement, luminal and basolateral „sides" can be distinguished on epithelial cells. The two membranes express different sets of transport proteins which result in the polarity of the epithelial tissue.[7] The polarized feature of these cells ensures the vectorial transport of the ions and water from the basolateral membrane to the lumen. This fluid secretion is a complex process and is highly regulated by both hormonal and neuronal mechanisms. Despite of the fact that epithelial cells play an important role in the maintenance of a standard environment, our knowledge of epithelial function is incomplete, especially in certain diseases, such as acute pancreatitis or dry eye syndrome. The general goal of our studies summarized in this thesis was to investigate the secretory mechanisms and intracellular regulation of various exocrine glands (especially the gastric gland, the lacrimal gland, and the pancreas) in normal and pathophysiological conditions. The better understanding of the mechanisms of epithelial ion transport processes may help us to develop drugs in the treatment of different diseases.

Research on gastric epithelial cell physiology has mainly focused on the role of gastrin in the regulation of acid secretion in parietal cell maturation. Several lines of evidence indicate that the gastric hormone gastrin is a potent stimulator of gastric acid secretion. [8, 9] It is well established that in addition to CCK-2 receptors, parietal cells also express H_2 histamine receptors and M3 muscarinic receptors.[10] Activation of each of these receptors is associated with parietal cell stimulation.[11] However, physiologically it is generally thought that gastrin acts primarily through release of histamine from enterochromaffin-like (ECL) cells, which then acts as a paracrine regulator of parietal cell function.[12] Studies in Gas-KO mice suggest that gastrin is involved in more than just the acute regulation of acid secretion. In these animals, parietal cells occur predominantly in an immature form so that they secrete little acid and are refractory to acute administration of gastrin, histamine or the muscarinic agonist carbachol.[13, 14] Interestingly, administration of gastrin over a period of a few days

induces acid secretion, and the capacity to respond to the main secretgogues,[14, 15] suggesting that in addition to its role in stimulating acid secretory responses during digestion, gastrin also plays a role in regulating the final steps of parietal cell maturation. The main focus of this study was to investigate the role of gastrin both in acid secretion and in parietal cell maturation demonstrated by H^+/K^+ ATPase activity.

The secretory properties of epithelial cells was not only investigated in gastric glands, but also in the lacrimal gland. In the lacrimal gland one of the main cell types is the ductal cell.[5, 6] The lacrimal gland ductal cells have a major role in fluid secretion which are essential in maintaining a healthy, normal function of the ocular surface. When tear secretion decreases in amount or changes in composition, dry eye syndrome (keratoconjunctivitis sicca) can develop and in the worst case can induce corneal ulceration and vascularisation leading to serious visual impairment.[16, 17] Most of the available methods to study protein and fluid secretion of lacrimal gland are focused on acinar cells,[18, 19] however much less is known about the LGDC.[20, 21] Ubels et al. have recently described a laser capture microdissection technique for cDNA microarray analysis and immunohistochemistry using frozen lacrimal gland,[21] however, no methods have been developed to characterize the LGDC secretion in viable ductal cells. Nevertheless, the secretory mechanisms of the ductal epithelia may play a physiological role in the maintenance of the standard environment of the cornea and the conjunctiva. In this part of my studies, our aim was to develop a method to isolate lacrimal ducts, in order to open up the possibility to obtain more information on the regulation of lacrimal gland epithelial tissue and to characterize LGDC acid/base ion transporters mediating fluid secretion.

We were interested in epithelial function not only under normal but also under pathophysiological conditions. Most of the pathophysiological investigations focus on the damaging factors, which alter the course of several diseases. For example in the pancreas a several factors have been shown to aggravate acute pancreatitis,[22, 23] however, the role of protective mechanisms are relatively less understood. Since acute pancreatitis is asociated with high morbidity and mortality our aim was to investigate which are those defensive mechanisms that may interfere with the aggravation of this disease. The pancreatic fluid hypersecretion during acute pancreatitis may be such a protective effect against pancreatic injury. The basal fluid secretion of the pancreas is responsible for washing out the digestive enzymes into the duodenum, and it contributes to the neutralization of the acid chyme entering the duodenum from the stomach.[1] The main transporters which are involved in this secretion across the luminal membrane are the Cl^-/HCO_3^- exchanger (luminal AE) and the

cAMP-activated cystic fibrosis transmembrane conductance regulator (CFTR).[24-27] It has been shown that this fluid secretion can increase in certain conditions,[28, 29] but the protective effect of this hypersecretion is poorly investigated.[30] We believe that the increased secretion is mainly due to pancreatic ductal epithelial cells, which may represent a defence mechanism against toxic factors. Since refluxed bile is one of the most common cause in the development of acute pancreatitis,[31-34] we investigated the effect of bile acids on pancreatic ductal HCO_3^- secretion. The pathogenesis underlying the development of acute biliary pancreatitis is not well understood. Although the bile can reach both acinar and ductal cells during biliary pancreatitis, much more research has been done on acinar cells.[35-38] To date, scientists have mostly examined the permeability and morphology of ductal cells following the administration of bile acids.[39-41] It has been shown that the permeability of the pancreatic ductal epithelium to HCO_3^- and Cl^- is increased by exposure to various bile salts at concentrations within the range normally found in the duodenum.[41] Although one of the main functions of the pancreatic ductal epithelium is to secrete the HCO_3^- ions found in pancreatic juice,[42, 43] no data are available on the effects of bile acids on HCO_3^- secretion. However, it has been shown, that retrograde injection of sodium taurocholate into the rat pancreatic duct induces fluid hypersecretion and decreases protein output in the initial phase of acute pancreatitis.[44] Our hypothesis is that the hypersecretory effect of bile acids, may represents a defence mechanism in order to avoid pancreatic injury. We planned in this study to characterize the effects of bile acids on ductal iontransport processes, especially on HCO_3^- secretion. We performed our experiments on intact isolated guinea pig pancreatic ducts, because the guinea pig pancreas secretes a juice containing ~140mM $NaHCO_3$ as does the human gland.[45]

Hyperlipidemia is also associated with acute pancreatitis,[46] however, the role of hyperlipidemia in the pathogenesis of acute pancreatitis is uncertain. Recent evidence indicates that a high-cholesterol diet alters the expression of HSP72 and the activation of nuclear factor κB (NF-κB).[47, 48] NF-κB plays a critical role in the pathogenesis of acute experimental pancreatitis by regulating the expressions of many proinflammatory genes.[49, 50] The possible protective factors during hyperlipidemic acute pancreatitis are unknown. Since it is well known that the accumulation of the highly stress-inducible member of the HSP72 in response to a variety of stressors confers long-lasting protection against further stress injury,[49, 50] we investigated whether hyperlipidemia alters the pancreatic heat stress response. In addition we examined the expression of IκB-α, the inhibitor protein of NF-κB,[51] during hyperlipidemic acute pancreatitis.

2. MATERIALS AND METHODS

2.1. Solutions and chemicals

The compositions of the solutions used are shown in Table 1. Hepes-buffered solutions were gassed with 100% O_2 and their pH was set to 7.4 with NaOH or HCl at 37°C. HCO_3^--buffered solutions were gassed with 95% O_2 / 5% CO_2 to set pH to 7.4 at 37°C. Chromatographically pure collagenase was purchased from Worthington (Lakewood, NJ, USA). CellTak was obtained from Becton Dickinson Labware (Bedford, MA, USA). 2.7-bis-(2-carboxyethyl)-5-(and-6-)carboxyfluorescein, acetoxymethyl ester (BCECF-AM), 5-Oxazolecarboxylic, 2-(6-(bis(carboxymethyl)amino)-5-(2-(2-(bis(carboxymethyl)amino)-5-methylphenoxy)ethoxy)-2-benzofuranyl)-5-oxazolecarboxylic acetoxymethyl ester (FURA 2-AM), dyhidro-4,4'-diisothiocyanostilbene-2,2'-disulfonic acid (H_2DIDS) and 1,2-bis(o-aminophenoxy)ethane-N,N,N',N'-tetraacetic acid (BAPTA-AM) were from Molecular Probes Inc. (Eugene, OR, USA). Nigericin was dissolved in absolute ethanol and amiloride in DMSO. COOH-terminally amidated, unsulphated, G17 was obtained from Bachem (St Helens, Merseyside, UK). Omeprazole was kindly donated by Astra Zeneca (London, U.K.). The rabbit anti-HSP72 antibody was a generous gift from Dr. István Kurucz (IVAX Drug Research Institute, Budapest, Hungary). The rabbit anti-IκB-α was purchased from Santa Cruz Biotechnology (Santa Cruz, CA, USA). The goat horseradish peroxidase conjugated anti-rabbit secondary antibody was from DAKO (Glostrup, Denmark). Bile acids and all other chemicals were obtained from Sigma-Aldrich (Budapest, Hungary).

Table 1. Composition of solutions.

	Standard HEPES	Standard HCO_3^-	High-K^+ HEPES	NH_4^+ in HEPES	NH_4^+ in HCO_3^-	Na^+-free HEPES	Na^+-free HCO_3^-	Cl^--free HEPES	Cl^--free HCO_3^-	Ca^{2+}-free HEPES
NaCl	130	115	5	110	95					132
KCl	5	5	130	5	5	5	5			5
$MgCl_2$	1	1	1	1	1	1	1			1
$CaCl_2$	1	1	1	1	1	1	1			
Na-HEPES	10		10	10						10
Glucose	10	10	10	10	10	10	10	10	10	10
$NaHCO_3$		25			25			25	25	
NH_4Cl				20	20					
HEPES						10				
NMDG-Cl						140	115			
Choline-HCO_3^-							25			
Atropine							0.01			
Na-gluconate								140	115	
Mg-gluconate								1	1	
Ca-gluconate								6	6	
KH_2-sulfate								5	5	

Values are concentrations in mM.

2.2. Animals and experimental protocols

2.2.1 Mice

We used mice in order to examine the priming effect of gastrin on gastrin knock-out parietal cells.

Gas-KO mice on a C57Bl/6 background have been described previously.[13] Mice were housed in polycarbonate-bottomed cages with a strict light cycle (lights on at 0700 and off at 1900) and fed on a commercial pellet diet (LATI, Gödöllő, Hungary) and water. The mice (10-12 weeks) were killed by standard carbon dioxide asphyxiation followed by cervical dislocation and then the stomach was rapidly removed. Approximately half of the non-secretory epithelium was removed, the pyloric sphincter was then directed through the newly created fundic opening and the stomach everted and sealed by ligation of the remaining non-secretory epithelium.

2.2.2 Rabbits

We used rabbits in order to characterize the acid/base ion transporters of lacrimal gland ductal cells.

Adult male New Zealand white rabbits weighing 2-2.5 kg were sedated with 50 mg/kg pentobarbital and humanely killed by cervical dislocation. The superotemporal and inferotemporal portions of the conjunctival fornices were dissected after wide temporal cantothomy. The eyeball was then dislocated inferonasally and the temporal part of the orbital connective tissues were excised using stereomicroscope. The preparation procedure revealed the main lobes of the lacrimal gland under the roof of the orbit, which were removed by gentle pressure with forceps and final separation with scissors. Both intraorbital lacrimal glands were carefully dissected.

2.2.3 Guinea pig

We used guinea pigs in order to examine the effect of bile acids on pancreatic ductal bicarbonate secretion.

Guinea pigs weighing 150-250g were kept at a constant room temperature of 22±2 ^{o}C, under 12-h light-dark cycles, and were allowed free access to water and standard laboratory chow. Guinea pigs were killed humanly by cervical dislocation, and then the pancreas was removed.

2.2.4 Rats

We used rats in order to investigate the role of hyperlipidemia in the pathogenesis of acute pancreatitis.

Wistar rats weighing 80-100 g were kept at a constant room temperature of 22±2 ^{o}C, under 12-h light-dark cycles, and were fed laboratory chow enriched with 3% cholesterol (cholesterol group) or standard chow (LATI, Gödöllő, Hungary) (control group) for 16 weeks. We used a necrotizing pancreatitis model to induce experimental pancreatitis.[52, 53]

At the end of this 16-week controlled-diet period, acute necrotizing pancreatitis was induced with 2x2 g/kg body weight of arginine (Arg) intraperitoneally in separate groups of normal and hyperlipidemic rats (Arg and cholesterol+Arg groups).[54-56] The control rats received 8.6% glycine in 0.9% physiological saline at the same times instead of Arg. 24 h after the first Arg injection, the rats were sacrificed by exsanguination through the abdominal aorta. The pancreas was quickly removed, cleaned from fat and lymph nodes, weighed, and frozen in liquid nitrogen and stored at –80 ^{o}C until use.

Akut nekrotizáló pankreatitiszt 2 g/2 kg testsúly dózisú arginin intraperitoneális adásával váltottunk ki, mind a kontrol mind pedig a koleszterinben gazdag diétán tartott állatokban.

2.3. Ethics

The experiments were conducted in compliance with the *Guide for the Care and Use of Laboratory Animals* (U.S.A. NIH publication No 85-23, revised 1985). In addition, the experimental protocols were approved by the local Ethical Board of the University of Szeged, Hungary.

2.4. Isolation and culture of primary tissues

2.4.1. Isolation of gastric gland

Stomachs were washed in ice-cold Hanks' balanced salt solution (HBSS) and were filled by injection via a 23-gauge needle with 0.5 ml of 0.5 mg.ml^{-1} collagenase A (Roche Molecular Biochemicals, East Sussex, UK). Using a modification of a previously described method,[57] glands were obtained by washing the stomach in pre-warmed (37°C) HBSS (3 times), followed by incubation in dithiothreitol (5 ml, 1 mM) for 15 minutes, washing again in

HBSS (3 times), and finally incubating in collagenase A (7.5 ml, 0.32 mg ml^{-1}, 30 minutes, 37°C) in an atmosphere of 95%O_2/5%CO_2 with shaking at 100 cycles per minute. Rupturing of the inverted stomach generally indicated adequate digestion to yield isolated glands. At this stage tissue was triturated using a wide mouthed plastic pipette, larger fragments were allowed to settle under gravity (45 seconds), leaving the isolated glands in suspension.[58] The supernatant containing isolated glands was then transferred to a clean tube, shaken to release additional glands, allowed to settle under gravity for 45 minutes on ice and the supernatant discarded. The isolated gastric glands from one mouse were suspended in 1.0 ml Dulbecco's Modified Eagle's Medium supplemented with 10% fetal bovine serum (FBS) and 1% antibiotic-antimycotic solution and cultured at 37°C in a humidified atmosphere of 95%O_2/5%CO_2. Medium was changed after 24 hours and experiments started 24 hours later. Two protocols were used: (1) For "priming", glands were incubated for 24 hours in medium containing G17 (1.0 nM). (2) For "acute" stimulation, glands were incubated for 1 hour with G17 or other drugs as appropriate. Typically, after priming glands were either incubated with an acute stimulant or with control medium.

2.4.2. Isolation of intra/interlobular lacrimal gland ducts

The isolation of the intra/interlobular ducts was similar to that described for the pancreas,[59] except that the isolation solution did not contain trypsin inhibitor.

2.4.3. Isolation of intra/interlobular guinea pig ducts

Intra/interlobular ducts were isolated by enzymatic digestion and microdissection as described previously.[59] The ducts were cultured overnight in a 37 ^oC incubator gassed with 5 % CO_2/95 % air. During the overnight incubation, both ends of the isolated ducts seal to form a closed sac that swells due to accumulation of secretion in the duct lumen.

2.5. Measurment of intracellular pH and calcium

Intacellular pH (pH_i) was estimated using the pH-sensitive fluorescent dye BCECF-AM. The gastric glands were cultured on coverslips (24mm), the pancreatic and lacrimal gland ducts were attached (using Cell Tak) to coverslips (24mm), which formed the base of a perfusion chamber mounted on a microscope (Olympus, Budapest, Hungary). The tissues were bathed in standard Hepes solution at 37 ^oC and loaded with the membrane permeable acetoxymethyl derivative of BCECF (2 μmol/L) for 20-30 min. After loading, the tissues were continuously perfused with solutions at a rate of 5-6 mL/min. pH_i was measured using a

Cell^R imaging system (Olympus, Budapest, Hungary). 4-5 small areas (Region of interests – ROIs) of 5-10 cells in each intact duct were excited with light at wavelengths of 490 and 440 nm, and the 490/440 fluorescence emission ratio was measured at 535 nm. One pH_i measurement was obtained per second. *In situ* calibration of the fluorescence signal was performed using the high K^+-nigericin technique.[60, 61]

Measurement of $[Ca^{2+}]_i$ was performed using the same method except that the cells were loaded with the Ca^{2+}-sensitive fluorescent dye FURA 2-AM (5 μmol/L) for 60 min. For excitation, 340 and 380 nm filters were used, and the changes in $[Ca^{2+}]_i$ were calculated from the fluorescence ratio (F_{340}/F_{380}) measured at 510 nm.

2.6. Microperfusion of pancreatic ducts

The lumen of the cultured pancreatic ducts was microperfused using a modification of the method described by Ishiguro et al.[62] Two concentric pipettes were used for the microperfusion. One end of a sealed duct was cut off and the other end was aspirated into the outer, holding pipette, then the inner, perfusion pipette, was gently inserted into the lumen while a negative pressure was applied to the holding pipette using a syringe. The duct was then perfused at a rate of 10-30 μl/min, the luminal perfusate left the duct at the open end. The high rate of the bath perfusion (5-6 mL/min), which was in the same direction as the flow of luminal perfusate, ensured that the outgoing luminal perfusate did not gain access to the basolateral surface of the duct cells. Replacement of the luminal perfusate took up to 2 minutes.

2.7. Measurment of bicarbonate secretion

We utilized three methods to determine the HCO_3^- efflux across the luminal membrane.

In the inhibitory stop method, the basolateral Na^+/HCO_3^- cotransporter (NBC) and the Na^+/H^+ exchanger (NHE) were blocked using H_2DIDS (0.5 mM) and amiloride (0.2 mM) for 3 min administered from the basolateral side. The inhibition of these transporters caused a marked decrease in pH_i. The rate of pH_i acidification after the exposure to H_2DIDS and amiloride reflects the intracellular buffering capacity and the rate at which HCO_3^- effluxes (i.e. is secreted) across the apical membrane via Cl^-/HCO_3^- exchangers and possibly CFTR.[63, 64] The initial rate of intracellular acidification (dpH/dt), over the first 60 seconds was

calculated by linear regression analysis using 60 data points (one pH_i measurements per second).

In the alkali load method, HCO_3^- secretion was estimated by the rate of pH_i recovery from an alkaline load. In these experiments ducts were exposed to 20 mM NH_4Cl in HCO_3^-/CO_2-buffered solution from the basolateral side which produced an immediate increase in pH_i due to the rapid influx of NH_3 across the membrane. After the alkalinisation there was a recovery in pH_i toward the basal value. Recently, we demonstrated that recovery of pH_i under these conditions was dependent on the presence of HCO_3^- in the bathing solution, suggesting that it results from HCO_3^- efflux (i.e. secretion) from the duct cells.[63] In the present study, the initial rate of recovery from alkalosis (dpH/dt) over the first 30 seconds (30 pH_i measurements) in the continued presence of NH_4Cl was calculated as described previously.[63]

In the Cl^- withdrawal technique, HCO_3^- secretion was characterized by the rate of pH_i elevation (alkalinization) after luminal Cl^- withdrawal.

2.8. Measurment of Na^+/HCO_3^- cotransporter and Na^+/H^+ exchanger activity

In the alkali load method, after the removal of NH_4Cl, there is a rapid decrease in pH_i, due to the diffusion of NH_3 out of the cell and the release of H^+. The recovery from this acid load mostly depends on the activity of NBC and NHE.[63] In order to study the transporters separately, the experiments were performed in the absence or presence of HCO_3^-. The initial rate of recovery (dpH/dt) over the first 60 seconds (60 pH_i measurements) was calculated as described previously.[63]

2.9. Determination of buffering capacity and base flux

The total buffering capacity ($ß_{total}$) of the pancreatic duct cells was estimated according to the NH_4^+ pre-pulse technique.[63, 65] Pancreatic duct cells were exposed to various concentrations of NH_4Cl in Na^+ and HCO_3^--free solution. $ß_i$ (which refers to the ability of intrinsic cellular components to buffer changes of pH_i) was estimated by the Henderson-Hasselbach equation. $ß_{total}$ was calculated from: $ß_{total} = ß_i + ß_{HCO3-} = ß_i + 2.3 \times [HCO_3^-]_i$, where $ß_{HCO3-}$ is the buffering capacity of the HCO_3^-/CO_2 system. The rates of pH_i change measured in the inhibitor stop, alkali and acid load experiments were converted to transmembrane base flux $J(B^-)$ using the equation: $J(B^-) = dpH/dt \times ß_{total}$. We denoted base influx as $J(B^-)$ and base efflux (secretion) as $-J(B^-)$.

2.10. Western blotting

Western blot analysis of pancreatic HSP72 and IκB-α expression was performed from the cytosolic fraction of the pancreas homogenate as described previously.[49, 50, 66] Pancreatic tissue was homogenized and diluted to load 40 µg of total protein on an 8-10 % polyacrylamide gel. After separation by electrophoresis, the proteins were blotted onto a nitrocellulose membrane. After blocking with 5% dry milk, the membranes were incubated with rabbit anti-HSP72 (1:2500 dilution, 60 min), or rabbit anti-IκB-α (1:500 dilution, 60 min) and with goat antirabbit secondary antibody for 60 min (1:1000). Bands were visualized by enhanced chemiluminescence (ECL Plus; GE Healthcare, Little Chalfont, Buckinghamshire, UK). Thereafter, they were scanned and quantified by using the ImageJ software (NHI, Bethesda, MD, USA). The band densities of the proteins were determined and summed in order to estimate the total level of nitrated proteins. Results are expressed in arbitrary units.

2.11. Transmission electron microscopy

For the electron microscopic studies, the ducts were fixed in 2.5% glutaraldehyde immediately following isolation. The samples were then post-fixed in 1 % osmium tetroxide, dehydrated in a series of graded ethanols, and subsequently embedded in epoxy resin. Ultrathin sections were contrasted with uranyl acetate and lead citrate. Tissue sections were analysed using a Philips CM10 transmission electron microscope.

2.12. Statistical analysis

Results are expressed as means ± S.E.M. Experiments were evaluated statistically with analysis of variance (ANOVA). P values ≤ 0.05 were accepted as significally significant.

3. RESULTS

3.1. Functional characterization of cultured gastric glands

In order to establish whether there are functional differences between wild-type and Gas-KO parietal cells in cultured glands we monitored pH_i. Parietal cells were identified by lectin staining before the experiments. The resting pH_i of wild-type parietal cells was 7.33 ± 0.02 (n=10) and was not significantly different in Gas-KO cells (7.30 ± 0.05). Removal of Na^+ from the standard Hepes solution caused a rapid and marked intracellular acidosis due to the inhibition of NHE activity (Fig. 1A). Exposure to 20 mM NH_4Cl induced an immediate rise in pH_i due to the rapid entry of NH_3 into the cells and its removal produced a rapid decrease in pH_i followed by a slower recovery due to activation of pH_i regulatory mechanisms. In the absence of Na^+ and HCO_3^-, the functionally active acid/base transporter/pump in these circumstances is the H^+/K^+-ATPase and the initial rate of recovery from acidosis reflects its activity. When 10-1000 pM G17 was included in the medium, there was a concentration-dependent stimulation of pH_i recovery after NH_4Cl due to the stimulated H^+ efflux (Fig. 1B) that was blocked by 100 μM omeprazole indicating that it was attributable to H^+/K^+ ATPase activity (Fig. 1C). The H_2 receptor antagonist ranitidine inhibited the response to 100 pM G17 (which is just above the physiological concentration in plasma), but only partially inhibited the effect of 1 nM G17 consistent with the idea that at physiological concentrations gastrin acts on parietal cells via histamine release from ECL cells, but can act directly at higher concentrations (Fig. 1D). Importantly, in Gas-KO mice the initial recovery of pH_i was significantly decreased compared with wild-type mice (Gas-KO, 0,0054 ± 0,001 U/min; wild type, 0.015 ± 0,002, $p<0.05$) and was completely refractory to 1 nM G17. However, priming with 1 nM G17, followed by a 2h wash-out period before the experiments, induced the capacity for an acute response to G17 (Fig. 1E).

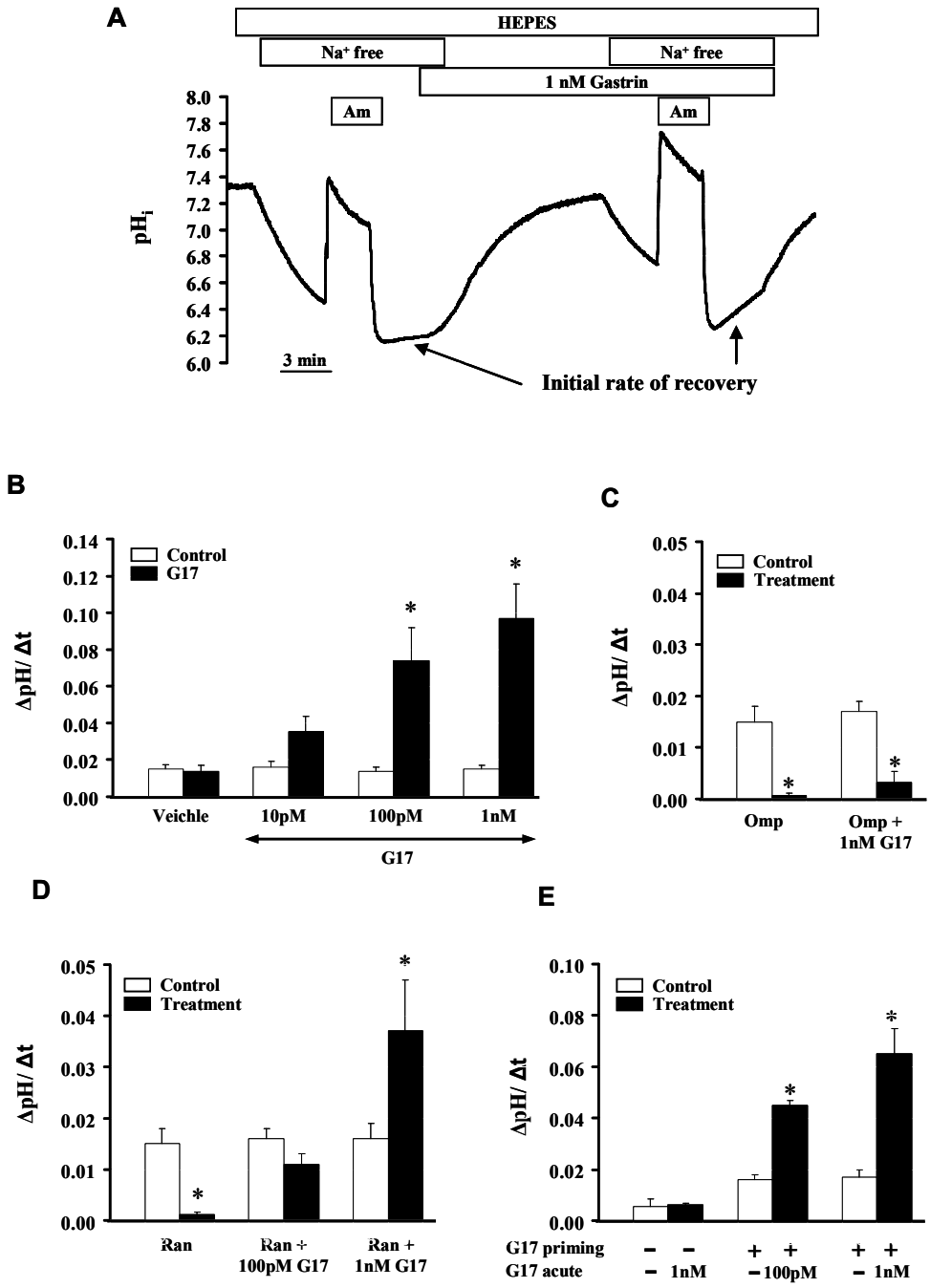

Figure 1. Functional characterisation of parietal cells in cultured gastric glands of Gas-KO and wild type mice. **A,** Representative pH_i trace of gastric gland parietal cells that were twice exposed to 3 min pulses of 20 mM NH_4Cl (Am) in a Na^+ free Hepes solution, the first exposure being the control and the second the test. The initial rates of pH_i recovery from the acid load (over the first 60sec) were determined for each exposure. G17 was administered for 20 minutes before and during the test exposure and the inhibitors (omeprazole or ranitidine, when used) were administered for 10 minutes between the measurements. **B,** Bar chart shows the summary of the results obtained using ammonium chloride pulses described above. Initial rates of pH_i recovery are shown by the open bars, compared with recovery in the test period (filled bars). Increasing concentrations of G17 stimulated the pH_i recovery after NH_4Cl pulses compatible with increased activity of H^+/K^+ ATPase. **C,** the proton pump inhibitor omeprazole (100 μM) completely blocked both unstimulated and G17-stimulated pH_i recovery. **D,** the H_2 receptor antagonist ranitidine (100 μM) inhibited pH_i recovery in response to a low concentration of G17, that could be overcome by higher concentrations of G17. **E,** in parietal cells from GAS-KO mice, incubation *in vitro* with gastrin (1nM, 24 h; "G17 priming") restored proton pump activity. Means ± SEM for groups of 3 glands/10-15 parietal cells are shown. * $p<0.05$.

3.2. Characterization of the acid/base transporters of the lacrimal gland ductal epithelia

3.3.1. Morphology of isolated ducts

The ultrastructural examination revealed that small ducts were characterized by numerous microvilli in the apical region, tight junctions, secretory granules, mitochondria and basolateral infoldings (interdigitations) of the cell membrane and basement membrane in the basal region. The cells were relatively rich in vesicles and secretory granules (Fig. 2).

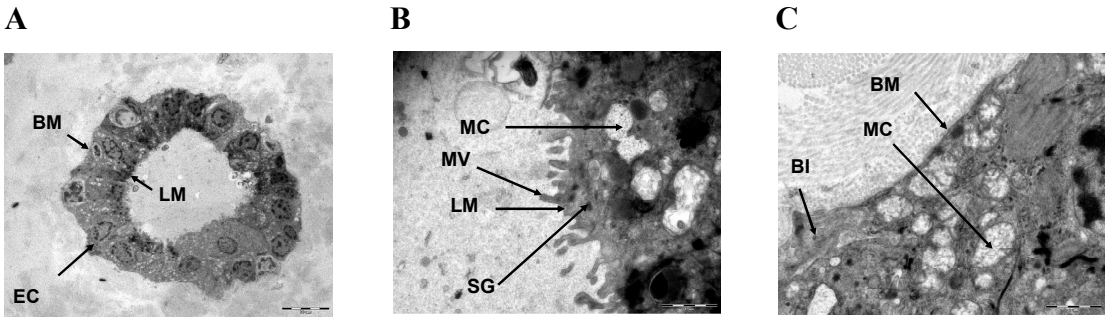

Figure 2. Electron micrographs of intact lacrimal ducts that had been maintained in culture for 24h. (A) Horizontal sections of isolated ducts. LM: luminal membrane, BM: basolateral membrane, EC: epithelial cell. **(B)** The luminal side of the lacrimal duct. MC: mitochondria, MV: microvilli, SG: secretory granule **(C)** The basolateral side of the lacrimal duct. BI: basolateral interdigitation. The bar represents 1 μm.

3.3.2. Resting pH_i of the lacrimal gland ductal epithelia

In the first series of experiments, we wanted to determine the resting pH_i of LGDC. Ducts were exposed to standard Hepes solution (pH:7.4), followed by an 8 min exposure to a high-K^+-Hepes solution (pH: 7.28), and then to an 8 min exposure to a high-K^+-Hepes solution (pH: 7.4). We used the classical linear model,[60, 61] to determine the resting pH_i. The resting-pH_i level of 5 ducts (22 ROIs) was found to be 7.40 ± 0.01. The resting pH_i of LGDC was virtually the same confirming that the experimental conditions can be kept constant for pH_i experiments (Fig. 3).

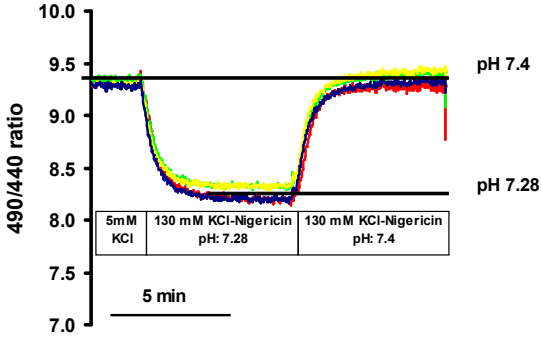

Figure 3. The resting pH_i of lacrimal ductal epithelial cells. Ducts were exposed to nigericin/high K^+-Hepes solutions of pH 7.28 and 7.4. Due to the relatively short time course of the experiment, the resting pH_i was calculated from this 2-point calibration by using the classic linear model. In this particular experiment, the pH_i was 7.4. The resting pH_i of 5 ducts (22 ROIs) was 7.40 ± 0.01.

3.3.3. Na^+/H^+ exchanger

In this series of experiments, we tested whether the isolated lacrimal glands are suitable for functional experiments. The Na^+/H^+ transport proteins that mediate the electroneutral exchange of Na^+ and H^+ ions were examined. Removal of Na^+ from the standard Hepes solution caused a rapid and marked intracellular acidosis (0.20 ± 0.01 pH U/min, n=3 ducts / 15 ROIs) (Fig. 4A). Re-addition of Na^+ to the solution resulted in a complete pH_i recovery. Since the solution did not contain HCO_3^-, this finding confirms the presence of a Na^+ dependent H^+ efflux mechanism on the basolateral side of the LGDC. Removal of Na^+ from the HCO_3^-/CO_2 containing solution also caused a mark acidification (0.22 ± 0.04 pH U/min, n=3 ducts / 15 ROIs) (Fig. 4B).

3.3.4. Na^+/HCO_3^- co-transporter

We also tested whether LGDC express a functionally active Na^+ dependent HCO_3^- transporter on the basolateral membrane (Fig. 4B). Administration of basolateral HCO_3^-/CO_2 rapidly and greatly decreased pH_i. This marked change in pH_i can be explained by the quick diffusion of CO_2 into the cytoplasm. A small pH_i recovery (0.04±0.02 pH U/min, n=6 ducts / 30 ROIs) was found after the acidification suggesting the marginal role of HCO_3^- efflux into the lacrimal duct cells.

3.3.5. Cl^-/HCO_3^- exchange activity

To test the activity of the Cl^-/HCO_3^- exchange mechanisms we utilized the Cl^- removal technique in the presence and absence of HCO_3^- ions. In the absence of HCO_3^-, Cl^- removal caused a small reversible alkalization in LGDC (Fig. 4C; 0.020±0.002 pH U/min), suggesting the small availability of HCO_3^- ions in the cytoplasm. However, in standard HCO_3^-/CO_2 solution a significantly higher alkalization was observed (Fig. 4D; 0.16±0.02 pH U/min, respectively).

In addition, the anion exchange inhibitor H_2DIDS (250 μM) significantly inhibited $\Delta pH/\Delta t$ (Figs. 4E and F; 0.067 ± 0.015 pH U/min). These results confirm functionally active Cl^-/HCO_3^- exchange mechanisms on the basolateral membrane of LGDC.

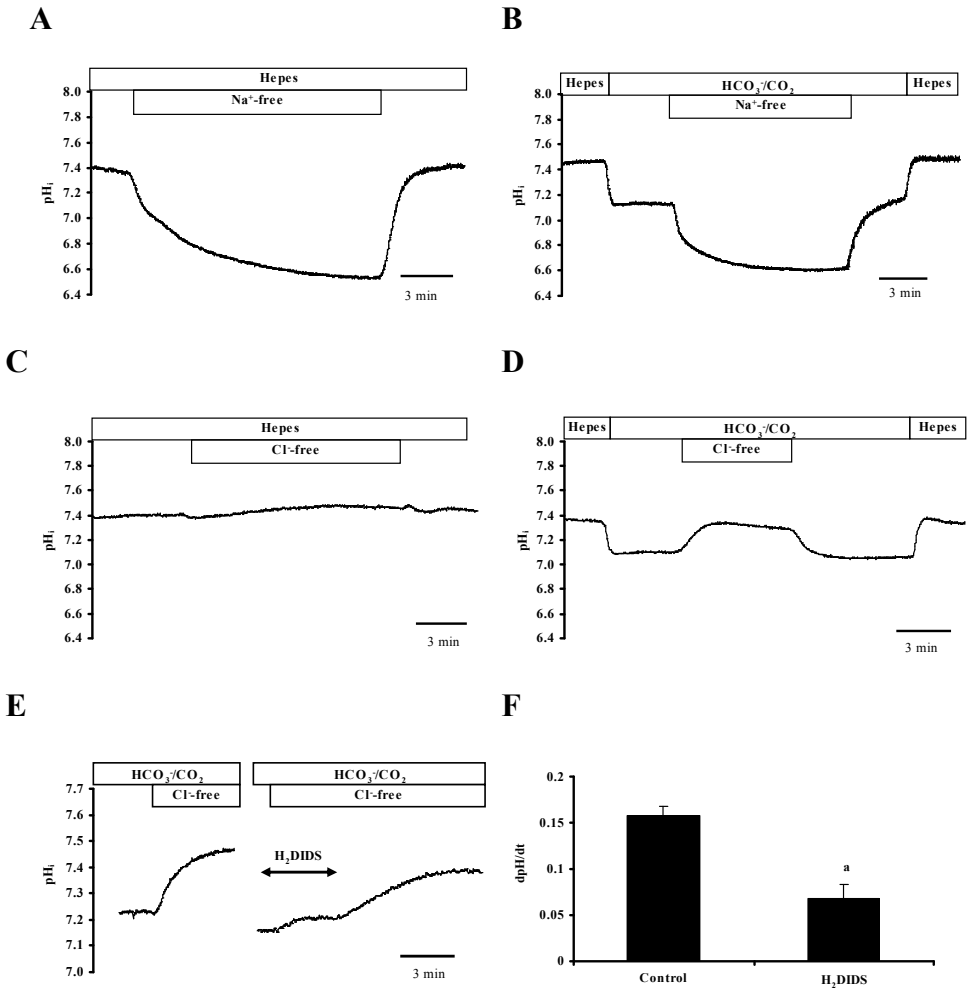

Figure 4. **Effects of removal and readdition of extracellular Na^+ or Cl^- with and without HCO_3^-/CO_2 on pH_i in lacrimal ductal epithelial cells. (A)** Removal of Na^+ resulted in a rapid reversable acidification of pH_i. **(B)** Standard HCO_3^-/CO_2 solution caused a rapid acidification of pH_i by the diffusion of CO_2 into the cells. Removal of Na^+ resulted in the same range of acidification as in Fig. 4A. **(C)** Removal of Cl^- from the HCO_3^--free (Hepes) solution resulted in a small reversable alkalization of pH_i, while in a HCO_3^- containing solution **(D)** this pH_i change was enhanced. Traces are representative of 3 experiments for each protocol. **(E).** Removal of Cl^- from the standard HCO_3^-/CO_2 solution resulted in an alkalization of pH_i; H_2DIDS (250 μM) strongly inhibited this alkalization, and this inhibitory effect of H_2DIDS was - at least partially – reversable. **(F).** Summary of the calculated initial rates of alkalization ($\Delta pH/\Delta t$) from Fig. 4E are shown. Means ± SEM for 14 ROIs of 3 ducts are shown. a: $p< 0.05$ vs control.

3.3.6. pH_i recovery from alkali and acid load

An alternate method for characterizing the above mentioned transporters is the ammonium-pulse technique.[63] Administration of 20 mM NH_4Cl initially increases pH_i due to the rapid entry of NH_3 into the cell. The recovery from alkali load may reflect the activity of the Cl^-/HCO_3^- exchanger.[63] Removal of NH_4Cl causes the typical acidic undershoot of pH_i (Fig. 5A). The transporters (if present in LGDC) most likely involved in the recovery process from acidosis are the basolateral Na^+/HCO_3^- cotransporter, the Na^+/H^+ exchanger and the H^+ pump.

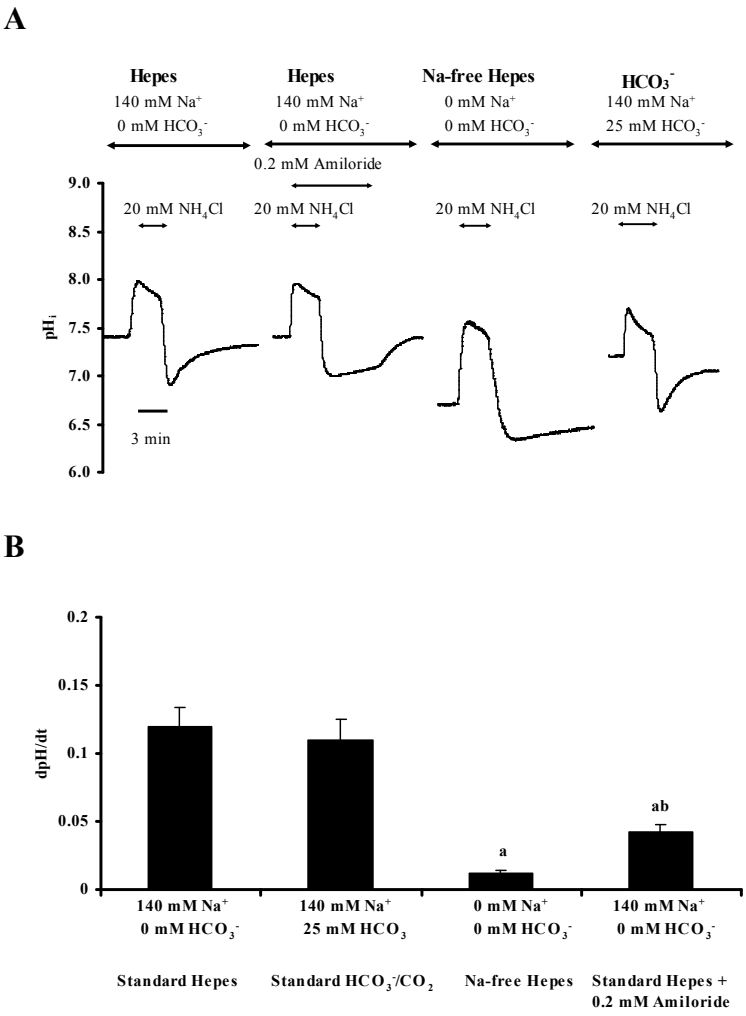

Figure 5. Recovery of pH_i after an acid load. (A). Duct cells were acid loaded by a 3 min exposure to 20 mM NH_4Cl, followed by its sudden withdrawal. The initial rates of pH_i recovery from the acid load (over the first 30 s) were calculated in each experiment. All experiments were performed at 37°C using standard Hepes (with or without Na^+) or HCO_3^-/CO_2 solution, respectively. Each experiment was performed on a different duct. **(B).** Summary of the calculated initial rate of recovery ($\Delta pH/\Delta t$) from Fig. 5A are shown. The effects of different solutions (HCO_3^--free and/or Na^+-free) and the NHE inhibitor, amiloride, are shown. Means ± SEM for 30 ROIs of 6 ducts are shown. a: $p< 0.001$ vs. Standard Hepes. b: $p< 0.05$ vs. Na^+-free Hepes.

The recovery ($\Delta pH/\Delta t$) from alkali load was significantly higher in the presence of HCO_3^- (0.049±0.004 pH U/min and 0.08±0.001 pH U/min, respectively) suggesting an active Cl^-/HCO_3^- exchanger. The recovery from acid load was 0.12±0.01 pH U/min in standard HCO_3^-/CO_2 solution (containing Na^+ and HCO_3^-/CO_2). The absence of HCO_3^- did not significantly change the rate of recovery (0.11±0.015 pH U/min). However, the removal of Na^+ from the standard Hepes solution significantly decreased the recovery from acid load to 0.012±0.002 pH U/min by switching off the Na^+/H^+ exchanger. The small remaining recovery from acid load may represent an active proton pump in LGDC. Finally, we tested the NHE inhibitor amiloride (0.2 mM). Amiloride administration greatly inhibited the Na^+/H^+ exchanger (0.04±0.01 pH U/min) located on the basolateral membrane of LGDC. Furthermore, the removal of amiloride immediately turned on the Na^+/H^+ exchanger suggesting the reversible effect of amiloride.

3.3.7. Ca^{2+} signaling during parasympathomimetic stimulation

The parasympathic neurotransmitters acetylcholine (Ach) and vasoactive intestinal peptide are potent stimuli of lacrimal gland secretion,[67] and have been shown to act through the intracellular Ca^{2+} signaling pathway. The parasympathomimetic carbachol was administered to LGDC in 3 different doses (10, 100 and 1000 µM, Fig. 6). Carbachol dose dependently stimulated the intracellular Ca^{2+} signaling in LGDC (F/F_0 14 ± 0.1, 20 ± 0.1 and 39±0.1%, respectively) suggesting the importance of this pathway in water and ion secretion. The parasympatholytic atropine (0.2 mM) completely blocked the stimulatory effect of carbachol (1 mM).

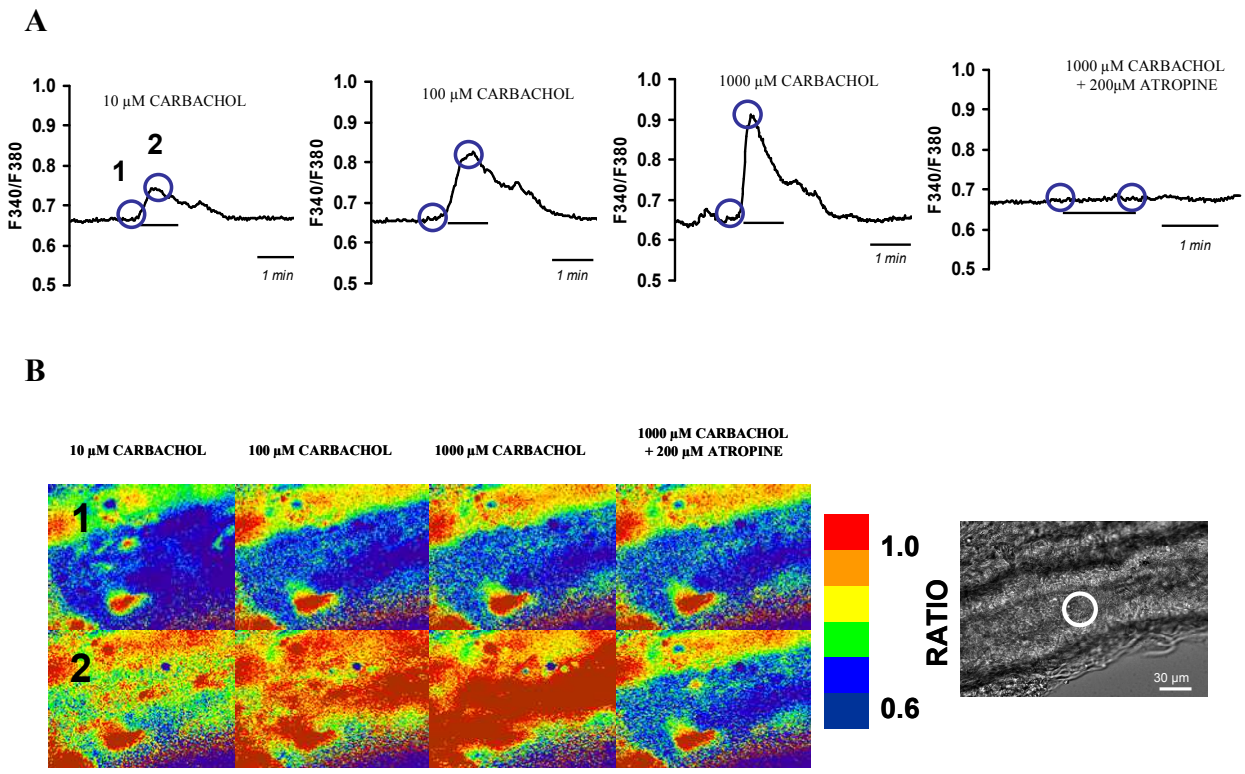

Figure 6. Effects of carbachol on intracellular Ca^{2+} concentration in lacrimal gland ductal epithelial cells. Cultured lacrimal ducts were attached to a coverslip as described in the methods. **(A)** 10, 100 and 1000 µM carbachol was administered to duct cells in standard Hepes solution. Carbachol dose dependently eleveted $[Ca^{2+}]_i$. Each experiment was performed on the same duct using a 10 min wash-out period between the pulses. Representative curves are shown. Maximal $[Ca^{2+}]_i$ elevation was observed 2 ± 0.5 s after stimulation. Similar results were obtained when the experiments were performed on different ducts (n=3). **(B)** Shown are the typical patterns of $[Ca^{2+}]_i$ changes in an intact duct perfused with different concentrations of carbachol. Increase in $[Ca^{2+}]_i$ is denoted by a change from a ''cold'' color (blue) to a ''warmer'' color (yellow to red; see color scale on the top). *Pictures 1-2* were taken at the times indicated by the *circles* in *A*. A representative duct is shown on the right. Data were taken from the ROI marked in the picture. The *bar* represents 30 µm.

3.3.8. The effects of carbachol on the Na^+/H^+ and anion exchangers

Administration of 1 mM carbachol significantly elevated the pH_i in standard Hepes solution (containing Na^+ and Cl^-, but no HCO_3^-) (Fig. 7A). However, this elevation was not observed in a Na^+-free Hepes solution (Fig. 7B). Since HCO_3^- was absent, the alkalization in the Na^+-containing solution must be due to a stimulated Na^+ dependent H^+ efflux mechanism via an NHE (Fig. 7A).

When the LGDCs were treated with 1 mM carbachol in standard HCO_3^-/CO_2 solution, a small pH_i elevation was observed (Fig. 7C). However, this brief alkalinization (most likely caused by the stimulation of an NHE) of pH_i was followed by an acidification. Importantly, this acidification was absent in a Cl^--free HCO_3^- solution suggesting that this decrease in pH_i is due to a Cl^- dependent HCO_3^- efflux mechanism via a Cl^-/HCO_3^- exchanger (Fig. 7D). These data indicate that carbachol stimulates Na^+ and Cl^- influx into the cell through the basolateral membrane of LGDC. Importantly, the parasympatholytic atropine (0.2 mM) totally blocked the stimulatory effect of 1 mM carbachol (Fig. 7E).

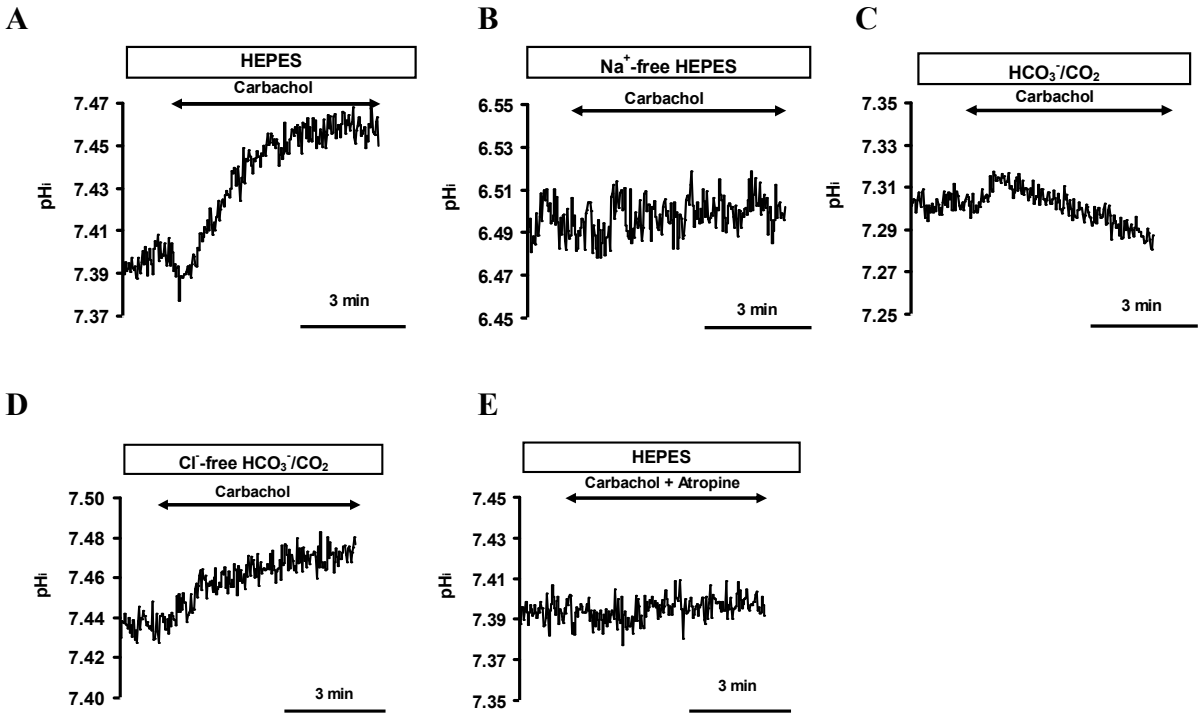

Figure 7. Effects of carbachol on pH_i. 1 mM carbachol was administered to duct cells in **(A)** standard Hepes solution (containing Na^+ and Cl^-,-but no HCO_3^-), **(B)** Na^+-free Hepes solution (containing Cl^-, but no Na^+ and HCO_3^-), **(C)** standard HCO_3^-/CO_2 solution (containing Na^+, Cl^- and HCO_3^-) or **(D)** Cl^--free HCO_3^-/CO_2 solution (containing Na^+ and HCO_3^-, but no Cl^-). **(E)** 1 mM carbachol and 200μM atropine were administered to duct cells in standard Hepes solution. Please note that alkalinization of pH_i was only observed in Na^+ containing solutions (A, C and D). Acidification of pH_i was observed only in a Cl^- and HCO_3 -containing solution (C).

To confirm this hypothesis we analysed the recoveries from acid and alkali load using the ammonium pulse technique. Fig. 8 shows a representative trace of the experiments. We found that 1 mM carbachol significantly stimulated the NHE (recovery from acid load in a HCO_3^- free solution, Figs. 8A and B). No differences were observed in the recovery from alkali load in a HCO_3^--free (Hepes) solution. However, when the experiments were performed in standard HCO_3^- solution, the AE (recovery from alkali load, Fig. 8C) was stimulated by 1 mM carbachol. As we found earlier, atropine (0.2 mM) totally blocked the stimulatory effect of carbachol on the NHE and AE (data not shown).

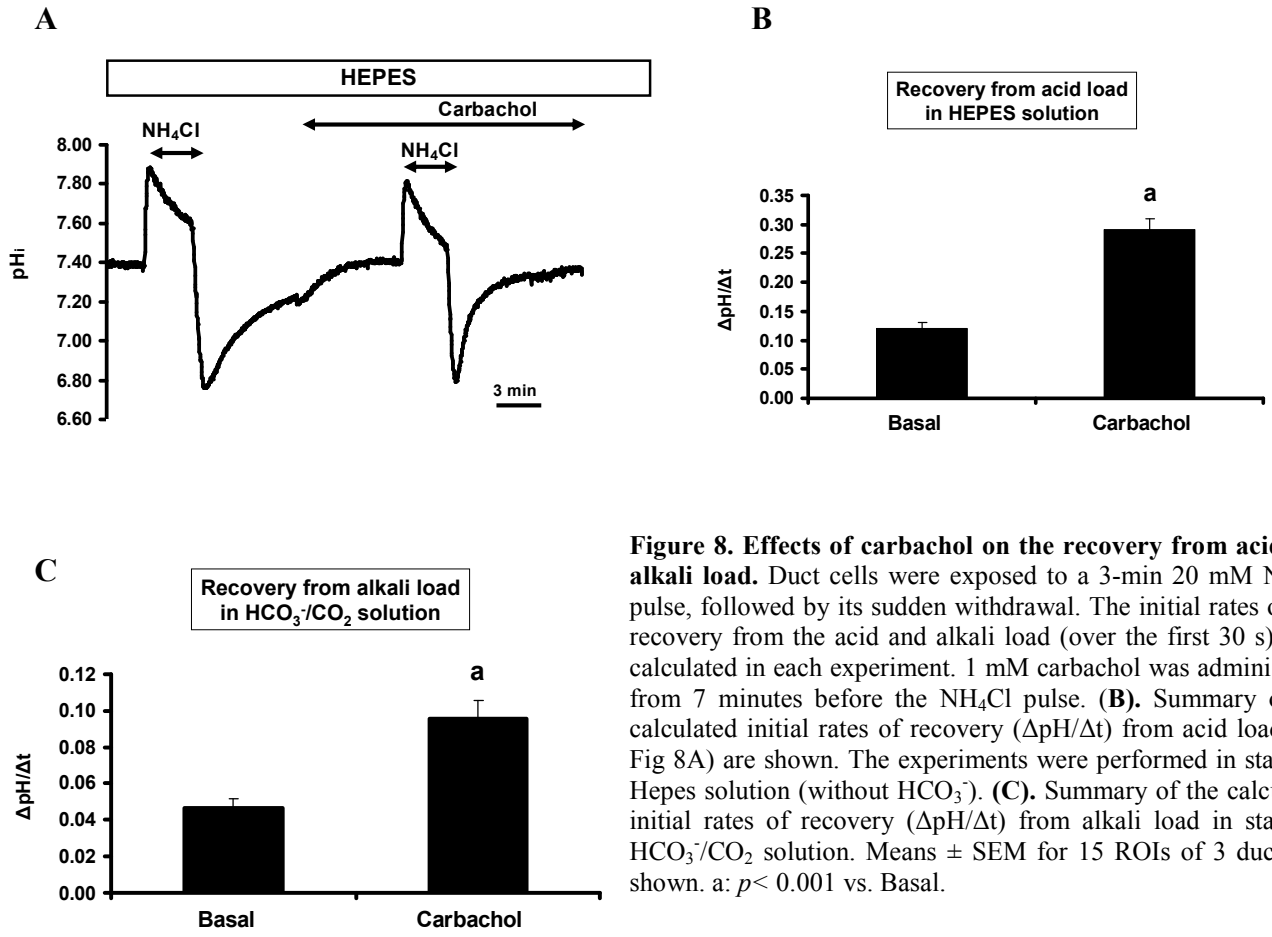

Figure 8. Effects of carbachol on the recovery from acid and alkali load. Duct cells were exposed to a 3-min 20 mM NH_4Cl pulse, followed by its sudden withdrawal. The initial rates of pH_i recovery from the acid and alkali load (over the first 30 s) were calculated in each experiment. 1 mM carbachol was administered from 7 minutes before the NH_4Cl pulse. **(B).** Summary of the calculated initial rates of recovery ($\Delta pH/\Delta t$) from acid load (see Fig 8A) are shown. The experiments were performed in standard Hepes solution (without HCO_3^-). **(C).** Summary of the calculated initial rates of recovery ($\Delta pH/\Delta t$) from alkali load in standard HCO_3^-/CO_2 solution. Means ± SEM for 15 ROIs of 3 ducts are shown. a: $p< 0.001$ vs. Basal.

3.3. Differential effect of bile acids on pancreatic ductal cells

3.3.1. Effect of basolateral exposure to bile acids on duct cell pH_i

Figure 9A-D shows the effect of basolateral administration of the non-conjugated CDC and the conjugated GCDC on the duct cell pH_i in perfused pancreatic ducts.

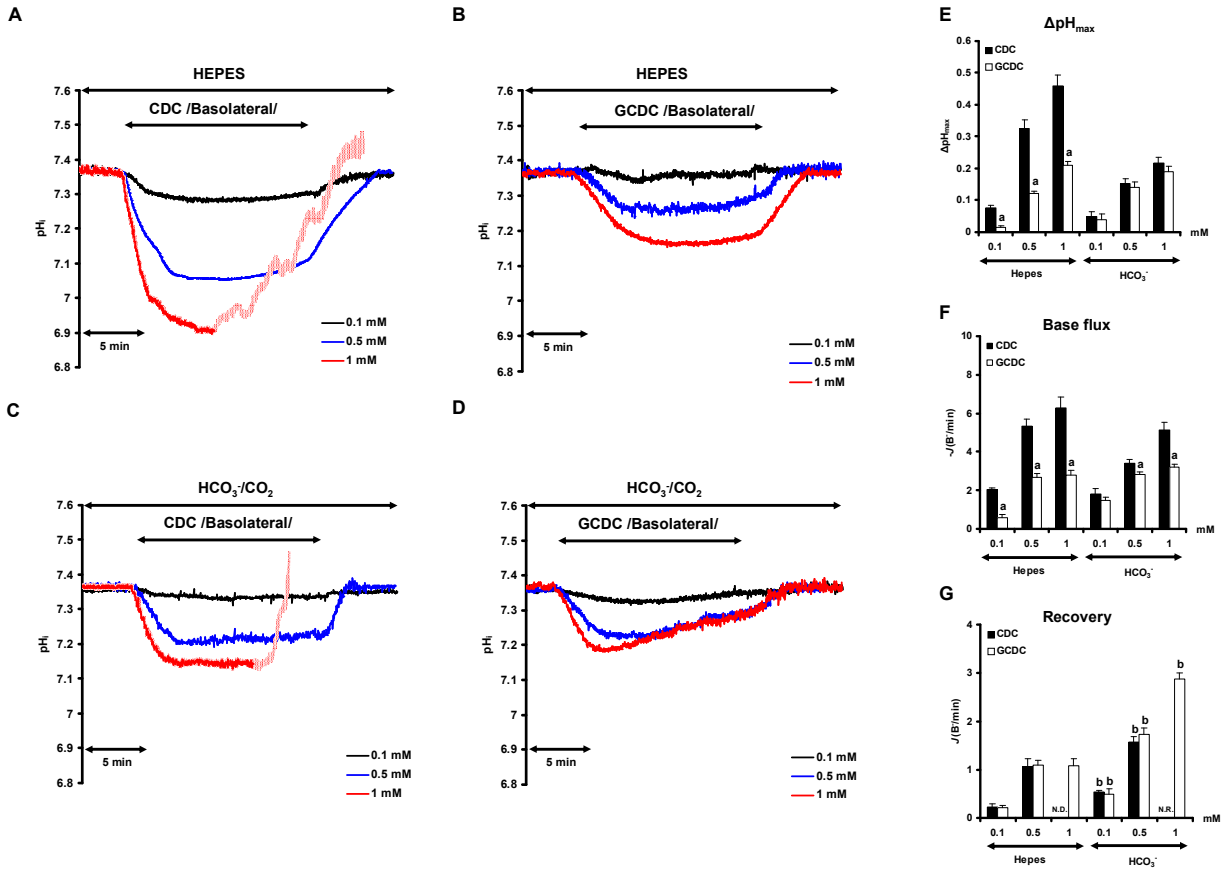

Figure 9. Effect of basolateral administration of bile acids on intracellular pH (pH_i) and base flux of pancreatic duct epithelial cells (PPDC). Panels A and B show representative pH_i traces demonstrating the effect of chenodeoxycholate (CDC; 0.1, 0.5, 1 mM) and glycochenodeoxycholate (GCDC; 0.1, 0.5, 1 mM) administered from the basolateral membrane in HCO_3^-/CO_2 and in standard Hepes-buffered solution (C and D). Summary data of the maximal pH_i changes (ΔpH_{max}), are shown in panel E and the mean base (bile acid) flux ($-J(B^-)$), in panel F. Panel G shows the recoveries ($J(B^-)$)during the addition of bile acids. Means ± SEM are from 36 regions of interests (ROIs) of 8 ducts. a: $p<0.001$ vs. CDC; b: $p<0.001$ *vs.* Hepes. N.D.: not detectable, N.R.: not recordable (due to dye leakage).

Typically, the response was an initial rapid, dose-dependent, fall in pH_i which then recovered to a variable degree during continued exposure to the bile acids. Note that the effect of the bile acids on pH_i was greatest in standard Hepes-buffered as compared to HCO_3^--buffered solutions (Figs. 9A-D). Also, when 1mM CDC was administered in standard Hepes solution, the fluorescence intensities at 440 and 490nm rapidly decreased after 6 ± 1 min (n = 6ducts/35ROIs), causing an elevation of the 490/440 ratio (Fig. 9A). This rapid decrease of the fluorescence intensities must be due to loss of BCECF from the cells. The presence of HCO_3^-/CO_2 delayed this event somewhat to 8 ± 1 min (n = 6ducts/38ROIs) (Fig. 9C). However, no dye leakage occurred with the same concentration of the conjugated GCDC (Figs. 9B and D).

The maximal pH_i change (ΔpH_{max}) and the base flux ($J(B^-)$) following exposure to the bile acids were calculated for each experiment and the summary data are shown in figures 9E and F. In standard Hepes-buffered solutions the unconjugated CDC had a much larger effect on ΔpH_{max} and $J(B^-)$ than the conjugated GCDC, most likely explained by slower permeation of the charged GCDC into the duct cells. In contrast, in HCO_3^-/CO_2 containing solutions the bile salts induced much smaller changes in ΔpH_{max} and $J(B^-)$ (Figs. 9E and F). This was particularly obvious for the unconjugated CDC and is consistent with the increased buffering capacity of the duct cells in the presence of HCO_3^-/CO_2.[58]

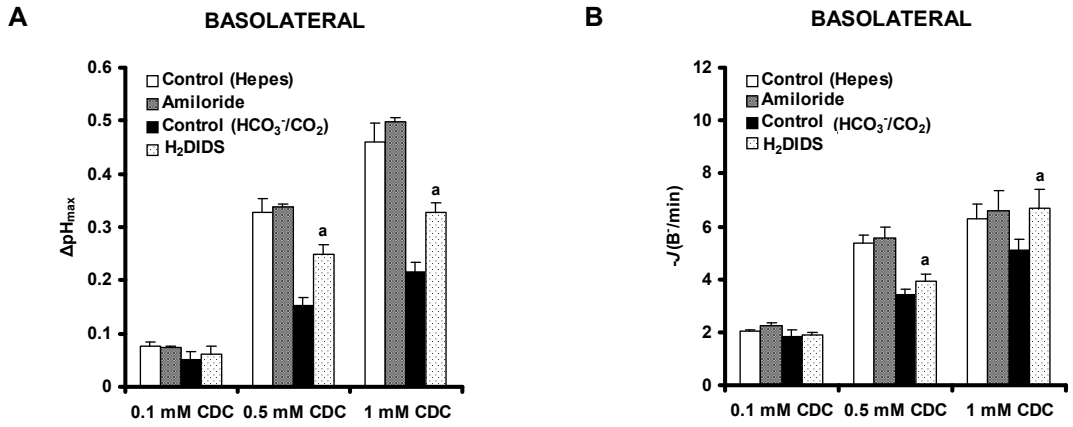

Figure 10. The effects of NBC and NHE activity on the CDC-induced acidification. Panels A and B show the effect of 0.5 mM H_2DIDS in HCO_3^-/CO_2 buffered solution or 0.2 mM amiloride in standard Hepes-buffered solution on the bile induced base flux ($-J(B^-)$) and ΔpH_{max} from the basolateral membrane. We found that amiloride did not have any effect on the initial phase of bile acid induced acidification or on the ΔpH_{max}. However, in the presence of H_2DIDS the rate of acidification and the CDC-induced pH_i change was significantly higher. Means ± SEM are from 23 ROIs of 4 ducts. a: $p<0.001$ vs the respective control.

Amiloride (0.2 mM) had no effect on the ΔpH_{max} and $J(B^-)$ caused by basolateral exposure to the unconjugated CDC in a standard Hepes-buffered solution, suggesting that Na^+/H^+ exchange is not activated during the acidification process (Figs. 10A and B). However, basolateral administration of 0.5 mM H_2DIDS significantly increased both the ΔpH_{max} and the $J(B^-)$ in response to CDC (Figs. 10A and B). This result suggests that the basolateral NBC normally acts to attenuate the fall in pH_i caused by CDC, presumably by transporting HCO_3^- ions into the duct cells.

3.3.2. Effect of luminal exposure to bile acids on duct cell pH_i

Figure 11A-F shows the effect of luminal administration of the bile acids on duct cell pH_i and $J(B^-)$ in perfused pancreatic ducts.

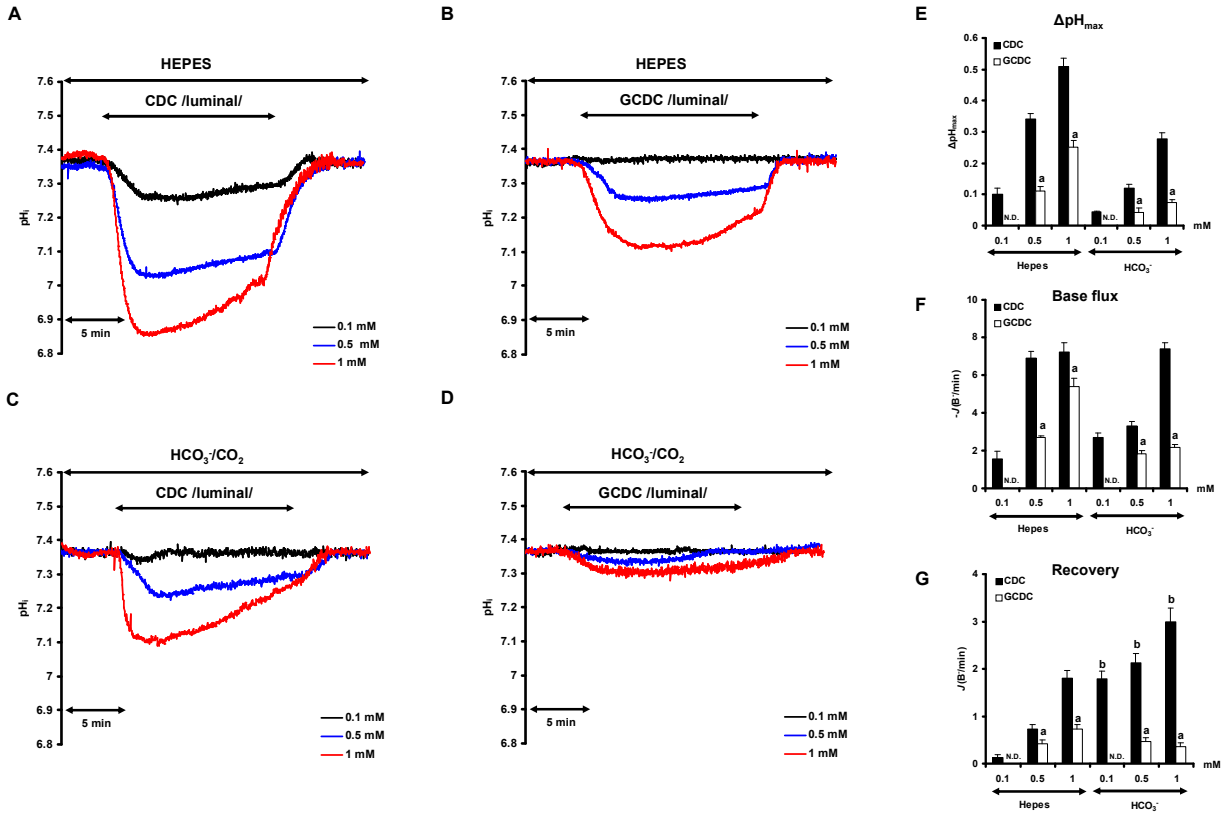

Figure 11. Effect of luminal administration of bile acids on intracellular pH (pH_i) and base flux of pancreatic duct epithelial cells. Panels A and B show representative pH_i traces demonstrating the effect of chenodeoxycholate (CDC; 0.1, 0.5, 1 mM) and glycochenodeoxycholate (GCDC; 0.1, 0.5, 1 mM) administered from the luminal membrane in HCO_3^-/CO_2 and in standard Hepes-buffered solution (C and D). Summary data of the maximal pH_i changes (ΔpH_{max}) are shown in panel E and the mean base (bile acid) flux ($-J(B^-)$), in panel F. Panel G shows the recoveries ($J(B^-)$) during the addition of bile acids. Means ± SEM are from 26 regions of interests (ROIs) of 5 ducts. a: $p<0.001$ vs. CDC; b: $p<0.001$ *vs.* Hepes. N.D.: not detectable.

As with basolateral exposure, there was: (i) a rapid fall in pH_i followed by a variable degree of pH_i recovery during continued exposure to the bile acid, (ii) the unconjugated CDC caused a much larger ΔpH_{max} and $J(B^-)$ than the conjugated GCDC, and (iii) luminal bile acids had a larger effect on pH_i when tested in a standard Hepes solution as compared to a HCO_3^-/CO_2 solution (Figs. 11A-F). However, note that luminal exposure to 1 mM CDC never caused the rapid dye loss that occurred following basolateral addition of the bile acid.

3.3.3. Recovery of duct cell pH_i during continued exposure to bile acids

The experimental traces in Figures 9 and 11 indicate that some degree of pH_i recovery occured during continuous exposure of the pancreatic duct epithelial cells (PPDC) to bile acids; except with 1 mM CDC administered from the basolateral side which damages the cells and causes dye leakage (Fig. 9). Initially, we calculated the $J(B^-)$ values during pH_i recovery with and without HCO_3^-/CO_2. A partial recovery of pH_i during continuous exposure to the bile salts (except 1 mM basolateral CDC) occurred in both Hepes and HCO_3^-/CO_2 solutions (Figs. 9A-D and Figs. 11 A-D). However, the calculated $J(B^-)$ values during pH_i recovery following basolateral administration of CDC and GCDC were 1.5- to 2.5-fold higher in the presence of HCO_3^-/CO_2 (Fig. 9G). Similarly, HCO_3^-/CO_2 enhanced the $J(B^-)$ during pH_i recovery following luminal exposure to CDC (Fig. 11G). However, no such effect was seen with luminal GCDC (Fig. 11G), presumably because luminal GCDC caused only small changes in duct cell pH_i under these conditions (Fig. 11D).

We sought to establish which acid/base transporters are involved in the pH_i recovery process; the most likely candidates being the basolateral NBC and the NHE.[68] Fig. 12A shows that amiloride (0.2 mM) strongly inhibited the $J(B^-)$ during pH_i recovery following exposure to basolateral CDC (0.1 and 0.5 mM) in standard Hepes solution, suggesting a major role for the NHE in pH_i recovery in the absence of HCO_3^- ions. In a more physiological HCO_3^-/CO_2 solution, amiloride was a somewhat less effective inhibitor (Fig. 12B). This suggests an involvement of the NBC in pH_i recovery when HCO_3^- is present and is consistent with the enhancing effect of HCO_3^-/CO_2 on $J(B^-)$ during pH_i recovery (Figs. 9G and 11G). Taken together, these data suggest that, when it occurs, pH_i recovery during exposure to bile acids is mediated both by the NHE and the NBC.

When a high dose of CDC (1 mM) was administered to the basolateral membrane in standard Hepes solution, PPDC started to lose dye and so pH_i recovery could not be studied (Fig. 9A). Leakage of dye was delayed in a HCO_3^-/CO_2 solution, however, no pH_i recovery

was observed before the cell membrane became permeable suggesting that the NBC and NHE were totally inhibited under these conditions (Fig. 9C).

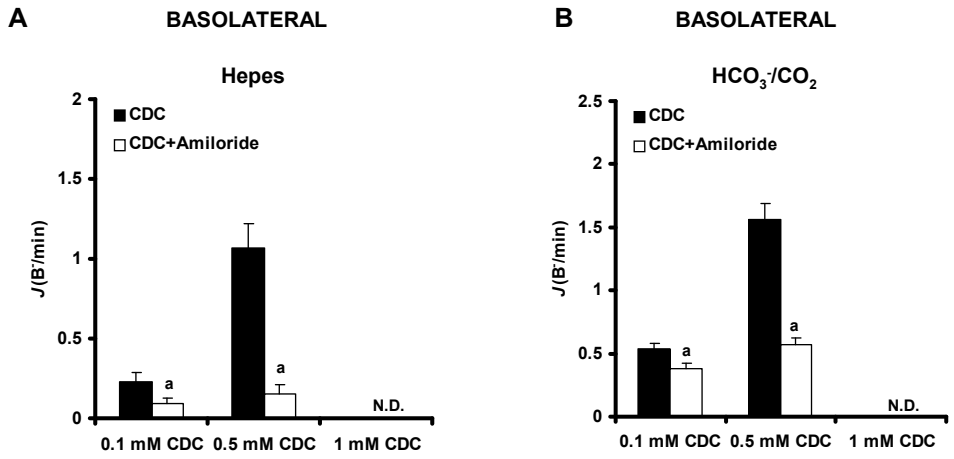

Figure 12. Amiloride inhibits the recovery of pH_i during chenodeoxycholate administration. Panels A and B show the effect of 0.2 mM amiloride on the recovery of pH_i during CDC administration (0.1, 0.5 and 1 mM) in the absence or presence of HCO_3^-/CO_2. We found that amiloride inhibited the recovery during CDC administration. However, this inhibitory effect was significantly lower in the presence of HCO_3^-/CO_2, which indicates that NBC is involved in the recovery process. Means ± SEM are from 27 ROIs of 5 ducts. a: $p<0.001$ vs the respective control. N.D.: not detectable.

3.3.4. Effect of bile acids on HCO_3^- secretion

To investigate the effects of bile acids on HCO_3^- secretion, we analysed the recovery of pH_i from an alkali load induced by exposure to NH_4Cl in a HCO_3^-/CO_2 containing solution (for original traces see Fig. 13). We have previously shown that the $J(B^-)$ calculated from the rate of pH_i recovery under these conditions reflects the rate of HCO_3^- efflux (i.e. secretion) on luminal Cl^-/HCO_3^- exchangers.[68] Basolateral administration of a low dose (0.1 mM) of the unconjugated CDC had no effect on $J(B^-)$; however, a higher dose of CDC (1 mM) strongly inhibited HCO_3^- secretion (Fig. 14A). Interestingly, luminal administration of 0.1 mM CDC had a stimulatory effect on HCO_3^- secretion (Fig. 14B), whereas the higher dose (1 mM) was inhibitory (Fig. 14B). The basal rate of HCO_3^- secretion and the stimulatory effect of luminal 0.1 mM CDC were unaffected by bumentanide or bromosulphophthalein (Fig. 14C), suggesting that neither the $Na^+/K^+/2Cl^-$ cotransporter nor bile acid/HCO_3^- exchange on the organic anion transporter protein (OATP) were involved in pH_i recovery (Fig. 14C). In contrast to the effects of CDC, neither basolateral nor luminal application of the conjugated GCDC (0.1 and 1 mM) had any effect on pH_i recovery from an alkali load (Figs. 14A and B).

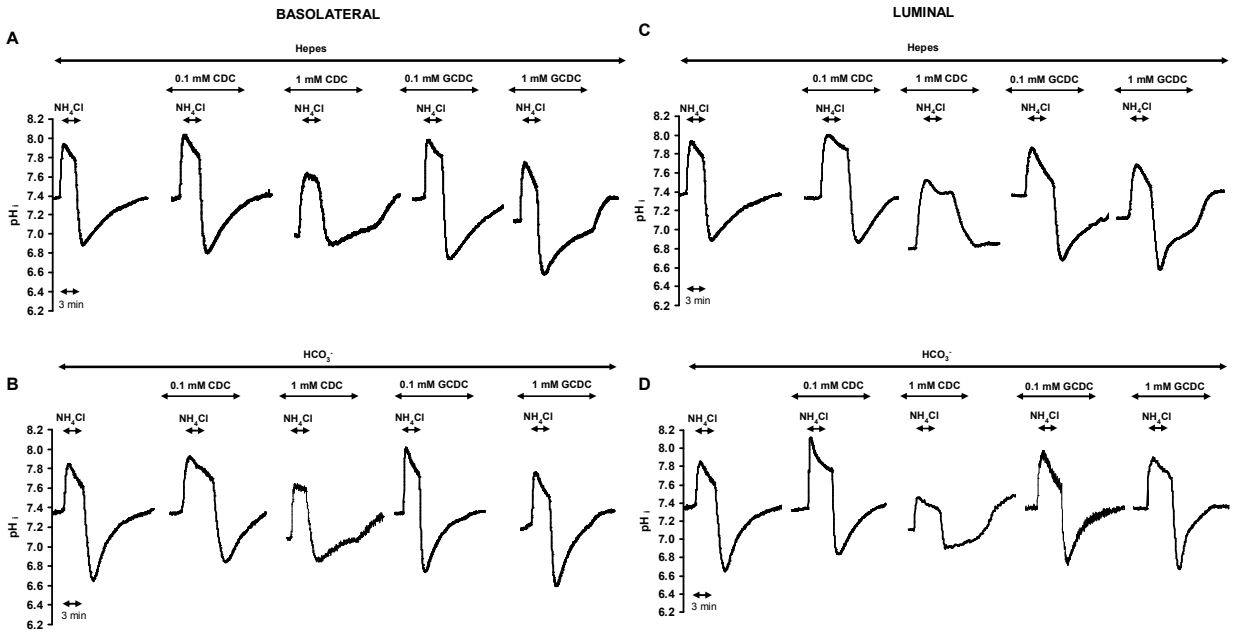

Figure 13. Effect of bile acids on the rate of pH_i recovery from an acid load. Panels A-D show the effect of bile acids (0.1 mM and 1 mM) administered from the basolateral membrane (A and B) or from the luminal membrane (C and D) on pH_i recovery from an acid load (20 mM NH_4Cl) in the absence (A and C) or presence (B and D) of HCO_3^-/CO_2. GCDC had no significant effect on the rate of pH_i recovery at either concentration, indicating that GCDC does not have a direct effect on the activity of NHE and NBC. In contrast, 1 mM CDC strongly inhibited the recovery from both the luminal and basolateral membranes in standard Hepes and HCO_3^-/CO_2 (blank bars) buffered solutions (E and F). Means ± SEM are from 25 ROIs of 5 duct.

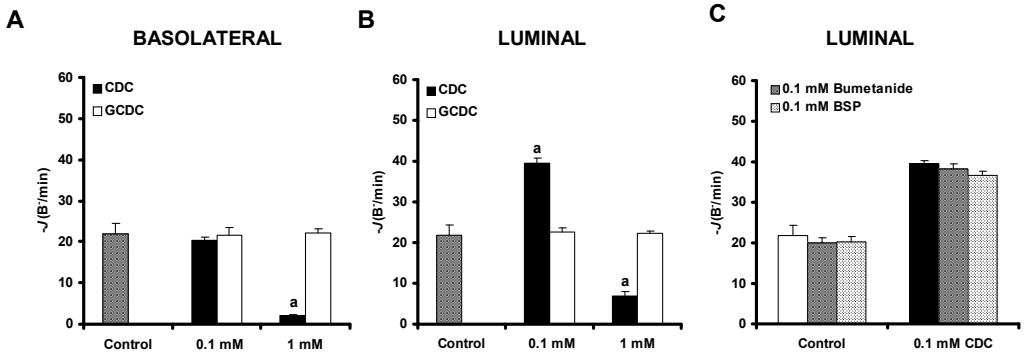

Figure 14. Effect of bile acids on the rate of pH_i recovery from an alkali load. Panel A shows the effect of basolaterally administered CDC (black bars) or GCDC (blank bars) (0.1 mM and 1 mM) on the rate of pH_i recovery from an alkali load (20 mM NH_4Cl in HCO_3^-/CO_2-buffered solution). A low concentration (0.1 mM) of CDC had no effect with respect to control, while 1 mM CDC stongly inhibited HCO_3^- efflux. In contrast 0.1 mM CDC administered from the luminal membrane (B) caused a significant increase in HCO_3^- secretion, whereas the high concentration (1 mM) blocked it. Panel C shows that the stimulatory effect of low dose CDC was not inhibited by bumetanide (0.1 mM) and bromosulphotalein (0.1 mM), inhibitors of the $Na^+K^+2Cl^-$ cotransporter, and the Oatp transporter, respectively. The initial rate of pH_i recovery was calculated in each experiment. Means ± SEM are from 25 ROIs of 5 ducts. a: $p<0.001$ vs control.

We used luminal H_2DIDS to investigate whether the stimulatory effect of luminal 0.1 mM CDC on HCO_3^- secretion was due to activation of Cl^-/HCO_3^- exchangers. We found that H_2DIDS inhibited the basal rate of HCO_3^- secretion by about 65% and completely blocked the stimulatory effect of 0.1mM luminal CDC, suggesting that the stimulatory effect must involve activation of luminal Cl^-/HCO_3^- exchangers (Fig. 15A). We confirmed these results using another method of measuring HCO_3^- secretion – the inhibitor stop technique.[63, 64] Again we found that luminal H_2DIDS totally blocked the stimulatory effect of low doses of CDC on HCO_3^- secretion (Fig. 15B).

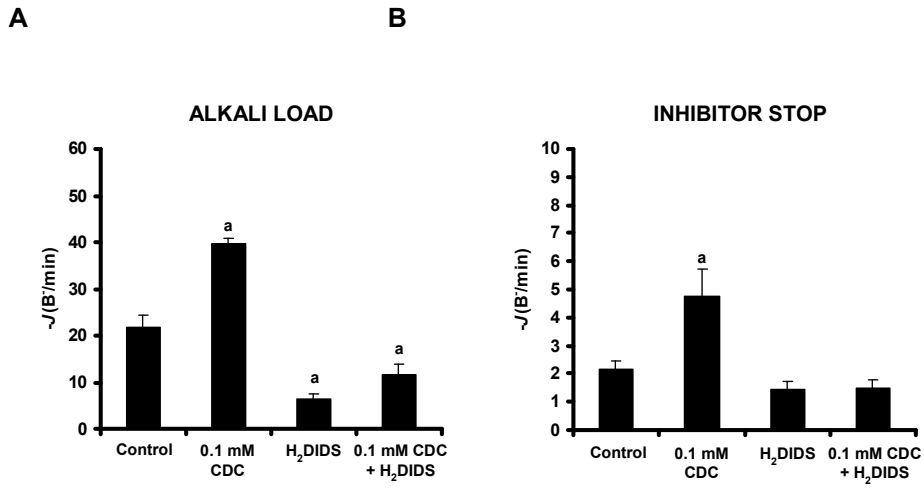

Figure 15. The luminal Cl^-/HCO_3^- exchanger is involved in the stimulatory effect of low doses of non-conjugated bile acids administered from the luminal side. Panel A shows the effect of CDC (0.1 mM) on the rate of pH_i recovery from an alkali load (20 mM NH_4Cl) in the presence and absence of 0.5 mM luminal H_2DIDS. Panel B shows the inhibitor stop method for determining HCO_3^- secretion. PPDC were exposed to 0.2 mM amiloride and 0.5 mM H_2DIDS which caused a marked decrease in pH_i due to the inhibition of NHE and NBC. The experiments were performed in the presence or absence of 0.5 mM luminal H_2DIDS. In the test experiments the bile acid was administered into the lumen from 5 minutes before exposure to 0.5 mM H_2DIDS and 0.2 mM amiloride, or 20 mM NH_4Cl. The initial rate of acidfication was calculated in each experiment. Means ± SEM are from 25 ROIs of 5 ducts. a: $p<0.001$ vs control.

Finally, we directly measured the effects of CDC on the activity of luminal Cl^-/HCO_3^- exchangers using the Cl^- removal technique. Figure 16A shows that CDC (0.1 mM) strongly stimulated pH_i alkalinization after removal of luminal Cl^-. The calculated $J(B^-)$ values indicate that base flux through the exchangers was increased about 8-fold under these conditions (Fig. 16B). Note that the rate of pH_i alkalinization and $J(B^-)$ on luminal Cl^- withdrawal were also slightly elevated when 1 mM CDC was used (which inhibits HCO_3^- secretion) (Figs. 16A and B). However, this apparent stimulation of anion exchange activity is most probably explained by the ongoing recovery of the pH_i that occurs during luminal administration of 1 mM CDC (see Fig. 11C).

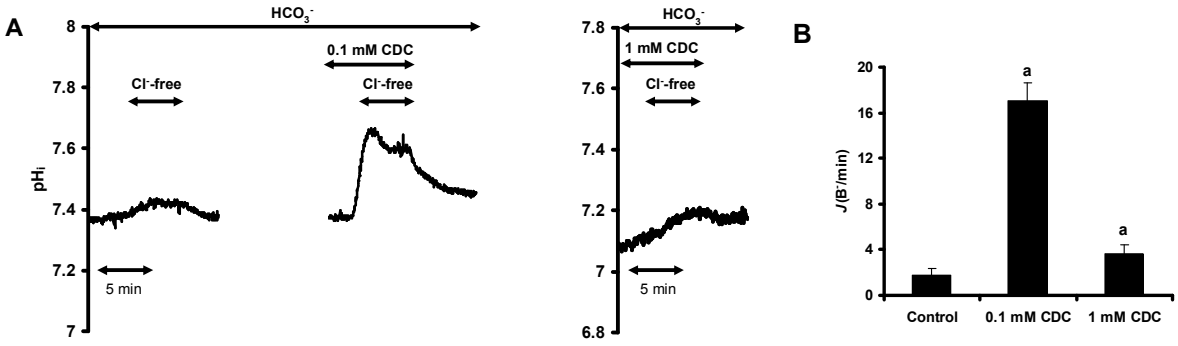

Figure 16. Effect of chenodeoxycholate on pH_i changes after Cl^- removal. Panel A shows representative traces demonstrating the effect of luminal CDC (0.1 and 1 mM) on pH_i changes after luminal Cl^- removal. 0.1 mM CDC induced a considerable increase both in the pH_i and in the maximal rate of alkalization. 1 mM CDC caused a slight increase in pH_i probably as a result of the activation of NBC and NHE. Panel B shows the summary data of the mean base (bile acid) flux ($J(B^-)$). Means ± SEM are from 32 ROIs of 6 ducts. a: $p<0.001$ vs control.

3.3.5. Relationship between the inhibitory and stimulatory effects of chenodeoxycholate on HCO_3^- secretion and chenodeoxycholate-induced changes in $[Ca^{2+}]_i$

We have clearly shown that luminal administration of low doses of CDC (i) stimulate HCO_3^- secretion through the luminal membrane and (ii) induce an IP_3-mediated $[Ca^{2+}]_i$ elevation. Therefore, we investigated whether preventing the elevation of $[Ca^{2+}]_i$ using the intracellular Ca^{2+}-chelator BAPTA-AM, had any effects on HCO_3^- secretion stimulated by luminal administration of low doses of CDC, using the alkali load method. We found that 40 μM BAPTA-AM inhibited basal HCO_3^- secretion by about 25 % and totally blocked the stimulatory effect of low doses of CDC on HCO_3^- secretion (Fig. 17A). Finally, we examined whether Ca^{2+} signaling evoked by a high dose of CDC modulates the inhibitory effect of this non-conjugated bile acid. In contrast to the stimulatory effect of low doses of CDC, the Ca^{2+}-chelator BAPTA-AM had no effect on the inhibitory effect of high doses of CDC (Fig. 17B).

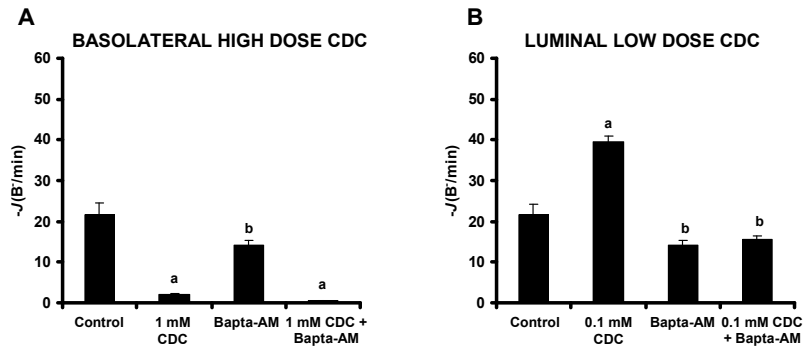

Figure 17. Elevation of intracellular Ca^{2+} concentration is responsible for the stimulatory effect of low doses of chenodeoxycholate on pancreatic HCO_3^- secretion. Panel A shows the effect of 40 μM BAPTA-AM pretreatment (30 minutes before the experiments) on the stimulatory effect of 0.1 mM CDC from the luminal membrane. (B) The effect of BAPTA-AM (40μM) pretreatment on the inhibitory effect of 1 mM CDC from the basolateral membrane. Means ± SEM are from 25 ROIs of 5 ducts. a: $p<0.001$ vs. control, b: $p<0.05$ vs. control.

3.4. The influence of hyperlipidemia on pancreatic HSP72 and IκB-α expression in acute necrotizing pancreatitis

We assessed if hyperlipidemia induced by cholesterol enriched diet affected the production of HSP72 in the pancreas in response to necrotizing pancreatitis. In the pancreas of the control rats, the basal level of HSP72 was very low, but the cholesterol-enriched diet significantly increased its expression. Arg-induced necrotizing pancreatitis resulted in further significant increases in pancreatic HSP72 content both in the animals on a normal diet and also in those on a high cholesterol diet as compared with the controls (Fig. 18A and B). Pancreatic IκB-α levels were not altered by cholesterol treatment vs the control. However, Arg administration significantly decreased IκB-α expression and this was further reduced in pancreatitic rats on a cholesterol diet (Fig. 19).

A

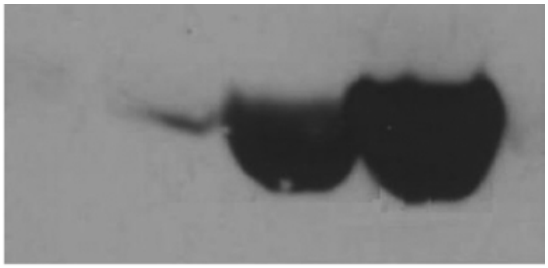

B

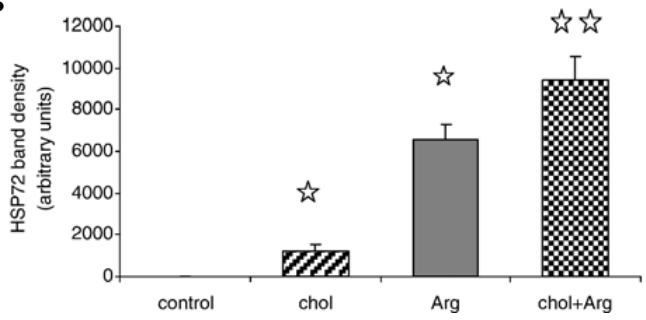

Figure 18. Pancreatic HSP72 expression is increased in hyperlipidemic rats. A. Representative Western immunoblot analysis of protein lysates (40 μg/lane) from the pancreata of rats. **B.** The bar diagram shows the densities of the Western blot bands in the control, cholesterol-fed (chol) groups, and in normal and hyperlipidemic rats with necrotizing pancreatitis (Arg and chol + Arg). The densities of the Western blot bands were quantified by using the ImageJ software. Results are means ± S.E.M. (n=7).☆: significant difference ($P<0.05$) vs. control group. ☆☆: significant difference ($P<0.05$) vs. chol group.

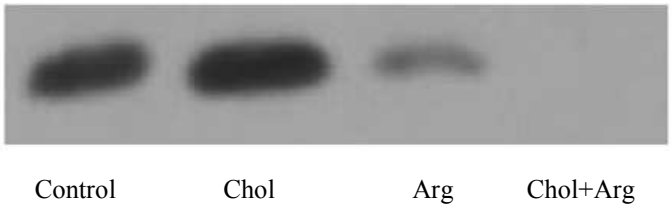

Figure 19. Pancreatic IκB-α levels. Pancreatic cytosolic protein fractions were analyzed by Western blot analysis (40 μg/lane), using a specific IκB-α antibody. Rats were treated in the same manner as described in the legend to Fig. 18.

4. DISCUSSION

In the first part of this thesis we described the secretory mechanisms of the gastric and lacrimal glands under normal conditions.

The secretion of the exocrine gastric gland is a complex process regulated by neural and hormonal mechanisms**.** One of the most important factors in the hormonal regulation is gastrin. It has been clear for some years that Gas-KO mice have substantially reduced gastric acid secretion and an inability to respond to the major gastric acid secretagogues but the relevant cellular mechanisms are largely unknown. [13, 14] The present studies made extensive use of cultured gastric glands. This preparation was selected because glands contain all the relevant cell types, and particularly histamine-secreting ECL cells, as well as parietal cells thereby facilitating studies of paracrine mechanisms. Using a protocol in which pH_i was employed to reflect H^+/K^+ATPase activity we showed that parietal cells from Gas-KO mice were refractory to the action of gastrin, but exposure to G17 for 24 hr restored responses to those seen in glands from wild-type mice. Crucially, the effect of near-physiological concentrations of gastrin in this system was mediated by histamine. However, the priming effect of gastrin was not blocked by the H-2 receptor antagonist, ranitidine. The present data are therefore compatible with the idea that while histamine relesased from ECL cells is a mediator of the acute, secretagogue effect of gastrin, but it does not mediate the effect of gastrin on parietal cell priming, and instead raises the possibility that gastrin acts directly on CCK-2 receptors on parietal cells to stimulate parietal cell maturation.

Lacrimal gland secretion consists of two fractions derived from the acinar and ductal cells. The regulation of ion and water secretion has been well investigated in intact glands,[67] however, no available method has been described to study the role of LGDC in the process of lacrimal fluid secretion. The preocular tear secreted by the lacrimal gland contains Na^+, Cl^- and K^+ in high concentration. This lacrimal gland fluid contains (mmol/L): 42 ± 4 K^+, 107 ± 4 Na^+, 126 ± 5 Cl^- in rabbit[69]; 46 ± 3 K^+, 135 ± 5 Na^+, 123 ±1 Cl^- in rat[70] and 38 ± 5 K^+, 144 ± 5 Na^+, 149 ± 16 Cl^- in mouse[71]. The ductal epithelia, at least in part, must be involved in this hypertonic fluid secretion. In the present study we developed an isolation technique which is suitable to investigate the ion transporters of LGDC and the regulation of fluid secretion. The micro-dissection technique is very similar to what we used for the pancreas.[60, 63] In order to show the viability of isolated and cultured interlobular lacrimal ducts, we characterized the most common acid/base transporters.

Our results showed the functional presence of a Na^+-dependent but HCO_3^--independent H^+ efflux mechanism (most probably through NHEs) on LGDC. Amiloride partially inhibited this Na^+/H^+ exchange mechanism. However, we must note that this K^+ sparing diuretic can also inhibit electrogenic Na^+ channels[72] and the Na^+/Ca^{2+} exchanger.[73] Since NHE1 and 2 are the most sensitive to amiloride inhibition while NHE3 and 4 are amiloride resistant,[74] our results indicate that approximately 66% of the functionally active NHEs are NHE1 and 2 isophorms. Many epithelial cells express proton pumps[26] and NBC [75] which, beside other physiological roles, can protect the epithelial cells from acidosis. We demonstrated that NBC ion transporters – if present - have only a marginal role in the pH_i regulation of LGDC. Following a CO_2-induced acidosis, only a small amount of HCO_3^- entry was detected (see Fig. 5B). Furthermore, no difference was found in the regeneration after acid load caused by an ammonium pulse between the presence and absence of HCO_3^-. Removal of Na^+ decreased this recovery by 93 % in standard Hepes solution suggesting a functionally very active Na^+ dependent H^+ efflux mechanism. We also detected a functionally active Cl^- dependent HCO_3^- efflux mechanism in LGDC. When HCO_3^- was absent from the solution, Cl^- removal only caused a small pH_i change, suggesting a reduced HCO_3^- concentration inside the cell. However, when HCO_3^- was present in the solution, Cl^- removal caused a marked pH_i elevation. We found that the classic and defining inhibitor of SLC4 family AE1-AE4,[76, 77] H_2DIDS, strongly inhibited the Cl^- dependent HCO_3^- efflux mechanism. AE1 has been identified in rat lacrimal ducts.[21] However, no other AEs have been confirmed in lacrimal ductal epithelium so far. In addition, we also tested whether the isolated and cultured ducts are suitable to study the regulation of LGDC secretion. Regulation of lacrimal gland secretion can be mediated by neurotransmitters (e.g. Ach) and growth factors (e.g. endothelial growth factor family).[78] Activation of muscarinic receptors by Ach released from parasympathetic nerves stimulates lacrimal gland secretion. The glandular subtype of M3 muscarinic receptors have been identified in the lacrimal gland.[79] It is more than likely that the ductal epithelia are involved in the hypersecretory effect of parasympathetic stimulation. In our study we tested the effect of carbachol on the intracellular Ca^{2+} signaling using the Ca^{2+} sensitive fluorescence dye FURA2-AM. Our results showed that carbachol dose dependently increased $[Ca^{2+}]_i$. Finally, we investigated the effects of parasympathetic stimulation on the acid/base transporters of LGDC. We found that carbachol strongly stimulates NHE activity, therefore drives Na^+ into the cell. This stimulation is followed by the activation of the AE on the basolateral membrane, which drives Cl^- into the LGDC. The Na^+ and Cl^- influx needs available H^+ and HCO_3^- inside the cell, which can come

after the dehydration of carbonic acid (H_2CO_3) by carbonic anhydrase.[80] The stimulatory effects of carbachol on NHE and AE have been shown in the lacrimal acinar cells [81, 82] indicating that there must be other differences in ion transport mechanisms on the basolateral membranes between the acinar cells and LGDC. Importantly, expression of Na^+/K^+ ATPase is three to five times higher on duct cells compared to acinar cells [83]. Therefore, the elevated intracellular Na^+ concentration after a parasympathetic activation may stimulate the basolateral Na^+/K^+ ATPase which will increase the intracellular K^+ concentration in LGDC. Our data suggests that the Na^+/K^+ ATPase may be a crucial basolateral transporter in the mechanisms of K^+ secretion in LGDC. Following the intracellular accumulation of K^+ and Cl^-, these ions can be secreted via a coupled mechanism (K^+ /Cl^- cotransporter)[21] and/or via a separate K^+ selective cation channel ($IK_{Ca}1$ and/or BK_{Ca}) and a Cl^- selective anion channel (CFTR and/or calcium-activated chloride channel CACC, Fig. 20).Taken together, we described a lacrimal gland duct isolation technique, in which the intact ducts remain viable and in which the role of duct cells in the pre-ocular tear film secretion can be characterized. In addition we added new insights into the regulation of lacrimal gland ductal secretion. Our data and new isolation method open up the possibility to understand the physiological and pathophysiological (such as dry eye syndrome or keratoconjuctivitis sicca) roles of the lacrimal gland ductal system. Furthermore, our results may lead to the development of drugs that stimulate preocular tear secretion in patients with dry eye syndrome.

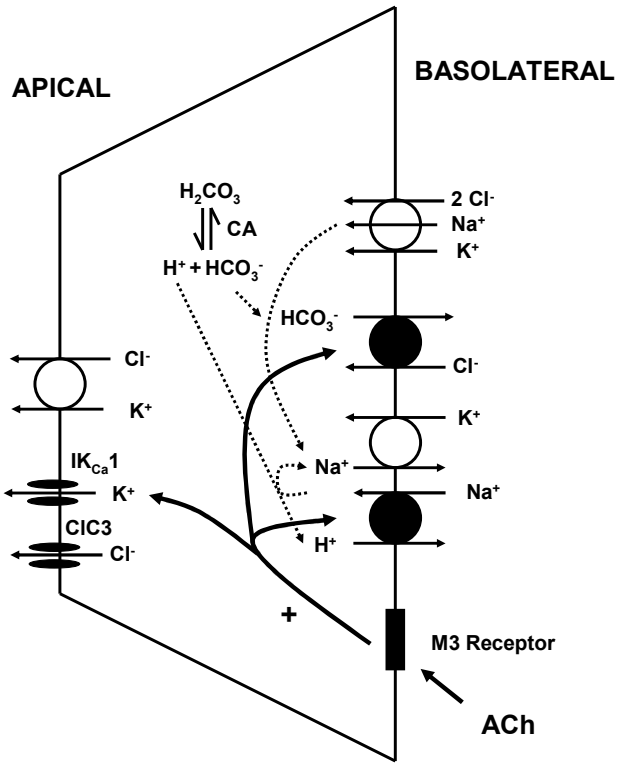

Figure 20. Model for secretion of K^+ and Cl^- by lacrimal gland ductal cells (LGDC). The model is based on the channels and transporters identified by Ubels et al.[11] and the functionally active acid/base transporters characterized in this study. Parasympathomimetic stimulation by carbachol strongly stimulate the NHE activity followed by the activation of AE on the basolateral membrane via Ca^{2+} signaling , which drive Na^+ and Cl^- into the LGDC. The Cl^- and Na^+ influx requires available H^+ and HCO_3^- inside the cell, generated from the dehydration of carbonic acid (H_2CO_3) by carbonic anhydrase[32]. The elevated intracellular Na^+ concentration can be exchanged for K^+ via the basolateral Na^+/K^+ ATPase which will increase the intracellular K^+ concentration in LGDC. The elevated intracellular Ca^{2+} concentration can also activate the $IK_{Ca}1$. CA: carbonic anhydrase, Ach: acetylcholine, ClC: chloride channel, $IK_{Ca}1$: calcium activated potassium channel.

In the second part of this thesis we utilized *in vitro* and *in vivo* experimental pancreatitis models, in which we investigated the protective role of hypersecretion and HSP72 in the course of acute pancreatitis. We also investigated the IκB-α level to monitor the severity of the pancreatitis.

Acute pancreatitis is a common disorder that results from acute inflamatory injury of the pancreas. The pathogenesis of acute pancreatitis is not fully understood, however, a number of conditions are known to induce this disease. One of the most common etiologic factors is the ampullary obstruction resulting in bile reflux into the pancreatic ductal system. Very little is known about the role of pancreatic ductal epithelium in acute pancreatitis, however, some recent studies have suggested that HCO_3^- and fluid secretion by pancreatic ductal cells may represent a defence mechanism against toxic factors that can induce pancreatitis.[30, 44] Since in previous studies it has been shown that bile acids stimulate secretion from different epithelia,[84-87] we investigated the secretory effect of bile acids on PPDC.

First we investigated the effects of bile acids on pH_i. We chose to use the unconjugated and conjugated forms of CDC for this investigation since the majority (62%) of guinea pig bile acids is CDC[88] and the human gallbladder bile also contains this bile acid in high concentrations.[89] We could only estimate the concentration of bile acid that can reach the small interlobular ducts during acute biliary pancreatitis. In our experiments we used 0.1 mM as a low dose and 1 mM as a high dose of bile acids. We found that basolateral or luminal administration of CDC dose-dependently and reversibly reduced the pH_i of duct cells. However, the conjugated GCDC had a significantly smaller effect than the unconjugated CDC and notably, low concentrations of GCDC had only a very small effect on pH_i when it was administered from the luminal side. Alvaro et al. reported that 0.5 – 1.5 mM ursodeoxycholate caused a dose-dependent rapid, intracellular acidification in bile duct epithelial cells.[90] In addition, the conjugated form of this bile acid (tauroursodeoxycholate) at 1 mM concentration had no effect on pH_i.[90] These results are in accordance with the diffusion characteristics of bile acids. Unconjugated bile salts are weak acids and they can traverse cell membranes by passive diffusion.[91] However, taurine or glycine conjugated bile acids are impermeable to cell membranes due to their lipid insolubility and require active transport mechanisms for cellular uptake.[92] Recently, an increasing number of bile acid transporters have been cloned and localized to either the luminal or basolateral membranes of polarized epithelial cells.[91, 93, 94] Basolateral administration of 1 mM CDC for 6-8 minutes damaged the membrane integrity and PPDC lost BCECF very quickly. The same concentration of CDC had no toxic effects on

the luminal membrane, however, a higher (2 mM) concentration of CDC also damaged the luminal membrane (unpublished data). In accordance with our findings, Okolo et al.[40] also found differences between the effects of bile acids on the luminal and basolateral membranes. The basolateral membrane was much more sensitive to bile acid-induced damage (transepithelial membrane resistance decreased much more when bile acids were administered from the basolateral side) than the luminal membrane.

We next investigated the effects of bile acids on the acid/base transporters of PPDC. A high concentration of CDC strongly inhibited the NHE, NBC and AE of PPDC. This observation indicates a possible toxic effect of high doses of CDC on the activity of the acid/base transport system which was also suggested by. Alvaro et al.[90] Using 1.5 mM ursodeoxycholate, spontaneous pH_i recovery did not occur during the administration of this bile acid; however, this finding was not further investigated using the NH_4Cl pulse technique.[90] Lower doses of ursodeoxycholate (0.5 mM) had no effect on the recovery from acid load in bile duct epithelial cells,[90] which is in accordance with our results. Importantly, luminal administration of low doses of CDC significantly stimulated HCO_3^- efflux i.e. secretion from PPDC. It has been shown that bile acids modulate AE and CFTR in different epithelia.[95-99] Low doses (20 µM) of taurocholic and taurolithocholic acid augmented the stimulatory effect of secretin on HCO_3^- secretion in cholangiocytes.[95, 96] Strazzabosco et al. also suggested that ursodeoxycholate stimulates HCO_3^- secretion in bile by a weak acid effect.[97] Luminal administration of 0.5 mM taurocholate has been shown to stimulate a CFTR dependent electrogenic Cl^- transport in the murine distal ileum.[99] Exposure of gastroduodenal mucosa to high concentrations of taurocholic acid was also shown to stimulate HCO_3^- secretion and therefore, can play a physiological role in the mucosal protective mechanisms.[98] In this study, we showed that low doses of CDC selectively act on the luminal membrane to stimulate HCO_3^- secretion. Inhibition of basolateral AE and NBC by H_2DIDS and NHE by amiloride had no effect on the secretory response to CDC. However, luminal administration of H_2DIDS totally blocked the stimulated HCO_3^- efflux. Three main anion transporters/channels have been identified on the luminal membrane of PPDC namely the CFTR chloride channel, the calcium-activated chloride channel (CACC) and two members of the SLC26 family (A3 and A6) anion exchangers. Since CFTR is unaffected by H_2DIDS,[100] it is unlikely to be involved in the stimulatory mechanism of CDC. Taurodeoxycholate was reported to activate a chloride conductance via IP_3-mediated Ca^{2+} signaling in the T84 colonic cell line[84] and in cultured PDEC.[40] Since SLC26A3 is only weakly inhibited by the disulphonic stilbene,[101, 102] the putative anion exchanger SLC26A6

and/or the CACC are the most likely candidates for the target of CDC.[102, 103] Most CACC are inhibited by DIDS, although human CACC in the HPAF cell line is not.[104] Finally, we provided evidence that the stimulatory effect of low doses of luminal CDC on HCO_3^- secretion is dependent on an elevation of $[Ca^{2+}]_i$. BAPTA-AM (40μM) slightly inhibited basal HCO_3^- secretion measured using the ammonium pulse method. In an earlier study, a lower concentration of BAPTA-AM (10 μM) had no effect on fluid secretion by guinea pig pancreatic duct cells,[105] suggesting a dose-dependent effect of this calcium chelator. Importantly, BAPTA-AM (40μM) totally blocked the stimulatory effect of low doses of CDC showing that this effect is Ca^{2+} dependent. However, BAPTA-AM had no effect on the inhibitory action of high doses of basolateral CDC on HCO_3^- secretion indicating that a Ca^{2+} independent mechanism is responsible for this effect. Our results suggest that the pancreatic ductal epithelium is remarkably resistant to attack by the conjugated bile salt GCDC, which is the major bile salt in the guinea pig's gall bladder. Whilst GCDC decreased pH_i and elevated $[Ca^{2+}]_i$ it had no detectable effect on HCO_3^- secretion. In contrast, the unconjugated CDC caused marked changes in pH_i and $[Ca^{2+}]_i$ and, depending on the dose, either stimulated or inhibited HCO_3^- secretion. Although, it has been shown that the triggering mechanisms of intracellular protease activation do not require bile influx into the pancreatic ductal tree,[106-108] a flow of bile into the pancreatic ductal system may occur after the first 24 to 48 h.[109, 110] Theoretically, when small stones obstruct the pancreatic duct and the 'common channel' is formed,[111] by the pancreatic and bile duct, bile acids start diffusing up into the ductal tree and reach the interlobular ducts in a low concentration, ductal cells may try to wash out the toxic acids and thus defend the acinar cells. The subsequent bile acid-induced stimulated HCO_3^- and fluid secretion may protect the pancreas in different ways. Firstly, the elevated luminal pressure stops or delays the bile acid diffusion towards the acinar tissue. Importantly, the higher ductal pressure may push the small stones through the papilla and open the way for the pancreatic and bile fluid. However, if this defense mechanism is not sufficient and the bile concentration rises further, thus leading to damage the epithelial barrier, the secretory mechanisms of pancreatic ductal cells are blocked and the ducts can no longer act as a defensive wall against the toxic bile. On the other hand, high concentrations of bile acids reaching the pancreatic ductal cells from the basolateral side (either from the blood and/or from the lumen due to the damage of the ductal barrier) inhibit HCO_3^- and fluid secretion, therefore, may contribute to the progression of acute pancreatitis. We postulate that these contrasting effects of bile acids may have an important role in the pathogenesis of bile-induced pancreatitis.

Another non-alcoholic etiologic factor which may play role during acute pancreatitis is hyperlipidemia. A hyperlipidemia prevalence of 12-38% has been reported in acute human pancreatitis in previous studies.[112-114] Even though a few animal studies have been published in this topic, the results are fairly contradictory, [115-118] therefore, the role of hyperlipidemia in acute pancreatitis is still debated. Hyperlipidemia has been shown to attenuate heat shock protein expression in the heart.[47] Although, it was not known whether hyperlipidemia leads to a decreased heat shock response in the pancreas, it was tempting to speculate that this mechanism is involved in the increased severity of pancreatitis in hyperlipidemia. Accordingly, we measured the pancreatic HSP72 production. Pancreatic HSP72 was induced by acute necrotizing pancreatitis using high doses of Arg[119] in animals on the high-cholesterol diet and in others on the normal diet. We found that the expression of HSP72 did not differ between the two groups. In addition we determined the pancreatic IκB-α levels and found that IκB-α expression was unaltered by cholesterol treatment. However, in the rats with acute necrotizing pancreatitis the high-cholesterol diet significantly decreased the expression of IκB-α as compared those receiving the normal diet.

In summary, we tried to provide a better insight into epithelial cell physiology under normal and pathophysiological conditions. Our results may represent a possible aid in the treatment of different diseases by contributing to the better understanding of epithelial cell function.

5. ACKNOWLEDGEMENTS

I would like to thank all of the people who have helped and inspired me during my doctoral study.

I am grateful to **Prof. Dr. János Lonovics** and **Prof. Dr. Tibor Wittman** past and present head of the First Department of Medicine, who gave me the opportunity to work in the department.

My warm thanks are due to **Prof. Tamás Takács**, who provided me the opportunity to start my Ph.D. in his scientific team. I am indeed grateful for his valuable advice and help.

I would like to express my deep and sincere gratitude to my supervisors **Dr. Péter Hegyi** and **Dr. Zoltán Rakonczay Jr.** Their wide knowledge and their logical way of thinking have been of great value for me. Their understanding and encouragement provided a good basis for the present thesis.

I wish to thank **Prof. Barry E. Argent** and **Dr. Mike A. Gray,** our collaborators from the University of Newcastle, UK for their extensive discussions of my work and interesting explorations.

I would also like to thank my colleagues and friends, **Béla Ózsvári**, **Imre Ignáth**, **József Maléth** and **Lajos Nagy** for all the emotional support, entertainment, and care they provided.

This work would not have been possible to accomplish without the assistance of **Zoltánné Fuksz**, **Edit Magyarné Pálfi**, **Ágnes Sitkei, Miklósné Árva**.

We are grateful to **Prof. András Varró**, the Head of Department of Pharmacology and Pharmacotherapy, who provided us the opportunity to work in his department .

This work was supported by Hungarian Scientific Research Fund grants to J.L. (T43066) and to Z.R. (PF6395), Bolyai Postdoctoral Fellowships to P.H. (00276/04) and to Z.R. (00218/06),

KPI Research Grant to A.V. (KPI/BIO-37), Joint International Grant (HAS and the Royal Society) to P.H and M.A.G, Asboth Grant to J.L. (XTPPSRT1), Hungarian Medical Research Council grant to J.L. (517/2006), and The Physiological Society Junior Fellowship to Z.R..

My deepest gratitude goes to **my family** for their unflagging love and support throughout my life; this dissertation would have been impossible to accomplish without their help. I dedicate this thesis to them.

6. REFERENCES

1. Argent BE, Gray MA. Regulation and formation of fluid and electrolyte secretions by pancreatic ductal epithelium. In:*Biliary and Pancreatic Ductal Epithelia. Pathobiology and Pathophysiology*, edited by Sirica AE and Longnecker DS. NewYork: Dekker, 1997, p. 349–377.

2. Bartle HJ, Harkins MJ. The gastric secretion: its bactericidalvalue to man. *Amer J Med Sci* 1925;**169**:373-388.

3. Gianella RA, Broitman SA, Zamcheck N. Gastric acid barrier to ingested microorganisms in man: Studies in vivo and in vitro. *Gut* 1972;**13**:251-256.

4. Bockman D. Anatomy and fine structure. In: Beger HG, Buchler M, Kozarek R, eds. *The Pancreas: An Integrated Textbook of Basic Science, Medicine and Surgery*. 2008. *In press*.

5. Martin CL, Munnell J, Kaswan R. Normal ultrastructure and histochemical characteristics of canine lacrimal glands. *Am J Vet Res* 1988;**49**:1566-72.

6. Millar TJ, Herok G, Koutavas H, et al. Immunohistochemical and histochemical characterisation of epithelial cells of rabbit lacrimal glands in tissue sections and cell cultures. *Tissue Cell* 1996;**28**:301-12.

7. M. Cereijido, RG Contreras, MR Garcia, et al. Epithelial polarity. In: NK Wills, L Reuss and SA Lewis, eds. Epithelial transport: *A guide to Methods and Experimental Analysis*. 1996.

8. Beltinger J, Hildebrand P, Drewe J, et al. Effect of spiroglumide, a gastrin receptor antagonist, on acid secretion in humans. *Eur J Clin Invest* 1999;**29**:153-59.

9. Kovacs TO, Walsch JH, Maxwell J, et al. Gastrin is a major regulator of the gastric of acid secretion in dogs: proof by monoclonal antibody neutralization. *Gastroenterology* 1989;**97**:1406-13.

10. Hersey SJ, Sachs G. Gastric acid secretion. *Physiol Rev* 1995;**75**:155-89.

11. Soll AH. The interaction of histamine with gastrin and carbamylcholine on oxygen uptake by isolated mammalian parietal cells. *J Clin Invest* 1978;**61**:381-9.

12. Black JW, Shankley NP. How does gastrin act on stimulate oxyntic cell secretion. *TIPS* 1987;**8**:486-90.

13. Koh TJ, Goldenring JR, Ito S, et al. Gastrin deficiency results in altered gastric differentiation and decreased colonic proliferation in mice. *Gastroenterology* 1997;**113**:1015-25.

14. Friis-Hansen L, Sundler F, Li Y, et al. Impaired gastric acid secretion in gastrin-deficient mice. *Am J Physiol* 1998;**274**:G561-8.

15. Chen D, Zao CM, Dockray GJ, et al. Glycine-extended gastrin synergizes with gastrin 17 to stimulate acid secretion in gastrin-deficient mice. *Gastroenterology* 2000;**119**:756-65.

16. Hemady R, Chu W, Foster CS. Keratoconjunctivitis sicca and corneal ulcers. *Cornea* 1990;**9**:170-3.

17. Golubovic S, Parunovic A. Corneal perforation in dry eye patients. *Fortschr Ophthalmol* 1987;**84**:33-7.

18. Rios JD, Ferdman D, Tepavcevic V, et al. Role of Ca^{2+} and protein kinase C in cholinergic, and alpha1-adrenergic agonists and EGF stimulated mitogen-activated protein kinase activity in lacrimal gland. *Adv Exp Med Biol* 2002;**506**:185-90.

19. Walcott B, Birzgalis A, Moore LC, et al. Fluid secretion and the Na^{+}-K^{+}-$2Cl^{-}$cotransporter in mouse exorbital lacrimal gland. *Am J Physiol Cell Physiol.* 2005;289:C860-7.

20. Saito Y, and Kuwahara S. Effect of acetylcholine on the membrane conductance of the intralobular duct cells of the rat exorbital lacrimal gland. *Adv Exp Med Biol* 1994;**350**:87-92.

21. Ubels JL, Hoffman HM, Srikanth S, et al. Gene expression in rat lacrimal gland duct cells collected using laser capture microdissection: evidence for K^{+} secretion by duct cells. *Invest Ophthalmol Vis Sci* 2006;**47**:1876-85.

22. Dobosz M, Hac S, Mionskowska L, et al. Organ Microcirculatory Disturbances in Experimental Acute Pancreatitis. A Role of Nitric Oxide. *Physiol Res* 2005;**54**:363-8.

23. Warzecha Z, Dembiñski A, Ceranowicz P, et al. Deleterious effect of Helicobacter pylori infection on the course of acute pancreatitis in rats. *Pancreatology* 2002;**2**:386-95.

24. Case RM, Hotz J, Hutson D, et al. Electrolyte secretion by the isolated cat pancreas during replacement of extracellular bicarbonate by organic anions and chloride by inorganic anions. *Journal of Physiology* 1979;**286**,563-76.

25. Noviak I, Greger R. Properties of the luminal membrane of isolated perfused rat pancreatic ducts: effect of cyclic AMP and blockers of chloride transport. *Pfluigers Archiv* 1988;**411**:546-53.

26. Zhao H, Star RA, Muallem S. A Membrane localization of H^{+} and HCO_3^{-} transporters in the rat pancreatic duct. *Journal of General Physiology* 1994;**104**:57-85.

27. Sewell WA, Young JA. Secretion of electrolytes by the pancreas of the anaestlhetized rat. Journtal of Physiology 1975;**252**:379-96.

28. Yamamoto A, Ishiguro H, Ko SBH, et al. Ethanol induces fluid hypersecretion from guinea-pig pancreatic duct cells. *J Physiol* 2003;**551.3**:917-26.

29. Yamamoto M, Shirohara H, Otsuki M. CCK-, secretin-, and cholinergic-independent pancreatic fluid hypersecretion in protease inhibitor-treated rats *Am J Physiol Gastrointest Liver Physiol* 1998;**274**: G406-12.

30. Hegyi P, Ördögh B, Rakonczai Z, et al. Effect of herpesvirus infection on pancreatic duct cell secretion. *World J Gastroenterol* 2006;**11**:5997-6002.

31. Opie EL. The etiology of acute haemorrhagic pancreatitis. *Johns Hopkins Hospital Bulletin* 1901;**12**:182-8.

32. Niederau C, Niedereu M, Luthen R, et al. Pancreatic exocrine secretion in acute experimental pancreatitis. *Gastroenterology* 1990;**99**:1120-7.

33. Senninger N. Bile-induced pancreatitis. *Eur Surg Res* 1992;**24**:68-73.

34. Pandol SJ, Saluja AK, Imrie CW, et al. Acute pancreatitis bench to the bedside. *Gastroenterology* 2007;**132**:1127-51.

35. Voronina S, Longbotton R, Sutton R, et al. Bile acids induce calcium signals in mouse pancreatic acinar cells: implications for bile-induced pancreatic pathology. *J Physiol* 2002;**540**:49-55.

36. Fischer L, Gukovskaya AS, Penninger JM, et al. Phosphatidylinositol 3-kinase facilitates bile acid-induced Ca^{2+} responses in pancreatic acinar cells. *Am J Physiol Gastrointest Liver Physiol* 2007;**292**:G875-86.

37. Raraty M, Ward J, Erdemli G, et al. Calcium-dependent enzyme activation and vacuole formation in the apical granular region of pancreatic acinar cells. *Proc Natl Acad Sci USA* 2000;**97**:13126-31.

38. Kim JY, Kim KH, Lee JA, et al. Transporter-mediated bile acid uptake causes Ca^{2+}-dependent cell death in rat pancreatic acinar cells. *Gastroenterology* 2002;**122**:1941-53.

39. Farmer RC, Tweedie J, Maslin S, et al. Effects of bile salts on permeability and morphology of main pancreatic duct in cats. *Dig Dis Sci* 1984;**29**:740-51.

40. Okolo C, Wong T, Moody MW, et al. Effect of bile acids on dog pancreatic duct epithelial cell secretion and monolayer resistance. *Am J Physiol Gastrointest Liver Physiol* 2002;**283**:G1042-50.

41. Reber HA, Mosley JG. The effect of bile salt on the pancreatic duct mucosal barrier. *Br J Surg* 1980;**67**:59-62.

42. Hegyi P, Rakonczay Z Jr, Tiszlavicz A, et al. SLC26 transporters and the inhibitory control of pancreatic ductal bicarbonate secretion. In: Novartis symposia series, Novartis Found Symp. No. 273. John Wiley & Sons, London 2006; 73:164-73; discussion 173-6, 261-4.

43. Hegyi P, Rakonczay Z Jr. The inhibitory pathways of pancreatic ductal bicarbonate secretion. *Intl J Biochem Cell Biol* 2007;**39**:25-30.

44. Czako L, Yamamoto M, Otsuki M. Exocrine pancreatic function in rats after acute pancreatitis. *Pancreas* 1997;**15**:83-90.

45. Argent BE, Case RM. Pancreatic ducts. Cellular mechanism and control of bicarbonate secretion. In: Physiology of the Gastrointestinal Tract. New York: Raven Press 1994:1473-97.

46. Dominguez-Munoz JE, Malfertheiner P, Ditschuneit HH, et al. Hyperlipidemia in acutepancreatitis. Relationship with etiology, onset, and severity of the disease. *Int J Pancreatol* 1991;**10**:261–7.

47. Csont T, Balogh G, Csonka C, et al. Hyperlipidemia induced by high cholesterol diet inhibits heat shock response in rat hearts. *Biochem Biophys Res Commun* 2002;**290**:1535-38.

48. Wilson SH, Caplice NM, Simari RD et al. Activated nuclear factor-kappa B is present in thecoronary vasculature in experimental hypercholesterolemia. *Atherosclerosis* 2000;**148**:23–30.

49. Rakonczay Jr Z, Jármay K, Kaszaki J, et al. NF-κB activation is detrimental in arginine-induced acute pancreatitis.*Free Radic Biol Med* 2003;**34**:696-709.

50. Rakonczay Jr Z, Takács T, Boros I, et al. Heat shock proteins and the pancreas. *J Cell Physiol* 2003;**195**:383-91.

51. Verma IM. Nuclear factor (NF)-kB proteins: therapeutic targets. *Ann Rheum Dis* 2004;**63**:57–61.

52. Hegyi P, Rakonczay Z Jr, Sari R et al. L-arginine induced experimental pancreatitis. Review. *World J Gastroenterol* 2004;**10**:2003-9.

53. Hegyi P, Takacs T, Jarmay K, et al. Spontaneous and cholecystokinin-octapeptide-promoted regeneration of the pancreas following L-arginine-induced pancreatitis in rat. *Int J Pancreatol* 1997;**22**:193-200.

54. Czakó L, Takács T, Varga IS, et al. Involvement of oxygen-derived free radicals in L-arginine-induced acute pancreatitis. *Dig Dis Sci* 1998;**43**:1770-7.

55. Hegyi P, Rakonczay Z Jr, Sari R, et al. Insulin is necessary for the hypertrophic effect of CCK-8 following acute necrotizing experimental pancreatitis. *World J Gastroenterol* 2004; **10**:2275-7.

56. Hegyi P, Czako L, Takacs T, et al. Pancreatic secretory responses in L-arginine-induced pancreatitis: comparison of diabetic and nondiabetic rats. *Pancreas* 1999;**19**:167-74.

57. Berglindh T, Obrink KJ. A method for preparing isolated glands from the rabbit gastric mucosa. *Acta Physiol Scand* 1976;**96**:150-9

58. Booth C, Patel S, Bennion GR, et al. The isolation and culture of adult mouse colonic epithelium. *Epithelial Cell Biol* 1995;**4**:76-86.

59. Argent BE, Arkle S, Cullen MJ, et al. Morphological, biochemical and secretory studies on rat pancreatic ducts maintained in tissue culture. *Q J Exp Physiol* 1986;**71**:633-48.

60. Hegyi P, Rakonczay Z Jr, Gray MA, et al. Measurement of intracellular pH in pancreatic duct cells. A new method to calibrating the fluorescence data. *Pancreas* 2004;**28**:427-34.

61. Thomas JA, Buchsbaum RN, Zimniak A, et al. Intracellular pH-measurements in Ehrlich ascites tumor cells utilizing spectroscopic probes generated in situ. *Biochemistry* 1979;**18**:2210-18.

62. Ishiguro H, Steward MC, Lindsay ARG, et al. Accumulation of intracellular HCO_3^- by Na^+- HCO_3^- cotransport in interlobular ducts from guinea-pig pancreas. *J Physiol* 1996;**495**:169-78.

63. Hegyi P, Gray MA, Argent BE. Substance P inhibits bicarbonate secretion from guinea-pig pancreatic ducts by modulating an anion exchanger. *Am J Physiol Cell Physiol* 2003;**285**:C268-76.

64. Szalmay G, Varga G, Kajiyama F, et al. Bicarbonate and fluid secretion by cholecystokinin, bombesin and acetylcholine in isolated guinea-pig pancreatic ducts. *J Physiol* 2001;**535**:795-807.

65. Weintraub WH, Machen TE. pH regulation in hepatoma cells: roles for Na-H exchange, Cl-HCO_3 exchange, and Na-HCO_3 cotransport. *Am J Physiol Gastrointest Liver Physiol* 1989;**257**:G317-27.

66. Giricz Z, Csonka C, Onody A et al. Role of cholesterol-enriched diet and the mevalonate pathway in cardiac nitric oxide synthesis. *Basic Res Cardiol* 2003;**98**:304–10.

67. Hodges RR, Dartt DA. Regulatory pathways in lacrimal gland epithelium. *Int Rev Cytol*. 2003;**231**:129-96.

68. Hegyi P, Rakonczay Z Jr, Tiszlavicz L, et al. Protein kinase C mediates the inhibitory effect of substance P on bicarbonate secretion from guinea pig pancreatic ducts. *Am J Physiol Cell Physiol* 2005;**288**:C1030-41.

69. Botelho SY, Martinez EV. Electrolytes in lacrimal gland fluid and in tears at various flow rates in the rabbit. *Am J Physiol* 1973;**225**:606-9.

70. Alexander JH, van Lennep EW, Young JA. Water and electrolyte secretion by the exorbital lacrimal gland of the rat studied by micropuncture and catheterization techniques. *Pflugers Arch* 1972;**337**:299-309.

71. Walcott B, Birzgalis A, Moore LC, et al. Fluid secretion and the Na^+-K^+-$2Cl^-$ cotransporter in mouse exorbital lacrimal gland. *Am J Physiol Cell Physiol* 2005;**289**:C860-7.

72. Koyama K, Sasaki I, Naito H, et al. Induction of epithelial Na^+ channel in rat ileum after proctocolectomy. *Am J Physiol* 1999;**276**:G975-84.

73. Romero JR, Rivera A, Lanca V, et al. Na^+/Ca^{2+} exchanger activity modulates connective tissue growth factor mRNA expression in transforming growth factor beta1- and Des-Arg10-kallidin-stimulated myofibroblasts. *J Biol Chem* 2005;**15**;280:14378-84.

74. Kiela PR, Ghishan FK. Na^+-H^+ exchange in mammalian digestive tract. *Physiology of the gastrointestinal tract*. 4th ed. Edited by Johnson LR., USA, Elsevier Academic Press; 2006:1847-81.

75. Soleimani M, Burnham CE. Na^+:$HCO(_3^-)$ cotransporters (NBC): cloning and characterization. *J Membr Biol* 2001;**183**:71-84.

76. Alper SL. The band 3-related anion exchanger (AE) gene family. *Annu Rev Physiol* 1991;**53**:549-64.

77. Ko SB, Luo X, Hager H, et al. AE4 is a DIDS-sensitive Cl^-/HCO_3^- exchanger in the basolateral membrane of the renal CCD and the SMG duct. *Am J Physiol Cell Physiol* 2002;**283**:C1206-18.

78. Dartt DA. Regulation of lacrimal gland secretion by neurotransmitters and the EGF family of growth factors. *Exp Eye Res* 2001;**73**:741-52.

79. Mauduit P, Jammes H, Rossignol B. M3 muscarinic acetylcholine receptor coupling to PLC in rat exorbital lacrimal acinar cells. *Am J Physiol Cell Physiol* 1993;**264**:C1550-60.

80. Ogawa Y, Toyosawa S, Inagaki T, et al. Carbonic anhydrase isozyme VI in rat lacrimal gland. *Histochem Cell Biol* 1995;**103**:387-94.

81. Lambert RW, Maves CA, Mircheff AK. Carbachol-induced increase of Na+/H+ antiport and recruitment of Na^+,K^+-ATPase in rabbit lacrimal acini. *Curr Eye Res* 1993;**12**:539-51.

82. Lambert RW, Bradley ME, Mircheff AK. pH-sensitive anion exchanger in rat lacrimal acinar cells. *Am J Physiol* 1991;**260**:G517-23.

83. Okami T, Yamamoto A, Takada T. Ultrastructural localization of Na^+,K^+-ATPase in the exorbital lacrimal gland of rat. *Invest Ophthalmol Vis Sci* 1992;**33**:196–204.

84. Devor DC, Sekar MC, Frizzell RA, et al. Taurodeoxycholate activates potassium and chloride conductances via an IP3-mediated release of calcium from intracellular stores in a colonic cell line (T84). *J Clin Invest* 1993;**92**:2173–81.

85. Dharmsathaphorn K, Huott PA, Vongkovit P, et al. Cl^- secretion induced by bile salts. A study of the mechanism of action based on a cultured colonic epithelial cell line. *J Clin Invest* 1989;**84**: 945–53.

86. Freel RW. Dihydroxy bile salt-induced secretion of rubidium ion across the rabbit distal colon. *Am J Physiol Gastrointest Liver Physiol* 1987;**252**:G554–61.

87. Freel RW, Hatch M, Earnest DL, et al. Dihydroxy bile salt-induced alterations in NaCl transport across the rabbit colon. *Am J Physiol Gastrointest Liver Physiol* 1983;245: G808–G815.

88. Ting GS, Xu GR, Batta AK, et al. Ursodeoxycholic acid, chenodeoxycholic acid, and 7-ketolithocholic acid are primary bile acids of the guinea pig. *J Lipid Res* 1990;31:1301-6.

89. Berr F, Stellaard F, Pratschke E, et al. Effects of cholecystectomy on the kinetics of primary and secondary bile acids. *J Clin Invest* 1989;**83**:1541-50.

90. Alvaro D, Mennone A, Boyer JL. Effect of ursodeoxcholic acid on intracellular pH regulation in isolated rat bile duct epithelial cells. *Am J Physiol Gastrointest Liver Physiol* 1993;**28**:G783-91.

91. Trauner M., Boyer JL. Bile salt transporters: Molecular characterization, function, and regulation. *Physiol Rev* 2003;**83**:633-71.

92. Meier PJ. Molecular mechanisms of hepatic bile salt transport from sinusoidal blood into bile. *Am J Physiol Gastrointest Liver Physiol* 1995;**269**:G801-12.

93. Hagenbuch B, Stieger B, Foguet M, et al. Functional expression cloning and characterization of the hepatocyte Na-bile acid cotransport system. *Proc Natl Acad Sci USA* 1991;**88**:10629-33.

94. Lazaridis KN, Pham L, Tietz P, et al. Rat cholangiocytes absorb bile acids at their apical domain via the ileal sodium-dependent bile acid transporter. *J Clin Invest* 1997;**100**:2714-21.

95. Alpini G, Glaser S, Robertson W, et al. Bile acids stimulate proliferative and secretory events in large bur not small cholangiocytes. *Am J Physiol Gastrointest Liver Physiol* 1997;**36**:G518-29.

96. Alpini G, Glaser S, Ueno Y, et al. Bile acid feeding induces cholangiocyte proliferation and secretion: evidence for bile acid-regulated ductal secretion. *Gastroenterology* 1999;**116**:179-86.

97. Strazzabosco M, Sakisaka S, Hayakawa T, et al. Effect of UDCA on intracellular and biliary pH in isolated rat hepatocyte couplets and perfused livers. *Am J Physiol Gastrointest Liver Physiol* 1991;**26**:G58-69.

98. Konturek SJ, Bilski J, Tasler J, et al. Gastroduodenal alkaline response to acid and taurocholate in conscious dogs. *Am J Physiol Gastrointest Liver Physiol* 1984;**247**:G149-54.

99. Bijvelds MJ, Jorna H, Verkade HJ, et al. Activation of CFTR by ASBT-mediated bile salt absorption. *Am J Physiol Gastrointest Liver Physiol* 2005;**289**:G870-9.

100. Paradiso AM, Ribeiro CMP, Boucher RC. Polarized signaling via purinoceptors in normal and cystic fibrosis airway epithelia. *J Gen Physiol* 2001;**117**:53-68.

101. Chernova MN, Jiang LW, Shmukler BE, et al. Acute regulation of the SLC26A3 congenital chloride diarrhoea anion exchanger (DRA) expressed in Xenopus oocytes. *J Physiol* 2003;**549**:3-19.

102. Ko SBH, Shcheynikov N, Choi JY, et al. A molecular mechanism for aberrant CFTR-dependent HCO3- transport in cystic fibrosis. *EMBO J* 2002;**21**:5662-72.

103. Wang Z, Petrovic S, Mann E, et al. Identification of an apical Cl^-/HCO_3^- exchanger in the small intestine. *Am J Physiol Gastrointest Liver Physiol* 2002;**282**:G573-9.

104. Winpenny JP, Harris A, Hollingsworth MA, et al. Calcium-activated chloride conductance in a pancreatic adenocarcinoma cell line of ductal origin (HPAF) and in freshly isolated human pancreatic duct cells. *Pflügers Arch-Eur J Physiol* 1998;**435**:796-803.

105. Yamamoto A, Ishiguro H, Shigeru BHK, et al. Ethanol induces fluid hypersecretion from guinea-pig panceatic duct cells. *J Physiol* 2003;**551**:917-26.

106. DiMagno EP, Shorter RG, Taylor WF, et al. Relationships between pancreaticobiliary ductal anatomy and pancreatic ductal and parenchymal histology. *Cancer* 1982;**49**:361-8.

107. Lerch MM, Hernandez CA, Adler G. Gallstones and acute pancreatitis--mechanisms and mechanics. *Dig Dis Sci* 1994;**12**:242-7.

108. Lerch MM, Weidenbach H, Hernandez CA, et al. Pancreatic outflow obstruction as the critical event for human gall stone induced pancreatitis. *Gut* 1994;**35**:1501-3.

109. Lerch MM, Saluja AK, Dawra R, et al. Acute necrotizing pancreatitis in the opossum: earliest morphological changes involve acinar cells. *Gastroenterology* 1992;**103**:205-13.

110. Lerch MM, Saluja AK, Runzi M, et al. Pancreatic duct obstruction triggers acute necrotizing pancreatitis in the opossum. *Gastroenterology* 1993;**104**:853-61.

111. Lerch MM. Clinical Course and Treatment Principles of Biliary Acute Pancreatitis. In: Beger HG, Buchler M, Kozarek R, eds. *The Pancreas: An Integrated Textbook of Basic Science, Medicine and Surgery*. 2008. *In press*.

112. Dominguez-Munoz JE, Malfertheiner P, Ditschuneit HH, et al. Hyperlipidemia in acute pancreatitis. Relationship with etiology, onset, and severity of the disease. *Int J Pancreatol* 1991;**10**:261-67.

113. Toskes PP.Hyperlipidemic pancreatitis. *Gastroenterol Clin North Am* 1990;**19**:783-91.

114. Yadav D, Pitchumoni CS. Issues in hyperlipidemic pancreatitis. *J Clin Gastroenterol* 2003;**36**:54-62.

115. Hofbauer B, Friess H, Weber A. Hyperlipaemia intensifies the course of acute oedematous and acute necrotising pancreatitis in the rat. *Gut* 1996;38:753-58.

116. Saharia P, Margolis S, Zuidema GD, et al. Acute pancreatitis withhyperlipemia: studies with an isolated perfused canine pancreas. *Surgery* 1997;**82**:60-67.

117. Kimura W, Mossner J. Role of hypertriglyceridemia in the pathogenesis ofexperimental acute pancreatitis in rats. *Int.J Pancreatol* 1996;**20**:177-84.

118. Paye F, Chariot J, Molas G, et al. Release of nonesterified fatty acids during cerulein-induced pancreatitis in rats. *Dig Dis Sci* 1996;**41**:1959-65.

119. Hegyi P, Takacs T, Tiszlavicz L, et al. Recovery of exocrine pancreas six months following pancreatitis induction with L-arginine in streptozotocin-diabetic rats**.** *J Physiol Paris* 2000; **94**:51-5.

7. ANNEX

Exp Physiol 93.11 pp 1174–1189

Experimental Physiology – *Research Paper*

Identification of ezrin as a target of gastrin in immature mouse gastric parietal cells

Adelina Pagliocca[1], Peter Hegyi[2], Viktoria Venglovecz[2], Stephen A. Rackstraw[1], Zara Khan[1], Galina Burdyga[1], Timothy C. Wang[3], Rod Dimaline[1], Andrea Varro[1] and Graham J. Dockray[1]

[1]*Physiological Laboratory, University of Liverpool, Liverpool, UK*
[2]*First Department of Medicine, University Medical School, Szeged, Hungary*
[3]*Department of Medicine, Columbia University, New York, NY, USA*

The gastric acid-secreting parietal cell exhibits profound morphological changes on stimulation. Studies in gastrin null (Gas-KO) mice indicate that maturation of parietal cell function depends on the hormone gastrin acting at the G-protein-coupled cholecystokinin 2 receptor. The relevant cellular mechanisms are unknown. The application of differential mRNA display to samples of the gastric corpus of wild-type (C57BL/6) and Gas-KO mice identified the cytoskeletal linker protein, ezrin, as a previously unsuspected target of gastrin. Gastrin administered *in vivo* or added to gastric glands *in vitro* increased ezrin abundance in Gas-KO parietal cells. In parietal cells of cultured gastric glands from wild-type mice treated with gastrin, histamine or carbachol, ezrin was localized to vesicular structures resembling secretory canaliculi. In contrast, in cultured parietal cells from Gas-KO mice, ezrin was typically distributed in the cytosol, and this did not change after incubation with gastrin, histamine or carbachol. However, priming with gastrin for approximately 24 h, either *in vivo* prior to cell culture or by addition to cultured gastric glands, induced the capacity for secretagogue-stimulated localization of ezrin to large vesicular structures in Gas-KO mice. Similarly, in a functional assay based on measurement of intracellular pH, cultured parietal cells from Gas-KO mice were refractory to gastrin unless primed. The priming effect of gastrin was not attributable to the paracrine mediator histamine, but was prevented by inhibitors of protein kinase C and transactivation of the epidermal growth factor receptor. We conclude that in gastrin null mice there is reduced ezrin expression and a defect in ezrin subcellular distribution in gastric parietal cells, and that both can be reversed by priming with gastrin.

(Received 14 March 2008; accepted after revision 9 June 2008; first published online 20 June 2008)
Corresponding author G. J. Dockray: Physiological Laboratory, University of Liverpool, Crown Street, Liverpool L69 3BX, UK. Email: g.j.dockray@liverpool.ac.uk

The capacity of the stomach to secrete hydrochloric acid provides a mechanism to destroy many potentially pathogenic micro-organisms ingested in food. Since gastric acid is also potentially damaging, its production is carefully regulated (Dockray *et al.* 1996; Dockray, 1999). Several lines of evidence indicate that the gastric hormone gastrin plays a central role in mediating acid secretory responses following the ingestion of food. For example, postprandial acid secretion is reduced by administration of antagonists to the receptor at which gastrin acts [cholecystokinin 2 (CCK2), or gastrin–CCK_B receptor], and by administration of neutralizing antibodies to gastrin (Kovacs *et al.* 1989; Beltinger *et al.* 1999). It is well established that in addition to CCK_2 receptors, parietal cells also express histamine H_2 receptors and muscarinic M_3 receptors (Hersey & Sachs, 1995). Activation of each of these receptors is associated with parietal cell stimulation (Soll, 1978). Physiologically, however, it is generally thought that gastrin acts primarily through release of histamine from enterochromaffin-like (ECL) cells, which then acts as a paracrine regulator of parietal cell function (Black & Shankley, 1987).

Studies in mice in which the *gastrin* gene has been deleted by homologous recombination (Gas-KO mice) suggest that gastrin is involved in more than the acute regulation of acid secretion. In these animals, parietal cells

DOI: 10.1113/expphysiol.2008.042648

occur predominantly in an immature form so that they secrete little acid and are refractory to acute administration of gastrin, histamine or the muscarinic agonist carbachol (Koh *et al.* 1997; Friis-Hansen *et al.* 1998; Chen *et al.* 2000). Interestingly, however, administration of gastrin over a period of a few days induces acid secretion and the capacity to respond to the main secretagogues (Friis-Hansen *et al.* 1998; Chen *et al.* 2000), suggesting that in addition to its role in stimulating acid secretory responses during digestion, gastrin also plays a role in regulating the final steps of parietal cell maturation.

In passing from the resting to the acid-secretory state, there is a profound morphological transformation of parietal cells (Forte *et al.* 1977; Okamoto & Forte, 2001). Although there has been some controversy over the relevant mechanisms, there is substantial evidence for the view that activation of these cells is associated with reorganization of the actin cytoskeleton and fusion of an extensive tubulo-vesicular network, to yield multiple secretory canaliculi continuous with the apical membrane and containing long microvilli (Okamoto & Forte, 2001). This morphological transformation occurs in conjunction with functional changes, including the insertion into the apical canalicular membrane of the H^+–K^+-ATPase responsible for transport of protons in exchange for luminal potassium (Agnew *et al.* 1999).

Recent work suggests the cytoskeletal linker protein, ezrin, plays an important role in the morphological transformation of parietal cells. Ezrin is a member of the ezrin–radixin–moesin family of proteins that serve to link the actin cytoskeleton to membrane proteins (Bretscher *et al.* 2000, 2002). It was first identified in parietal cells as a phosphorylated membrane protein (Urushidani *et al.* 1987; Hanzel *et al.* 1991; Zhou *et al.* 2005), and it is now clear that in stimulated cells it is localized to the apical canalicular membrane in association with activation of H^+–K^+-ATPase (Agnew *et al.* 1999; Yao & Forte, 2003). There is evidence that in these circumstances ezrin provides an anchoring point for protein kinase A (PKA), and that PKA-mediated phosphorylation of ezrin is a key component of the relocation of H^+–K^+-ATPase to the apical membrane for stimulation of acid secretion (Hanzel *et al.* 1991; Dransfield *et al.* 1997; Zhou *et al.* 2003). Interestingly, knockdown of ezrin in mice results in severe achlorhydria that has been attributed to an inability to form canalicular apical membranes in parietal cells (Tamura *et al.* 2005).

In the present study, we sought to identify genes that might be targets of gastrin in controlling parietal cell maturation. We report here that differential mRNA display identified ezrin as downregulated in parietal cells in Gas-KO mice; we show that priming with gastrin restores the functional response of parietal cells demonstrated by H^+–K^+-ATPase activity, increases ezrin expression in parietal cells and induces the capacity for ezrin localization to vesicular structures compatible with secretory canaliculi. We suggest that these events are part of the process of parietal cell maturation required for acid secretion.

Methods

Animals

Gastrin null mice on a C57BL/6 background have been described previously (Koh *et al.* 1997). Mice were housed in polycarbonate-bottomed cages in normal animal house conditions with a strict light–dark cycle (lights on at 06.00 h and off at 18.00 h) and fed on a commercial pelleted diet and water *ad libitum*. Mice (10–12 weeks old) were killed by increasing CO_2 concentration followed by cervical dislocation. Some C57BL/6 and Gas-KO mice fed *ad libitum* were treated with heptadecapeptide gastrin (G17; 20 nmol I.P., at 09.00 and 16.00 h on day 1 and 09.00 h on day 2 and killed 3 h later).

Chemicals

Carboxy-terminally amidated, unsulphated G17 was obtained from Bachem (St Helens, UK); AG1478, Ro32-0432 and GM6001 were obtained from CN Biosciences (Beeston, UK); U0126 was obtained from Cell Signaling Technology (Beverly, MA, USA); and 2.7-bis-(2-carboxyethyl)-5-(and-6-)carboxyfluorescein, acetoxymethyl ester (BCECF-AM) was obtained from Invitrogen (Karlsruhe, Germany). Omeprazole was kindly donated by Astra Zeneca (London, UK). Unless otherwise stated, all other chemicals were obtained from Sigma (Poole, UK).

Differential display

Differential mRNA display was performed as described previously (Khan *et al.* 2003). Total RNA from the gastric corpus of Gas-KO or C57BL/6 control mice was DNAse treated and reverse transcribed in four separate reactions employing the anchored oligonucleotide primers T(12)VA, T(12)VC, T(12)VG and T(12)VT, where V is A, C or G. Primary polymerase chain reaction (PCR) was performed on cDNA pools using an arbitrary decamer together with the relevant anchored oligonucleotide in reactions that included [α-^{35}S]dATP. Reaction products were separated using 6% acrylamide solution containing 8M urea sequencing gels and differentially expressed bands excised, the DNA recovered and amplified in a second PCR reaction using the original primers. Secondary PCR products were gel purified, cloned into pGEMTeasy (Promega, Southampton, UK) and sequenced by the dideoxy method.

Western blotting

Protein was extracted from gastric mucosal scrapings in Radioimmuno precipitation assey (RIPA) lysis buffer (Upstate Biotechnology, Cambridge, UK) containing 1% protease inhibitor cocktail set III ($10\,\mu l\,ml^{-1}$) and 1% phosphatase inhibitor cocktail set II ($10\,\mu l\,ml^{-1}$; Calbiochem, Beeston, UK). Alternatively, protein was extracted from adherent gastric glands (see subsection 'Gastric gland isolation and primary culture') in 2× Laemmli buffer containing protease and phosphatase inhibitors. Western blotting was performed as previously described (Varro *et al.* 2002*a*), and Ponceau Red or Coomassie Blue staining was performed. Lysates ($40\,\mu g$ protein) were electrophoresed on 8% SDS–polyacrylamide gels. After electrophoresis, the proteins were blotted on nitrocellulose membranes, and immunodetection of the proteins was performed using a goat anti-ezrin antibody (Santa Cruz Biotechnology, Santa Cruz, CA, USA). Samples were reprobed either with a goat anti-β-actin antibody (Santa Cruz Biotechnology) or a mouse anti-glyceraldehyde-3-phosphate dehydrogenase (GAPDH) antibody (Biodesign International, AMS biotech, Abingdon, UK). Enhanced chemiluminescence (SuperSignal® West Pico chemiluminescent substrate; Pierce, Little Chalfont, UK) and HyperFilm (Amersham, UK) were used to identify the proteins of interest. Bands of interest were quantified using a BioRad Gel-Doc 1000 system (Hemel Hempstead, UK).

Gastric gland isolation and primary culture

Mouse stomachs were ligated at both the oesophageal and pyloric sphincters, rapidly removed and washed in Hanks' balanced salts solution (HBSS). Approximately half of the non-secretory epithelium was removed. The pyloric sphincter was then directed through the newly created fundic opening and the stomach everted and sealed by ligation of the remaining non-secretory epithelium. Stomachs were washed in ice-cold HBSS and filled by injection via a 23-gauge needle with 0.5 ml of $0.5\,mg\,ml^{-1}$ collagenase A (Roche Molecular Biochemicals, Welwyn Garden City, UK). Using a modification of a previously described method (Berglindh & Obrink, 1976), glands were obtained by washing the stomach in prewarmed (37°C) HBSS (3 times), followed by incubation in dithiothreitol (5 ml, 1 mM) for 15 min, washing again in HBSS (3 times), and finally incubating in collagenase A (7.5 ml, $0.32\,mg\,ml^{-1}$, 30 min, 37°C) in an atmosphere of $95\%O_2$–$5\%CO_2$ with shaking at $100\,cycles\,min^{-1}$. Rupturing of the inverted stomach generally indicated adequate digestion to yield isolated glands. At this stage, tissue was triturated using a wide-mouthed plastic pipette. Larger fragments were allowed to settle under gravity (45 s), leaving the isolated glands in suspension (Booth *et al.* 1995). The supernatant containing isolated glands was then transferred to a clean tube, shaken to release additional glands, allowed to settle under gravity for 45 min on ice and the supernatant discarded. The isolated gastric glands from one mouse were suspended in 1.0 ml Dulbecco's modified Eagle's medium supplemented with 10% fetal bovine serum and 1% antibiotic–antimycotic proprietary solution (Sigma-Aldrich, Gillingham, UK) and cultured at 37°C in a humidified atmosphere of $95\%O_2$–$5\%CO_2$. Medium was changed after 24 h and experiments started 24 h after that. Two protocols were used. For 'priming', glands were incubated for 23 h in serum-free medium containing G17 (1.0 nM), phorbol-12-myristate-13-acetate (PMA, 100 nM) or epidermal growth factor (EGF, $10\,ng\,ml^{-1}$; or other drugs, see text and figure legends). For 'acute' stimulation, glands were incubated in serum-free medium for 1 h with G17 or other drugs as appropriate (see text and figure legends). Typically, after priming, glands were either incubated with an acute stimulant or with control medium.

Immunohistochemistry

Isolated glands were cultured at 150 μl gland suspension per well on four-well chamber slides (Nunc, Naperville, IL, USA) for 48 h. The following antibodies were used in indirect immunofluorescence studies: mouse anti-trefoil factor-2 (NovoCastra, Newcastle-upon-Tyne, UK), rabbit anti/pepsinogen (a gift from Mike Samloff, Centre for Ulcer Research, Los Angeles, CA, USA), rabbit anti-H^+/K^+-ATPase (Calbiochem), goat anti-ezrin (Santa Cruz Biotechnology), rabbit anti-chromogranin A (Hussain *et al.* 1999), guinea-pig anti-gastrin (Hussain *et al.* 1999), mouse anti-vimentin and α-smooth muscle actin (Research Diagnostics, Flanders, NJ, USA). Fluorescein isothiocyanate (FITC)-conjugated donkey anti-mouse immunoglobulin M or anti-rabbit immunoglobulin G (Jackson ImmunoResearch Laboratories, West Grove, PA, USA) were used as appropriate, and glands were mounted under Vectashield containing propidium iodide (Vector Laboratories, Peterborough, UK) to preserve fluorescence and stain cell nuclei, respectively. In co-localization studies, rabbit anti-H^+–K^+-ATPase and goat anti-ezrin were used with Texas-Red-labelled donkey anti-rabbit and FITC-conjugated donkey anti-goat, respectively, and samples were mounted under Vectashield containing 4′6-diamidino-2-phenylindole (DAPI) (Vector Laboratories) to label cell nuclei. Slides were examined using a Zeiss Axioplan-2 microscope (Zeiss Vision, Welwyn Garden City, UK), and images captured using a JVC-3 charge-coupled device camera using ×40 magnification (oil immersion) and KS300 software (Zeiss Vision).

For confocal microscopy, three-way immunofluorescence was performed using tetramethylrhodamine B isothiocyanate (TRITC)-conjugated phalloidin, rabbit anti-H^+–K^+-ATPase visualized using FITC-donkey anti-rabbit and goat anti-ezrin visualized with Alexa Fluor

649–donkey anti-goat (Molecular Probes, Eugene, OR, USA). A Zeiss LSM 510 was used, and optical sections of 1 μm were taken under oil at 1024 × 1024 pixel resolution through a Plan-Apochromat ×63 objective.

Receptor autoradiography

Isolated glands (150 μl suspension per well) were cultured on four-well chamber slides for 48 h, washed in phosphate-buffered saline (PBS; 3 times) and fixed in 4% w/v paraformaldehyde (30 min, 22°C). In some experiments, parietal cells were identified using FITC-conjugated *Dolichos biflorus* lectin (10 ng ml^{-1}; Sigma; Falk *et al.* 1994) before the autoradiography protocol. Receptor autoradiography was performed using a modification of a previously described protocol (Herkenham & Pert, 1982). Adherent gastric glands were incubated in buffer containing 20 pM [^{125}I]-G17 (Amersham Pharmacia Biotech, Little Chalfont, UK), in a humidified atmosphere for 4 h at 22°C; control glands were incubated in the presence of excess unlabelled G17 (40 nM). Samples were coated with emulsion using radiosensitive LM-1 (Amersham Pharmacia Biotech), dried, transferred to a light-sensitive slide-box and maintained in a dry atmosphere at 4°C for 12–16 weeks. Slides were developed using Kodak D-19 developer (Kodak, New York, NY, USA) for 2 min at 15°C, washed (20 s, distilled water), and fixed in Kodak rapid fix (Kodak) for 90 s at 15°C. Glands were examined by dark-field microscopy using a Zeiss Axioplan-2 microscope, and images were captured using a JVC-3 charge-coupled device camera using ×40 magnification and KS300 software (Zeiss Vision).

Intracellular pH determination

The following solutions were used: standard Hepes-buffered solution contained (in mmol l^{-1}): 130 NaCl, 5 KCl, 1 $CaCl_2$, 1 $MgCl_2$, 10 D-glucose and 10 sodium-Hepes; Na^+-free Hepes-buffered solution contained (in mmol l^{-1}): 140 N-methyl-D-glucamine (NMDG)-chloride, 5 KCl, 1 $CaCl_2$, 1 $MgCl_2$, 10 D-glucose and 10 Hepes-acid; and ammonium-pulse Na^+-free Hepes-buffered solution contained (in mmol l^{-1}): 120 NMDG-chloride, 20 NH_4Cl, 5 KCl, 1 $CaCl_2$, 1 $MgCl_2$, 10 D-glucose and 10 Hepes-acid. Hepes-buffered solutions were gassed with 100% O_2 and their pH was set to 7.4 with NaOH or HCl at 37°C. The high-K^+ Hepes-buffered solution contained (in mmol l^{-1}): 130 KCl, 5 NaCl, 1 $CaCl_2$, 1 $MgCl_2$, 10 D-glucose, 10 sodium-Hepes and 0.01 nigericin. Gastric glands were cultured on 24 mm coverslips for 48 h and mounted in a perfusion chamber on an Olympus microscope. The glands were bathed in standard Hepes solution at 22°C and exposed to 20 ng ml^{-1} FITC-conjugated *Dolichos biflorus* lectin (Sigma) for 1 h to identify parietal cells. Glands were then loaded with the pH-sensitive fluorescent dye BCECF-AM (2 μmol l^{-1}) for 20–30 min and thereafter were continuously perfused at 4–5 ml min^{-1}. Intracellular pH (pH_i) was measured using a Cell® imaging system (Olympus, Budapest, Hungary), excited with light at wavelengths of 490 and 440 nm, and the 490/440 fluorescence emission ratio was recorded from parietal cells identified by lectin staining. One pH_i measurement was obtained per second. *In situ* calibration of the fluorescence signal was performed using the high-K^+–nigericin technique (Thomas *et al.* 1979; Hegyi *et al.* 2004) using high-K^+ Hepes solution containing 10 μM nigericin and extracellular pH stepped between 5.95 and 8.46 (Hegyi *et al.* 2004). In order to determine H^+–K^+-ATPase activity, glands were exposed to 3 min pulses of 20 mM NH_4Cl in a Na^+-free standard Hepes solution twice, the first exposure being the control and the second the test. Gastrin (G17, 10–1000 pM) or vehicle were administered for 20 min between the two measurements (Hegyi *et al.* 2003; Dufner *et al.* 2005). In some experiments, ranitidine (100 μM) or omeprazole (100 μM) was applied for 10 min between the two measurements. The initial rate of pH_i recovery (dpH/dt) was measured over the first 60 s (60 data points) after removal of NH_4Cl using linear regression analysis.

Flow cytometry

Gastric glands were cultured as described above, and cells recovered in suspension by mild digestion with trypsin, suspended in 2% paraformaldehyde (37°C, 15 min), permeabilized by the addition of methanol to a final concentration of 90% and incubated on ice (1 h). Cells were then washed twice in 5% bovine serum albumin in PBS, incubated with rabbit anti-ezrin antibody (Cell Signalling Technology; 4°C overnight with gentle shaking), washed twice in 4% donkey serum in PBS and incubated in donkey anti-rabbit antibody conjugated to FITC (Jackson Immunoresearch Laboratories; 22°C, 1 h with gentle shaking). Finally, cells were washed twice in 5% bovine serum albumin and fluorescence-activated cell sorting (FACS) analysis carried out using a BD FACSVantage flow cytometer (Becton, Dickinson and Company, Oxford, UK). Data were recorded and analysed using CellQuest Pro-software (Becton, Dickinson and Company). Parietal cells were identified by gating cells with a high forward scatter and side scatter as previously described (Dixit & Dikshit, 2001). Changes in the abundance of parietal cell ezrin were measured as an increase or decrease in the geometric mean fluorescence for cells in this region.

Determination of ezrin subcellular localization

For studies of ezrin localization, adherent gastric glands consisting of more than 80 cells and containing at least

eight parietal cells were scored for the localization of ezrin to large vesicular structures. Thus, the number of parietal cells exhibiting ezrin localization to one or more large vesicular structures was determined as a percentage of the total number of ezrin-containing parietal cells within that gland. For each treatment, observations were made from a minimum of eight glands from a single mouse, and the mean for the experimental treatment was typically calculated from at least three individual mice.

Statistics

Results are presented as means ± S.E.M.; comparisons within individual strains were made using Student's paired *t* test and between-strain comparisons were made by analysis of variance (ANOVA). In both cases, comparisons were considered significant at $P < 0.05$.

Results

Gastrin regulates ezrin expression

When differential mRNA display was applied to samples of gastric corpus of wild-type and Gas-KO mice (Khan *et al.* 2003), one of the differentially expressed bands was identified as corresponding to approximately 280 bp immediately upstream of the polyadenylation site of mouse ezrin mRNA. To confirm the differential expression of ezrin at the protein level, we then showed that in Western blots its abundance in gastric mucosal samples from Gas-KO mice was significantly lower than in wild-type mice (Fig. 1*A* and *B*); whereas, for example, the abundance of the α-subunit of H^+–K^+-ATPase was similar in the two strains (not shown). The depression in ezrin expression in the stomach of Gas-KO mice could be rescued by gastrin, since in Gas-KO mice treated with G17 there was a significant increase in ezrin abundance (Fig. 1*C* and *D*). In contrast, treatment of C57BL/6 mice with gastrin had no effect on the abundance of gastric ezrin (Fig. 1*E* and *F*).

Characterization of cultured gastric glands

We then asked whether the effect of gastrin was exerted directly at the level of the gastric epithelium. Previous studies have made use of purified, dissociated parietal cells (Soll, 1978; Chew, 1994; Agnew *et al.* 1999); since, however, many effects of gastrin are exerted via paracrine

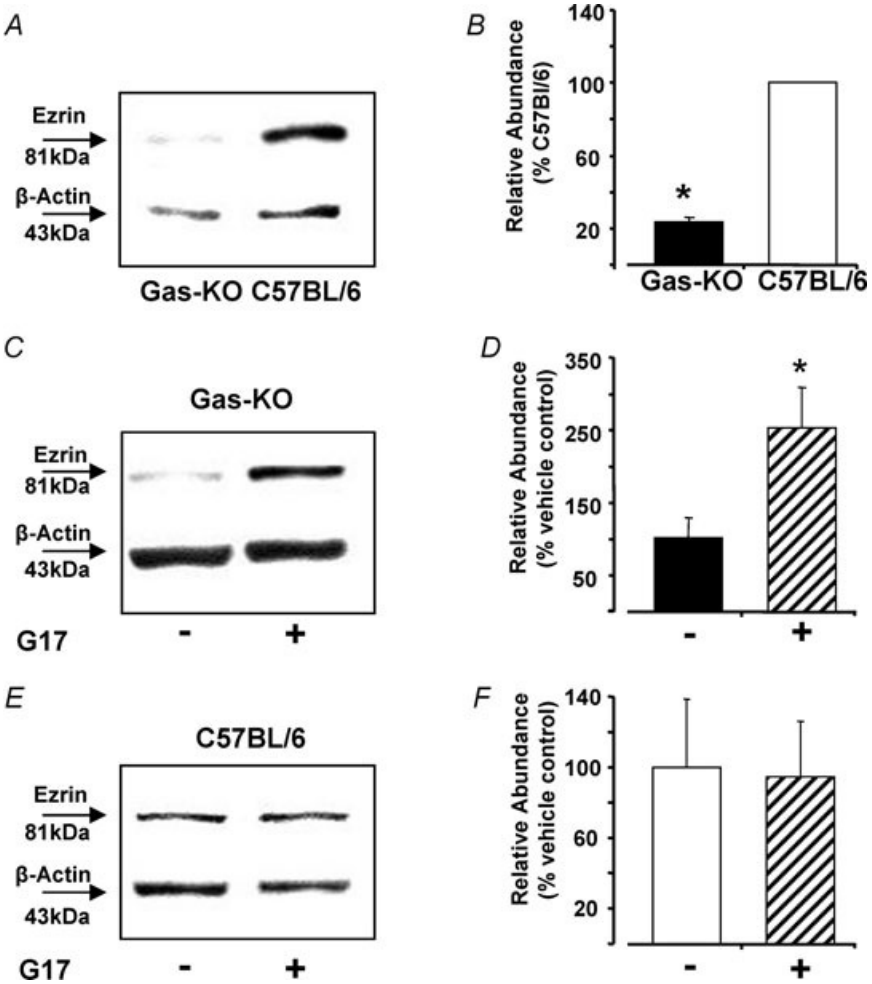

Figure 1. Gastrin-dependent expression of ezrino
A, Western blot of mucosal scrapings from untreated Gas-KO and C57BL/6 mice showing ezrin and β-actin. *B*, quantification of bands indicates a fivefold higher ezrin abundance in C57BL/6 mice. *C*, Western blot of mucosal scrapings from Gas-KO mice treated with gastrin (20 nmol, I.P., 3 times in 27 h) or saline. *D*, quantification of bands indicates a three- to fourfold increase in ezrin with gastrin; ezrin values are normalized to β-actin in the same sample. *E* and *F*, in C57BL/6 mice, treatment with gastrin had no effect on ezrin abundance. Values are means + S.E.M., $n = 3$ mice in each group. $^*P < 0.05$.

mediators, we sought a preparation in which different cell types were represented in physiological proportions and which could be used in prolonged culture. We therefore adapted a previously described method for preparing rabbit gastric glands (Berglindh *et al.* 1979) to mice and established culture conditions that allowed gland cells to survive for at least 7 days. When cultured on either glass or plastic surfaces, isolated mouse gastric glands spread after about 18 h to form a monolayer in which all the epithelial cells were preserved (Fig. 2*A* and *B*). Time lapse videomicroscopy (Wroblewski *et al.* 2003) indicated that cell division and cell loss through apoptosis were relatively rare events. Immunohistochemical studies indicated that the major differentiated cell types, i.e. parietal cells, zymogen cells, endocrine cells and mucus cells, were represented in proportions similar to those reported previously (Karam & Leblond, 1992; Fig. 2*C*–*F*). The presence of parietal cells defined the glands as originating from the corpus part of the stomach; staining for gastrin (to identify G-cells and therefore glands originating from the antral part of the stomach) was negative. Myofibroblasts, identified by staining for α-smooth muscle actin, were rare (approximately one positive cell in 5% of glands). The cultured glands included large cells that expressed the CCK_2 receptor as indicated by autoradiography using [^{125}I]-G17 (Fig. 2*G* and *H*), and these were identified as parietal cells by staining with *Dolichos biflorus* lectin (data not shown). In addition, receptor autoradiography revealed occasional small round cells which expressed the CCK_2 receptor, presumably corresponding to ECL cells (Fig. 2*H*).

We then verified the localization of ezrin to cultured parietal cells. Thus, over 90% of cells that were immunoreactive for H^+–K^+-ATPase also stained with antibodies to ezrin, and there was no difference between Gas-KO and C57BL/6 mice in this regard (Fig. 3*A*–*C*); we did not find co-localization of ezrin with either pepsinogen or mucin (not shown), indicating that in cultured glands, as *in vivo*, ezrin was not expressed in the other major secretory cell types (mucus or chief cells). There was, however, ezrin in some ECL cells. In order to quantify ezrin in parietal cells, we applied FACS analysis to dissociated cells from cultured glands (Dixit & Dikshit, 2001; Zavros *et al.* 2002). In parietal cells from the cultured gastric glands of Gas-KO mice, ezrin abundance was significantly lower than in C57BL/6 mice (wild-type, $100 \pm 11.4\%$; Gas-KO, 52.6 ± 12.2, $P < 0.05$; $n = 10$). Inclusion of gastrin (1–10 nM, 24–48 h) in the culture medium significantly increased ezrin abundance in Gas-KO parietal cells (Fig. 3*D*), but had no effect on ezrin abundance in parietal cells of wild-type mice (control, $100 \pm 23\%$; 1 nM G17, $93 \pm 14\%$).

In order to establish whether there were functional differences between wild-type and Gas-KO parietal cells in cultured glands, we monitored intracellular pH using BCECF-AM and microfluorometry. The resting pH_i of wild-type parietal cells was 7.33 ± 0.02 ($n = 10$) and was not significantly different in Gas-KO mice (7.30 ± 0.5). In these cells, removal of Na^+ from the standard Hepes solution caused a rapid and marked intracellular acidosis owing to the inhibition of Na^+–H^+ exchanger activity

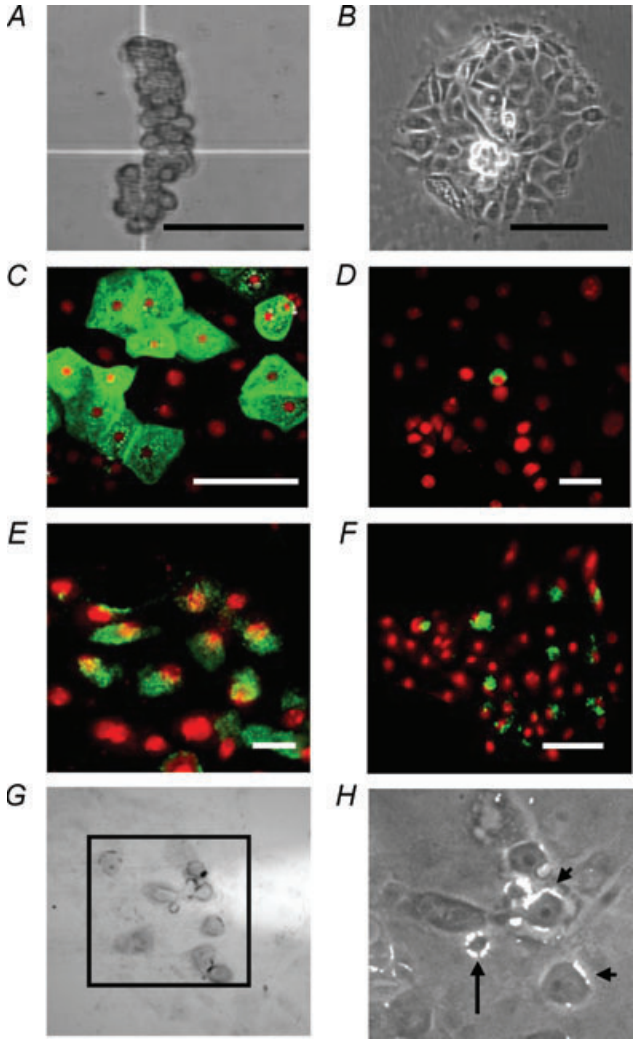

Figure 2. Cultured mouse gastric glands
A, phase contrast microscopy of an acutely dissociated mouse gastric gland, showing characteristic tubular shape. *B*, a comparable gland after culture on plastic for 24 h, showing that cells adhere and spread to form a monolayer. Also shown are immunohistochemical localization of: H^+–K^+-ATPase (*C*, parietal cells are green), chromogranin A (*D*, enterochromaffin-like cells are green), trefoil factor-2 (*E*, mucous neck cells are green) and pepsinogen (*F*, chief cells are green). In *C*–*F*, nuclei are counterstained red with propidium iodide. In addition, the figure shows expression of the CCK_2 receptor in cultured gastric glands indicated by [^{125}I]-G17 autoradiography (*G*, bright field) and dark field (*H*, showing the region indicated by the box in *G*). Receptor was expressed around the entire plasma membrane of small cells (arrow in *H*) and in patches on the plasma membrane of larger cells (arrowheads) within cultured gastric glands. In *A*–*F*, scale bars represent 100 μm. In *G* and *H*, scale bars as in *F*.

(Fig. 4). Moreover, exposure to 20 mM NH_4Cl induced an immediate rise in pH_i owing to the rapid entry of NH_3 into the cells, and its removal produced a rapid decrease in pH followed by a slower recovery owing to activation of pH_i regulatory mechanisms. In the absence of Na^+ and HCO_3^-, the functionally active acid–base transporter/pump in these circumstances is the H^+–K^+-ATPase and therefore the initial rate of recovery from acidosis reflects its activity. When 10–1000 pM G17 was included in the medium, there was a concentration-dependent stimulation of pH_i recovery after NH_4Cl owing to the stimulated H^+ efflux (Fig. 4) that was blocked by 100 μM omeprazole, indicating that it was attributable to H^+–K^+-ATPase activity. The H_2 receptor antagonist, ranitidine, inhibited the response to 100 pM G17 (which is just above the physiological concentration in plasma), but only partly inhibited the effect of 1 nM G17, which is consistent with the idea that at physiological concentrations gastrin acts on parietal cells via histamine release from ECL cells, but can act directly at higher concentrations. In contrast, in Gas-KO mice, the initial recovery of pH_i was significantly decreased compared with wild-type mice (Gas-KO, 0.0054 ± 0.001 units min^{-1}; wild-type, 0.015 ± 0.002 units min^{-1}, $P < 0.05$) and was completely refractory to 1 nM G17. However, incubation for 24 h *in vitro* with 1 nM G17 (which we refer to as 'priming'), followed by a 2 h wash-out period before the experiments, induced the capacity for an acute response to G17 (Fig. 4). The data are therefore compatible with studies *in vivo* indicating that gastrin priming restores secretagogue sensitivity to parietal cells in Gas-KO mice (Fig. 4).

Cellular localization of ezrin

Ezrin is normally localized to the apical canalicular secretory membrane of stimulated parietal cells (Hanzel *et al.* 1991; Yao *et al.* 1996; Agnew *et al.* 1999). In approximately 90% of parietal cells from C57BL/6 mice in the absence of secretagogues, confocal microscopy indicated a distribution of ezrin that was distinct from that of H^+–K^+-ATPase (Fig. 5*A*–*C*). In these cells, ezrin was localized in aggregates that were within the cytosol and to the base of the adherent cells. However, in a minority of cells (10.0 ± 1.7%), ezrin was localized to large vesicular structures in close association with H^+–K^+-ATPase and with F-actin stained by phalloidin, compatible with localization at the canalicular membrane (Fig. 5*D*–*F*). Stimulation with G17 for 1 h significantly increased the population of parietal cells from C57BL/6 mice that exhibited ezrin association with large vesicular structures, and similar results were obtained with the two other main gastric secretagogues, histamine and carbachol (Fig. 6*A*). The H_2 receptor antagonist, ranitidine, inhibited the effect of gastrin in stimulating ezrin association with large vesicular structures in C57BL/6 mice, indicating

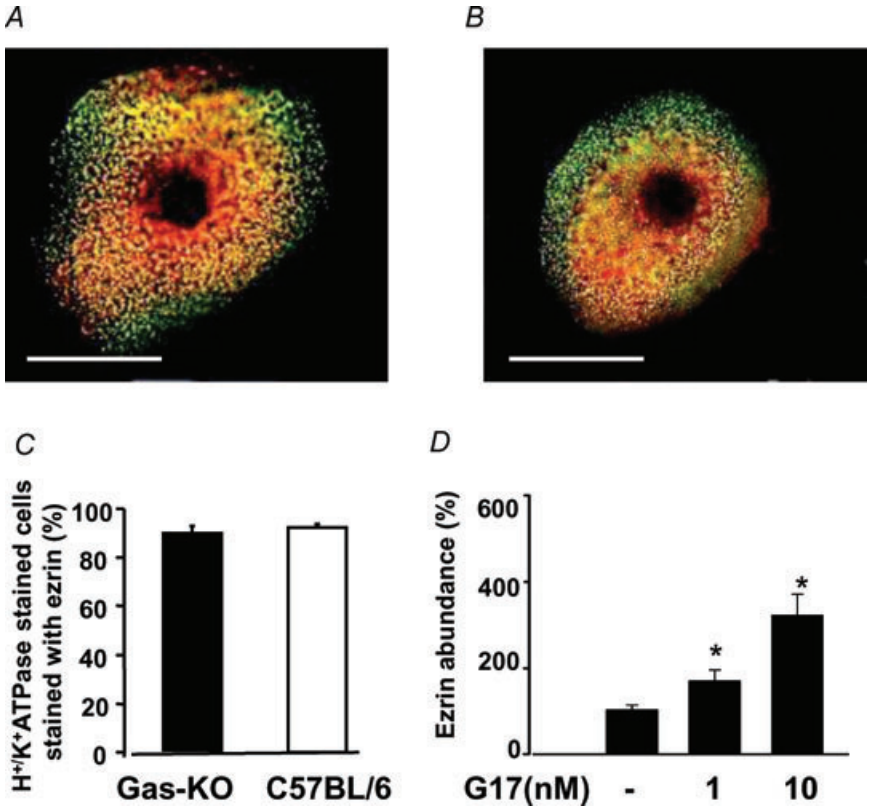

Figure 3. Localization of ezrin to parietal cells in Gas-KO mice
Immunohistochemical localization of ezrin (green) to unstimulated parietal cells (stained with antibody to H^+–K^+-ATPase, red) from Gas-KO (*A*) and C57BL/6 mice (*B*) Scale bars represent 20 μm.
C, approximately 90% of parietal cells stained with antibody to H^+–K^+-ATPase also contained ezrin immunoreactivity, and there was no difference between Gas-KO and C57BL/6 mice. *D*, flow cytometry indicated that the relative abundance of ezrin (determined by comparison of the integrated peak in control *versus* treated parietal cells) in cultured gastric glands was increased in Gas-KO mice in response to 1 and 10 nM G17 (48 h. $^*P < 0.05$. Values are means + S.E.M., $n = 3$–9.

a role for histamine in mediating this effect of gastrin (not shown). In contrast, in parietal cells from Gas-KO mice, the distribution of ezrin was predominantly in cytosolic aggregates, and this was not influenced by acute (1 h) stimulation by gastrin (1 nM), histamine (10 μM) or carbachol (10 μM; Fig. 6*B*).

Gastrin primes ezrin redistribution in parietal cells from Gas-KO mice

We then examined whether pretreatment of Gas-KO mice with gastrin restored the capacity for ezrin redistribution to vesicular structures similar to that seen in the parietal cells of wild-type mice. When Gas-KO mice were treated with G17 *in vivo*, and parietal cells subsequently cultured, there was a significant increase in the proportion of cells exhibiting localization of ezrin to large vesicular structures in response to acute stimulation with gastrin (Fig. 7*A*). We then used the proportion of parietal cells exhibiting localization of ezrin to one or more large vesicular structures as a simple assay of the response to gastrin. Thus, in order to determine whether prolonged incubation *in vitro* with gastrin might also induce the capacity for ezrin redistribution, we cultured gastric glands from Gas-KO mice in the presence of gastrin and then substituted fresh medium either without secretagogue or containing gastrin, histamine or carbachol for a further 1 h (i.e. acute stimulation after priming; Fig. 7*B*). We found that each of the three secretagogues increased the proportion of parietal cells exhibiting ezrin association with large vesicular structures compared with control cells (primed with gastrin and unstimulated for the last hour). The data suggest that prolonged exposure to gastrin either *in vivo* or *in vitro* primes parietal cells from Gas-KO mice, enabling ezrin association with secretory canaliculi in response to acute secretagogue stimulation.

Histamine is not involved in gastrin-stimulated parietal cell priming

Since histamine mediates the acute response to gastrin after priming, we then examined whether the priming response to gastrin described above was histamine dependent. Priming of cultured gastric glands from Gas-KO mice with histamine (10 μM, 23 h) had no effect on the capacity of parietal cells to exhibit ezrin redistribution in response to subsequent stimulation by gastrin for 1 h (histamine priming, $12.8 \pm 2.8\%$ parietal cells exhibiting ezrin localization to vesicular structures; histamine priming followed by gastrin, $15.6 \pm 2.6\%$ exhibiting ezrin localization to vesicular structures). Moreover, ranitidine did not inhibit the capacity of gastrin to prime Gas-KO parietal cells (Fig. 7*C*). The evidence suggests that the priming effect of gastrin is neither mediated by, nor replicated by, histamine.

Roles for epidermal growth factor (EGF) receptor and protein kinase C (PKC) in gastrin-stimulated parietal cell priming

Previous work has shown that CCK_2 receptor stimulation activates PKC which, through stimulation of a metalloproteinase, is able to promote shedding of EGF receptor ligands such as transforming growth factor (TGF)α and heparin-binding epidermal growth factor (HB-EGF) that in turn stimulate EGF receptors and activate the mitogen activated protein (MAP) kinase pathway (Wang *et al.* 2000; Varro *et al.* 2002*b*). An indication of the involvement of this pathway in gastrin-stimulated priming of parietal cells was provided by the observation that when cells were primed with G17 in the presence of the broad spectrum metalloproteinase inhibitor GM6001, the EGF receptor tyrosine kinase inhibitor AG1478, the MAP kinase kinase (MEK) inhibitor U0126 or the PKC inhibitor Ro-32-0432, the subsequent increase in parietal cells exhibiting ezrin translation in response to acute stimulation by gastrin was significantly reduced (Fig. 8*A*). Moreover, consistent with a role for transactivation of the EGF receptor by HB-EGF (Miyazaki *et al.* 1999; Varro *et al.* 2002*b*; Sinclair *et al.* 2004), we found that the mutant diphtheria toxin, CRM197, which inhibits the effect of HB-EGF, also blocked the priming effect of G17 (Fig. 8*A*).

To further explore the role of PKC, we cultured parietal cells from Gas-KO mice in the presence of phorbol-12-myristate-13-acetate (PMA); medium was then replaced, and the effect of stimulation with gastrin for a period 1 h examined. Using this protocol, gastrin significantly increased the proportion of cells exhibiting ezrin redistribution compared with PMA-primed cells not subsequently exposed to gastrin (Fig. 8*B*). Consistent with the evidence in other systems that PKC is associated with transactivation of the EGF receptor (Prenzel *et al.* 1999), we found that GM6001 completely inhibited the priming effect of PMA (Fig. 8*B*), as did the EGF receptor tyrosine kinase inhibitor AG1478 and the MEK inhibitor U0126. In support of the idea that EGF receptor activation was able to prime cells, we showed that pretreatment of glands with EGF (10 ng ml^{-1}, 23 h) also increased the proportion of cells exhibiting ezrin redistribution in response to subsequent acute stimulation by gastrin (EGF pretreatment alone, $24.7 \pm 0.2\%$ of parietal cells exhibiting ezrin redistribution; EGF pretreatment followed by 0.1 nM gastrin for 1 h, $35.2 \pm 1.0\%$ of parietal cells exhibiting ezrin redistribution, $P < 0.05$). Finally, we made use of the mutated diphtheria toxin CRM197, which inhibits the action of HB-EGF, to examine the role of this member of the EGF family. The presence of CRM197 during the priming phase of gastrin treatment was associated with a significant reduction in the number of parietal cells exhibiting ezrin redistribution in response

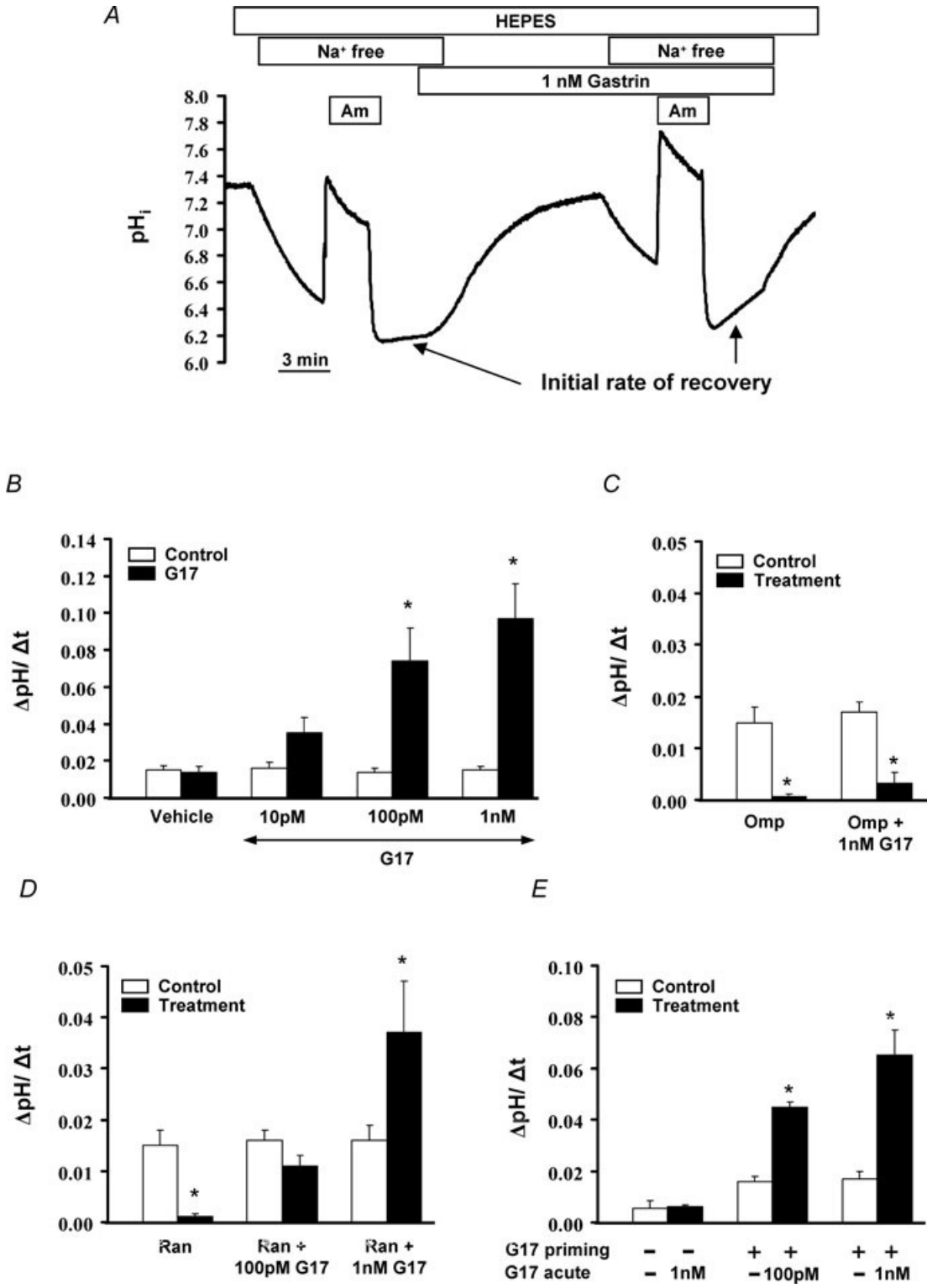

Figure 4. Functional characterization of parietal cells in cultured gastric glands of Gas-KO and wild-type mice

A, representative pH_i trace. Gastric glands from wild-type mice were exposed to 3 min pulses of 20 mM NH_4Cl (Am) in a Na^+-free standard Hepes solution twice, the first exposure being the control and the second the test. The initial rates of pH_i recovery from the acid load (over the first 60 s) were determined for each exposure. Gastrin (G17) was administered for 20 min before and during the test exposure and the inhibitors (omeprazole or ranitidine, when used) were administered for 10 min between the measurements. *B*, summary of the results obtained using the ammonium chloride pulses. Initial rates of pH_i recovery are shown by the open bars, compared.

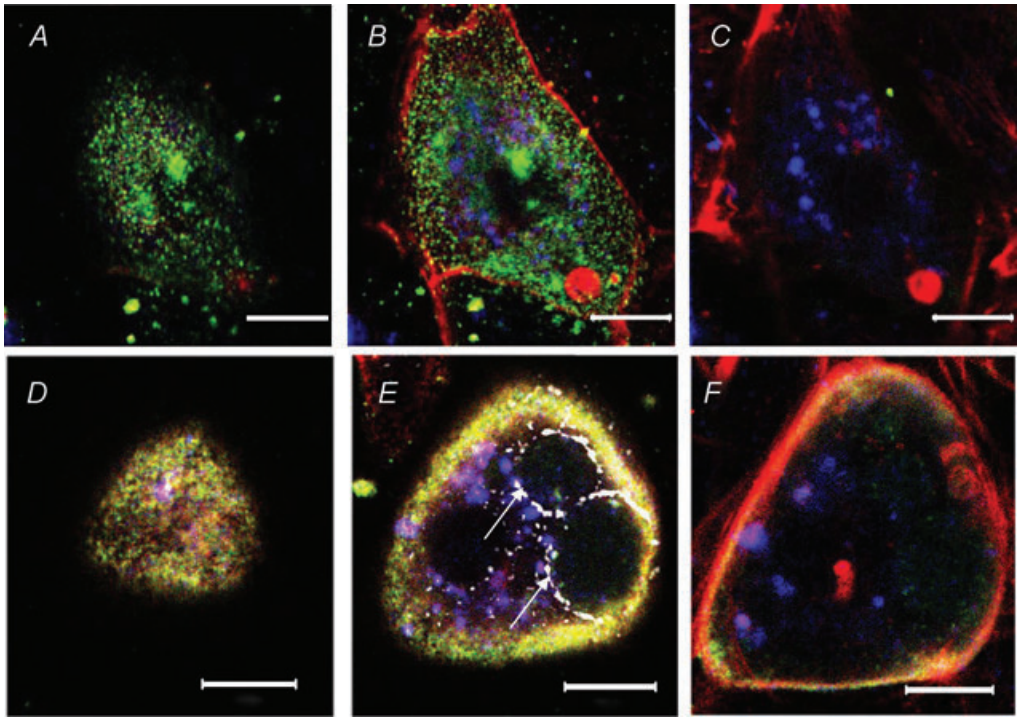

Figure 5. Confocal microscopy of quiescent and stimulated parietal cells
Triple labelling of cultured parietal cells from C57BL/6 mice with antibodies to ezrin (blue) and H^+–K^+-ATPase (green), and with phalloidin (red). Optical sections through an unstimulated parietal cell in the apical (*A*), mid (*B*) and basal region (*C*). Note cytosolic aggregations of ezrin. *D*–*F*, slices through a gastrin-stimulated cell (1 nM, 1 h), showing similar regions (apical, *D*; mid, *E*; and basal region, *F*). Note redistribution of ezrin in the mid-region of cells (*E*) to large vesicular structures and localization at these loci with H^+–K^+-ATPase and F-actin (white arrows). Scale bars represent 10 μm.

to subsequent stimulation with gastrin (gastrin priming and stimulation alone, $43.7 \pm 3.2\%$ cells exhibiting ezrin redistribution; gastrin priming in presence of CRM197 followed by gastrin stimulation for 1 h, 16.3 ± 4.5 cells exhibiting redistribution, $P < 0.05$).

Discussion

The main findings of the present study are that in mice in which the *gastrin* gene has been deleted by homologous recombination, there is depressed expression of the cytoskeletal linker protein, ezrin, in gastric parietal cells. This is associated with changes in the subcellular distribution of ezrin and, in cultured cells, with a failure to respond to gastric acid secretagogues. Administration of gastrin for approximately 24 h or more *in vivo* or *in vitro* increased ezrin abundance and induced the capacity for secretagogue-stimulated subcellular redistribution of ezrin. The latter effects were not mediated by histamine but appeared to involve activation of PKC, metalloproteinase shedding of the EGF receptor ligand HB-EGF and transactivation of the EGF receptor. The data provide new insights into the mechanisms by which gastrin regulates the maturation of parietal cells and suggest that these mechanisms are distinct from those involved in the acute regulation of gastric acid secretion (Dockray *et al.* 2005).

The starting point for the present study was the discovery by differential mRNA display that expression of the cytoskeletal linker protein, ezrin, was depressed in the gastric corpus of Gas-KO mice and that this phenotype was rescued by gastrin. Importantly, gastrin had little or no effect on ezrin abundance in wild-type

with recovery in the test period (filled bars). Increasing concentrations of G17 stimulated the pH_i recovery after NH_4Cl pulses, compatible with increased activity of H^+–K^+-ATPase. *C*, the proton pump inhibitor omeprazole (100 μM) completely blocked both unstimulated and G17-stimulated recovery. *D*, the H_2 receptor antagonist ranitidine (100 μM) inhibited recovery in response to a low concentration of G17, which could be overcome by higher concentrations of G17. *E*, in glands from Gas-KO mice, incubation *in vitro* with gastrin (1 nM, 24 h; 'G17 priming') restored proton pump activity. Values are means + S.E.M.; data from at least 3 glands containing 10–15 parietal cells are shown. $^*P < 0.05$.

mice, consistent with the idea that it does not play a major role in maintaining ezrin expression in mature parietal cells. These findings were considered interesting in view of the extensive evidence implicating ezrin in the acid secretory responses of the parietal cell (Urushidani *et al.* 1987; Agnew *et al.* 1999; Yao & Forte, 2003; Zhou *et al.* 2003). In particular, ezrin is generally recognized to be highly concentrated in parietal cells compared with other cells of the gastric epithelium (Hanzel *et al.* 1991; Yao & Forte, 2003), and reduction of ezrin expression in the stomach of transgenic mice to <5% of that in control animals results in a defect in the assembly of the parietal cell canalicular apical membrane and severe achlorhydria (Tamura *et al.* 2005). Ezrin is therefore essential for the capacity to secrete acid.

It has been clear for some years that Gas-KO mice have substantially reduced gastric acid secretion and an inability to respond to the major gastric acid secretagogues (gastrin, histamine and cholinergic muscarinic agonists) but the relevant cellular mechanisms are largely unknown (Koh *et al.* 1997; Friis-Hansen *et al.* 1998). The present data indicate that the defects include reduced ezrin expression and changes in the subcellular distribution of the residual ezrin. Whether depressed ezrin abundance is sufficient on its own to account for the inability to secrete acid remains to be determined. We think this is unlikely, however, since many other proteins are required for secretagogue-evoked acid secretion and functional genomic studies have identified many other genes that exhibit differential expression in gastrin null mice (Jain *et al.* 2006). In Gas-KO mice, we find ezrin in cytosolic aggregates and evidence of redistribution to large vesicular structures, presumably corresponding to secretory cannaliculi, following stimulation after gastrin priming. Moreover, in wild-type parietal cells, acute stimulation with gastrin, histamine or carbachol was also associated with the redistribution of ezrin to large vesicular structures that were absent from the majority of unstimulated cells. Previous studies using rabbit parietal cells have noted that ezrin does not relocate from cytoplasm to other structures on stimulation (Zhu *et al.* 2005). Whether or not there are differences between rabbit and mouse parietal cells, or whether the method of culture (isolated cells *versus* cultured glands) influences the localization of ezrin, will require further work. It is, however, worth noting that in other cell types, such as prostate cancer cells (Chuan *et al.* 2006), stimulation has been reported to be associated with a redistribution of ezrin to the plasma membrane.

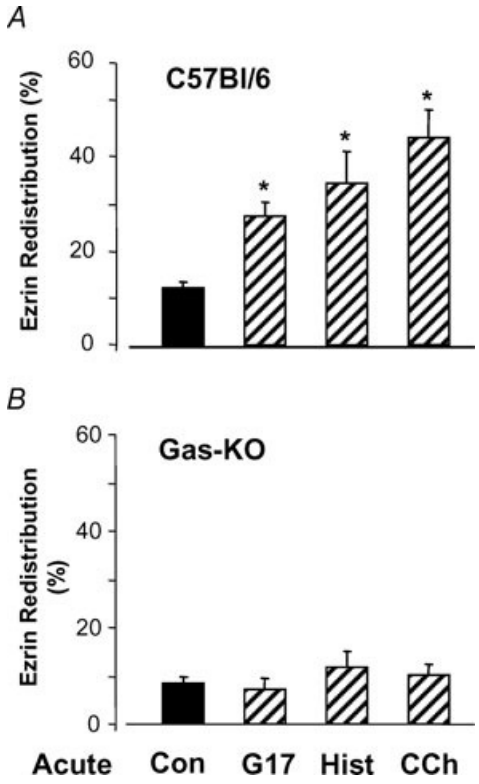

Figure 6. Effects of gastrin on ezrin distribution
The proportion of the parietal cell population (%) in glands cultured for 48 h exhibiting at least one large vesicular structure (see Fig. 4*E*) with associated ezrin immunoreactivity after treatment in serum-free medium for 1 h with gastrin (G17, 1 nM), histamine (Hist, 10 μm), carbachol (CCh, 10 μM) or vehicle (Con). *A*, in parietal cells from C57BL/6 mice, a significantly increased proportion of the parietal cell population exhibits ezrin redistribution in response to each secretagogue (*$P < 0.05$). *B*, in contrast, in parietal cells from Gas-KO mice, there is no change in the proportion of cells exhibiting redistribution in response to any of the three secretagogues. Values are means + S.E.M., $n = 3$–7.

It is well established that morphologically identifiable parietal cells are present in Gas-KO mice (Koh *et al.* 1997; Chen *et al.* 2000). The first descriptions of the phenotype in Gas-KO mice also noted a possible reduction in parietal cell numbers compared with wild-type mice (Koh *et al.* 1997). More strikingly, however, the parietal cells that do occur in Gas-KO mice are insensitive to acute secretagogue stimulation (Friis-Hansen *et al.* 1998; Chen *et al.* 2000), while administration of gastrin for about 24 h or longer induces the capacity for secretagogue-induced secretion. The idea has emerged, therefore, that gastrin is required for completion of relatively late events in the differentiation of parietal cells, and we use the term 'priming' to describe these events (and to distinguish them from the acute effects of gastrin on normal parietal cells). Calcium signalling in response to gastrin has been reported to be retained in parietal cells from Gas-KO mice (Hinkle *et al.* 2003), suggesting that the inability to respond to acute stimulation by gastrin is located elsewhere on the signalling pathway.

There has been some controversy over the mechanisms by which gastrin acts on parietal cells (Soll, 1978; Black & Shankley, 1987). Receptors for each of the three main gastric acid secretagogues are expressed by parietal

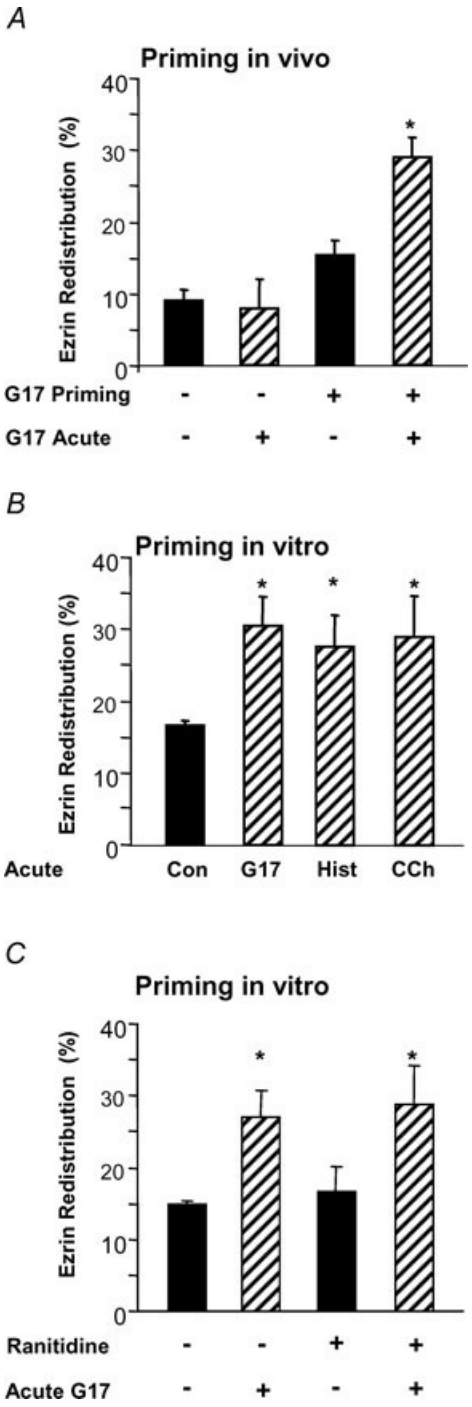

Figure 7. Gastrin priming rescues the capacity for ezrin redistribution

The proportion of the parietal cell population (%) in glands from Gas-KO mice cultured for 48 h exhibiting at least one large vesicular structure (see Fig. 4*E*) with associated ezrin immunoreactivity after pretreatment with gastrin either *in vivo* or *in vitro* is shown. *A*, prior to culture, mice were treated with G17 (3 × 20 nmol, I.P., over 27 h, i.e. 'priming *in vivo*') or vehicle, and gastric glands were then cultured for 48 h followed by the subsequent addition of G17 (hatched bars) or vehicle (filled bars) for 1 h; note significant increase in the proportion of cells showing redistribution in response to acute gastrin stimulation following gastrin priming. *B*, similarly, when cultured gastric glands. from Gas-KO mice were treated in serum-free medium for 23 h with G17 (1 nM; 'priming *in vitro*') and then washed, the subsequent addition for 1 h (hatched bars) of G17 (100 pM), histamine (Hist, 10 μM) or carbachol (CCh, 10 μM) significantly increased the proportion of the parietal cell population exhibiting ezrin distribution to large vesicular structures compared with primed cells in vehicle (filled bar; Con, control). *C*, moreover, priming with gastrin *in vitro* (1 nM, 23 h) in the presence of the H_2 receptor antagonist ranitidine (100 μM) did not block the subsequent response to acute stimulation by gastrin (hatched bars) compared with acute exposure to vehicle (filled bars). $^*P < 0.05$; values are means + S.E.M., $n = 3$–6.

cells. Earlier evidence for interactions between these secretagogues at the level of the parietal cell (Soll, 1978) has received some support from recent studies in mice in which the muscarinic M_3 receptor has been deleted (Aihara *et al.* 2003). Even so, it appears that histamine release from adjacent ECL cells accounts for a substantial proportion of the acid secretory response to gastrin *in vivo* (Dockray *et al.* 2001). The preparation used in this study contains the main epithelial cell types, notably histamine-secreting ECL cells and parietal cells, thereby facilitating studies of paracrine mechanisms. Using a protocol in which determination of intracellular pH is used to reflect H^+–K^+-ATPase activity, we showed that parietal cells from Gas-KO mice were refractory to the action of gastrin, but exposure to G17 for 24 h restored responses to those seen in glands from wild-type mice. Crucially, the effect of near-physiological concentrations of gastrin in this system was mediated by histamine. However, the priming effect of gastrin on ezrin distribution was not replicated by histamine and was not blocked by an H_2 antagonist. The present data are therefore compatible with the idea that while histamine released from ECL cells is a mediator of the acute, secretagogue effects of gastrin, it does not mediate the effect of gastrin on parietal cell priming, and instead raise the possibility that gastrin acts directly on CCK_2 receptors on parietal cells to stimulate parietal cell maturation.

The CCK_2 receptor is coupled to $G\alpha_{q/11}$ and is known to activate PKC and increase intracellular calcium (Delvalle *et al.* 1992; Todisco *et al.* 1997). Since the priming effect of gastrin was replicated by PMA and blocked by a PKC inhibitor, we suggest that activation of PKC by gastrin is part of the priming response that renders parietal cells susceptible to acute secretagogue stimulation. The role of PKC in parietal cells has been the subject of discussion. Some studies suggest that activation leads to weak stimulation of acid secretion; others indicate an inhibitory effect (Chew *et al.* 1997; Yao & Forte, 2003). The picture is somewhat complicated by the fact that different PKC isoforms may have different roles so, for example, PKCα appears to inhibit acid secretion while PKCε stimulates it (Fahrmann *et al.* 2002, 2003). Further work will be needed to determine the isoforms

relevant for parietal cell maturation. Interestingly, there is already evidence that ezrin is a target of PKC and that ezrin phosphorylation is associated with relocation to the membrane, compatible with the present data (Chew *et al.* 1997). However, for reasons discussed below we think that the priming effect of gastrin may involve an indirect action mediated by a paracrine/autocrine loop involving transactivation of the EGF receptor.

There is growing evidence from studies in many cell types that activation of PKC, or increased intracellular calcium concentrations, induces shedding of EGF receptor ligands, such as HB-EGF and amphiregulin (Prenzel *et al.* 1999). In the case of CCK_2 receptor stimulation, this type of mechanism can mediate proliferative responses in cell lines (Varro *et al.* 2002*b*). Moreover, there is abundant evidence that CCK_2 receptors activate the MAP kinase pathway (Takeuchi *et al.* 1997; Todisco *et al.* 1997; Daulhac *et al.* 1999), possibly secondary to release of EGF receptor ligands. The role of EGF-related growth factors produced in parietal cells has attracted considerable attention. It has,

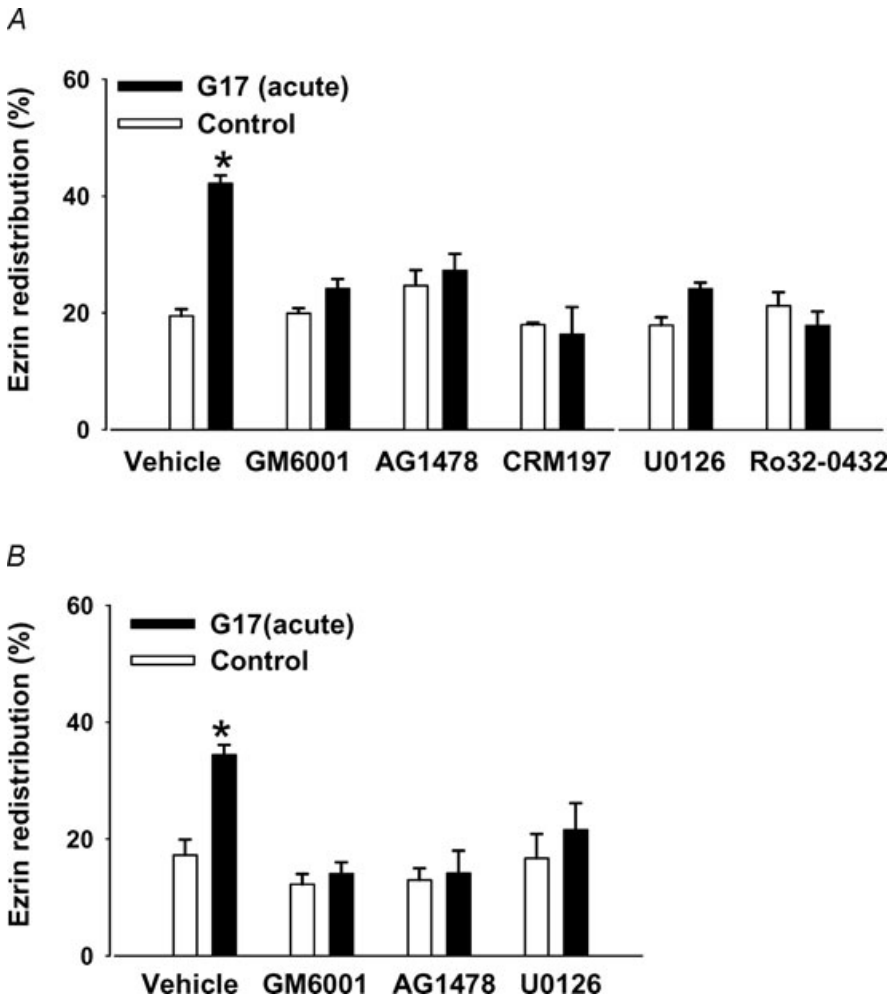

Figure 8. Protein kinase C and EGF receptor activation mediate the effects of gastrin
A, when cultured gastric glands from Gas-KO mice were treated with G17 (1 nM, 23 h) in serum-free medium, washed, and then incubated for 1 h in fresh medium containing gastrin [filled bars; 'G17 (acute)'], there was an increase in the proportion of the parietal cell population exhibiting ezrin distribution to large vesicular structures (*$P < 0.05$) compared with glands that were primed but then incubated with vehicle for 1 hour (open bars; 'control'). The response was absent when priming (but not the acute phase stimulation) was carried out in the presence of a metalloproteinase inhibitor GM6001 (12.5 μM), the EGF receptor tyrosine kinase inhibitor AG1478 (30 nM), the mutant diphtheria toxin CRM197 (1 μg ml^{-1}), the MEK inhibitor U0126 (10 μM) or the PKC inhibitor Ro-32-0432 (1 μM). *B*, when gastric glands from Gas-KO mice were primed *in vitro* with phorbol-12-myristate-13-acetate (PMA; 100 nM, 23 h) to stimulate PKC, washed, and then incubated in fresh medium containing gastrin [filled bars; 'G17 (acute)'], there was an increased proportion of parietal cells exhibiting ezrin redistribution (*$P < 0.05$) compared with glands that were primed but then incubated with vehicle for 1 h (open bars; 'control'). The response was absent when priming (but not the acute phase stimulation) was carried out in the presence of GM6001, AG1478 or U0126. Values are means + S.E.M., $n = 3$–5.

for example, been argued that the proliferative effects of gastrin in the gastric epithelium might be mediated by release of HB-EGF, amphiregulin or TGFα from parietal cells (Miyazaki *et al.* 1999; Wang *et al.* 2000; Dockray *et al.* 2001). In addition, though, it is well recognized that EGF-related peptides influence parietal cell function. In isolated canine parietal cells, EGF produces acute inhibition and chronic stimulation of acid secretion (Takeuchi *et al.* 1997). For the most part, these studies have not taken into account the possibility that EGF receptor transactivation might be downstream of gastrin and a component of the maturation of the parietal cells. The observation that inhibitors of the EGF receptor and of MAP kinase both blocked the effect of gastrin on parietal cell priming, and that EGF itself was sufficient for priming, is compatible with a role for this mechanism in parietal cell maturation. Moreover, studies involving inhibition of HB-EGF indicate that this mediator is at least partly involved in the priming action of gastrin.

As a whole, the present data indicate that the terminal differentiation of parietal cells involves the activation by gastrin of mechanisms involving ezrin expression and ezrin distribution. Further work will be required to determine the extent to which ezrin phosphorylation is implicated in the mechanisms described here. In any event, the relevant signalling events are distinct from those involved in the acute regulation of acid secretion. We consider it likely that ezrin is just one example of many proteins that are regulated by gastrin in immature parietal cells. Moreover, given that *in vivo* studies in Gas-KO mice implicate non-classical gastrins in maintaining the parietal cell phenotype, there will also need to be studies of the role of these signalling pathways (Chen *et al.* 2000). However, it is already clear that ezrin plays a key role in parietal cell function (Yao & Forte, 2003; Zhou *et al.* 2003; Tamura *et al.* 2005); our data now indicate that ezrin is functionally linked to gastrin-dependent maturation of these cells.

References

Agnew BJ, Duman JG, Watson CL, Coling DE & Forte JG (1999). Cytological transformations associated with parietal cell stimulation: critical steps in the activation cascade. *J Cell Sci* **112**, 2639–2646.

Aihara T, Fujishita T, Kanatani K, Furutani K, Nakamura E, Taketo MM, Matsui M, Chen D & Okabe S (2003). Impaired gastric secretion and lack of trophic responses to hypergastrinemia in M3 muscarinic receptor knockout mice. *Gastroenterology* **125**, 1774–1784.

Beltinger J, Hildebrand P, Drewe J, Christ A, Hlobil K, Ritz M, D'Amato M, Rovati L & Beglinger C (1999). Effects of spiroglumide, a gastrin receptor antagonist, on acid secretion in humans. *Eur J Clin Invest* **29**, 153–159.

Berglindh T, Helander H & Sachs G (1979). Secretion at the parietal cell level—a look at rabbit gastric glands. *Scand J Gastroenterol Suppl* **55**, 7–20.

Berglindh T & Obrink KJ (1976). A method for preparing isolated glands from the rabbit gastric mucosa. *Acta Physiol Scand* **96**, 150–159.

Black JW & Shankley NP (1987). How does gastrin act to stimulate oxyntic cell secretion. *Trends Pharmacol Sci* **8**, 486–490.

Booth C, Patel S, Bennion GR & Potten CS (1995). The isolation and culture of adult mouse colonic epithelium. *Epithelial Cell Biol* **4**, 76–86.

Bretscher A, Chambers D, Nguyen R & Reczek D (2000). ERM-Merlin and EBP50 protein families in plasma membrane organization and function. *Annu Rev Cell Dev Biol* **16**, 113–143.

Bretscher A, Edwards K & Fehon RG (2002). ERM proteins and merlin: integrators at the cell cortex. *Nat Rev Mol Cell Biol* **3**, 586–599.

Chen D, Zhao CM, Dockray GJ, Varro A, Van Hoek A, Sinclair NF, Wang TC & Koh TJ (2000). Glycine-extended gastrin synergizes with gastrin 17 to stimulate acid secretion in gastrin-deficient mice. *Gastroenterology* **119**, 756–765.

Chew CS (1994). Parietal cell culture: new models and directions. *Annu Rev Physiol* **56**, 445–461.

Chew CS, Zhou CJ & Parente JA Jr (1997). Ca^{2+}-independent protein kinase C isoforms may modulate parietal cell HCl secretion. *Am J Physiol Gastrointest Liver Physiol* **272**, G246–G256.

Chuan YC, Pang ST, Cedazo-Minguez A, Norstedt G, Pousette A & Flores-Morales A (2006). Androgen induction of prostate cancer cell invasion is mediated by ezrin. *J Biol Chem* **281**, 29938–29948.

Daulhac L, Kowalski-Chauvel A, Pradayrol L, Vaysse N & Seva C (1999). Src-family tyrosine kinases in activation of ERK-1 and p85/p110- phosphatidylinositol 3-kinase by G/CCKB receptors. *J Biol Chem* **274**, 20657–20663.

Delvalle J, Tsunoda Y, Williams JA & Yamada T (1992). Regulation of $[Ca^{2+}]_i$ by secretagogue stimulation of canine gastric parietal cells. *Am J Physiol Gastrointest Liver Physiol* **262**, G420–G426.

Dixit C & Dikshit M (2001). A flowcytometric method for evaluation of acid secretion from isolated rat gastric mucosal cells. *J Pharmacol Toxicol Methods* **45**, 47–53.

Dockray G, Dimaline R & Varro A (2005). Gastrin: old hormone, new functions. *Pflugers Arch* **449**, 344–355.

Dockray GJ (1999). Topical review. Gastrin and gastric epithelial physiology. *J Physiol* **518**, 315–324.

Dockray GJ, Varro A & Dimaline R (1996). Gastric endocrine cells: gene expression, processing, and targeting of active products. *Physiol Rev* **76**, 767–798.

Dockray GJ, Varro A, Dimaline R & Wang T (2001). The gastrins: their production and biological activities. *Annu Rev Physiol* **63**, 119–139.

Dransfield DT, Bradford AJ, Smith J, Martin M, Roy C, Mangeat PH & Goldenring JR (1997). Ezrin is a cyclic AMP-dependent protein kinase anchoring protein. *EMBO J* **16**, 35–43.

Dufner MM, Kirchhoff P, Remy C, Hafner P, Muller MK, Cheng SX, Tang LQ, Hebert SC, Geibel JP & Wagner CA (2005). The calcium-sensing receptor acts as a modulator of gastric acid secretion in freshly isolated human gastric glands. *Am J Physiol Gastrointest Liver Physiol* **289**, G1084–G1090.

Fahrmann M, Kaufhold M, Pfeiffer AF & Seidler U (2003). Protein kinase C-α attenuates cholinergically stimulated gastric acid secretion of rabbit parietal cells. *Br J Pharmacol* **139**, 545–554.

Fahrmann M, Kaufhold M, Rieg T & Seidler U (2002). Different actions of protein kinase C isoforms α and ε on gastric acid secretion. *Br J Pharmacol* **136**, 938–946.

Falk P, Roth KA & Gordon JI (1994). Lectins are sensitive tools for defining the differentiation programs of mouse gut epithelial cell lineages. *Am J Physiol Gastrointest Liver Physiol* **266**, G987–1003.

Forte TM, Machen TE & Forte JG (1977). Ultrastructural changes in oxyntic cells associated with secretory function: a membrane-recycling hypothesis. *Gastroenterology* **73**, 941–955.

Friis-Hansen L, Sundler F, Li Y, Gillespie PJ, Saunders TL, Greenson JK, Owyang C, Rehfeld JF & Samuelson LC (1998). Impaired gastric acid secretion in gastrin-deficient mice. *Am J Physiol Gastrointest Liver Physiol* **274**, G561–G568.

Hanzel D, Reggio H, Bretscher A, Forte JG & Mangeat P (1991). The secretion-stimulated 80K phosphoprotein of parietal cells is ezrin, and has properties of a membrane cytoskeletal linker in the induced apical microvilli. *EMBO J* **10**, 2363–2373.

Hegyi P, Gray MA & Argent BE (2003). Substance P inhibits bicarbonate secretion from guinea pig pancreatic ducts by modulating an anion exchanger. *Am J Physiol Cell Physiol* **285**, C268–C276.

Hegyi P, Rakonczay Z Jr, Gray MA & Argent BE (2004). Measurement of intracellular pH in pancreatic duct cells: a new method for calibrating the fluorescence data. *Pancreas* **28**, 427–434.

Herkenham M & Pert CB (1982). Light microscopic localization of brain opiate receptors: a general autoradiographic method which preserves tissue quality. *J Neurosci* **2**, 1129–1149.

Hersey SJ & Sachs G (1995). Gastric acid secretion. *Physiol Rev* **75**, 155–189.

Hinkle KL, Bane GC, Jazayeri A & Samuelson LC (2003). Enhanced calcium signaling and acid secretion in parietal cells isolated from gastrin-deficient mice. *Am J Physiol Gastrointest Liver Physiol* **284**, G145–G153.

Hussain I, Bate GW, Henry J, Djali P, Dimaline R, Dockray GJ & Varro A (1999). Modulation of gastrin processing by vesicular monoamine transporter type 1 (VMAT1) in rat gastrin cells. *J Physiol* **517**, 495–505.

Jain RN, Brunkan CS, Chew CS & Samuelson LC (2006). Gene expression profiling of gastrin target genes in parietal cells. *Physiol Genomics* **24**, 124–132.

Karam SM & Leblond CP (1992). Identifying and counting epithelial cell types in the "corpus" of the mouse stomach. *Anat Rec* **232**, 231–246.

Khan ZE, Wang TC, Cui G, Chi AL & Dimaline R (2003). Transcriptional regulation of the human trefoil factor, TFF1, by gastrin1. *Gastroenterology* **125**, 510–521.

Koh TJ, Goldenring JR, Ito S, Mashimo H, Kopin AS, Varro A, Dockray GJ & Wang TC (1997). Gastrin deficiency results in altered gastric differentiation and decreased colonic proliferation in mice. *Gastroenterology* **113**, 1015–1025.

Kovacs TO, Walsh JH, Maxwell V, Wong HC, Azuma T & Katt E (1989). Gastrin is a major mediator of the gastric phase of acid secretion in dogs: proof by monoclonal antibody neutralization. *Gastroenterology* **97**, 1406–1413.

Miyazaki Y, Shinomura Y, Tsutsui S, Zushi S, Higashimoto Y, Kanayama S, Higashiyama S, Taniguchi N & Matsuzawa Y (1999). Gastrin induces heparin-binding epidermal growth factor-like growth factor in rat gastric epithelial cells transfected with gastrin receptor. *Gastroenterology* **116**, 78–89.

Okamoto CT & Forte JG (2001). Vesicular trafficking machinery, the actin cytoskeleton, and H^+–K^+-ATPase recycling in the gastric parietal cell. *J Physiol* **532**, 287–296.

Prenzel N, Zwick E, Daub H, Leserer M, Abraham R, Wallasch C & Ullrich A (1999). EGF receptor transactivation by G-protein-coupled receptors requires metalloproteinase cleavage of proHB-EGF. *Nature* **402**, 884–888.

Sinclair NF, Ai W, Raychowdhury R, Bi M, Wang TC, Koh TJ & McLaughlin JT (2004). Gastrin regulates the heparin binding epidermal-like growth factor promoter via a PKC/EGFR dependent mechanism. *Am J Physiol Gastrointest Liver Physiol* **286**, G992–G999.

Soll AH (1978). The interaction of histamine with gastrin and carbamylcholine on oxygen uptake by isolated mammalian parietal cells. *J Clin Invest* **61**, 381–389.

Takeuchi Y, Yamada J, Yamada T & Todisco A (1997). Functional role of extracellular signal-regulated protein kinases in gastric acid secretion. *Am J Physiol Gastrointest Liver Physiol* **273**, G1263–G1272.

Tamura A, Kikuchi S, Hata M, Katsuno T, Matsui T, Hayashi H, Suzuki Y, Noda T, Tsukita S & Tsukita S (2005). Achlorhydria by ezrin knockdown: defects in the formation/expansion of apical canaliculi in gastric parietal cells. *J Cell Biol* **169**, 21–28.

Thomas JA, Buchsbaum RN, Zimniak A & Racker E (1979). Intracellular pH measurements in Ehrlich ascites tumor cells utilizing spectroscopic probes generated in situ. *Biochemistry* **18**, 2210–2218.

Todisco A, Takeuchi Y, Urumov A, Yamada J, Stepan VM & Yamada T (1997). Molecular mechanisms for the growth factor action of gastrin. *Am J Physiol Gastrointest Liver Physiol* **273**, G891–G898.

Urushidani T, Hanzel DK & Forte JG (1987). Protein phosphorylation associated with stimulation of rabbit gastric glands. *Biochim Biophys Acta* **930**, 209–219.

Varro A, Hemers E, Archer D, Pagliocca A, Haigh C, Ahmed S, Dimaline R & Dockray GJ (2002*a*). Identification of plasminogen activator inhibitor-2 as a gastrin-regulated gene: role of Rho GTPase and menin. *Gastroenterology* **123**, 271–280.

Varro A, Noble PJ, Wroblewski LE, Bishop L & Dockray GJ (2002*b*). Gastrin-cholecystokinin$_B$ receptor expression in AGS cells is associated with direct inhibition and indirect stimulation of cell proliferation via paracrine activation of the epidermal growth factor receptor. *Gut* **50**, 827–833.

Wang TC, Dangler CA, Chen D, Goldenring JR, Koh T, Raychowdhury R, Coffey RJ, Ito S, Varro A, Dockray GJ & Fox JG (2000). Synergistic interaction between hypergastrinemia and *Helicobacter* infection in a mouse model of gastric cancer. *Gastroenterology* **118**, 36–47.

Wroblewski LE, Noble PJ, Pagliocca A, Pritchard DM, Hart CA, Campbell F, Dodson AR, Dockray GJ & Varro A (2003). Stimulation of MMP-7 (matrilysin) by *Helicobacter pylori* in human gastric epithelial cells: role in epithelial cell migration. *J Cell Sci* **116**, 3017–3026.

Yao X, Cheng L & Forte JG (1996). Biochemical characterization of ezrin-actin interaction. *J Biol Chem* **271**, 7224–7229.

Yao X & Forte JG (2003). Cell biology of acid secretion by the parietal cell. *Annu Rev Physiol* **65**, 103–131.

Zavros Y, Rieder G, Ferguson A, Samuelson LC & Merchant JL (2002). Genetic or chemical hypochlorhydria is associated with inflammation that modulates parietal and G-cell populations in mice. *Gastroenterology* **122**, 119–133.

Zhou R, Cao X, Watson C, Miao Y, Guo Z, Forte JG & Yao X (2003). Characterization of protein kinase A-mediated phosphorylation of ezrin in gastric parietal cell activation. *J Biol Chem* **278**, 35651–35659.

Zhou R, Zhu L, Kodani A, Hauser P, Yao X & Forte JG (2005). Phosphorylation of ezrin on threonine 567 produces a change in secretory phenotype and repolarizes the gastric parietal cell. *J Cell Sci* **118**, 4381–4391.

Zhu L, Liu Y & Forte JG (2005). Ezrin oligomers are the membrane-bound dormant form in gastric parietal cells. *Am J Physiol Cell Physiol* **288**, C1242–C1254.

Acknowledgements

We are grateful to the Wellcome Trust and Medical Research Council for support. Dr David Spiller kindly helped with confocal microscopy, and Mike Samloff donated antibody to pepsinogen.

New Experimental Method to Study Acid/Base Transporters and Their Regulation in Lacrimal Gland Ductal Epithelia

Edit Tóth-Molnár,[1,2] *Viktória Venglovecz,*[2,3] *Béla Ózsvári,*[3] *Zoltán Rakonczay, Jr,*[3] *András Varró,*[4,5] *Julius G. Papp,*[4,5] *András Tóth,*[4] *János Lonovics,*[3] *Tamás Takács,*[3] *Imre Ignáth,*[3] *Béla Iványi,*[6] *and Péter Hegyi*[3,4]

Purpose. The main function of the lacrimal gland is to produce the most aqueous component of the tear film covering the surfaces of the cornea and the conjunctiva. Studies have been conducted that characterize the mixed fluid and protein secretion of isolated acini, but no methods have been developed to characterize lacrimal gland ductal cell (LGDC) secretion. Secretory mechanisms of ductal epithelia may play physiological roles in the maintenance of the standard environments for the cornea and the conjunctiva.

Methods. In this study, the authors developed a rapid method to isolate large quantities of intact lacrimal ducts. The preparation of isolated intact lacrimal gland ducts for the first time enabled the performance of real-time functional experiments on cleaned ducts. Electron microscopy and fluorescence measurements were used to evaluate the viability of lacrimal ducts.

Results. Fluorescence measurements showed that LGDCs express functionally active Na^+/H^+ exchanger (NHE) and Cl^-/HCO_3^- exchanger (AE). Parasympathomimetic stimulation by carbachol stimulated NHE and AE through the elevation of intracellular calcium concentration. This mechanism can play a role in the regulation of ion and water secretion by LGDCs.

Conclusions. The authors have described a lacrimal gland duct isolation technique in which the intact ducts remain viable and the role of duct cells in tear film secretion can be characterized. These data combined with the novel isolation facilitated understanding of the regulation mechanisms of ductal cell secretion at cellular and molecular levels under normal and pathologic conditions. (*Invest Ophthalmol Vis Sci.* 2007;48: 3746–3755) DOI:10.1167/iovs.06-1291

From the Departments of [1]Ophthalmology, [4]Pharmacology and Pharmacotherapy, and [6]Pathology, and the [3]First Department of Medicine, Faculty of Medicine, University of Szeged, Szeged, Hungary; and the [5]Division of Cardiovascular Pharmacology, Hungarian Academy of Sciences, Szeged, Hungary.

[2]These authors contributed equally to the work presented here and should therefore be regarded as equivalent authors.

Supported by Hungarian Scientific Research Fund Grants T43066 (JL), PF6395 (ZR), and NI61902 (AV), Bolyai Postdoctoral Fellowships 00276/04 (PH) and 00218/06 (ZR), and Agency for Research Fund Management and Research Exploitation (KPI) Research Grant KPI/BIO-37 (AV).

Submitted for publication October 26, 2006; revised January 25 and March 20, 2007; accepted May 8, 2007.

Disclosure: **E. Tóth-Molnár**, None; **V. Venglovecz**, None; **B. Ózsvári**, None; **Z. Rakonczay, Jr**, None; **A. Varró**, None; **J.G. Papp**, None; **A. Tóth**, None; **J. Lonovics**, None; **T. Takács**, None; **I. Ignáth**, None; **B. Iványi**, None; **P. Hegyi**, None

The publication costs of this article were defrayed in part by page charge payment. This article must therefore be marked "*advertisement*" in accordance with 18 U.S.C. §1734 solely to indicate this fact.

Corresponding author: Péter Hegyi, University of Szeged, Faculty of Medicine, First Department of Medicine, P.O. Box 469, H-6701, Szeged, Hungary; hep@in1st.szote.u-szeged.hu.

The function of the lacrimal gland is to produce the preocular component of the tear film covering the surfaces of the cornea and the conjunctiva. This secreted fluid, which contains proteins, ions, and water, is essential for maintaining healthy, normal function of the ocular surface. When tear secretion decreases in amount or changes in composition, dry eye syndrome (keratoconjunctivitis sicca) can develop and, in the worst case, can induce corneal ulceration and vascularization leading to serious visual impairment.[1,2]

As do all exocrine glands, such as the pancreas and the submandibular gland, the lacrimal gland has three major cell types—acinar, ductal, and myoepithelial (surrounding acinar and ductal cells).[3,4] Preocular tear film is mostly secreted by acini and ductal cells. Because of the convenient accessibility of the external end of the lacrimal gland duct, the preocular tear has been characterized in detail using tear-collecting techniques in which the main duct is cannulated and the secreted fluid is collected.[5]

Methods have been published by which proteins and fluids secreted by the acini can be studied.[6] In principle, the gland is removed and minced into small pieces. These pieces undergo enzymatic digestion, resulting in small groups of acini or single acinar cells.[7] These techniques are mostly used for animal studies. However, some investigators have also isolated acini from human lacrimal gland biopsy specimens or cadavers.[8,9] Despite the large number of studies on the whole lacrimal gland and acini, less is known about the lacrimal gland ductal cell (LGDC).[10,11] Ubels et al.[11] have recently described a laser capture microdissection technique for cDNA microarray analysis and immunohistochemistry using frozen lacrimal gland, but no methods have been developed to characterize the LGDC secretion in viable ductal cells. Nevertheless, the secretory mechanisms of ductal epithelia may play a physiological role in the maintenance of the standard environment of the cornea and the conjunctiva. More important, the failure of ion and water secretion, as may occur in dry eye syndrome or in cystic fibrosis,[12,13] has serious consequences for the integrity of the cornea and can lead to potentially sight-threatening disease that diminishes the patient's quality of life. Therefore, it is imperative to separate the functions of acini and ductal cells in the secretion of preocular tear. Better understanding of LGDC secretion at the cellular and molecular levels under normal and pathologic conditions may help in the development of drugs that stimulate tear secretion in patients with dry eye.

Our aims in this study were to develop a method to isolate lacrimal ducts, to make it possible to obtain more information on the regulation of lacrimal gland epithelial tissue, and to characterize LGDC acid/base ion transporters (mediating fluid secretion).

Materials and Methods

Ethics

All experiments were conducted in compliance with the National Institutes of Health Guide for the Care and Use of Laboratory Animals

Investigative Ophthalmology & Visual Science, August 2007, Vol. 48, No. 8

and with the ARVO Statement for the Use of Animals in Ophthalmic and Vision Research. In addition, the experimental protocol was approved by the local ethical board of the University of Szeged, Hungary.

Solutions and Chemicals

The standard HEPES-buffered solution contained 130 mM NaCl, 5 mM KCl, 1 mM $CaCl_2$, 1 mM $MgCl_2$, 10 mM [SCAP]D-glucose, and 10 mM Na-HEPES. The Na^+-free HEPES-buffered solution contained 140 mM NMDG-Cl, 5 mM KCl, 1 mM $CaCl_2$, 1 mM $MgCl_2$, 10 mM [SCAP]D-glucose, and 10 mM HEPES-acid. The ammonium pulse HEPES-buffered solution contained 110 mM NaCl, 20 mM NH_4Cl, 5 mM KCl, 1 mM $CaCl_2$, 1 mM $MgCl_2$, 10 mM D-glucose, and 10 mM Na-HEPES. The Cl^--free HEPES solution contained 140 mM Na-gluconate, 2.5 mM K-sulfate, 6 mM Ca-gluconate, 1 mM Mg-gluconate, 10 mM [SCAP]D-glucose, and 10 mM Na-HEPES. The high K^+-HEPES-buffered solution contained 130 mM KCl, 5 mM NaCl, 1 mM $CaCl_2$, 1 mM $MgCl_2$, 10 mM [SCAP]D-glucose, 10 mM Na-HEPES, and 0.01 mM nigericin. HEPES-buffered solutions were gassed with 100% O_2, and their pH was set to 7.4 with NaOH or HCl at 37°C. The standard HCO_3^--buffered solution contained 115 mM NaCl, 25 mM $NaHCO_3$, 5 mM KCl, mM 1 $CaCl_2$, mM 1 $MgCl_2$, and 10 mM D-glucose. The ammonium pulse HCO_3^--buffered solution contained 95 mM NaCl, 20 mM NH_4Cl, 25 mM $NaHCO_3$, 5 mM KCl, 1 mM $CaCl_2$, 1 mM $MgCl_2$, and 10 mM [SCAP]D-glucose. The Na^+-free HCO_3^--buffered solution contained 115 mM NMDG-Cl, 5 mM KCl, 1 mM $CaCl_2$, 1 mM $MgCl_2$, 10 mM [SCAP]D-glucose, 25 mM choline-HCO_3^-, and 0.01 mM atropine, and pH was set to 8.0 with HCl. The Cl^--free HCO_3^- solution contained 115 mM Na-gluconate, 25 mM $NaHCO_3$, 2.5 mM K-sulfate, 6 mM Ca-gluconate, 1 mM Mg-gluconate, and 10 mM D-glucose. HCO_3^--buffered solutions were gassed with 95% O_2/5% CO_2 to set pH to 7.4 at 37°C. Cell and tissue adhesive was obtained from Becton Dickinson Labware (Cell Tak; Bedford, MA). 2.7-bis-(2-carboxyethyl)-5-(and-6-)carboxyfluorescein, acetoxymethyl ester (BCECF-AM), FURA 2AM, and 4,4′-diisothiocyanodihydrostilbene-2,2′-disulfonate (H_2DIDS) were obtained from Molecular Probes (Eugene, OR). BCECF was dissolved in dimethyl sulfoxide (DMSO), and FURA 2AM was dissolved in DMSO containing 20% Pluronic acid. Nigericin was dissolved in absolute ethanol, and amiloride was dissolved in DMSO. All other chemicals were obtained from Sigma-Aldrich (Budapest, Hungary).

Solutions and Chemicals for Isolation

Chromatographically pure collagenase was obtained from Worthington (Lakewood, NJ). Ingredients for culture medium (Dulbecco modified Eagle medium [DMEM], McCoy 5A medium modified [McCoy 5A], fetal calf serum, glutamine, and bovine serum albumin) were from Sigma-Aldrich. The isolation solution contained DMEM supplemented with 100 U/mL collagenase and 1 mg/mL bovine serum albumin. The storage solution contained DMEM and 3% (wt/vol) bovine serum albumin. The culture solution contained McCoy 5A tissue culture medium, 10% (vol/vol) fetal calf serum, and 2 mM glutamine.

Preparation of Micropipettes

Micropipettes were prepared for transferring ducts after isolation. Glass tubes were obtained from Drummond Scientific Company (Broomall, PA) and were pulled by a vertical pipette puller (Technical Product International Inc., St. Louis, MO) from glass tubing (inside diameter, 0.075 inch; outside diameter, 0.090 inch). Inside diameters of tips were between 50 and 150 μm.

Animals

Adult male New Zealand White rabbits weighing 2 to 2.5 kg were sedated with 50 mg/kg pentobarbital and humanely killed by cervical dislocation. Superotemporal and inferotemporal portions of the conjunctival fornices were dissected after wide temporal canthotomy. The eyeball was then dislocated inferonasally, and the temporal part of the orbital connective tissues were excised using stereomicroscopy. The preparation procedure revealed the main lobes of the lacrimal gland under the roof of the orbit, which were removed by gentle pressure with forceps and final separation with scissors. Both intraorbital lacrimal glands were carefully dissected.

Isolation Process

Intraorbital lacrimal glands were dissected as described above and were transferred to a sterile, small, flat-bottom glass Erlenmeyer flask containing cold (4°C) storage solution, as described, to minimize damage to the cells. Then the glands were placed on a 4°C sterile glass plate. First, the glands were trimmed of fat and then 1 mL isolation solution was injected into the interstitium of the glands using 26-gauge × 0.5-inch (0.45 × 12 mm) medical stainless steel needles (Braun Melsungen AG, Melsungen, Germany). Microinjected glands were cut into small pieces using a razor blade and were transferred, using Pasteur pipettes, to a glass flask containing 2 mL isolation solution. The flask was briefly gassed with 100% O_2 and was incubated in a shaking water bath (80 cyc/min) at 37°C for 25 minutes. After incubation, the isolation solution was removed, and 5 mL fresh cold storage solution was added to the flask. Digested tissue was washed two more times with storage solution to minimize the amount of collagenase in the solution. Finally, the tissue was transferred to a disposable 10 mL polycarbonate tube and was kept at 4°C until microdissection.

Tissue sample suspension was transferred, using a Pasteur pipette, to a glass microscope slide and viewed under a stereo microscope (Jencons-PLS; Nikon, Grinstead, UK) equipped with a cold-light source. Intralobular and interlobular ducts were microdissected under 50× magnification with 26-gauge × 0.5 inch (0.45 × 12 mm) medical stainless steel needles. Isolated ducts were aspirated into a micropipette (described in Methods) and transferred to a Petri dish containing storage solution. After 20 to 30 minutes, the tissue sample was discarded and replaced by a fresh cold piece of tissue. Fifteen to 25 ducts were isolated from each animal.

Culturing

After microdissection, intact lacrimal gland ducts were transferred to a polycarbonate hydrophilic membrane (10-μm pore size; Whatman International Ltd., Kent, UK) placed on top of the culture solution in a Petri dish. Ducts were cultured overnight in a 37°C incubator gassed with 5% CO_2/95% air.

Transmission Electron Microscopy

For electron microscopic studies, ducts were fixed in 2.5% glutaraldehyde immediately after isolation. Samples were then postfixed in 1% osmium tetroxide, dehydrated in a series of graded ethanols, and subsequently embedded in epoxy resin. Ultrathin sections were contrasted with uranyl acetate and lead citrate. Tissue sections were analyzed under a transmission electron microscope (CM10; Philips, Eindhoven, The Netherlands; Fig. 1).

Intracellular pH Measurement

Cultured lacrimal ducts were attached, using an adhesive (Cell Tak; Becton Dickinson Labware), to a coverslip (24 mm) forming the base of a perfusion chamber mounted on a microscope (Olympus, Budapest, Hungary). Ducts were bathed in standard HEPES solution at 37°C and loaded with the pH-sensitive fluorescent dye BCECF-AM (2 μM) for 20 to 30 minutes Thereafter, the ducts were continuously perfused with solutions at a rate of 4 to 5 mL/min. Intracellular pH (pH_i) was measured using an imaging system (Cell; Olympus). Four to five small areas (regions of interest [ROIs]) of 5 to 10 cells each in an intact duct were excited with light at wavelengths of 490 nm and 440 nm, and the 490/440 fluorescence emission ratio was measured at 535 nm (Fig. 2). One pH_i measurement was recorded per second. In situ calibration of the fluorescence signal was performed using the high K^+-nigericin technique.[14,15] During calibration, ducts were bathed in high K^+-

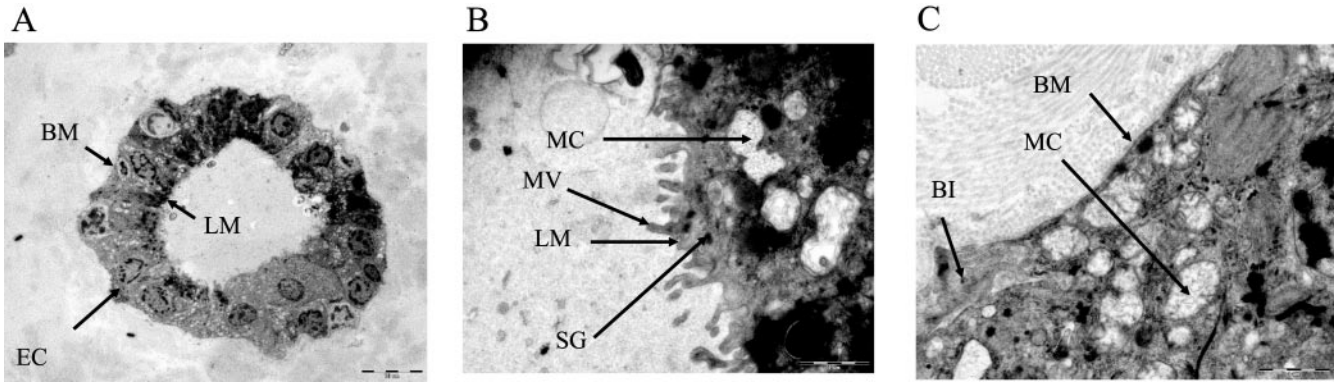

FIGURE 1. Electron micrographs of intact lacrimal ducts that had been maintained in culture for 24 hours. (**A**) Horizontal sections of isolated ducts. LM, luminal membrane; BM, basolateral membrane; EC, epithelial cell. (**B**) Luminal side of the lacrimal duct. MC, mitochondria; MV, microvilli; SG, secretory granule. (**C**) Basolateral side of the lacrimal duct. BI, basolateral interdigitation.

HEPES solution containing 10 μM nigericin, and extracellular pH was stepped between 5.95 and 8.46.[15] Initial rates of pH_i recovery (over the first 30 seconds) were calculated by linear regression analysis.

Measurement of Intracellular Ca^{2+} Concentration

Cultured lacrimal ducts were attached to a coverslip and mounted on an microscope (Olympus), as described above. The ducts were bathed in standard HEPES solution at 37°C and loaded with the Ca^{2+}-sensitive fluorescent dye FURA 2AM (4–5 μM) for 60 minutes. After loading, the ducts were continuously perfused with solutions at a rate of 4 to 5 mL/min. Changes in intracellular Ca^{2+} concentration ($[Ca^{2+}]_i$) were measured using an imaging system (Cell; Olympus). Four to 5 small ROIs of 5 to 10 cells in each intact duct were excited with light at wavelengths of 340 nm and 380 nm, and the 380/340 fluorescence emission ratio was measured at 510 nm (see Fig. 5). One $[Ca^{2+}]_i$ measurement was obtained per second.

Statistical Analysis

Results are expressed as mean ± SEM (n = 3–6 ducts/10–30 ROIs). Statistical analyses were performed using ANOVA. $P \leq 0.05$ was accepted as significant.

RESULTS

Morphology of Isolated Ducts

Ultrastructural examination revealed that small ducts were characterized by numerous microvilli in the apical regions, tight junctions, secretory granules, mitochondria, and basolateral infoldings (interdigitations) of the cell membrane and basement membrane in the basal region (Fig. 1). Cells were relatively rich in vesicles and secretory granules (Fig. 1). Figure 2A shows an isolated interlobular duct attached to a coverslip, as described in Methods. Lumen (L), epithelial cells (ECs), and connective tissue (CT) are visible. This figure confirms that acini-free epithelial cells can be chosen for data recordings (ROI).

pH Regulation in Lacrimal Gland Ductal Epithelia

In the first series of experiments, we wanted to determine the resting pH_i of LGDC. Ducts were exposed to standard HEPES solution (pH 7.4), followed by an 8-minute exposure to a high-K^+-HEPES solution (pH 7.28) and then to an 8-minute

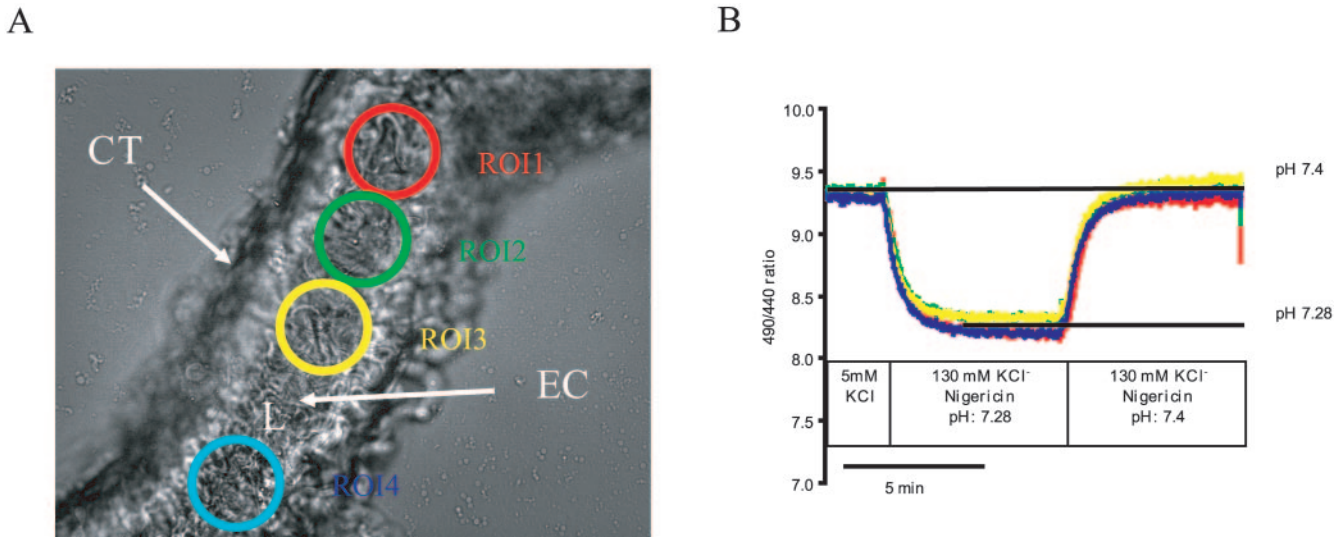

FIGURE 2. Resting pH_i of lacrimal ductal epithelial cells. Cultured lacrimal ducts were attached to a coverslip. (**A**) Four to five small areas (ROIs) of 5 to 10 cells each in an intact duct were excited with light at wavelengths of 490 nm and 440 nm, and the 490:440 fluorescence emission ratio was measured at 535 nm. CT, connective tissue; EC, epithelial cell; L, lumen. (**B**) Ducts were exposed to nigericin/high K^+-HEPES solutions of pH 7.28 and 7.4. Because of the relatively short time course of the experiment, the resting pH_i was calculated from this two-point calibration by using the classic linear model. In this particular experiment, the pH_i was 7.4, and the resting pH_i of five ducts (22 ROIs) was 7.40 ± 0.01.

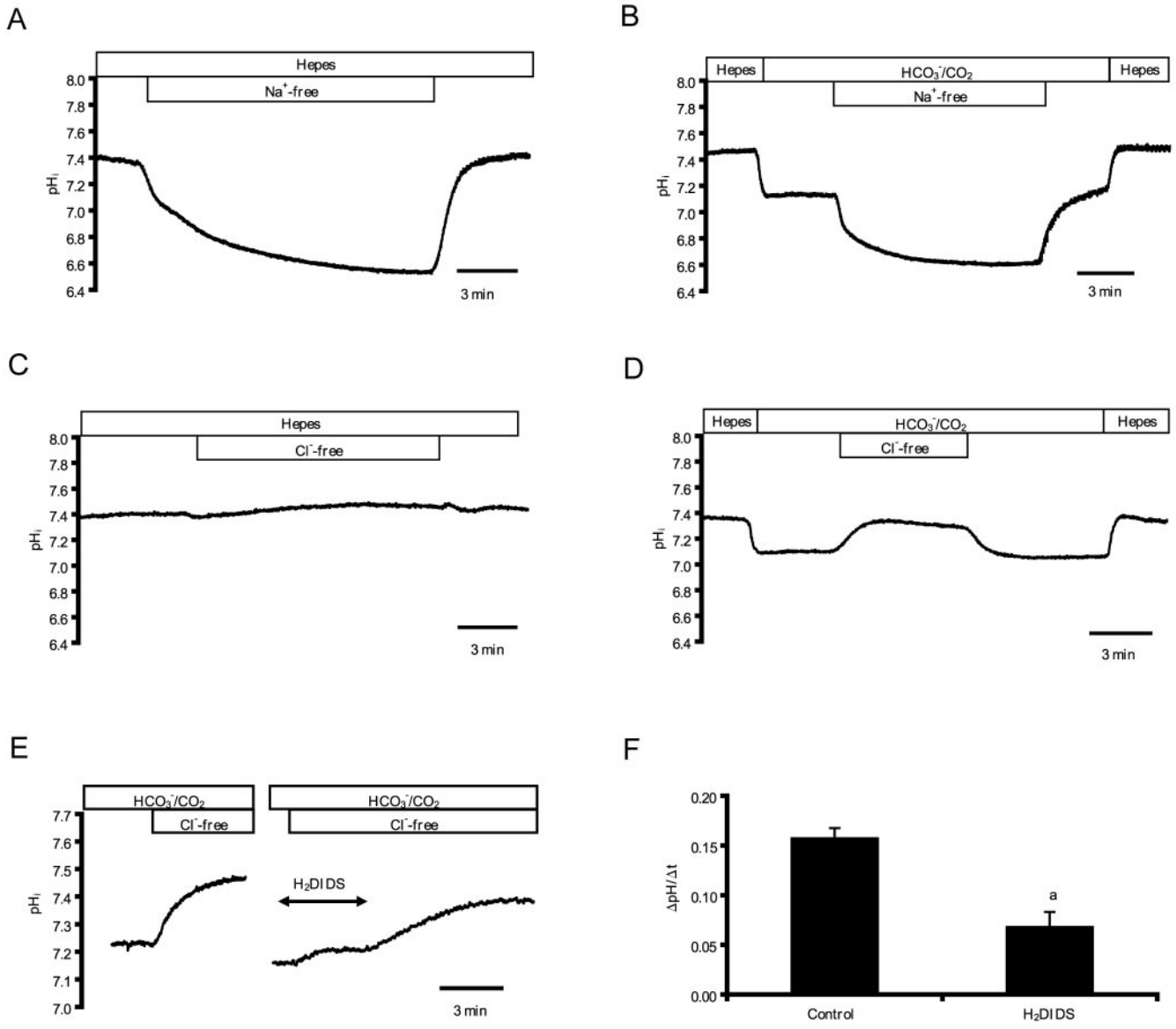

FIGURE 3. Effect of removal and readdition of extracellular Na^+ and Cl^- with and without HCO_3^-/CO_2 on pH_i in lacrimal ductal epithelial cells. (**A**) Removal of Na^+ resulted in rapid, reversible acidification of pH_i. (**B**) Standard HCO_3^-/CO_2 solution caused rapid acidification of pH_i by the diffusion of CO_2 into the cells. Removal of Na^+ resulted in the same range of acidification as in (**A**). (**C**) Removal of Cl^- from the HCO_3^--free (HEPES) solution resulted in small, reversible alkalization of pH_i, whereas in an HCO_3^--containing solution (**D**), this pH_i change was enhanced. Traces are representative of three experiments for each protocol. (**E**). Removal of Cl^- from the standard HCO_3^-/CO_2 solution resulted in an alkalization of pH_i. H_2DIDS (250 μM) strongly inhibited this alkalization, and this inhibitory effect of H_2DIDS was, at least in part, reversible. (**F**). Summary of the calculated initial rates of alkalization ($\Delta pH/\Delta t$) from (**E**) are shown. Mean ± SE for 14 ROIs of 3 ducts are shown. $^aP < 0.05$.

exposure to a high-K^+-HEPES solution (pH 7.4). We used the classical linear model[14,15] to determine the resting pH_i. The resting pH_i level of five ducts (22 ROIs) was found to be 7.40 ± 0.01. The resting pH_i of LGDCs was virtually the same, confirming that the experimental conditions could be kept constant for pH_i experiments (Fig. 2B).

Na^+/H^+ Exchanger (NHE). In this series of experiments, we tested whether isolated lacrimal glands were suitable for functional experiments. Na^+/H^+ transport proteins that mediate the electroneutral exchange of Na^+ and H^+ ions were examined. Removal of Na^+ from the standard HEPES solution caused rapid and marked intracellular acidosis (0.20 ± 0.01 pH U/min; $n = 3$ ducts/15 ROIs; Fig. 3A). Adding Na^+ back to the solution resulted in complete pH_i recovery. Because the solution did not contain HCO_3^-, this finding confirms the presence of an Na^+-dependent H^+ efflux mechanism on the basolateral side of each LGDC. Removal of Na^+ from the HCO_3^-/CO_2-containing solution also caused mark acidification (0.22 ± 0.04 pH U/min; $n = 3$ ducts/15 ROIs; (Fig. 3B).

Na^+/HCO_3^- Cotransporter (NBC). We also tested whether LGDCs express a functionally active Na^+-dependent HCO_3^- transporter on the basolateral membrane (Fig. 3B). The administration of basolateral HCO_3^-/CO_2 rapidly and greatly decreased pH_i. This marked change in pH_i could be explained by the quick diffusion of CO_2 into the cytoplasm. A small pH_i recovery (0.04 ± 0.02 pH U/min; $n = 6$ ducts/30 ROIs) was found after acidification, suggesting the marginal role of HCO_3^- efflux into the lacrimal duct cells.

Cl^-/HCO_3^- Exchange Activity. To test the activity of the Cl^-/HCO_3^- exchange mechanisms, we used the Cl^- removal technique in the presence and absence of HCO_3^- ions. In the absence of HCO_3^-, Cl^- removal caused a small reversible

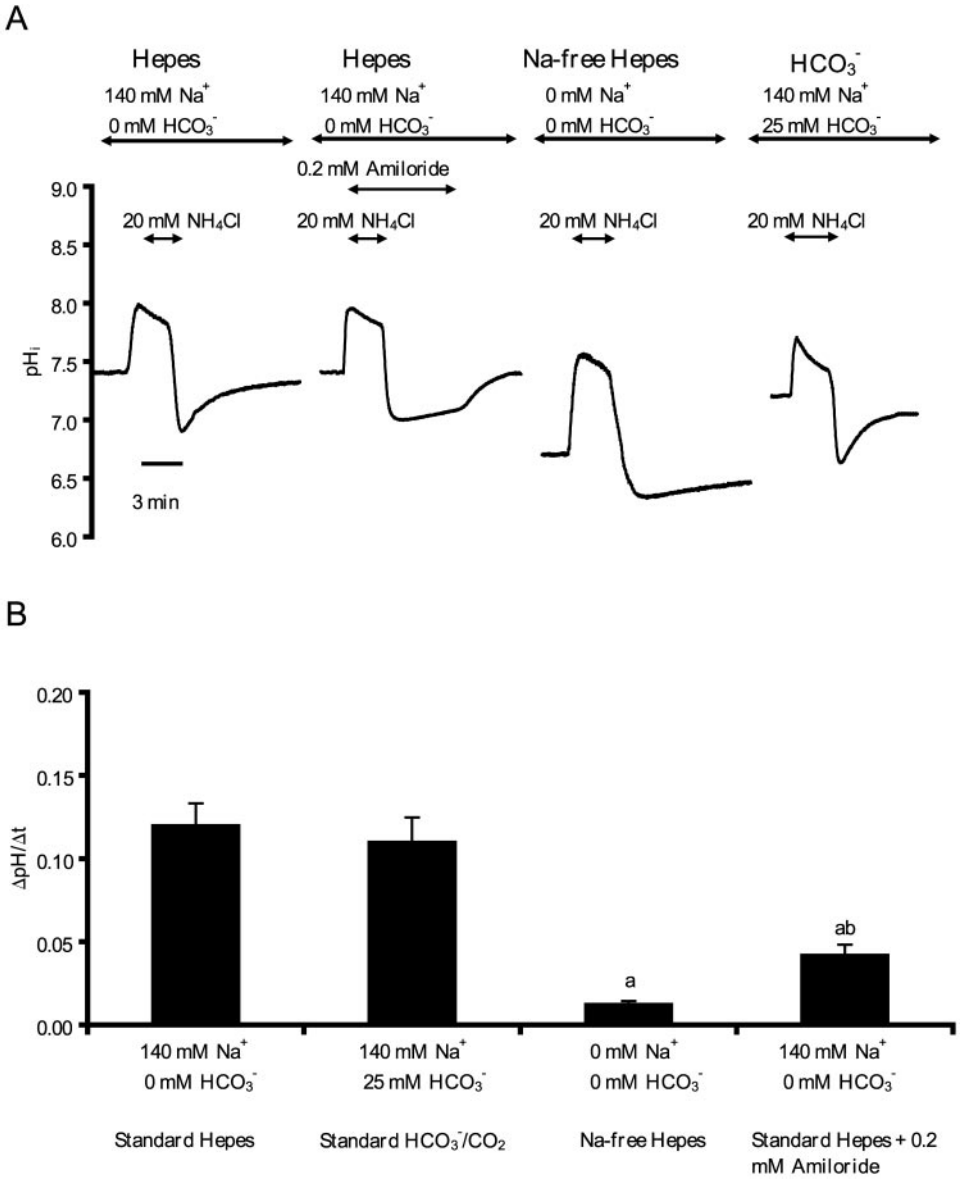

FIGURE 4. Recovery of pH_i after an acid load. (**A**) Duct cells were acid loaded by a 3-minute exposure to 20 mM NH_4Cl, followed by its sudden withdrawal. Initial rates of pH_i recovery from the acid load (over the first 30 seconds) were calculated in each experiment. All experiments were performed at 37°C using a standard HEPES solution with or without Na^+ or HCO_3^-/CO_2, respectively. Each experiment was performed on a different duct. (**B**) Summary of the calculated initial rate of recovery ($\Delta pH/\Delta t$) from (**A**) are shown. Effects of different solutions (HCO_3^--free, Na^+-free, or both) and the NHE inhibitor, amiloride, are shown. Mean ± SE for 30 ROIs of 6 ducts are shown. $^aP < 0.001$. $^bP < 0.05$.

alkalization in LGDC (Fig. 3C; 0.020 ± 0.002 pH U/min), suggesting the small availability of HCO_3^- ions in the cytoplasm. However, in standard HCO_3^- solution, significantly higher alkalization was observed (0.16 ± 0.02 pH U/min, respectively). In addition, the anion exchange inhibitor H_2DIDS (250 μM) significantly inhibited $\Delta pH/\Delta t$ (Figs. 3E, 3F; 0.067 ± 0.015 pH U/min). These results confirmed functionally active Cl^-/HCO_3^- exchange mechanisms on the basolateral membranes of LGDCs.

pH_i Recovery from Alkali and Acid Load

An alternative method for characterizing these transporters is the ammonium-pulse technique.[16] Administration of 20 mM NH_4Cl initially increases pH_i because of the rapid entry of NH_3 into the cell. Recovery from alkali load may reflect the activity of the Cl^-/HCO_3^- exchanger (AE).[16] Removal of NH_4Cl causes the typical acidic undershoot of pH_i (Fig. 4A). Transporters (if present in LGDCs) most likely involved in the recovery process from acidosis are the basolateral Na^+/HCO_3^- cotransporter, the Na^+/H^+ exchanger, and the H^+ pump.

Recovery ($\Delta pH/\Delta t$) from alkali load was significantly higher in the presence of HCO_3^- (0.049 ± 0.004 pH U/min and 0.08 ± 0.001 pH U/min, respectively), suggesting an active Cl^-/HCO_3^- exchanger.

Recovery from acid load was 0.12 ± 0.01 pH U/min in standard HCO_3^- solution (containing Na^+ and HCO_3^-/CO_2). The absence of HCO_3^- did not significantly change the rate of recovery (0.11 ± 0.015 pH U/min). However, the removal of Na^+ from the HEPES solution significantly decreased recovery from acid load to 0.012 ± 0.002 pH U/min by switching off the NHE. The small remaining recovery from acid load may represent an active proton pump in LGDCs. Finally, we tested the NHE inhibitor amiloride (0.2 mM). Amiloride administration greatly inhibited the NHE (0.04 ± 0.01 pH U/min) located on the basolateral membranes of LGDCs. Furthermore, the removal of amiloride immediately turned on the NHE, suggesting the reversible effect of amiloride.

Ca^{2+} Signaling during Parasympathomimetic Stimulation

Parasympathetic neurotransmitters acetylcholine (ACh) and vasoactive intestinal peptide are potent stimuli of lacrimal gland secretion[17] and have been shown to act through the intracel-

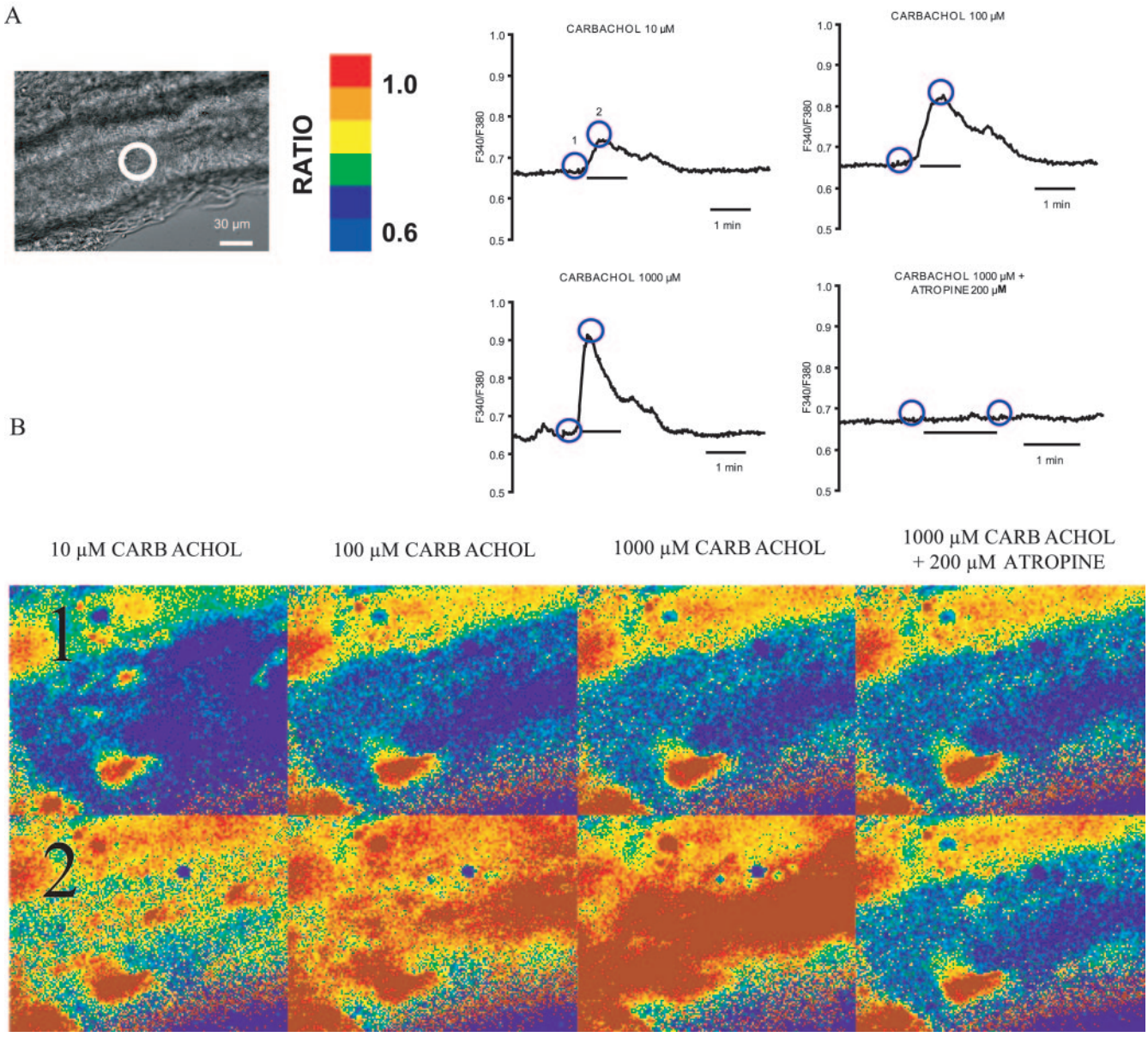

FIGURE 5. Effects of carbachol on intracellular Ca^{2+} concentration in lacrimal gland ductal epithelial cells. (**A**) Cultured lacrimal ducts were attached to a coverslip. A representative duct is shown. Carbachol (10, 100, and 1000 μM) was administered to duct cells. Carbachol dose dependently elevated $[Ca^{2+}]_i$. Each experiment was performed on the same duct using a 10-minute washout period between the pulses. Representative curves are shown. Maximal $[Ca^{2+}]_i$ elevation was observed 2 ± 0.5 seconds after stimulation. Data were taken from the ROI marked in the image. Similar results were obtained when the experiments were performed on different ducts (n = 3). (**B**) Typical patterns of $[Ca^{2+}]_i$ changes in an intact duct perfused with different concentrations of carbachol. Increase in $[Ca^{2+}]_i$ is denoted by a change from a cold color (*blue*) to a warmer color (*yellow* to *red*; see color scale at the top). Pictures 1 and 2 were taken at the times indicated by the *circles* in (**A**). Bar, 30 μm.

lular Ca^{2+} signaling pathway. Parasympathomimetic carbachol was administered to LGDCs in three different doses (10, 100, and 1000 μM; Fig. 5). Carbachol dose dependently stimulated intracellular Ca^{2+} signaling in LGDCs (F/F_0 14% ± 0.1%, 20% ± 0.1%, and 39 ± 0.1%, respectively, for the three different doses), suggesting the importance of this pathway in water and ion secretion. Parasympatholytic atropine (0.2 mM) completely blocked the stimulatory effect of carbachol (1 mM).

Effects of Carbachol on NHE and AE

Administration of 1 mM carbachol significantly elevated the pH_i in standard HEPES solution (containing Na^+ and Cl^- but not HCO_3^-; Fig. 6A). However, this elevation was not observed in an Na^+-free HEPES solution (Fig. 6B). Because HCO_3^- was absent, the alkalization in the Na^+-containing solution must have been the result of a stimulated Na^+-dependent H^+ efflux mechanism through the NHE (Fig. 6A). When the LGDCs were treated with 1 mM carbachol in standard HCO_3^- solution, a small pH_i elevation was observed (Fig. 6C). However, this brief alkalization (most likely caused by the stimulation of an NHE) was followed by acidification. Importantly, this acidification was absent in a Cl^--free HCO_3^- solution, suggesting that this decrease in pH_i was caused by a Cl^--dependent HCO_3^- efflux mechanism through a Cl^-/HCO_3^- exchanger (Fig. 6D). These data indicate that carbachol stimulates Na^+ and Cl^- influx into the cell through the basolateral membrane of the LGDC. Parasympatholytic atropine (0.2 mM) totally blocked the stimulatory effect of 1 mM carbachol (Fig. 6E).

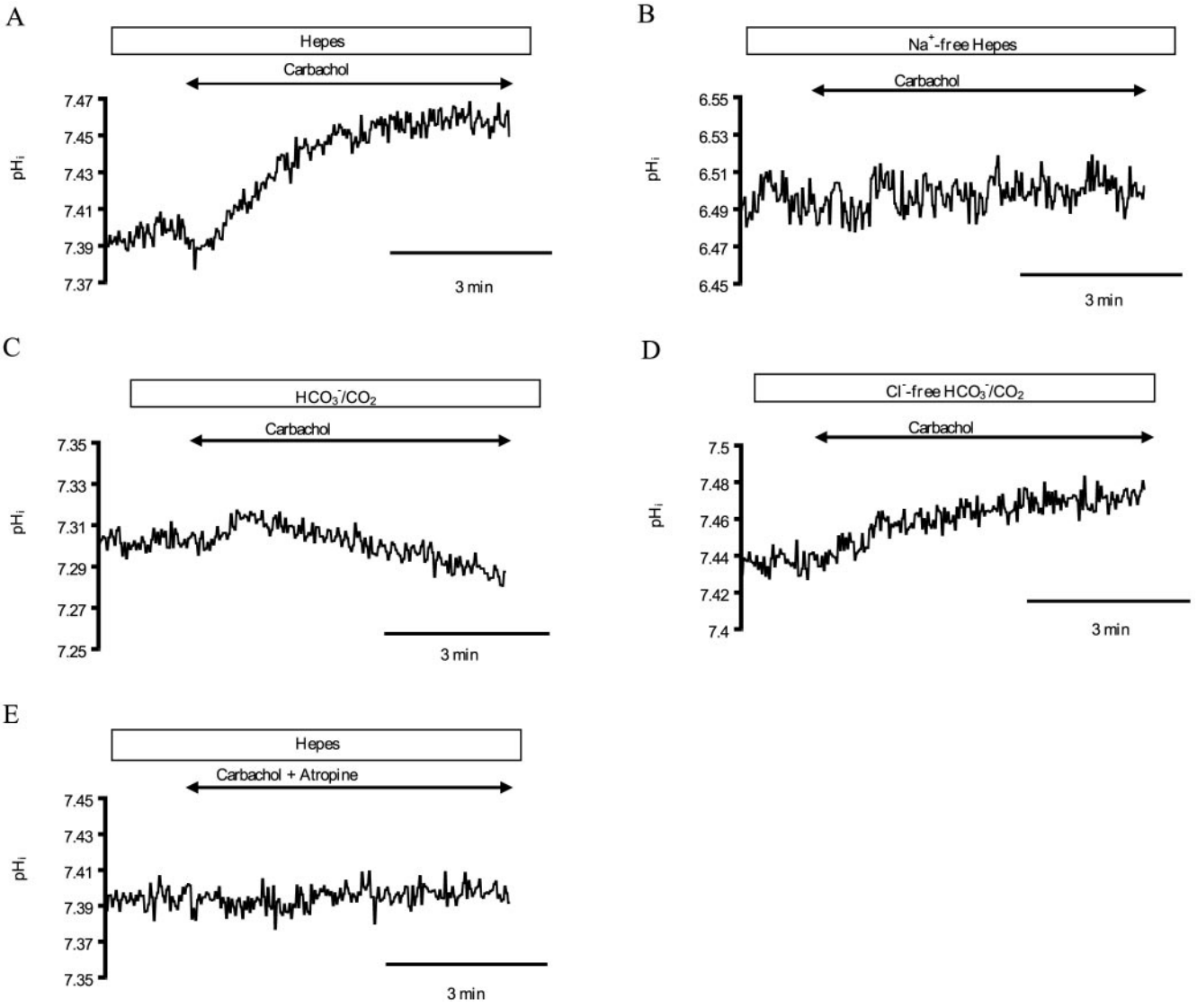

FIGURE 6. Effects of carbachol on pH_i. Carbachol (1 mM) was administered to duct cells in (**A**) standard HEPES solution (containing Na^+ and Cl^-, but no HCO_3^-), (**B**) Na^+-free HEPES solution (containing Cl^- but no Na^+ or HCO_3^-), (**C**) standard HCO_3^-/CO_2 solution (containing Na^+, Cl^-, and HCO_3^-), or (**D**) Cl^--free HCO_3^-/CO_2 solution (containing Na^+ and HCO_3^- but no Cl^-). (**E**) Carbachol (1 mM) and 200 μM atropine were administered to duct cells in standard HEPES solution (containing Na^+ and Cl^- but no HCO_3^-). Alkalization of pH_i was only observed in Na^+-containing solutions (**A**, **C**, **D**). Acidification of pH_i was observed only in a Cl^- and HCO_3^--containing solution (**C**).

To confirm this hypothesis, we analyzed the recoveries from acid and alkali load using the ammonium pulse technique. Figure 7 shows a representative trace of the experiments. We found that 1 mM carbachol significantly stimulated NHE (recovery from acid load in an HCO_3^--free solution; Figs. 7A, 7B). No differences were observed in the recovery from alkali load in a HCO_3^--free (HEPES) solution. However, when the experiments were performed in standard HCO_3^- solution, the AE (recovery from alkali load; Fig. 7C) was stimulated by 1 mM carbachol. As we found earlier, atropine (0.2 mM) totally blocked the stimulatory effect of carbachol on the NHE and AE (data not shown).

DISCUSSION

Lacrimal gland secretion consists of two fractions derived from acinar and ductal cells. The regulation of ion and water secretion has been well investigated in intact glands,[17] but no available method has been described to study the role of LGDCs in the process of lacrimal fluid secretion. The preocular tear secreted by the lacrimal gland contains Na^+, Cl^-, and K^+ in high concentrations. This lacrimal gland fluid contains 42 ± 4 mM K^+, 107 ± 4 mM Na^+, 126 ± 5 mM Cl^- in rabbit[18]; 46 ± 3 mM K^+, 135 ± 5 mM Na^+, 123 ±1 mM Cl^- in rat[19]; and 38 ± 5 mM K^+, 144 ± 5 mM Na^+, 149 ± 16 mM Cl^- in mouse.[7] Ductal epithelia, at least in part, must be involved in this hypertonic fluid secretion.

In other secretory glands, such as the pancreas, duct isolation techniques have been described,[20] and the secretion by acini and ductal cells can therefore be studied separately. In the present study, we developed an isolation technique suitable for investigating the ion transporters of LGDCs and the regulation of fluid secretion. The microdissection technique was similar to what we used in the pancreas.[15,16] However, because the connective tissue sticks to the lacrimal ducts more strongly than in the pancreas, isolation takes more time and fewer ducts can be isolated.

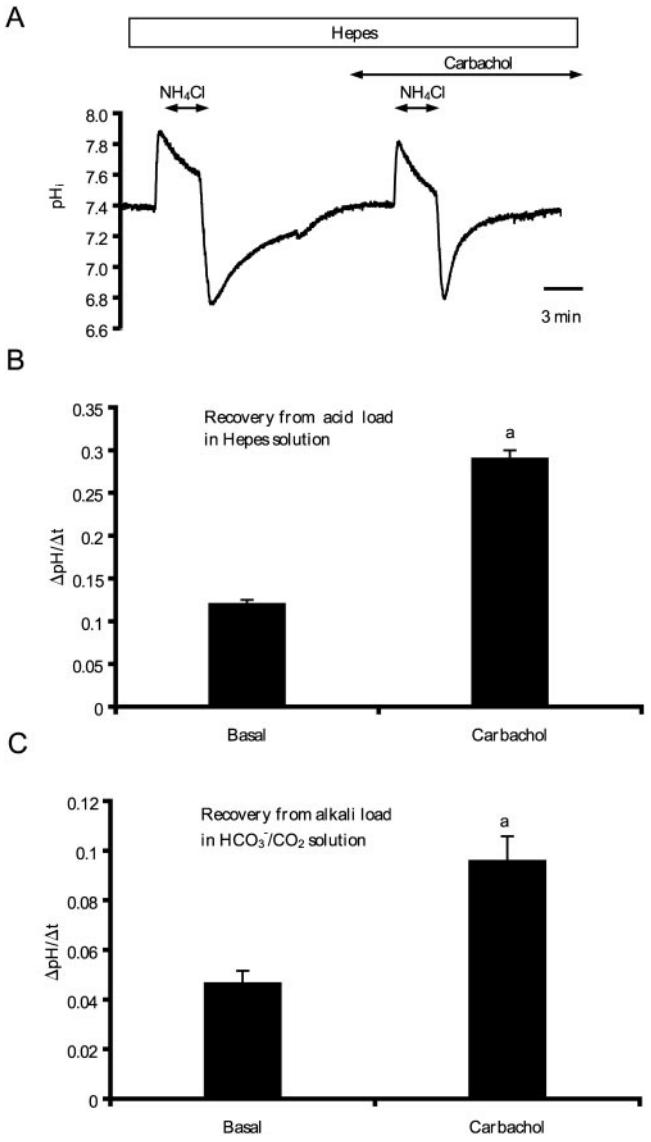

FIGURE 7. Effects of carbachol on recovery from acid and alkali load. Duct cells were exposed to a 3-minute, 20-mM NH_4Cl pulse, followed by its sudden withdrawal. Initial rates of pH_i recovery from the acid and alkali load (over the first 30 seconds) were calculated in each experiment. Carbachol (1 mM) was administered from 7 minutes before the NH_4Cl pulse. All experiments were performed at 37°C. Each experiment was performed on a different duct. (**B**) Summary of the calculated initial rates of recovery ($\Delta pH/\Delta t$) from acid load (**A**). Experiments were performed in standard HEPES solution (without HCO_3^-). (**C**) Summary of the calculated initial rates of recovery ($\Delta pH/\Delta t$) from alkali load in standard HCO_3^-/CO_2 solution.

The regulation of pH_i in epithelial cells is important because most of the biological processes (e.g., water and ion secretion) are pH sensitive.[21] Epithelial cells have a polarized membrane that is able to transport acid/base equivalents through the cell.[21] Therefore, to show the viability of isolated and cultured interlobular lacrimal ducts, we characterized the most common acid/base transporters.

Our results showed the functional presence of an Na^+-dependent but HCO_3^--independent H^+ efflux mechanism (most probably through NHEs) on LGDCs. Amiloride partially inhibited this Na^+/H^+ exchange mechanism. However, we must note that this K^+-sparing diuretic can also inhibit electrogenic Na^+ channels[22] and the Na^+/Ca^{2+} exchanger.[23] Given that NHE1 and NHE2 are the most sensitive to amiloride inhibition and NHE3 and NHE4 are amiloride resistant,[24] our results indicate that approximately 66% of the functionally active NHEs are NHE1 and NHE2 isoforms.

Many epithelial cells express proton pumps[25] and NBC,[26] which, in addition to other physiological roles, can protect epithelial cells from acidosis. We demonstrated that NBC ion transporters, if present, have only a marginal role in the pH_i regulation of LGDCs. After CO_2-induced acidosis, only a small amount of HCO_3^- entry was detected (Fig. 3B). Furthermore, no difference was found in the regeneration after acid load caused by an ammonium pulse between the presence and absence of HCO_3^-. Removal of Na^+ decreased this recovery by 93% in HEPES solution, suggesting a functionally very active Na^+-dependent H^+ efflux mechanism.

We also detected a functionally active Cl^--dependent HCO_3^- efflux mechanism in LGDCs. When HCO_3^- was absent from the solution, Cl^- removal only caused a small pH_i change, suggesting reduced HCO_3^- concentration inside the cell. However, when HCO_3^- was present in the solution, Cl^- removal caused a marked pH_i elevation. We found that the classic and defining inhibitor of SLC4 family AE1-AE4,[27,28] H_2DIDS, strongly inhibited the Cl^--dependent HCO_3^- efflux mechanism. AE1 has been identified in rat lacrimal ducts.[11] Thus far, however, no other AEs have been confirmed in lacrimal ductal epithelium.

We also tested whether the isolated and cultured ducts are suitable for studying the regulation of LGDC secretion. The main function of the lacrimal gland is to secrete water, electrolytes, and proteins onto the eye surface. The relative contribution of acinar cells and LGDCs to this secretion is yet to be determined. Regulation of lacrimal gland secretion can be mediated by neurotransmitters (e.g., ACh) and growth factors (e.g., endothelial growth factor family).[29] Activation of muscarinic receptors by ACh released from parasympathetic nerves stimulates lacrimal gland secretion. The glandular subtype of M3 muscarinic receptors have been identified in the lacrimal gland.[30] It is more than likely that the ductal epithelia are involved in the hypersecretory effect of parasympathetic stimulation. We tested the effect of carbachol on the intracellular Ca^{2+} signaling using the Ca^{2+}-sensitive fluorescence dye FURA 2AM. Our results showed that carbachol dose dependently increased $[Ca^{2+}]_i$.

Finally, we investigated the effects of parasympathetic stimulation on the acid/base transporters of LGDCs and found that carbachol strongly stimulates NHE activity, hence driving Na^+ into the cell. This stimulation is followed by the activation of the AE on the basolateral membrane, which drives Cl^- into the LGDC. Na^+ and Cl^- influxes require H^+ and HCO_3^- inside the cell; they become available after the dehydration of carbonic acid (H_2CO_3) by carbonic anhydrase.[31]

The stimulatory effects of carbachol on NHE and AE have been shown in lacrimal acinar cells,[32,33] indicating that there must be other differences in ion transport mechanisms on the basolateral membranes between the acinar cells and LGDCs. Na^+/K^+ ATPase expression is three to five times higher on duct cells than on acinar cells.[34] Therefore, elevated intracellular Na^+ concentration after parasympathetic activation may stimulate the basolateral Na^+/K^+ ATPase, which increases the intracellular K^+ concentration in LGDC. Our data suggest that Na^+/K^+ ATPase may be a crucial basolateral transporter in the mechanisms of K^+ secretion in LGDCs. After the intracellular accumulation of K^+ and Cl^-, these ions can be secreted through a coupled mechanism (K^+/Cl^- cotransporter)[11] or through a separate K^+-selective cation channel ($IK_{Ca}1$, BK_{Ca}, or both) and a Cl^- selective anion channel (cystic fibrosis transmembrane conductance regulator[CFTR], chloride channel [ClC], or both; Fig. 8).

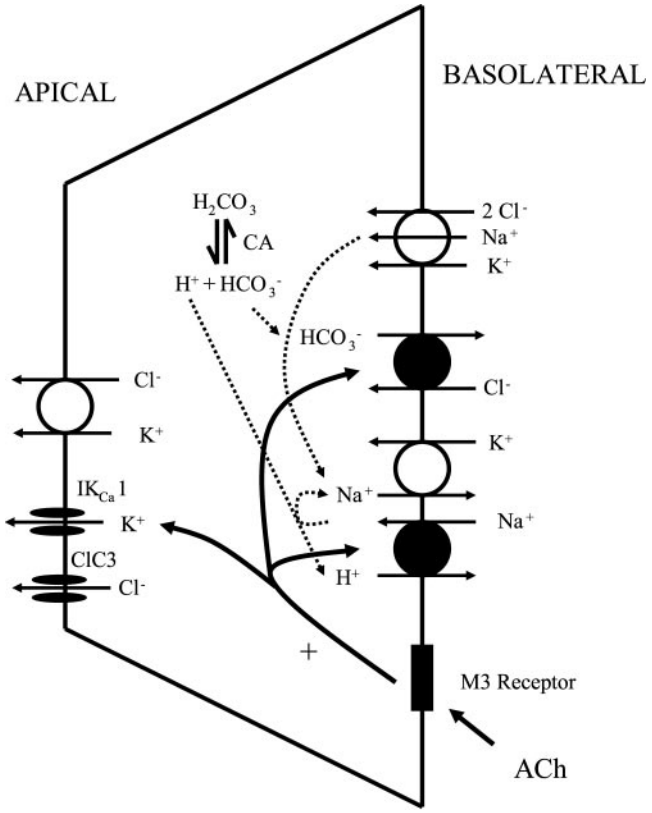

FIGURE 8. Model for secretion of K^+ and Cl^- by LGDCs. The model is based on the channels and transporters identified by Ubels et al.[11] and the functionally active acid/base transporters characterized in this study. Parasympathomimetic stimulation by carbachol strongly stimulates NHE activity, followed by the activation of AE on the basolateral membrane through Ca^{2+} signaling that drives Na^+ and Cl^- into the LGDCs. Cl^- and Na^+ influx requires available H^+ and HCO_3^- inside the cell, generated from the dehydration of carbonic acid (H_2CO_3) by carbonic anhydrase.[31] The elevated intracellular Na^+ concentration can be exchanged for K^+ through the basolateral Na^+/K^+ ATPase, which increases the intracellular K^+ concentration in LGDCs. The elevated intracellular Ca^{2+} concentration can also activate $IK_{Ca}1$. CA, carbonic anhydrase; $IK_{Ca}1$, calcium-activated potassium channel.

Taken together, we described a lacrimal gland duct isolation technique in which the intact ducts remain viable and in which the role of duct cells in preocular tear film secretion can be characterized. We also added new insights into the regulation of lacrimal gland ductal secretion. Our data and our new isolation method open up the possibility of understanding the physiological and pathophysiological (such as dry eye syndrome or keratoconjuctivitis sicca) roles of the lacrimal gland ductal system. Furthermore, our results may lead to the development of drugs that stimulate preocular tear secretion in patients with dry eye syndrome.

References

1. Hemady R, Chu W, Foster CS. Keratoconjunctivitis sicca and corneal ulcers. *Cornea*. 1990;9:170–173.
2. Golubovic S, Parunovic A. Corneal perforation in dry eye patients. *Fortschr Ophthalmol*. 1987;84:33–37.
3. Martin CL, Munnell J, Kaswan R. Normal ultrastructure and histochemical characteristics of canine lacrimal glands. *Am J Vet Res*. 1988;49:1566–1572.
4. Millar TJ, Herok G, Koutavas H, Martin DK, Anderton PJ. Immunohistochemical and histochemical characterisation of epithelial cells of rabbit lacrimal glands in tissue sections and cell cultures. *Tissue Cell*. 1996;28:301–312.
5. Jones DT, Monroy D, Pflugfelder SC. A novel method of tear collection: comparison of glass capillary micropipettes with porous polyester rods. *Cornea*. 1997;16:450–458.
6. Rios JD, Ferdman D, Tepavcevic V, Hodges R, Zoukhri D, Dartt DA. Role of Ca^{2+} and protein kinase C in cholinergic, and alpha1-adrenergic agonists and EGF stimulated mitogen-activated protein kinase activity in lacrimal gland. *Adv Exp Med Biol*. 2002;506:185–190.
7. Walcott B, Birzgalis A, Moore LC, Brink PR. Fluid secretion and the Na^+-K^+-2Cl^- cotransporter in mouse exorbital lacrimal gland. *Am J Physiol Cell Physiol*. 2005;289:C860–C867.
8. Paulsen F, Langer G, Hoffmann W, Berry M. Human lacrimal gland mucins. *Cell Tissue Res*. 2004;316:167–177.
9. Yoshino K, Tseng SC, Pflugfelder SC. Substrate modulation of morphology, growth, and tear protein production by cultured human lacrimal gland epithelial cells. *Exp Cell Res*. 1995;220:138–151.
10. Saito Y, Kuwahara S. Effect of acetylcholine on the membrane conductance of the intralobular duct cells of the rat exorbital lacrimal gland. *Adv Exp Med Biol*. 1994;350:87–92.
11. Ubels JL, Hoffman HM, Srikanth S, Resau JH, Webb CP. Gene expression in rat lacrimal gland duct cells collected using laser capture microdissection: evidence for K^+ secretion by duct cells. *Invest Ophthalmol Vis Sci*. 2006;47:1876–1885.
12. Castagna I, Roszkowska AM, Fama F, Sinicropi S, Ferreri G. The eye in cystic fibrosis. *Eur J Ophthalmol*. 2001;11:9–14.
13. Mrugacz M, Zak J, Bakunowicz-Lazarczyk A, Wysocka J, Minarowska A. Flow cytometric analysis of HLA-DR antigen in conjunctival epithelial cells of patients with cystic fibrosis. *Eye*. 2006; May 19 (E-pub ahead of print).
14. Thomas JA, Buchsbaum RN, Zimniak A, Racker E. Intracellular pH-measurements in Ehrlich ascites tumor cells utilizing spectroscopic probes generated in situ. *Biochemistry*. 1979;18:2210–2218.
15. Hegyi P, Rakonczay Z Jr, Gray MA, Argent BE. Measurement of intracellular pH in pancreatic duct cells: a new method for calibrating the fluorescence data. *Pancreas*. 2004;28:427–434.
16. Hegyi P, Gray MA, Argent BE. Substance P inhibits bicarbonate secretion from guinea-pig pancreatic ducts by modulating an anion exchanger. *Am J Physiol Cell Physiol*. 2003;285:C268–C276.
17. Hodges RR, Dartt DA. Regulatory pathways in lacrimal gland epithelium. *Int Rev Cytol*. 2003;231:129–196.
18. Botelho SY, Martinez EV. Electrolytes in lacrimal gland fluid and in tears at various flow rates in the rabbit. *Am J Physiol*. 1973;225:606–609.
19. Alexander JH, van Lennep EW, Young JA. Water and electrolyte secretion by the exorbital lacrimal gland of the rat studied by micropuncture and catheterization techniques. *Pflugers Arch*. 1972;337:299–309.
20. Argent BE, Arkle S, Cullen MJ, Green R. Morphological, biochemical and secretory studies on rat pancreatic ducts maintained in tissue culture. *Q J Exp Physiol*. 1986;71:633–648.
21. Boron WF. Intracellular pH regulation in epithelial cells. *Annu Rev Physiol*. 1986;48:377–388.
22. Koyama K, Sasaki I, Naito H, et al. Induction of epithelial Na^+ channel in rat ileum after proctocolectomy. *Am J Physiol*. 1999;276:G975–G984.
23. Romero JR, Rivera A, Lanca V, Bicho MD, Conlin PR, Ricupero DA. Na^+/Ca^{2+} exchanger activity modulates connective tissue growth factor mRNA expression in transforming growth factor beta1- and Des-Arg10-kallidin-stimulated myofibroblasts. *J Biol Chem*. 2005;15:280:14378–14384.
24. Kiela PR, Ghishan FK. Na^+-H^+ exchange in mammalian digestive tract. *Physiology of the Gastrointestinal Tract*. 4th ed. Johnson LR, ed. Burlington, MA: Elsevier Academic Press; 2006:1847–1881.
25. Zhao H, Star RA, Muallem S. Membrane localization of H^+ and HCO_3^- transporters in the rat pancreatic duct. *J Gen Physiol*. 1994;104:57–85.
26. Soleimani M, Burnham CE. Na^+:$HCO(_3^-)$ cotransporters (NBC): cloning and characterization. *J Membr Biol*. 2001;183:71–84.

27. Alper SL. The band 3-related anion exchanger (AE) gene family. *Annu Rev Physiol*. 1991;53:549–564.
28. Ko SB, Luo X, Hager H, et al. AE4 is a DIDS-sensitive Cl^-/HCO_3^- exchanger in the basolateral membrane of the renal CCD and the SMG duct. *Am J Physiol Cell Physiol*. 2002;283:C1206–C1218.
29. Dartt DA. Regulation of lacrimal gland secretion by neurotransmitters and the EGF family of growth factors. *Exp Eye Res*. 2001;73:741–752.
30. Mauduit P, Jammes H, Rossignol B. M3 muscarinic acetylcholine receptor coupling to PLC in rat exorbital lacrimal acinar cells. *Am J Physiol Cell Physiol*. 1993;264:C1550–C1560.
31. Ogawa Y, Toyosawa S, Inagaki T, Hong SS, Ijuhin N. Carbonic anhydrase isozyme VI in rat lacrimal gland. *Histochem Cell Biol*. 1995;103:387–394.
32. Lambert RW, Maves CA, Mircheff AK. Carbachol-induced increase of Na^+/H^+ antiport and recruitment of Na^+,K^+-ATPase in rabbit lacrimal acini. *Curr Eye Res*. 1993;12:539–551.
33. Lambert RW, Bradley ME, Mircheff AK. pH-Sensitive anion exchanger in rat lacrimal acinar cells. *Am J Physiol*. 1991;260:G517–G523.
34. Okami T, Yamamoto A, Takada T, Omori K, Uyama M, Tashiro Y. Ultrastructural localization of Na^+,K^+-ATPase in the exorbital lacrimal gland of rat. *Invest Ophthalmol Vis Sci*. 1992;33:196–204.

Effects of bile acids on pancreatic ductal bicarbonate secretion in guinea pig

V Venglovecz, Z Rakonczay, Jr, B Ózsvári, et al.

Gut 2008 57: 1102-1112 originally published online February 26, 2008
doi: 10.1136/gut.2007.134361

Effects of bile acids on pancreatic ductal bicarbonate secretion in guinea pig

V Venglovecz,[1] Z Rakonczay Jr,[1] B Ózsvári,[1] T Takács,[1] J Lonovics,[1] A Varró,[2,3] M A Gray,[4] B E Argent,[4] P Hegyi[1,2]

See Commentary, p 1037

► Additional figures are published online only at http://gut.bmj.com/content/vol57/issue8

[1] First Department of Medicine, University of Szeged, Szeged, Hungary; [2] Department of Pharmacology and Pharmacotherapy, University of Szeged, Szeged, Hungary; [3] Division for Cardiovascular Pharmacology, Hungarian Academy of Sciences, Szeged, Hungary; [4] Epithelial Research Group, Institute for Cell and Molecular Biosciences, Newcastle University, Newcastle upon Tyne, UK

Correspondence to: Dr Péter Hegyi, University of Szeged, Faculty of Medicine, First Department of Medicine, PO Box 427, H-6701, Szeged, Hungary; hep@in1st.szote.u-szeged.hu

Revised 8 February 2008
Accepted 15 February 2008
Published Online First 26 February 2008

ABSTRACT

Background and aims: Acute pancreatitis is associated with significant morbidity and mortality. Bile reflux into the pancreas is a common cause of acute pancreatitis and, although the bile can reach both acinar and ductal cells, most research to date has focused on the acinar cells. The aim of the present study was to investigate the effects of bile acids on HCO_3^- secretion from the ductal epithelium.

Methods: Isolated guinea pig intralobular/interlobular pancreatic ducts were microperfused and the effects of unconjugated chenodeoxycholate (CDC) and conjugated glycochenodeoxycholate (GCDC) on intracellular calcium concentration ($[Ca^{2+}]_i$) and pH (pH_i) were measured using fluorescent dyes. Changes of pH_i were used to calculate the rates of acid/base transport across the duct cell membranes.

Results: Luminal administration of a low dose of CDC (0.1 mM) stimulated ductal HCO_3^- secretion, which was blocked by luminal H_2DIDS (dihydro-4,4′-diisothiocyanostilbene-2,2′-disulfonic acid). In contrast, both luminal and basolateral administration of a high dose of CDC (1 mM) strongly inhibited HCO_3^- secretion. Both CDC and GCDC elevated $[Ca^{2+}]_i$, and this effect was blocked by BAPTA-AM (1,2-bis(*o*-aminophenoxy)ethane-*N*,*N*,*N*′,*N*′-tetra-acetic acid), caffeine, xestospongin C and the phospholipase C inhibitor U73122. BAPTA-AM also inhibited the stimulatory effect of low doses of CDC on HCO_3^- secretion, but did not modulate the inhibitory effect of high doses of CDC.

Conclusions: It is concluded that the HCO_3^- secretion stimulated by low concentrations of bile acids acts to protect the pancreas against toxic bile, whereas inhibition of HCO_3^- secretion by high concentrations of bile acids may contribute to the progression of acute pancreatitis.

The close relationship between the passage of a gallstone and the development of acute pancreatitis has been known for nearly a hundred years,[1] and has been confirmed in a number of studies.[2–4] However, the pathogenesis underlying the development of acute pancreatitis is not well understood. Exposure of the pancreas to bile acids is considered to be one of the possible causes of acute pancreatitis. Since the pancreatic and bile ducts share a common outflow into the duodenum, obstruction of the ampulla of Vater may cause bile to penetrate into the pancreatic duct, exposing the pancreas to bile acids.[1]

Although the bile can reach both acinar and ductal cells during biliary pancreatitis, much more research has been done on acinar cells. Bile acids have been shown to induce Ca^{2+} signalling in pancreatic acinar cells via an inositol trisphosphate (IP_3)-dependent mobilisation of intracellular Ca^{2+} and an inhibition of SERCA (sarco/endoplasmic reticulum Ca^{2+} ATPase)-dependent Ca^{2+} reloading into intracellular pools.[5 6] The elevated intracellular Ca^{2+} concentration ($[Ca^{2+}]_i$) can lead to enzyme activation[7] and/or cell death,[8] and result in severe acute necrotising pancreatitis. These data suggest that Ca^{2+} toxicity could be an important factor contributing to bile acid-induced cellular damage.

To date, researchers have mostly examined the permeability and morphology of the ductal cells following the administration of bile acids. High doses (1–15 mM) make the ducts permeable to molecules as large as 20 000 Da, whereas they are normally impermeable to molecules over 3000 Da.[9] Bile acids in millimolar concentrations also decrease the transepithelial resistance of dog pancreatic ductal cells.[10] In addition, the permeability of the pancreatic ductal epithelium to HCO_3^- and Cl^- is increased by exposure to various bile salts at concentrations within the range normally found in the duodenum.[11] Although one of the main functions of the pancreatic ductal epithelium is to secrete the HCO_3^- ions found in pancreatic juice,[12] no data are available on the effects of bile acids on HCO_3^- secretion. However, it has been shown that retrograde injection of Na-taurocholate into the rat pancreatic duct induces fluid hypersecretion and decreases protein output in the initial phase of acute pancreatitis.[13] We believe that the pancreatic ductal epithelium is at least partly involved in the hypersecretory effect of bile acids, which may represent a defence mechanism against bile acids in order to avoid pancreatic injury. The aim of this study was to characterise the effects of bile acids on pancreatic ductal HCO_3^- secretion. We performed our experiments on intact isolated guinea pig pancreatic ducts, because the guinea pig pancreas secretes a juice containing ~140 mM $NaHCO_3$, as does the human gland.[12]

MATERIALS AND METHODS

Ethics

All experiments were conducted in compliance with the *Guide for the care and use of laboratory animals* (USA NIH publication No 85-23, revised 1985). In addition, the experimental protocol was approved by the local Ethical Board of the University of Szeged, Hungary.

Solutions and chemicals

The compositions of the solutions used are shown in Table 1. HEPES-buffered solutions were gassed

with 100% O_2 and their pH was set to 7.4 with NaOH or HCl at 37°C. HCO_3^--buffered solutions were gassed with 95% O_2/5% CO_2 to set the pH to 7.4 at 37°C. Chromatographically pure collagenase was purchased from Worthington (Lakewood, New Jersey, USA). CellTak was obtained from Becton Dickinson Labware (Bedford, Massachusetts, USA). 2,7-Bis-(2-carboxyethyl)-5-(and-6-)carboxyfluorescein, acetoxymethyl ester (BCECF-AM), 5-oxazolecarboxylic, 2-(6-(bis(carboxymethyl) amino)-5-(2-(2-(bis(carboxymethyl)amino)-5-methylphenoxy)-ethoxy)-2-benzofuranyl)-5-oxazolecarboxylic acetoxymethyl ester (FURA 2-AM), dihydro-4,4′-diisothiocyanostilbene-2,2′-disulfonic acid (H_2DIDS) and 1,2-bis(o-aminophenoxy)ethane-*N*,*N*,*N*′,*N*′-tetraacetic acid (BAPTA-AM) were from Molecular Probes (Eugene, Oregon, USA). Bile acids and all other chemicals were obtained from Sigma-Aldrich (Budapest, Hungary).

Isolation and culture of the ducts

Small intralobular/interlobular ducts were isolated from the pancreas of guinea pigs weighing 150–250 g. The guinea pig was humanely killed by cervical dislocation, the pancreas removed and intralobular/interlobular ducts were isolated as described previously.[14] The ducts were cultured overnight in a 37°C incubator gassed with 5% CO_2/95% air.

Microperfusion

The lumen of the cultured ducts was microperfused using a modification of the method described by Ishiguro *et al*.[15] Two concentric pipettes were used. One end of a sealed duct was cut off and the other end was aspirated into the outer, holding pipette. Then, whilst applying a negative pressure to the holding pipette with a syringe, the inner perfusion pipette was gently advanced into the duct lumen. The duct was then perfused at a rate of 10–30 µl/min, with the luminal perfusate flowing out at the open end. The high rate of bath perfusion (5–6 ml/min), which was in the same direction as the flow of luminal perfusate, ensured that the escaping luminal perfusate did not gain access to the basolateral surface of the duct cells. Replacement of the luminal perfusate took up to 2 min.

Measurement of intracellular pH and Ca^{2+} concentration

Intacellular pH (pH_i) was estimated using the pH-sensitive fluorescent dye BCECF-AM. Briefly, ducts were bathed in standard HEPES solution at 37°C and loaded with the membrane-permeable acetoxymethyl derivative of BCECF (2 µmol/l) for 20–30 min. After loading, the ducts were continuously perfused with solutions at a rate of 5–6 ml/min. pH_i was measured using a Cell^R imaging system (Olympus, Budapest, Hungary). Four to five small areas (region of interests (ROIs)) of 5–10 cells in each intact duct were excited with light at wavelengths of 490 and 440 nm, and the 490/440 fluorescence emission ratio was measured at 535 nm. One pH_i measurement was obtained per second. In situ calibration of the fluorescence signal was performed using the high K^+-nigericin technique.[16 17]

Measurement of $[Ca^{2+}]_i$ was performed using the same method except that the cells were loaded with the Ca^{2+}-sensitive fluorescent dye FURA 2-AM (5 µmol/l) for 60 min. For excitation, 340 and 380 nm filters were used, and the changes in $[Ca^{2+}]_i$ were calculated from the fluorescence ratio (F_{340}/F_{380}) measured at 510 nm.

Measurement of HCO_3^- secretion

We utilised two methods to determine the HCO_3^- efflux across the luminal membrane. In the inhibitory stop method, basolateral Na^+/HCO_3^- co-transporters (NBCs) and Na^+/H^+ exchangers (NHEs) were blocked using H_2DIDS (0.5 mM) and amiloride (0.2 mM) administered from the basolateral side for 3 min. The inhibition of these transporters caused a marked decrease in pH_i. The rate of pH_i acidification after the exposure to H_2DIDS and amiloride reflects the intracellular buffering capacity and the rate at which HCO_3^- effluxes (ie, is secreted) across the luminal membrane via Cl^-/HCO_3^- exchangers and possibly cystic fibrosis transmembrane conductance regulator (CFTR) channels.[18 19] The initial rate of intracellular acidification (dpH/dt), over the first 60 s from the administration of inhibitors was calculated by linear regression analysis using 60 data points (one pH_i measurements per second). Therefore, the start point for the calculation of dpH/dt was the pH_i immediately before exposure to the inhibitors.

In the alkali load method, HCO_3^- secretion was estimated by the rate of pH_i recovery from an alkaline load. In these experiments, ducts were exposed to 20 mM NH_4Cl in HCO_3^--buffered solution from the basolateral side, which produced an immediate increase in pH_i due to the rapid influx of NH_3 across the membrane. After the alkalinisation, there was a recovery in pH_i toward the basal value. Recently, we

Table 1 Composition of solutions

	Standard HEPES	Standard HCO_3^-	High-K^+ HEPES	NH_4^+ in HEPES	NH_4^+in HCO_3^-	Na^+-free HEPES	Ca^{2+}-free HEPES	Cl^--free HCO_3^-
NaCl	130	115	5	110	95		132	
KCl	5	5	130	5	5	5	5	
$MgCl_2$	1	1	1	1	1	1	1	
$CaCl_2$	1	1	1	1	1	1		
Na-HEPES	10		10	10			10	
Glucose	10	10	10	10	10	10	10	10
$NaHCO_3$		25			25			25
NH_4Cl				20	20			
HEPES						10		
NMDG-Cl						140		
Na-gluconate								115
Mg-gluconate								1
Ca-gluconate								6
KH_2-sulfate								2.5

Values are concentrations in mM.
NMDG, *N*-methyl-D-glutamine.

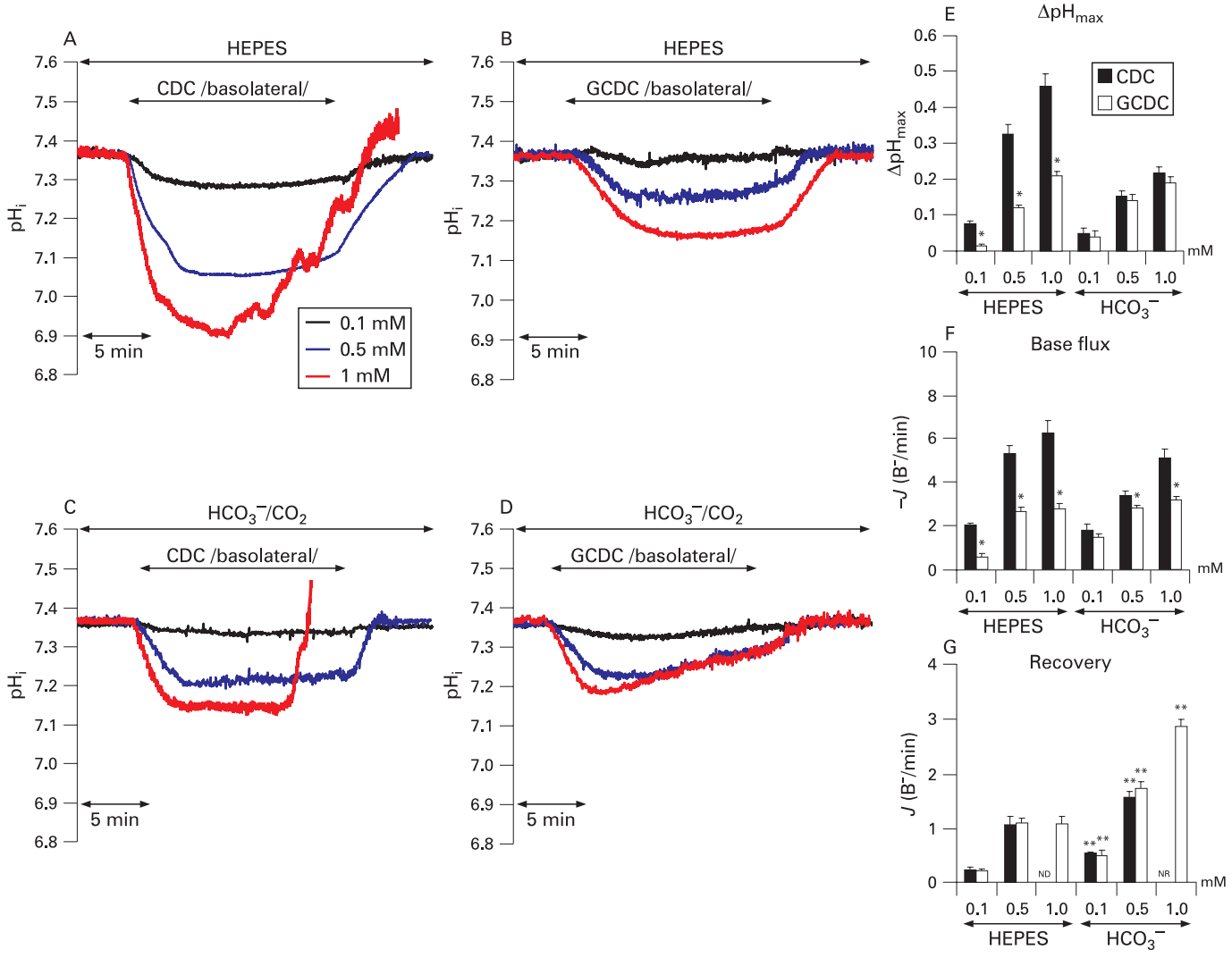

Figure 1 Effect of basolateral administration of bile acids on intracellular pH (pH_i) and base flux ($J(B^-)$) in perfused pancreatic ducts. (A–D) Representative pH_i traces demonstrating the effect of unconjugated chenodeoxycholate (CDC; 0.1, 0.5, 1 mM) and conjugated glycochenodeoxycholate (GCDC; 0.1, 0.5, 1 mM) administered from the basolateral membrane in HEPES- (A and B) and HCO_3^-/CO_2-buffered solutions (C and D). The red traces in A and C show a rapid elevation of the 490/440 nm ratio due to the loss of 2.7-bis-(2-carboxyethyl)-5-(and-6-)carboxyfluorescein (BCECF) from the cells. (E and F) Summary data for the maximal pH_i change (ΔpH_{max}) (E) and the calculated base flux ($J(B^-)$) (F) induced by the bile acids. $J(B^-)$ was calculated from the dpH/dt obtained by linear regression analysis of pH_i measurements made over the first 60 s after bile acid administration (one pH_i measurements was made per second). The start point for the measurement of dpH/dt was the pH_i immediately before exposure to the bile acids (7.36 (0.01), n = 36). The buffering capacity at the start point pH_i was used for the calculation of $J(B^-)$ (see the Materials and methods section). (G) Recovery of $J(B^-)$ during application of the bile acids. The recovery (dpH/dt) was measured over 60 s from the lowest pH_i level (7.36–ΔpH_{max}, see E) induced by the bile acids, and $J(B^-)$ was calculated as described above. Data are shown as means (SEM) from 36 regions of interests in eight ducts. *p<0.001 vs CDC; **p<0.001 vs HEPES. ND, not detectable; NR, not recordable (due to dye leakage).

demonstrated that recovery of pH_i under these conditions was dependent on the presence of HCO_3^- in the bathing solution, suggesting that it results from HCO_3^- efflux (ie, secretion) from the duct cells.[18] In the present study, the initial rate of recovery from alkalosis (dpH/dt) over the first 30 s (30 pH_i measurements) from the highest pH_i value obtained in the presence of NH_4Cl was calculated as described previously.[18]

Measurement of Cl^-/HCO_3^- exchanger activity

Luminal membrane Cl^-/HCO_3^- exchanger activity was measured from the rate of pH_i elevation (alkalinisation) after luminal Cl^- withdrawal. dpH/dt was calculated by linear regression analysis of pH_i measurements made over the first 60 s after exposure to the Cl^--free solution. The start point for the calculation of dpH/dt was the pH_i immediately before exposure to the Cl^--free solution.

Determination of buffering capacity and base efflux

The total buffering capacity (β_{total}) of duct cells was estimated according to the NH_4^+ pre-pulse technique.[18 20] Pancreatic duct cells were exposed to various concentrations of NH_4Cl in an Na^+- and HCO_3^--free solution. β_i (which refers to the ability of intrinsic cellular components to buffer changes of pH_i) was estimated by the Henderson–Hasselbach equation. β_{total} was calculated from: $\beta_{total} = \beta_i + \beta_{HCO_3^-} = \beta_i + 2.3 \times [HCO_3^-]_i$, where $\beta_{HCO_3^-}$ is the buffering capacity of the HCO_3^-/CO_2 system. The measured rates of pH_i change (dpH/dt) were converted to transmembrane base flux $J(B^-)$ using the equation:

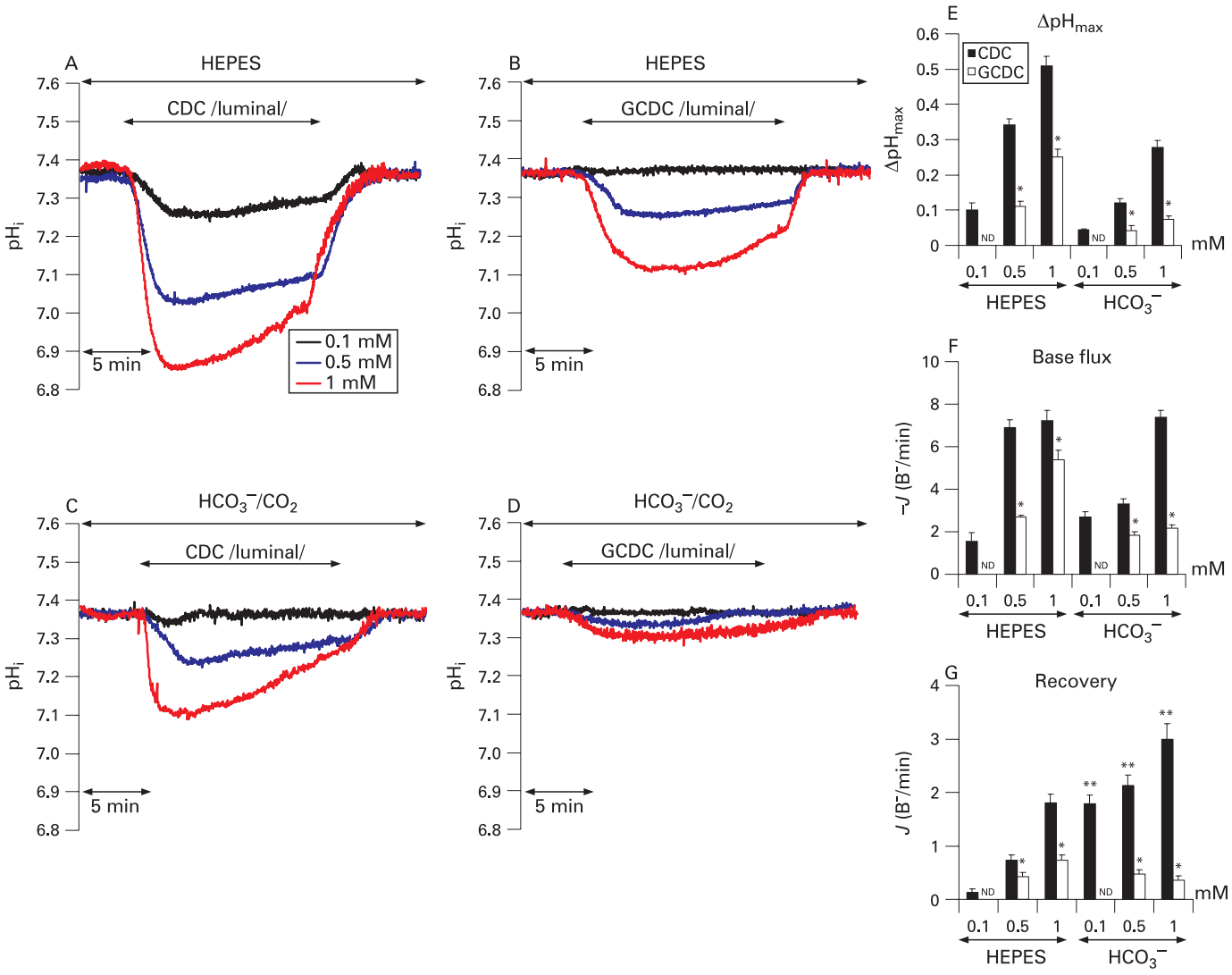

Figure 2 Effect of luminal administration of bile acids on intracellular pH (pH_i) and base flux ($J(B^-)$) in perfused pancreatic ducts. (A–D) Representative pH_i traces demonstrating the effect of unconjugated chenodeoxycholate (CDC; 0.1, 0.5, 1 mM) and conjugated glycochenodeoxycholate (GCDC; 0.1, 0.5, 1 mM) administered from the luminal membrane in HEPES- (A and B) and HCO_3^-/CO_2^-- (C and D) buffered solutions. (E and F) Summary data for the maximal pH_i change (ΔpH_{max}) (E) and the calculated base flux ($J(B^-)$) (F) induced by the bile acids. $J(B^-)$ was calculated as described in the legend to Fig. 1. The start point pH_i was 7.36 (0.01), n = 26. (G) Recovery of $J(B^-)$ during application of the bile acids. $J(B^-)$ was calculated as described in the legend to Fig.1. The start point pH_i was 7.36–ΔpH_{max} (see E). Data are shown as means (SEM) from 26 regions of interest in five ducts. *p<0.001 vs CDC; *p<0.001 vs HEPES. ND, not detectable.

$J(B^-) = dpH/dt \times \beta_{total}$. The β_{total} value at the start point pH_i (see figure legends) was used for the calculation of $J(B^-)$. We denote base influx as $J(B^-)$ and base efflux (secretion) as $-J(B^-)$.

Statistical analyses

Results are expressed as means (SEM) (n = 5–7 ducts/20–36 ROIs). Statistical analyses were performed using analysis of variance. p Values $\leqslant 0.05$ were accepted as significant.

RESULTS

Effect of basolateral exposure to bile acids on duct cell pH_i

Figure 1A–D shows the effect of basolateral administration of the non-conjugated chenodeoxycholate (CDC) and the conjugated glycochenodeoxycholate (GCDC) on the duct cell pH_i in perfused pancreatic ducts. Typically, the response was an initial rapid, dose-dependent fall in pH_i which then recovered to a variable degree during continued exposure to the bile acids. Note that the effect of the bile acids on pH_i was greatest in HEPES-buffered as compared with HCO_3^--buffered solutions (fig 1A–D). Also, when 1 mM CDC was administered in HEPES, the fluorescence intensities at 440 and 490 nm rapidly decreased after 6±1 min (n = 6 ducts/35 ROIs), causing an elevation of the 490/440 ratio (fig 1A). This rapid decrease of the fluorescence intensities must be due to loss of BCECF from the cells. The presence of HCO_3^-/CO_2 delayed this event somewhat, 8±1 min (n = 6 ducts/38 ROIs) (fig 1C). However, no dye leakage occurred with the same concentration of the conjugated GCDC (fig 1B,D).

The maximal pH_i change (ΔpH_{max}) and the base flux ($J(B^-)$) following exposure to the bile acids were calculated for each experiment and the summary data are shown in fig 1E and F. In HEPES-buffered solutions, the unconjugated CDC had a much larger effect on ΔpH_{max} and $J(B^-)$ than the conjugated GCDC, most probably explained by slower permeation of the charged GCDC into the duct cells. In contrast, in HCO_3^-/CO_2-containing solutions, the bile salts induced rather smaller

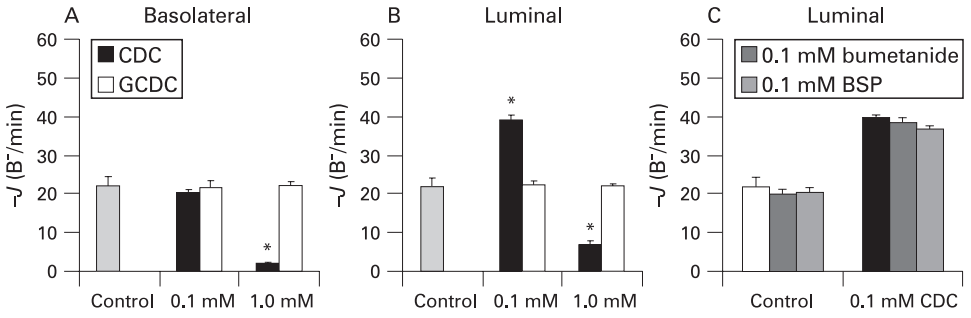

Figure 3 Effect of bile acids on HCO_3^- secretion in perfused pancreatic ducts. The initial rate of pH_i recovery from an alkali load (20 mM NH_4Cl in a HCO_3^-/CO_2-buffered solution) was measured and the $J(B^-)$ calculated. Under these conditions, $J(B^-)$ is the rate of HCO_3^- secretion by the duct cells. (A) Effect of basolateral chenodeoxycholate (CDC; filled bars) and glycochenodeoxycholate (GCDC; open bars) (0.1 or 1 mM) on HCO_3^- secretion. $J(B^-)$ was calculated from the dpH/dt obtained by linear regression analysis of pH_i measurements made over the first 30 s of recovery from the highest pH_i level (start point pH_i) achieved in the presence of NH_4Cl. Start point pH_i values were: control, 7.87 (0.03): 0.1 mM CDC, 7.96 (0.03); 1 mM CDC, 7.62 (0.03); 0.1 mM GCDC, 8.10 (0.01); 1 mM GCDC, 7.78 (0.02); n = 25 for all conditions. The buffering capacity at the start point pH_i was used for the calculation of $J(B^-)$. (B) Effect of luminal CDC and GDCD on HCO_3^- secretion. $J(B^-)$ was calculated as described above. The start point pH_i values were: control, 7.87 (0.03); 0.1 mM CDC, 8.10 (0.03); 1 mM CDC, 7.48 (0.04); 0.1 mM GCDC, 7.89 (0.02); 1 mM GCDC, 7.90 (0.02); n = 25 for all conditions. (C) Nil effect of bumetanide (0.1 mM) and bromosulfophtalein (BSP, 0.1 mM) on HCO_3^- secretion stimulated by 0.1 mM CDC. The inhibitors had no effects on the maximal pH_i level induced by NH_4Cl—that is, the start point pH. Means (SEM) are from 25 regions of interest in five ducts. *$p<0.001$ vs the control.

changes in ΔpH_{max} and $J(B^-)$ (fig 1E,F). This was particularly obvious for the unconjugated CDC and is consistent with the increased buffering capacity of the duct cells in the presence of HCO_3^-/CO_2.[18]

Amiloride (0.2 mM) had no effect on the ΔpH_{max} and $J(B^-)$ caused by basolateral exposure to the unconjugated CDC in a HEPES-buffered solution, suggesting that Na^+/H^+ exchange is not activated during the acidification process (Supplementary fig 1A,B). However, basolateral administration of 0.5 mM H_2DIDS significantly increased both the ΔpH_{max} and the $J(B^-)$ in response to CDC (Supplementary fig 1A, B). This result suggests that the basolateral NBC normally acts to attenuate the fall in pH_i caused by CDC, presumably by transporting HCO_3^- ions into the duct cells.

Effect of luminal exposure to bile acids on duct cell pH_i

Figure 2A–F shows the effect of luminal administration of the bile acids on duct cell pH_i and $J(B^-)$ in perfused pancreatic duct cells (PPDCs). As with basolateral exposure: (1) there was a rapid fall in pH_i followed by a variable degree of pH_i recovery during continued exposure to the bile acid, (2) the unconjugated CDC caused a much larger ΔpH_{max} and $J(B^-)$ than the conjugated GCDC and (3) luminal bile acids had a larger effect on pH_i when tested in a HEPES solution as compared with a HCO_3^-/CO_2 solution (fig 2A–F). However, note that luminal exposure to 1 mM CDC never caused the rapid dye loss that occurred following basolateral addition of the bile acid.

Recovery of duct cell pH_i during contined exposure to bile acids

The experimental traces in figs 1 and 2 indicate that some degree of pH_i recovery occurs during continuous exposure of the perfused pancreatic ducts to bile acids, except with 1 mM CDC administered from the basolateral side which damages the cells and causes dye leakage (fig 1). Initially, we calculated the $J(B^-)$ values during pH_i recovery with and without HCO_3^-/CO_2. A partial recovery of pH_i during continuous exposure to the bile salts (except 1 mM basolateral CDC) occurred in both HEPES and HCO_3^-/CO_2 solutions (figs 1A–D and 2A–D). However, the calculated $J(B^-)$ values during pH_i recovery following basolateral administration of CDC and GCDC were 1.5- to 2.5-fold higher in the presence of HCO_3^-/CO_2 (fig 1G). Similarly, HCO_3^-/CO_2 enhanced the $J(B^-)$ during pH_i recovery following luminal exposure to CDC (fig 2G). However, no such effect was seen with luminal GCDC (fig 2G), presumably because luminal GCDC caused only small changes in duct cell pH_i under these conditions (fig 2D).

We sought to establish which acid/base transporters are involved in the pH_i recovery process, with the most likely candidates being the basolateral NBC and the NHE.[21] Supplementary fig 2A shows that amiloride (0.2 mM) strongly inhibited the $J(B^-)$ during pH_i recovery following exposure to basolateral CDC (0.1 and 0.5 mM) in a HEPES solution, suggesting a major role for the NHE in pH_i recovery in the absence of HCO_3^- ions. In a more physiological HCO_3^-/CO_2 solution, amiloride was a somewhat less effective inhibitor (Supplementary fig 2B). This suggests an involvement of the NBC in pH_i recovery when HCO_3^- is present and is consistent with the enhancing effect of HCO_3^-/CO_2 on $J(B^-)$ during pH_i recovery (figs 1G and 2G). Taken together, these data suggest that, when it occurs, pH_i recovery during exposure to bile acids is mediated by both the NHE and the NBC.

When a high dose of CDC (1.0 mM) was administered to the basolateral membrane in a HEPES solution, perfused pancreatic ducts started to lose dye and so pH_i recovery could not be studied (fig 1A). Leakage of dye was delayed in a HCO_3^-/CO_2 solution; however, no pH_i recovery was observed before the cell membrane became permeable, suggesting that the NBC and NHE were totally inhibited under these conditions (fig 1C).

Effect of bile acids on HCO_3^- secretion

To investigate the effects of bile acids on HCO_3^- secretion, we analysed the recovery of pH_i from an alkali load induced by exposure to NH_4Cl in a HCO_3^-/CO_2-containing solution (for original traces see Supplementary fig 3). We have previously shown that the $J(B^-)$ calculated from the rate of pH_i recovery under these conditions reflects the rate of HCO_3^- efflux (ie, secretion) on luminal Cl^-/HCO_3^- exchangers.[21] Basolateral administration of a low dose (0.1 mM) of the unconjugated CDC had no effect on $J(B^-)$; however, a higher dose of CDC (1 mM) strongly inhibited HCO_3^- secretion (fig 3A). Interestingly, luminal administration of 0.1 mM CDC had a

stimulatory effect on HCO_3^- secretion (fig 3B), whereas the higher dose (1 mM) was inhibitory (fig 3B). The basal rate of HCO_3^- secretion and the stimulatory effect of 0.1 mM luminal CDC were unaffected by bumentanide and bromosulfophthalein (fig 3C), suggesting that neither the $Na^+/K^+/2Cl^-$ co-transporter nor bile acid/HCO_3^- exchange on the organic anion transporting polypeptide transporter were involved in pH_i recovery (fig 3C). In contrast to the effects of CDC, neither basolateral nor luminal application of the conjugated GCDC (0.1 and 1 mM) had any effect on pH_i recovery from an alkali load (fig 3A and B).

We used luminal H_2DIDS to investigate whether the stimulatory effect of 0.1 mM luminal CDC on HCO_3^- secretion was due to activation of Cl^-/HCO_3^- exchangers. We found that H_2DIDS inhibited the basal rate of HCO_3^- secretion by about 65% and completely blocked the stimulatory effect of 0.1 mM luminal CDC, suggesting that the stimulatory effect must involve activation of luminal Cl^-/HCO_3^- exchangers (fig 4A). We confirmed these results using another method of measuring HCO_3^- secretion—the inhibitor stop technique.[18 19] Again we found that luminal H_2DIDS totally blocked the stimulatory effect of low doses of CDC on HCO_3^- secretion (fig 4B).

Finally, we directly measured the effects of CDC on the activity of luminal Cl^-/HCO_3^- exchangers using the Cl^- removal technique. Figure 5A shows that CDC (0.1 mM) strongly stimulated pH_i alkalinisation after removal of luminal Cl^-. The calculated $J(B^-)$ values indicate that base flux through the exchangers was increased about 8-fold under these conditions (fig 5B). Note that the rate of pH_i alkalinisation and $J(B^-)$ on luminal Cl^- withdrawal were also slightly elevated when 1 mM CDC was used (which inhibits HCO_3^- secretion) (fig 5A,B). However, this apparent stimulation of anion exchange activity is most probably explained by the ongoing recovery of the pH_i that occurs during luminal administration of 1 mM CDC (see fig 2C).

Bile acids evoke a dose-dependent rise in $[Ca^{2+}]_i$

Our results clearly show differential effects of the unconjugated CDC and the conjugated GCDC on the perfused pancreatic ducts. CDC had marked effects on pH_i and, depending on the dose and route of administration, either stimulated or inhibited HCO_3^- secretion. In contrast, GCDC has smaller effects on pH_i and no effect on HCO_3^- secretion. We next sought to establish the intracellular pathways responsible for these actions. Bile acids have been shown to evoke Ca^{2+} signalling in pancreatic acinar cells; therefore, we first tested whether bile acids had any effect on $[Ca^{2+}]_i$ in PPDC.

Figure 6A and B show that basolateral administration of CDC and GCDC caused a dose-dependent increase in $[Ca^{2+}]_i$. The unconjugated CDC was the most effective, causing what appeared to be repetitive $[Ca^{2+}]_i$ transients at a dose of 0.1 mM and a large initial peak in $[Ca^{2+}]_i$ followed by a sustained plateau at 1.0 mM (fig 6A). In contrast, 0.1 mM of the conjugated GCDC had little or no effect on $[Ca^{2+}]_i$ while 1.0 mM GCDC caused a small initial peak followed by a sustained plateau which was similar in magnitude to the plateau obtained with 1.0 mM CDC (fig 6B).

Luminal application of 0.1 mM CDC again caused slow $[Ca^{2+}]_i$ transients which appeared to decline during continued exposure to the bile acid. However, 1.0 mM luminal CDC caused a very large sustained increase in $[Ca^{2+}]_i$ (fig 6C). In contrast, 0.1 mM of the conjugated GCDC had no effect on $[Ca^{2+}]_i$ when applied from the lumen, whereas 1.0 mM caused a rise in $[Ca^{2+}]_i$ comparable with that observed when the same dose was applied from the basolateral membrane (compare fig 6B and D).

Figure 6E shows fluorescent ratio images of perfused pancreatic ducts exposed to CDC, which confirm the results described above. Basolateral application of 0.1 mM CDC caused localised increases in $[Ca^{2+}]_i$ within the duct, whereas all cells appeared to be affected by 1 mM CDC (fig 6E, left panel).

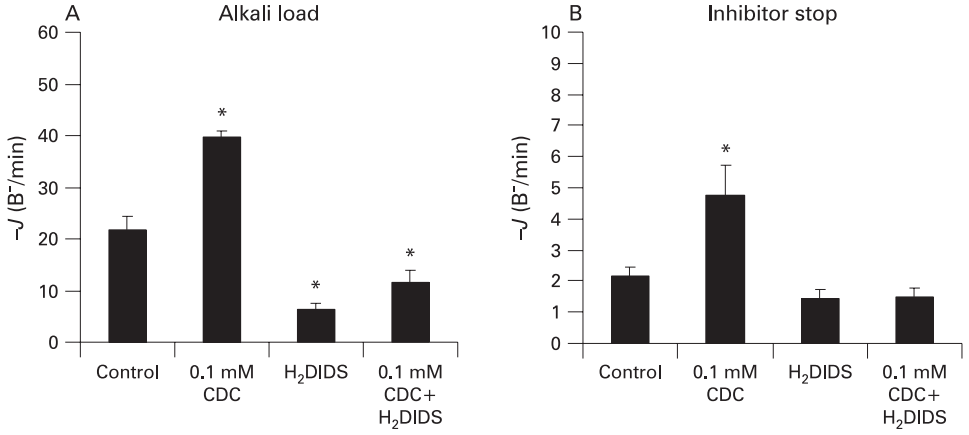

Figure 4 Role of luminal Cl^-/HCO_3^- exchangers in the stimulatory effect of chenodeoxycholate (CDC) on HCO_3^- secretion in perfused pancreatic ducts. (A) HCO_3^- secretion was measured using the alkali load method (see the Materials and methods section) and is expressed as the calculated $J(B^-)$. $J(B^-)$ was calculated as described in the legend to Fig. 3. Start point pH_i values were: control, 7.87 (0.02); 0.1 mM CDC, 8.1 (0.03); dihydro-4,4′-diisothiocyanostilbene-2,2′-disulfonic acid (H_2DIDS), 7.83 (0.03); 0.1 mM CDC+H_2DIDS, 7.89 (0.03); n = 25 for all conditions. H_2DIDS (0.5 mM), a blocker of the SLC26A6 anion exchanger, was applied from the luminal side. (B) The same experiment repeated using the inhibitor stop method for measuring HCO_3^- secretion (see the Materiala and methods section). $J(B^-)$ was calculated from the dpH/dt obtained by linear regression analysis of pH_i measurements made over the first 60 s after exposure to the transport inhibitors. The start point for the calculation of dpH/dt was the pH_i immediately before exposure to the inhibitors. Start point pH_i values were: control, 7.36 (0.01); 0.1 mM CDC, 7.34 (0.02); H_2DIDS, 7.33 (0.02); 0.1 mM CDC+H_2DIDS, 7.33 (0.02); n = 25 for all conditions. The buffering capacity at the start point pH_i was used for the calculation of base flux, $J(B^-)$. As we have previously reported, the absolute rates of $J(B^-)$ (ie, HCO_3^- secretion) are much higher when measured using the alkali load method as compared with the inhibitor stop method.[18 21] This difference probably reflects the higher HCO_3^- concentration in the cells following alkali loading.[18 20] Means (SEM) are from 25 regions of interest in five ducts. *p<0.001 vs the control.

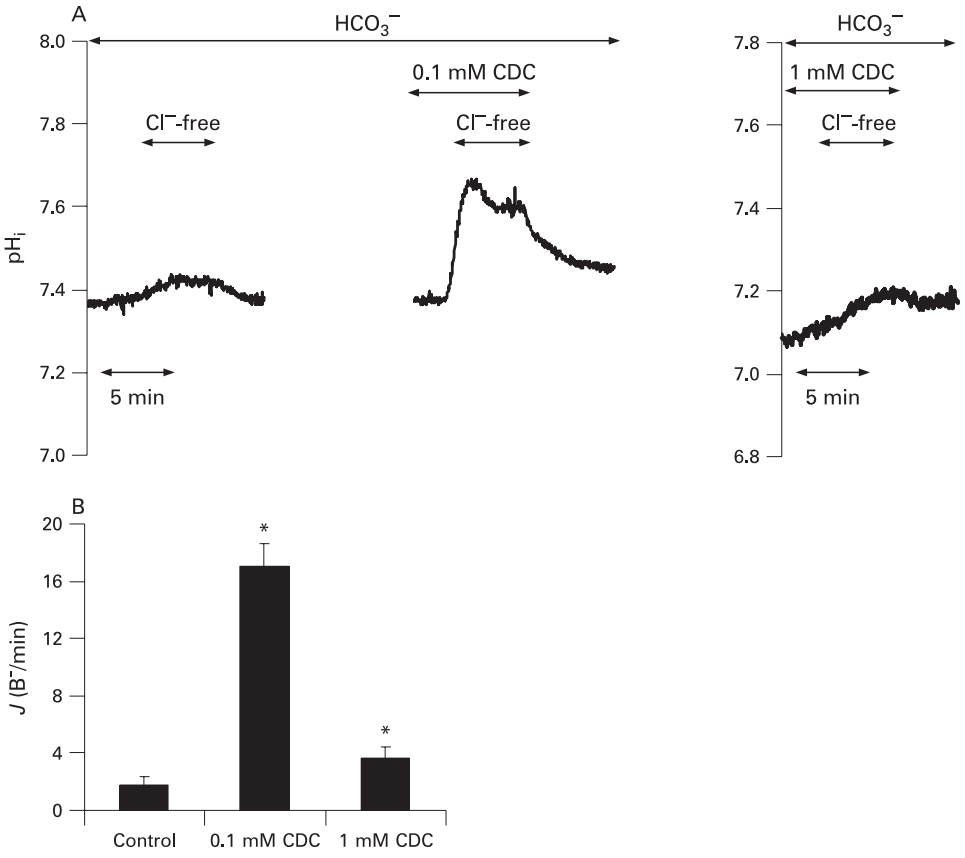

Figure 5 Effect of chenodeoxycholate (CDC) on luminal Cl^-/HCO_3^- exchange activity in perfused pancreatic ducts. (A) Representative experimental traces showing the effects of CDC (0.1 and 1 mM) on pH_i after removal of luminal Cl^-. (B) Summary data. Base flux, $J(B^-)$, was calculated from the dpH/dt obtained by linear regression analysis of pH_i measurements made over the first 60 s after exposure to the Cl^--free solution. The start point for the calculation of dpH/dt was the pH_i immediately before exposure to the Cl^--free solution. The start point pH_i values were: control, 7.36 (0.01); 0.1 mM CDC, 7.33 (0.01); 1 mM CDC, 7.1 (0.03); n = 32 for all conditions. The buffering capacity at the start point pH_i was used for the calculation of base flux, $J(B^-)$. Means (SEM) are from 32 regions of interest of six ducts. *p<0.001 vs the control.

Following luminal application, localised increases in $[Ca^{2+}]_i$ were also observed with 0.1 mM CDC, but these were more extensive compared with when the same dose was administered basolaterally. Luminal 1.0 mM CDC caused a very large generalised increase in $[Ca^{2+}]_i$.

Neither atropine (100 μM) nor removal of extracellular Ca^{2+} had any effect on the $[Ca^{2+}]_i$ rise evoked by basolateral administration of 0.1 mM CDC (fig 7A). However, the IP_3 receptor antagonist caffeine (20 mM), the Ca^{2+}-chelator BAPTA-AM (40 μM), the IP_3 receptor inhibitor xestospongin C (50 μM) and the phospholipase C (PLC) inhibitor U73122 (10 μM) all completely blocked the rise in $[Ca^{2+}]_i$ evoked by this low close of CDC (fig 7A). The inhibitors also reduced, albeit less so, the rise in $[Ca^{2+}]_i$ evoked by 1.0 mM basolateral CDC (fig 7B). Similar results were obtained when CDC was applied from the luminal membrane (fig 7C,D). Taken together, these data indicate that the mechanism by which basolateral and luminal CDC increases $[Ca^{2+}]_i$ involves activation of PLC and IP_3 receptors.

Relationship between the inhibitory and stimulatory effects of CDC on HCO_3^- secretion and CDC-induced changes in $[Ca^{2+}]_i$

The unconjugated CDC increases $[Ca^{2+}]_i$ and has a dual effect on HCO_3^- secretion, causing inhibition and stimulation at high and low doses, respectively. We investigated whether chelation of intracellular Ca^{2+} with BAPTA had any effect on these HCO_3^- secretory responses using the alkali load method. Figure 8A shows that loading the duct cells with BAPTA-AM had no effect on the inhibitory action of 1.0 mM basolateral CDC on HCO_3^- secretion. In contrast, the stimulatory effect of 0.1 mM luminal CDC on HCO_3^- secretion was completely blocked by BAPTA-AM (Fig 8B).

DISCUSSION

Acute pancreatitis is a sudden inflammation of the pancreas which usually develops either as a result of gallstones impacting in the papilla of Vater resulting in bile reflux into the pancreatic ductal system, or as a result of moderate to heavy alcohol consumption. Very little is known about the pancreatic ductal epithelium in acute pancreatitis. Some recent studies have suggested that HCO_3^- and fluid secretion by pancreatic ductal cells may represent a defence mechanism against toxic factors that can induce pancreatitis. For instance, activation of proteinase-activated receptor-2 (PAR-2) receptors by trypsin not only stimulates acinar cell secretion in the early stage of acute pancreatitis,[22] but also activates anion transporters in pancreatic duct cells, such as calcium-activated chloride channel (CACC)[23] and luminal anion exchanger (AE).[24] It has been reported that 0.3–30 mM ethanol directly augments pancreatic ductal fluid secretion stimulated by physiological and pharmacological concentrations of secretin (cAMP pathway) and via Ca^{2+} mobilisation.[25] Moreover, we have recently shown that pseudorabies virus infection can stimulate pancreatic ductal HCO_3^- secretion by four- to fivefold.[26] Bile acids have been shown to increase the HCO_3^- and Cl^- permeability of the pancreatic duct mucosa at a concentration of 15–42 mM,[11] but no data are available concerning changes in the secretory function of PPDCs. Here we report, for the first time, that bile acids can stimulate HCO_3^- secretion from PPDCs.

First we investigated the effects of bile acids on pH_i. We chose to use the unconjugated and conjugated forms of CDC for this investigation since the majority (62%) of guinea pig bile acids is CDC[27] and the human gallbladder bile also contains this bile acid in high concentrations.[28] We can only estimate the possible concentration of bile acid that can reach the small interlobular

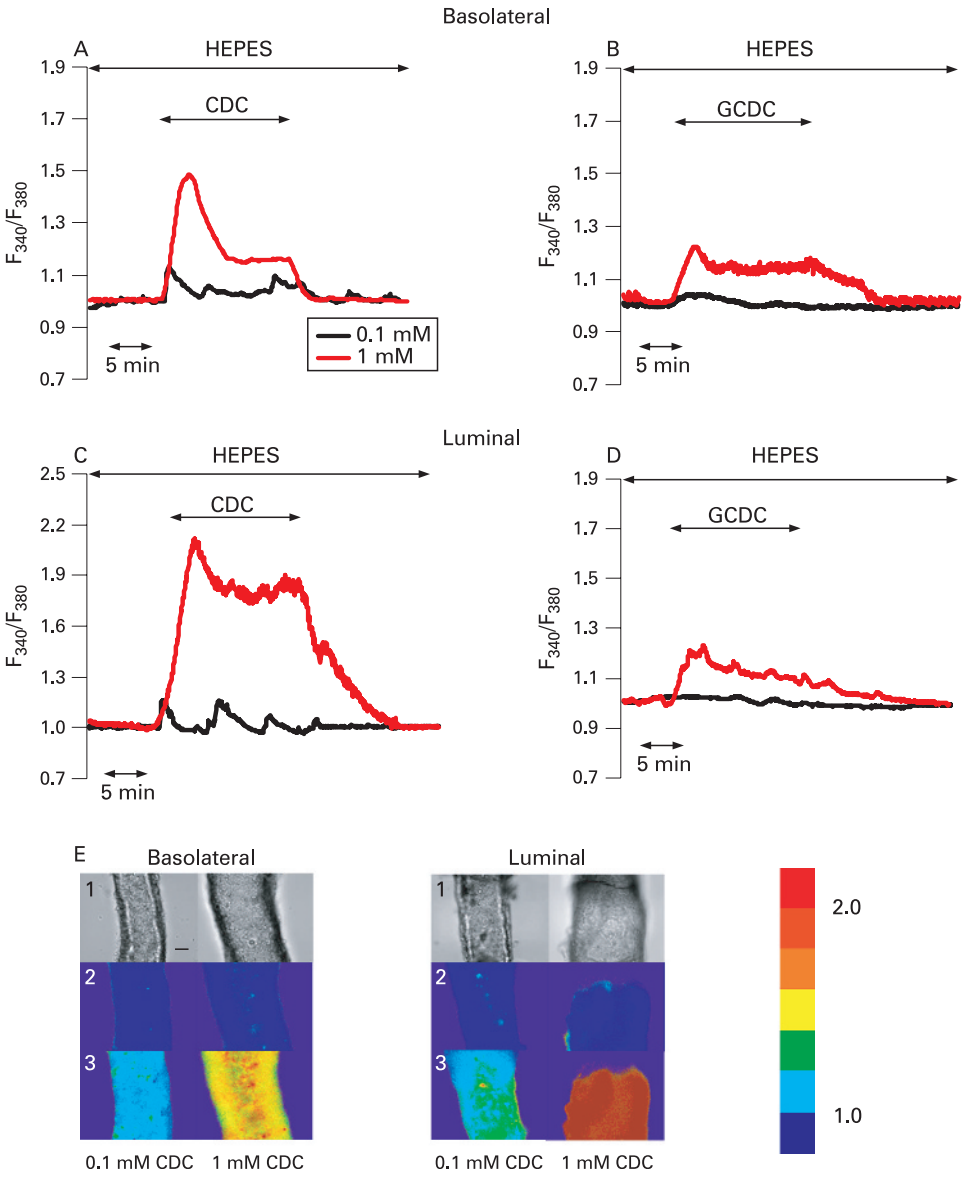

Figure 6 Effect of bile acids on $[Ca^{2+}]_i$ in perfused pancreatic ducts.
(A–D) Representative experimental traces showing the effect of basolateral (A and B) and luminal (C and D) administration of either chenodeoxycholate (CDC) or glycochenodeoxycholate (GCDC; 0.1 and 1 mM) on $[Ca^{2+}]_i$ in perfused ducts. The experiments were performed in a HEPES-buffered solution. (E) Light (1) and fluorescent ratio images (2 and 3) of pancreatic ducts perfused with either 0.1 or 1 mM CDC from either the basolateral (left panel) or luminal side (right panel). An increase in $[Ca^{2+}]_i$ is denoted by a change from a "cold" colour (blue) to a "warmer" colour (yellow to red); see scale on the right. Pictures were taken before (1 and 2) and 1 min after (3) exposure of the ducts to CDC.
Bar = 50 μm.

ducts during acute biliary pancreatitis. The normal concentration of bile salts in human gallbladder bile is approximately 5–10 mM. However, this can be increased by cholecystokinin infusion.[28] Looking at the very distal end of the duct, 25 μM of the natural bile acid taurolithocholic-acid-3-sulfate induced Ca^{2+} signalling in only 11% of mouse acinar cells, 37% of the cells responded to 50 μM, 69% to 100 μM and almost all acinar cells responded to 200 μM taurolithocholic-acid-3-sulfate.[5] This suggests that at least 50–100 μM of bile acids have to pass through the small ducts to induce intra-acinar cell changes. Therefore, in our experiments we used 0.1 mM as a low dose and 1 mM as a high dose of bile acids.

We found that either basolateral or luminal administration of CDC dose-dependently and reversibly reduced the pH_i of duct cells. However, the conjugated GCDC had a significantly smaller effect than the unconjugated CDC and, notably, low concentrations of GCDC had only a very small effect on pH_i when it was administered from the luminal side. Alvaro *et al* reported that 0.5–1.5 mM ursodeoxycholate caused a dose-dependent rapid, intracellular acidification in bile duct epithelial cells.[29] In addition, the conjugated form of this bile acid (tauroursodeoxycholate) at 1 mM concentration had no effect on pH_i.[29] These results are in accordance with the diffusion characteristics of bile acids. Unconjugated bile salts are weak acids and they can traverse cell membranes by passive diffusion.[30] However, taurine- or glycine-conjugated bile acids cannot cross cell membranes due to their lipid insolubility, and they require active transport mechanisms for cellular uptake.[31] Recently, an increasing number of bile acid transporters have been cloned and localised to either the luminal or basolateral membranes of polarised epithelial cells.[30 32–34] Basolateral administration of 1 mM CDC for 6–8 min damaged the membrane integrity, and the duct cells lost BCECF very quickly. The same concentration of CDC had no toxic effects on the luminal membrane; however, a higher (2 mM) concentration of CDC also damaged the luminal membrane (data not shown). Okolo *et al*[10] also found differences between the effects of bile acids on the luminal and basolateral membranes. The basolateral membrane was much more sensitive to bile acid-induced damage (transepithelial membrane resistance decreased much more when bile acids were administered from the basolateral side) than the luminal membrane.

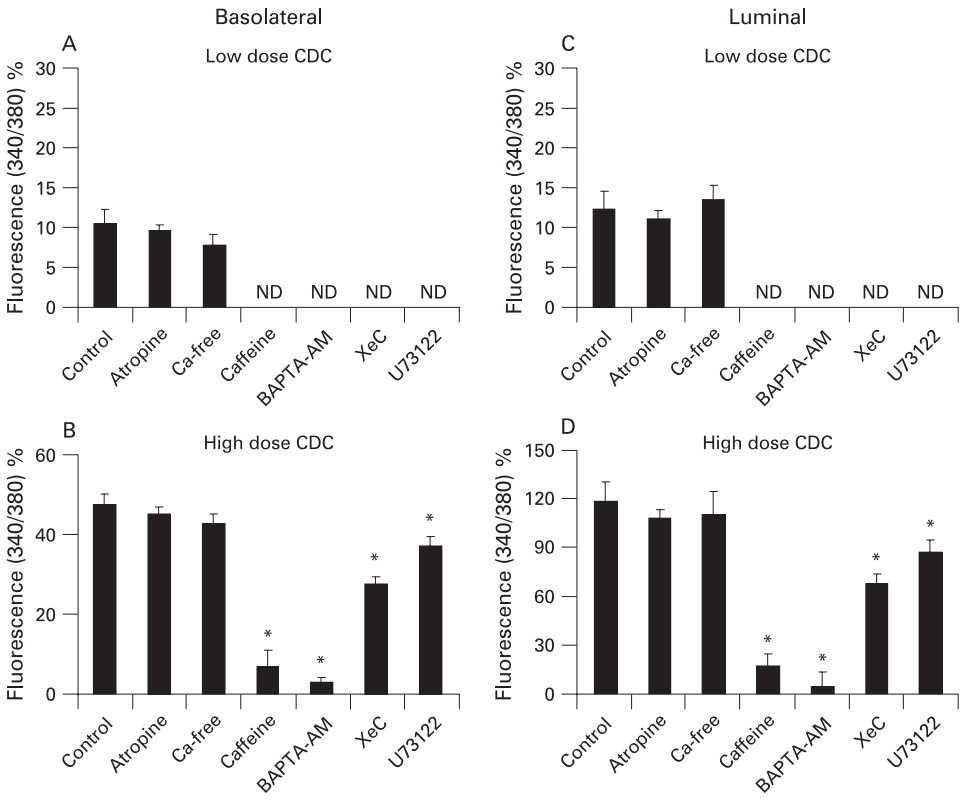

Figure 7 Effect of extracellular calcium removal and pharmacological inhibitors on the rise in $[Ca^{2+}]_i$ caused by chenodeoxycholate (CDC). (A and B) Effect of atropine (100 μM), extracellular calcium removal, caffeine (20 mM), pre-loading the ducts with BAPTA-AM (1,2-bis(*o*-aminophenoxy)ethane-*N*,*N*,*N*′,*N*′-tetraacetic acid; 40 μM), the inositol trisphosphate (IP_3) receptor inhibitor xestospongin C (XeC, 50 μM) and the phospholipase C inhibitor U73122 (10 μM) on the rise in $[Ca^{2+}]_i$ caused by basolateral CDC (high dose is 1 mM; low dose is 0.1 mM). (C and D) The same experiments performed with luminal CDC administration. Controls represent response to CDC only. Means (SEM) are from 25 regions of interest in five ducts. *$p<0.001$ vs the control. ND, not detectable.

We next investigated the effects of bile acids on the acid/base transporters of PPDCs. A high concentration of CDC strongly inhibited the NHE, NBC and AE of PPDCs. This observation indicates a possible toxic effect of high doses of CDC on the activity of the acid/base transport system. Alvaro *et al* also suggested a possible toxic effect of bile acids on the acid-extruding system of bile duct epithelial cells.[29] Using 1.5 mM ursodeoxycholate, spontaneous pH_i recovery did not occur during the administration of this bile acid; however, this finding was not further investigated using the NH_4Cl pulse technique.[29] Lower doses of ursodeoxycholate (0.5 mM) had no effect on the recovery from acid load in bile duct epithelial cells,[29] which is in accordance with our results. Alterations in cell metabolism and/or changes in membrane structure might therefore underlie the global inhibition of ion transporters (NHE, NBC and AE) that we observed with high concentrations of bile acids. Bile acids have been found to release components from cell membranes (eg, proteins, membrane enzymes and phospholipids) prior to the occurrence of significant cell lysis.[35 36] In addition, bile acids can cause concentration-related increases in membrane fluidity over the range 0.1–1.0 mM.[37].

Importantly, luminal administration of low doses of CDC significantly stimulated HCO_3^- efflux—that is, secretion from PPDCs. It has been shown that bile acids modulate AE and CFTR in different epithelia.[34 38–41] Low doses (20 μM) of taurocholic and taurolithocholic acid augmented the stimulatory effect of secretin on HCO_3^- secretion in cholangiocytes.[34 38] Strazzabosco *et al* also suggested that ursodeoxycholate stimulates HCO_3^- secretion in bile by a weak acid effect.[39] Luminal administration of 0.5 mM taurocholate has been shown to stimulate a CFTR-dependent electrogenic Cl^- transport in the murine distal ileum.[41] Exposure of gastroduodenal mucosa to taurocholic acid at high concentration was also shown to stimulate HCO_3^- secretion and, therefore, can play a physiological role in the mucosal protective mechanisms.[40]

In this study, we showed that low doses of CDC selectively act on the luminal membrane to stimulate HCO_3^- secretion. Inhibition of basolateral AE and NBC by H_2DIDS, and of NHE by amiloride had no effect on the secretory response to CDC. However, luminal administration of H_2DIDS totally blocked the stimulated HCO_3^- efflux. Three main anion transporters/channels have been identified on the luminal membrane of PPDCs, namely the CFTR chloride channel, the CACC and two members of the SLC26 family (A3 and A6) of AEs. Since CFTR is unaffected by H_2DIDS,[42] it is unlikely to be involved in the stimulatory mechanism of CDC. Taurodeoxycholate was reported to activate a chloride conductance via IP_3-mediated Ca^{2+} signalling in the T84 colonic cell line[43] and in cultured pancreatic ductal epithelial cells (PDECs).[10] Since SLC26A3 is only weakly inhibited by the disulfonic stilbene,[44 45] the putative anion exchanger SLC26A6 and/or the CACC are the most likely candidates for the target of CDC.[45 46] Most CACCs are inhibited by DIDS, although human CACC in the HPAF cell line is not.[47]

The next challenge was to identify the intracellular mechanisms by which CDC stimulates/inhibits pancreatic HCO_3^- secretion. Bile acids induce an elevation in $[Ca^{2+}]_i$ in various cell types including pneumocytes,[48] hepatocytes,[49 50] colonocytes,[43] gastric mucosal cells,[51] vascular endothelial cells[52] and, importantly, pancreatic acinar cells.[5 6 8 53] The fact that taurodeoxycholic acid-induced DIDS-sensitive $^{125}I^-$ efflux can be inhibited by BAPTA-AM in dog PDECs suggests that bile acids may induce Ca^{2+} signals in PDECs.[10] In the present study, we showed, for the first time, that both unconjugated and conjugated bile acids induce a dose-dependent elevation of $[Ca^{2+}]_i$ in PPDCs. Similarly to the pH_i effects, the unconjugated CDC had significantly larger effects than the conjugated GCDC. Notably, the effect of luminal administration of a low

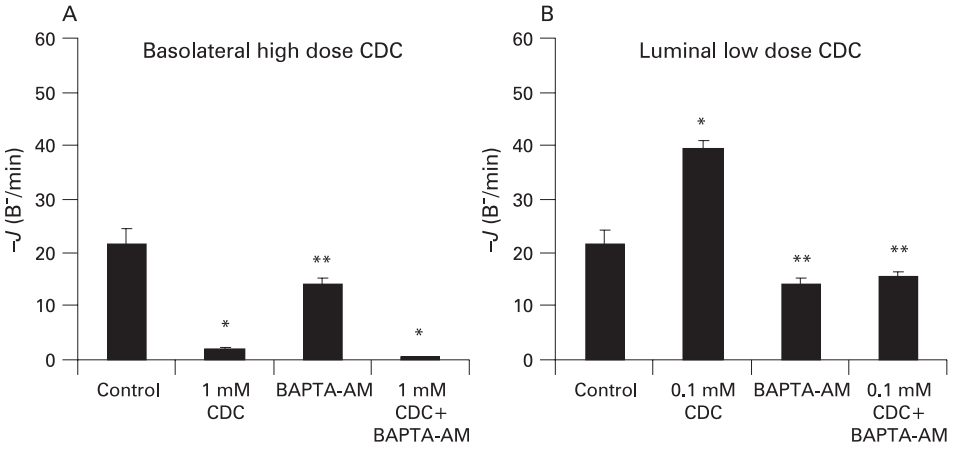

Figure 8 Effect of BAPTA-AM (1,2-bis(*o*-aminophenoxy)ethane-*N*,*N*,*N*′,*N*′-tetraacetic acid) on the inhibitory and stimulatory effects of chenodeoxycholate (CDC) on HCO_3^- secretion. HCO_3^- secretion was measured using the alkali load method and is expressed as the calculated $J(B^-)$. A shows that the pre-treatment of ducts with 40 μM BAPTA-AM (30 min before the experiments) had no effect on the inhibitory action of 1 mM basolateral CDC on HCO_3^- secretion. $J(B^-)$ was calculated as described in the legend to Fig. 3. Start point pH_i values were: control, 7.87 (0.03); 1 mM CDC, 7.62 (0.03); BAPTA-AM, 7.92 (0.02); BAPTA-AM+1 mM CDC, 7.57 (0.04); n = 25 for all conditions. B shows that pre-treatment with BAPTA-AM blocked the stimulatory effect of 0.1 mM luminal CDC on HCO_3^- secretion. Start point pH_is were: control, 7.87 (0.03); 1 mM CDC, 8.10 (0.03); BAPTA-AM, 7.92 (0.02); BAPTA-AM+1 mM CDC, 7.96 (0.03); n = 25 for all conditions. Means (SEM) are from 25 regions of interest in five ducts. *p<0.001 vs the control, **p<0.05 vs the control.

dose of GCDC was almost undetectable. We also showed that the Ca^{2+} signal induced by luminal administration of low doses of CDC was totally blocked by the calcium chelator BAPTA-AM, caffeine, the IP_3 receptor inhibitor xestospongin C and the PLC inhibitor U73122, but unaffected by removal of extracellular Ca^{2+}. The above-mentioned inhibitors also had a similar effect on the $[Ca^{2+}]_i$ elevation evoked by basolateral administration of a high dose of CDC.

Finally, we provided evidence that the stimulatory effect of low doses of luminal CDC on HCO_3^- secretion is dependent on an elevation of $[Ca^{2+}]_i$. BAPTA-AM (40 μM) slightly inhibited basal HCO_3^- secretion measured using the ammonium pulse method. In an earlier study, a lower concentration of BAPTA-AM (10 μM) had no effect on fluid secretion by guinea pig pancreatic duct cells,[25] suggesting a dose-dependent effect of this calcium chelator. Importantly, BAPTA-AM (40 μM) totally blocked the stimulatory effect of low doses of CDC, showing that this effect is Ca^{2+} dependent. However, BAPTA-AM had no effect on the inhibitory action of high doses of basolateral CDC on HCO_3^- secretion, indicating that a Ca^{2+}-independent mechanism is responsible for this effect.

Our results suggest that the pancreatic ductal epithelium is remarkably resistant to attack by the conjugated bile salt GCDC, which is probably the major bile salt in the guinea pig's gall bladder. Whilst GCDC decreased pH_i and elevated $[Ca^{2+}]_i$, it had no detectable effect on HCO_3^- secretion. In contrast, the unconjugated CDC caused marked changes in pH_i and $[Ca^{2+}]_i$ and, depending on the dose, either stimulated or inhibited HCO_3^- secretion. Although it has been shown that the triggering mechanisms of intracellular protease activation do not require bile influx into the pancreatic ductal tree,[54–56] a flow of bile into the pancreatic ductal system may occur after the first 24–48 h.[57 58] Theoretically, when small stones obstruct the pancreatic duct and a "common channel" is formed with the bile ducts, bile acids will start diffusing up into the pancreatic ductal tree and reach the interlobular ducts in a low concentration. The subsequent bile acid-induced stimulated of HCO_3^- and fluid secretion may protect the pancreas in different ways. First, the elevated luminal pressure stops or delays bile acid diffusion towards the acinar tissue. Importantly, the higher ductal pressure may help push small stones through the papilla and open the way for the pancreatic and bile fluids. However, if this defence mechanism is not sufficient and the bile concentration rises further, thus leading to damage of the epithelial barrier, the secretory mechanisms of pancreatic ductal cells are blocked and the ducts can no longer act as a defensive wall against the toxic bile. On the other hand, high concentrations of bile acids reaching the pancreatic ductal cells from the basolateral side (either from the blood and/or from the lumen due to the damage of the ductal barrier) inhibit HCO_3^- and fluid secretion, and therefore may contribute to the progression of acute pancreatitis.

In conclusion, luminal administration of low doses of CDC stimulates HCO_3^- secretion via PLC- and IP_3-mediated Ca^{2+} signalling in pancreatic ductal cells. High doses of CDC also induce Ca^{2+} signalling, but inhibit HCO_3^- secretion. We postulate that these contrasting effects of bile acids may have an important role in the pathogenesis of bile-induced pancreatitis.

Acknowledgements: Supported by Hungarian Scientific Research Fund grants to JL (T43066) and to ZR (PF6395), Bolyai Postdoctoral Fellowships to PH (00276/04) and to ZR (00218/06), a KPI Research Grant to AV (KPI/BIO-37), a Joint International Grant (HAS and the Royal Society) to PH and MAG, an Asboth Grant to JL (XTPPSRT1), a Hungarian Medical Research Council grant to JL (517/2006), and The Physiological Society Junior Fellowship to ZR.

Competing interests: None.

Ethics approval: All experiments were conducted in compliance with the *Guide for the care and use of laboratory animals*. The experimental protocol was approved by the local Ethical Board of the University of Szeged, Hungary.

REFERENCES

1. **Opie EL.** The etiology of acute hemorrhagic pancreatitis. *Johns Hopkins Hosp Bull* 1901;**12**:182–8.
2. **Niederau C,** Niedereu M, Luthen R, *et al*. Pancreatic exocrine secretion in acute experimental pancreatitis. *Gastroenterology* 1990;**99**:1120–7.
3. **Senninger N.** Bile-induced pancreatitis. *Eur Surg Res* 1992;**24**:68–73.
4. **Pandol SJ,** Saluja AK, Imrie CW, *et al*. Acute pancreatitis: bench to the bedside. *Gastroenterology* 2007;**132**:1127–51.
5. **Voronina S,** Longbotton R, Sutton R, *et al*. Bile acids induce calcium signals in mouse pancreatic acinar cells: implications for bile-induced pancreatic pathology. *J Physiol* 2002;**540**:49–55.

6. **Fischer L,** Gukovskaya AS, Penninger JM, *et al*. Phosphatidylinositol 3-kinase facilitates bile acid-induced Ca^{2+} responses in pancreatic acinar cells. *Am J Physiol Gastrointest Liver Physiol* 2007;**292**:G875–86.
7. **Raraty M,** Ward J, Erdemli G, *et al*. Calcium-dependent enzyme activation and vacuole formation in the apical granular region of pancreatic acinar cells. *Proc Natl Acad Sci USA* 2000;**97**:13126–31.
8. **Kim JY,** Kim KH, Lee JA, *et al*. Transporter-mediated bile acid uptake causes Ca^{2+}-dependent cell death in rat pancreatic acinar cells. *Gastroenterology* 2002;**122**:1941–53.
9. **Farmer RC,** Tweedie J, Maslin S, *et al*. Effects of bile salts on permeability and morphology of main pancreatic duct in cats. *Dig Dis Sci* 1984;**29**:740–51.
10. **Okolo C,** Wong T, Moody MW, *et al*. Effect of bile acids on dog pancreatic duct epithelial cell secretion and monolayer resistance. *Am J Physiol Gastrointest Liver Physiol* 2002;**283**:G1042–50.
11. **Reber HA,** Mosley JG. The effect of bile salt on the pancreatic duct mucosal barrier. *Br J Surg* 1980;**67**:59–62.
12. **Argent BE,** Gray MA, Steward MC, *et al*. Cell physiology of pancreatic ducts. In: Johnson LR, ed. *Physiology of the gastrointestinal tract*. 4th edn. San Diego: Elsevier, 2006:1371–96.
13. **Czako L,** Yamamoto M, Otsuki M. Exocrine pancreatic function in rats after acute pancreatitis. *Pancreas* 1997;**15**:83–90.
14. **Argent BE,** Arkle S, Cullen MJ, *et al*. Morphological, biochemical and secretory studies on rat pancreatic ducts maintained in tissue culture. *Q J Exp Physiol* 1986;**71**:633–48.
15. **Ishiguro H,** Steward MC, Lindsay ARG, *et al*. Accumulation of intracellular HCO_3^- by Na^+–HCO_3^- cotransport in interlobular ducts from guinea-pig pancreas. *J Physiol* 1996;**495**:169–78.
16. **Hegyi P,** Rakonczay Z Jr, Gray MA, *et al*. Measurement of intracellular pH in pancreatic duct cells: a new method for calibrating the fluorescence data. *Pancreas* 2004;**28**:427–34.
17. **Thomas JA,** Buchsbaum RN, Zimniak A, *et al*. Intracellular pH-measurements in Ehrlich ascites tumor cells utilizing spectroscopic probes generated in situ. *Biochemistry* 1979;**18**:2210–18.
18. **Hegyi P,** Gray MA, Argent BE. Substance P inhibits bicarbonate secretion from guinea-pig pancreatic ducts by modulating an anion exchanger. *Am J Physiol Cell Physiol* 2003;**285**:C268–76.
19. **Szalmay G,** Varga G, Kajiyama F, *et al*. Bicarbonate and fluid secretion by cholecystokinin, bombesin and acetylcholine in isolated guinea-pig pancreatic ducts. *J Physiol* 2001;**535**:795–807.
20. **Weintraub WH,** Machen TE. pH regulation in hepatoma cells: roles for Na–H exchange, Cl–HCO_3 exchange, and Na–HCO_3 cotransport. *Am J Physiol Gastrointest Liver Physiol* 1989;**257**:G317–27.
21. **Hegyi P,** Rakonczay Z Jr, Tiszlavicz L, *et al*. Protein kinase C mediates the inhibitory effect of substance P on bicarbonate secretion from guinea pig pancreatic ducts. *Am J Physiol Cell Physiol* 2005;**288**:C1030–41.
22. **Singh VP,** Bhagat L, Navina S, *et al*. PAR-2 protects against pancreatitis by stimulating exocrine secretion. *Gut* 2007;**56**:958–64.
23. **Nguyen TD,** Moody MW, Steinhoff M, *et al*. Trypsin activates pancreatic duct epithelial cell ion channels through proteinase-activated receptor-2. *J Clin Invest* 1999;**103**:261–9.
24. **Namkung W,** Lee JA, Ahn W, *et al*. Ca^{2+} activates cystic fibrosis transmembrane conductance regulator- and Cl^--dependent HCO_3 transport in pancreatic duct cells. *J Biol Chem* 2003;**278**:200–7.
25. **Yamamoto A,** Ishiguro H, Shigeru BHK, *et al*. Ethanol induces fluid hypersecretion from guinea-pig panceatic duct cells. *J Physiol* 2003;**551**:917–26.
26. **Hegyi P,** Ördögh B, Rakonczai Z, *et al*. Effect of herpesvirus infection on pancreatic duct cell secretion. *World J Gastroenterol* 2006;**11**:5997–6002.
27. **Ting GS,** Xu GR, Batta AK, *et al*. Ursodeoxycholic acid, chenodeoxycholic acid, and 7-ketolithocholic acid are primary bile acids of the guinea pig. *J Lipid Res* 1990;**31**:1301–6.
28. **Berr F,** Stellaard F, Pratschke E, *et al*. Effects of cholecystectomy on the kinetics of primary and secondary bile acids. *J Clin Invest* 1989;**83**:1541–50.
29. **Alvaro D,** Mennone A, Boyer JL. Effect of ursodeoxycholic acid on intracellular pH regulation in isolated rat bile duct epithelial cells. *Am J Physiol Gastrointest Liver Physiol* 1993;**28**:G783–91.
30. **Trauner M,** Boyer JL. Bile salt transporters: molecular characterization, function, and regulation. *Physiol Rev* 2003;**83**:633–71.
31. **Meier PJ.** Molecular mechanisms of hepatic bile salt transport from sinusoidal blood into bile. *Am J Physiol Gastrointest Liver Physiol* 1995;**269**:G801–12.
32. **Hagenbuch B,** Stieger B, Foguet M, *et al*. Functional expression cloning and characterization of the hepatocyte Na–bile acid cotransport system. *Proc Natl Acad Sci USA* 1991;**88**:10629–33.
33. **Lazaridis KN,** Pham L, Tietz P, *et al*. Rat cholangiocytes absorb bile acids at their apical domain via the ileal sodium-dependent bile acid transporter. *J Clin Invest* 1997;**100**:2714–21.
34. **Alpini G,** Glaser S, Robertson W, *et al*. Bile acids stimulate proliferative and secretory events in large but not small cholangiocytes. *Am J Physiol Gastrointest Liver Physiol* 1997;**36**:G518–29.
35. **Coleman R,** Holdsworth G. The release of membrane components prior to haemolysis during extraction of intact erythrocytes with bile salts. *Biochim Biophys Acta* 1976;**426**:776–80.
36. **Vyvoda OS,** Coleman R, Holdsworth G. Effects of different bile salts upon the composition and morphology of a liver plasma membrane preparation: deoxycholate is more membrane damaging than cholate and its conjugates. *Biochim Biophys Acta* 1977;**465**:68–76.
37. **Zhao DL,** Hirst BH. Comparison of bile salt perturbation of duodenal and jejunal isolated brush-border membranes. *Digestion* 1990;**47**:200–7.
38. **Alpini G,** Glaser S, Ueno Y, *et al*. Bile acid feeding induces cholangiocyte proliferation and secretion: evidence for bile acid-regulated ductal secretion. *Gastroenterology* 1999;**116**:179–86.
39. **Strazzabosco M,** Sakisaka S, Hayakawa T, *et al*. Effect of UDCA on intracellular and biliary pH in isolated rat hepatocyte couplets and perfused livers. *Am J Physiol Gastrointest Liver Physiol* 1991;**26**:G58–69.
40. **Konturek SJ,** Bilski J, Tasler J, *et al*. Gastroduodenal alkaline response to acid and taurocholate in conscious dogs. *Am J Physiol Gastrointest Liver Physiol* 1984;**247**:G149–54.
41. **Bijvelds MJ,** Jorna H, Verkade HJ, *et al*. Activation of CFTR by ASBT-mediated bile salt absorption. *Am J Physiol Gastrointest Liver Physiol* 2005;**289**:G870–9.
42. **Paradiso AM,** Ribeiro CMP, Boucher RC. Polarized signaling via purinoceptors in normal and cystic fibrosis airway epithelia. *J Gen Physiol* 2001;**117**:53–68.
43. **Devor DC,** Sekar MC, Frizzell RA, *et al*. Taurodeoxycholate activates potassium and chloride conductances via an IP3-mediated release of calcium from intracellular stores in a colonic cell line (T84). *J Clin Invest* 1993;**92**:2173–81.
44. **Chernova MN,** Jiang LW, Shmukler BE, *et al*. Acute regulation of the SLC26A3 congenital chloride diarrhoea anion exchanger (DRA) expressed in Xenopus oocytes. *J Physiol* 2003;**549**:3–19.
45. **Ko SBH,** Shcheynikov N, Choi JY, *et al*. A molecular mechanism for aberrant CFTR-dependent HCO_3^- transport in cystic fibrosis. *EMBO J* 2002;**21**:5662–72.
46. **Wang Z,** Petrovic S, Mann E, *et al*. Identification of an apical Cl^-/HCO_3^- exchanger in the small intestine. *Am J Physiol Gastrointest Liver Physiol* 2002;**282**:G573–9.
47. **Winpenny JP,** Harris A, Hollingsworth MA, *et al*. Calcium-activated chloride conductance in a pancreatic adenocarcinoma cell line of ductal origin (HPAF) and in freshly isolated human pancreatic duct cells. *Pflügers Arch-Eur J Physiol* 1998;**435**:796–803.
48. **Oelberg DG,** Downey SA, Flynn MM. Bile salt-induced intracellular Ca^{++} accumulation in type II pneumocytes. *Lung* 1990;**168**:297–308.
49. **Combettes L,** Berthon B, Doucet E, *et al*. Bile acids mobilise internal Ca^{2+} independently of external Ca^{2+} in rat hepatocytes. *Eur J Biochem* 1990;**190**:619–23.
50. **Beuers U,** Nathanson MH, Boyer JL. Effects of tauroursodeoxycholic acid on cytosolic Ca^{2+} signals in isolated rat hepatocytes. *Gastroenterology* 1993;**104**:604–12.
51. **Molloy M,** Batzri S, Dziki AJ, *et al*. Reversibility of deoxycholate-induced cellular hypercalcemia in rabbit gastric mucosal cells. *Surgery* 1996;**119**:89–97.
52. **Nakajima T,** Okuda Y, Chisaki K, *et al*. Bile acids increase intracellular Ca(2+) concentration and nitric oxide production in vascular endothelial cells. *Br J Pharmacol* 2000;**130**:1457–67.
53. **Gerasimenko JV,** Flowerdew SE, Voronina SG, *et al*. Bile acids induce Ca^{2+} release from both the endoplasmic reticulum and acidic intracellular calcium stores through activation of inositol trisphosphate receptors and ryanodine receptors. *J Biol Chem* 2006;**281**:40154–63.
54. **DiMagno EP,** Shorter RG, Taylor WF, *et al*. Relationships between pancreaticobiliary ductal anatomy and pancreatic ductal and parenchymal histology. *Cancer* 1982;**49**:361–8.
55. **Lerch MM,** Hernandez CA, Adler G. Gallstones and acute pancreatitis—mechanisms and mechanics. *Dig Dis Sci* 1994;**12**:242–7.
56. **Lerch MM,** Weidenbach H, Hernandez CA, *et al*. Pancreatic outflow obstruction as the critical event for human gall stone induced pancreatitis. *Gut* 1994;**35**:1501–3.
57. **Lerch MM,** Saluja AK, Dawra R, *et al*. Acute necrotizing pancreatitis in the opossum: earliest morphological changes involve acinar cells. *Gastroenterology* 1992;**103**:205–13.
58. **Lerch MM,** Saluja AK, Runzi M, *et al*. Pancreatic duct obstruction triggers acute necrotizing pancreatitis in the opossum. *Gastroenterology* 1993;**104**:853–61.
59. **Lerch MM.** Clinical course and treatment principles of biliary acute pancreatitis. In: Beger HG, Buchler M, Kozarek R, eds. *The pancreas: an integrated textbook of basic science, medicine and surgery*. 2008. In press.

Available online at www.sciencedirect.com
ScienceDirect
European Journal of Pharmacology xx (2007) xxx–xxx
www.elsevier.com/locate/ejphar

Hyperlipidemia induced by a cholesterol-rich diet aggravates necrotizing pancreatitis in rats

László Czakó [a,*], Annamária Szabolcs [a], Ágota Vajda [a], Sándor Csáti [a], Viktória Venglovecz [a], Zoltán Rakonczay Jr. [a], Péter Hegyi [a], László Tiszlavicz [b], Tamás Csont [c], Anikó Pósa [d], Anikó Berkó [d], Csaba Varga [d], Szőllősiné Varga Ilona [e], Imre Boros [f], János Lonovics [a]

[a] *First Department of Medicine, University of Szeged, Hungary*
[b] *Department of Pathology, University of Szeged, Hungary*
[c] *Department of Biochemistry, University of Szeged, Hungary*
[d] *Department of Comparative Physiology, University of Szeged, Hungary*
[e] *Biological Isotope Laboratory, University of Szeged, Hungary*
[f] *Hungarian Academy of Sciences, Biological Research Center, Institute of Biochemistry, Szeged, Hungary*

Received 19 February 2007; received in revised form 21 May 2007; accepted 23 May 2007

Abstract

The aim of the present study was to investigate whether hyperlipidemia can cause acute pancreatitis or alter its severity. Male Wistar rats were fed a 3% cholesterol-enriched diet or a normal diet for 16 weeks. Edematous and necrotizing pancreatitis was induced with 3×75 μg/kg body weight of cholecystokinin s.c. and 2×2 g/kg body weight of L-arginine i.p., respectively, in separate groups of normal and hyperlipidemic rats. The severity of the pancreatitis was assessed. We studied the influence of hyperlipidemia on the formation of oxygen-derived free radicals, endogenous scavengers, nitric oxide synthases (NOS), peroxynitrite ($ONOO^-$), heat shock protein 72 (HSP72) and nuclear factor-kappa B (NF-κB) activation in the pancreas during acute edematous and necrotizing pancreatitis. Hyperlipidemia did not worsen edematous, but aggravated necrotizing pancreatitis. The cholesterol-enriched diet significantly reduced the catalase and Mn-superoxide dismutase (SOD) and constitutive NOS (cNOS) activities and increased the inducible NOS (iNOS) in the pancreas relative to those in the rats on the normal diet. The pancreatic nitrotyrosine level, as a marker of $ONOO^-$, and the NF-κB DNA-binding activity in the pancreas, were significantly elevated in the cholesterol-fed rats. The pancreatic HSP72 expression during necrotizing pancreatitis was not influenced by the hyperlipidemia. The pancreatic Mn-SOD, Cu, Zn-SOD, glutathione peroxidase, total glutathione and cNOS activities were significantly reduced, while the catalase, iNOS and NF-κB DNA-binding activities were significantly increased in the animals with necrotizing pancreatitis on the cholesterol diet as compared with those with pancreatitis and receiving the normal diet. Hyperlipidemia induced with this cholesterol-enriched diet leads to decreases in endogenous scavenger and cNOS activities, results in iNOS and NF-κB activation and stimulates $ONOO^-$ generation in the pancreas, which may be responsible for the aggravation of acute necrotizing pancreatitis.

Keywords: Hyperlipidemia; Acute edematous pancreatitis; Acute necrotizing pancreatitis; Peroxynitrite; NF-κB; Heat shock protein; Nitric oxide synthases; Endogenous scavengers

1. Introduction

Hyperlipidemia is reported to be associated with acute pancreatitis in 12–38% of the cases. Hyperlipidemia, which may lead to acute pancreatitis, may be seen as an epiphenomenon of pancreatitis. Lipid levels increase above the normal in up to

* Corresponding author. First Department of Medicine, University of Szeged, Szeged, P.O. Box: 427, H-6701, Hungary. Tel.: +36 62 545187; fax: +36 62 545185.
E-mail address: czal@in1st.szote.u-szeged.hu (L. Czakó).

0014-2999/$ - see front matter © 2007 Elsevier B.V. All rights reserved.
doi:10.1016/j.ejphar.2007.05.064

50% of patients with acute pancreatitis of any cause. The relationship between the two and the role of hyperlipidemia in the pathogenesis of acute pancreatitis is uncertain (Dominguez-Munoz et al., 1991; Toskes, 1990; Yadav and Pitchumoni, 2003).

Hyperlipidemia may be primary in origin or secondary to other clinical conditions, such as alcohol abuse, diabetes mellitus, pregnancy and the use of oral contraceptives. Consequently, most clinical reports have a high proportion of patients with alcoholism, which can itself induce acute pancreatitis. For ethical reasons, an experimental design that convincingly demonstrates causative or contributory effects of hyperlipidemia on acute pancreatitis is difficult to apply clinically. The role of hyperlipidemia in the pathogenesis of pancreatitis might therefore, not be deduced from clinical studies. It has been suggested that animal experiments should be resorted in order to assess the effect of hyperlipidemia on the course of acute pancreatitis (Zieve, 1968).

The mechanism of hyperlipidemic acute pancreatitis is not known. The increasing evidence that has accumulated in recent years indicates that a high-cholesterol diet impairs nitric oxide (NO)-cGMP signaling in both endothelial and nonendothelial cells (Ferdinandy et al., 1997; Deliconstantinos et al., 1995). In the normal pancreas, NO is synthesized from L-arginine (Arg) on the action of nitric oxide synthase (NOS), which exists in 3 isoforms: endothelial NOS (eNOS) and neuronal NOS (nNOS), which are constitutive (cNOS), and an inducible form (iNOS). NO appears to have a biphasic (protective and deleterious) role in acute pancreatitis (Vallance, 2003; Moncada and Higgs, 1993; Werner et al., 1998).

Experimental hypercholesterolemia is associated with an increased production of reactive oxygen species (ROS) (Parker et al., 1995), decreased activities of endogenous radical scavengers (Napoli et al., 1999), and a decreased bioavailability of NO (Ignarro et al., 1999). A reduced level of vascular NO release in hyperlipidemia has been revealed as a consequence of the enhanced formation of superoxide, which then reacts with NO to form the highly toxic peroxynitrite ion ($ONOO^-$) (White et al., 1994).

One of the most important transcription factors that control proinflammatory gene expression during acute pancreatitis is nuclear factor κB (NF-κB). In most cells, NF-κB is normally sequestered in the cytoplasm in an inactive form associated with a class of inhibitory proteins called IκBs. NF-κB is rapidly activated during acute pancreatitis, is translocated to the nucleus, binds to specific κB sequences in the promoter regions and transactivates the downstream genes, including interleukins, chemokines, adhesion molecules, receptors and enzymes (Barnes and Karin, 1997; Rakonczay et al., 2003a,b). Experimental hypercholesterinemia has been demonstrated to be associated with NF-κB activation in the coronary vasculature (Wilson et al., 2000). Moreover, NF-κB has been shown to play a critical role in the pathogenesis of acute experimental pancreatitis by regulating the expressions of many proinflammatory genes in the pancreas (Rakonczay et al., 2003a,b).

It is well known that the accumulation of the inducible member of the 70-kD heat shock protein family (HSP72) in response to a variety of stressors such as heat, mechanical stress, and ischemia confers long-lasting protection against further stress injury (Rakonczay et al., 2003a,b; Welch, 1993). Attenuation of HSP expression has been revealed in certain pathological conditions, such as aging, cardiac hypertrophy and hyperlipidemia (Csont et al., 2002; Locke and Tanguay, 1996; Tajima et al., 1997).

The aims of the present study were to investigate whether hyperlipidemia induced by a cholesterol-enriched diet can cause acute pancreatitis or alter its severity in rats and to analyze the possible pathomechanism. The effects of hyperlipidemia were examined on the levels of malondialdehyde (MDA), a marker of lipid peroxidation, endogenous scavengers and the various forms of NOS, on the generation of $ONOO^-$ and on the activation of NF-κB in the pancreas. A study was also made whether hyperlipidemia interacts with the pancreatic heat stress response.

2. Materials and methods

The experimental protocol followed the principles of Laboratory Animal Care of the National Institutes of Health, USA, and was approved by the ethics committee of the University of Szeged.

2.1. Animals and experimental protocol

80–100 g male Wistar rats were used. The animals were kept at a constant room temperature of 22±2 °C, under 12-h light–dark cycles, and were fed laboratory chow enriched with 3% cholesterol (cholesterol group) or standard chow (LATI, Gödöllő, Hungary) (control group) for 16 weeks. At the end of this 16-week controlled-diet period, acute edematous pancreatitis was induced with 3×75 μg/kg body weight of cholecystokinin (CCK) (Takács et al., 1996) s.c. (CCK and cholesterol+CCK groups), and acute necrotizing pancreatitis with 2×2 g/kg body weight of Arg i.p. (Czakó et al., 1998), in separate groups of normal and hyperlipidemic rats (Arg and cholesterol+Arg groups). The control rats received the same amount of 0.9% saline or an 8.6% solution of glycine in 0.9% saline at the same times instead of the CCK and Arg. At 6 h following the first CCK injection and at 24 h following the first Arg injection, the rats were sacrificed by aortic exsanguinations respectively, and the severity of the pancreatitis was assessed by measurement of the serum amylase and lipase concentrations, and the ratio pancreatic weight/body weight, and via the histology.

2.2. Serum assays

For serum assays, blood samples were centrifuged for 20 min at 2500×*g*. The serum amylase and lipase activities were determined by an Auto Analyzer (Prestige-24, Tokyo Boeki Medical System, Japan). Serum triglycerides and total cholesterol concentrations were measured in triplicates using commercially available colorimetric assay kits (Diagnosticum Rt, Budapest, Hungary) adapted to 96-well plates as described previously (Bjelik et al., 2006). The accuracy of the assays was monitored by using Standard Lipid Controls (Sentinel, Milan, Italy).

Please cite this article as: Czakó, L. et al. Hyperlipidemia induced by a cholesterol-rich diet aggravates necrotizing pancreatitis in rats. Eur. J. Pharmacol. (2007), doi:10.1016/j.ejphar.2007.05.064

2.3. Redox status

The pancreata were homogenized in 4-fold excess (w/v) of ice-cold buffer containing 100 mM K_2HPO_4, 150 mM KCl, 100 mM EDTA, (pH=7.4), and 0.2% (w/v) butylated hydroxytoluene using an Ultra-Turrax homogenizer (IKA-Werk, Staufen, Germany) for 2 min. The homogenates were centrifuged at 3000 ×*g* for 10 min and the supernatants were used for measurements. MDA levels were measured after reaction with thiobarbituric acid, according to the method of Placer et al. (1966), and were corrected for the protein content of the tissue. Superoxide dismutase (SOD) activity was determined on the basis of the inhibition of epinephrine-adrenochrome autoxidation (Misra and Fridovich, 1972). Mn-SOD activity was measured by the autoxidation method in the presence of 5×10^{-3} M KCN (Beauchamp and Fridovich, 1971). Cu, Zn-SOD activity was calculated by subtracting the Mn-SOD activity from the overall SOD activity. Catalase activity was determined spectrophotometrically at 240 nm by the method of Beers et al. (Beers and Sizer, 1951) and was expressed in Bergmeyer units (BU) (1 BU=the decomposition of 1 g of H_2O_2/min at 25 °C). The total glutathione (GSH) content in the supernatant was measured spectrophotometrically with Ellman's reagent, and was corrected for the protein content of the tissue (Sedlak and Lindsay, 1968). Glutathione peroxidase activity was determined by the method of using cumene hydroperoxide and reduced glutathione as substrates of glutathion peroxidase (Chiu et al., 1976)).

2.4. Preparation of nuclear protein extracts and electrophoretic mobility shift assay (EMSA) of NF-κB

Preparation of nuclear protein extracts and EMSA was performed as described previously (Rakonczay et al., 2003a,b). Briefly, a 250–300-mg pancreatic tissue sample was lysed on ice in hypotonic *buffer A* by 20 strokes in a glass Dounce homogenizer. The hypotonic buffer was supplemented with 1 mM phenylmethylsulphonyl fluoride (PMSF), 4 mM benzamidine, 100 IU/ml aprotinin, and 1 mM dithiothreitol (DTT). The homogenate was left on ice for 25 min, and Nonidet P-40 was then added to a final concentration of 0.3–0.4% (v/v). The samples were briefly vortexed and incubated on ice for an additional 2 min. The nuclear pellet was collected by centrifugation of the lysed tissue for 50 s at 13,000 ×*g* in a microfuge. The supernatant (cytosolic fraction) was saved for Western blot analysis. The nuclear pellet was resuspended in *buffer C* supplemented with 1 mM DTT, 1.5 mM PMSF, 4 mM benzamidine, and 100 IU/ml aprotinin. After rotation at 4 °C for 30–45 min, the nuclear membranes were pelleted by microcentrifugation for 10 min and the supernatant (nuclear extract) was aliquoted and stored at −70 °C. For the EMSA of NF-κB DNA-binding activity, a 21-basepair oligonucleotide 5′-GGCAGAGGGGACTTTCCGAGA-3′ containing the NF-κB consensus sequence (underlined) was annealed with its complementary oligonucleotide (with 5′ G overhangs at both ends) to generate a double-stranded probe and was end-labeled with [γ-^{32}P] by T_4 polynucleotide kinase. To determine the NF-κB binding activity, aliquots of nuclear protein (15 μg) were mixed with a buffer containing 10 mM HEPES (pH=7.9), 50 mM KCl, 1 mM EDTA, 1 mM DTT, 10% (v/v) glycerol, and 4.5 μg poly(dI/dC). The binding reaction was started by adding 5–8000 cpm of the radiolabeled double-stranded probe and was allowed to proceed for 30–40 min on ice. The specificity of NF-κB binding was confirmed in competition experiments. DNA-protein complexes were resolved by PAGE at 4 °C on a nondenaturing 4.5% gel in a buffer containing 6.7 mM Tris base, 3.3 mM sodium acetate, and 1 mM EDTA (pH=7.5). Gels were vacuum-dried and exposed to Fuji RX films with intensifying screens at −70 °C. The intensities of the bands were quantified by using the ImageJ software (NIH, Bethesda, MD, USA).

2.5. Measurement of NOS

The activities of iNOS and cNOS were determined through the conversion of L-[^{14}C]arginine monohydrochloride to L-[^{14}C] citrulline (Takács et al., 2002). The protein concentration of the

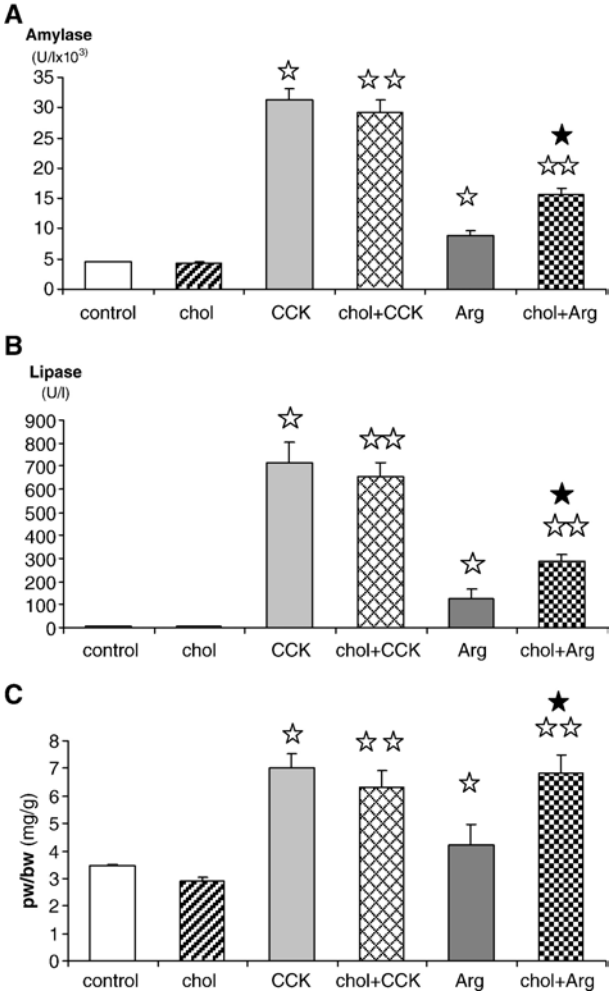

Fig. 1. Serum (A) amylase and (B) lipase activities, and (C) pancreatic edema expressed as the ratio pancreatic weight/body weight in the control, cholesterol-fed (chol) groups, and in normal and hyperlipidemic rats with edematous (CCK and chol+CCK) or necrotizing pancreatitis (Arg and chol+Arg). Results are means±S.E.M. (n=7). ☆: significant difference (P<0.05) vs. control group. ★: significant difference (P<0.05) vs. Arg group. ☆☆: significant difference (P<0.05) vs. chol group.

Please cite this article as: Czakó, L. et al. Hyperlipidemia induced by a cholesterol-rich diet aggravates necrotizing pancreatitis in rats. Eur. J. Pharmacol. (2007), doi:10.1016/j.ejphar.2007.05.064

Table 1
Histological alterations in the control, cholesterol-fed (chol) groups, and in normal and hyperlipidemic rats with edematous (CCK and chol+CCK) and necrotizing pancreatitis (Arg and chol+Arg)

	Edema	Leukocyte infiltration	Acinar vacuolization	Hyperaemia	Necrosis	Total damage
Control	0.00±0.00	0.00±0.00	0.00±0.00	0.20±0.20	0.00±0.00	0.20±0.20
chol	0.00±0.00	0.00±0.00	0.00±0.00	0.20±0.20	0.00±0.00	0.20±0.20
CCK	1.33±0.34[a]	1.67±0.33[a]	1.00±0.17[a]	1.50±0.21[a]	0.00±0.00	5.5±0.47[a]
chol+CCK	1.33±0.34[b]	1.33±0.29[b, c]	0.66±0.28[b]	1.67±0.18[b; d]	0.00±0.00	4.99±0.42[b]
Arg	1.50±0.34[a]	1.67±0.33[a]	1.17±0.17[a]	1.67±0.21[a]	1.14±0.14[a]	7.15±0.65[a]
chol+Arg	2.00±0.00[b, d]	2.29±0.29[b]	1.00±0.00[b]	2.29±0.18[b, d]	1.83±0.31[b, d]	9.41±0.42[b, d]

Results are means±S.E.M. ($n=7$).
[a] Significant difference ($P<0.05$) vs. the control group.
[b] Significant difference ($P<0.05$) vs. the chol group.
[c] Significant difference ($P<0.05$) vs. the CCK group.
[d] Significant difference ($P<0.05$) vs. the Arg group.

pancreatic tissue was determined by the method of Goa (Goa, 1953).

2.6. Western blotting

Western blot analysis of pancreatic HSP72, IκB-α expression and markers of $ONOO^-$ formation (by detecting 3-nitrotyrosine residues) was performed from the cytosolic fraction of the pancreas homogenate as described previously (Rakonczay et al., 2003a,b; Giricz et al., 2003). Pancreatic tissue was homogenized and diluted to load 20–40 μg of total protein on an 8–10% polyacrylamide gel. After separation by electrophoresis, the proteins were blotted onto nitrocellulose membrane. After blocking, the membranes were incubated with mouse monoclonal anti-nitrotyrosine antibody (Chemicon International, 1:1000 dilution, 80 min), rabbit anti-HSP72 (1:2500 dilution, 60 min), or rabbit anti-IκB-α (1:500 dilution, 60 min, Santa Cruz Biotechnology, Santa Cruz, CA, USA) and with a rabbit anti-mouse or goat anti-rabbit secondary antibody for 60 min (DakoCytomation Denmark A/S, Glostrup, Denmark, 1:1000). Bands were visualized by enhanced chemiluminescence (ECL Plus; GE Healthcare, Little Chalfont, Buckinghamshire, UK). Thereafter, they were scanned and quantified by using the ImageJ software (NIH, Bethesda, MD, USA). The band densities of all 3-nitrotyrosine-containing proteins were determined and summed in order to estimate the total level of nitrated proteins. Results are expressed in arbitrary units.

2.7. Histologic examination

A portion of the pancreas was fixed overnight in 6% neutral formaldehyde solution and embedded in paraffin. Tissue slices were subjected to hematoxylin and eosin staining and histologic study by light microscopy. Slides were coded and examined blind by the pathologist for the grading of histologic alterations. Intestinal edema, vacuolization, inflammation, hemorrhage and acinar cell necrosis were graded on a scale of 1 to 3. The total histological damage was calculated by adding the scores for the different parameters.

2.8. Statistical analysis

Results are expressed as means±S.E.M. Experiments were evaluated statistically with two-way analysis of variance (ANOVA). P values <0.05 were accepted as statistically significant.

3. Results

3.1. Serum lipids

At the end of the 16-week controlled-diet period, the animals weighed 500–600 g. The hyperlipidemic rats were heavier, but not significantly so than the rats on the normal diet. The 16-week cholesterol-enriched diet significantly increased serum cholesterol and triglyceride levels from 1.88±0.15 and 0.52±0.05 mmol/L to

Table 2
The pancreatic activities of MDA and endogenous scavengers in the control, cholesterol-fed (chol) groups, and in normal and hyperlipidemic rats with necrotizing pancreatitis (Arg and chol+Arg)

	Malonyl dialdehyde (nM/mg protein)	Total glutathione (μM/mg protein)	Catalase (BU/mg protein × 10^{-4})	Glutathion peroxidase (U/mg protein × 10^{-3})	Mn-SOD (U/mg protein)	Cu, Zn-SOD (U/mg protein)
Control	0.10±0.005	1.01±0.12	1.7±0.14	4.97±0.25	0.81±0.06	2.63±0.15
Chol	0.12±0.01	1.08±0.18	1.1±0.10[a]	5.92±0.34	0.64±0.05[a]	2.55±0.20
Arg	3.21±0.18[a]	1.71±0.14[a]	6.51±0.51[a]	12.07±0.63[a]	0.31±0.03[a]	5.28±0.33[a]
Chol+Arg	3.42±0.20[b]	1.24±0.11[b, c]	8.74±0.73[b, c]	9.1±0.60[b, c]	0.20±0.02[b, c]	4.01±0.26[b, c]

Results are means±S.E.M. ($n=7$).
[a] Significant difference ($P<0.05$) vs. the control group.
[b] Significant difference ($P<0.05$) vs. the chol group.
[c] Significant difference ($P<0.05$) vs. the Arg group.

Please cite this article as: Czakó, L. et al. Hyperlipidemia induced by a cholesterol-rich diet aggravates necrotizing pancreatitis in rats. Eur. J. Pharmacol. (2007), doi:10.1016/j.ejphar.2007.05.064

2.52±0.18 ($P<0.05$) and 1.07±0.12 ($P<0.05$) mmol/L, respectively.

3.2. Severity of acute pancreatitis

The cholesterol-enriched diet did not modify the serum amylase and lipase activities or the ratio pancreatic weight/body weight as compared with those of the rats on normal diet, and did not cause any histological alteration in the pancreas. Likewise, the cholesterol diet did not worsen the activities of serum amylase and lipase, the ratio pancreatic weight/body weight or the histological score in the animals with edematous pancreatitis. In marked contrast, in the animals with necrotizing pancreatitis, the serum amylase and lipase activities, the ratio pancreatic weight/body weight and the histological score were significantly increased in the hyperlipidemic animals as compared with the nonhyperlipidemic rats (Fig. 1, Table 1).

3.3. Oxidative stress

To analyze the mechanism by which hypercholesterinemia intensifies the course of acute necrotizing pancreatitis, we studied whether this high-cholesterol diet increased the extent of lipid peroxidation or the levels of endogenous scavengers due to oxidative stress in the pancreatic tissue. The pancreatic MDA concentration was not altered by the cholesterol diet in the rats without pancreatitis, while it was increased, but not significantly so in the hyperlipidemic group as compared with the nonhyperlipidemic rats with pancreatitis. Among the endogenous scavengers, the catalase and the Mn-SOD activities were significantly reduced following the cholesterol diet in the rats without pancreatitis. The Mn-SOD, Cu, Zn-SOD, glutathion peroxidase and GSH activities were significantly reduced, while the catalase activity was significantly increased in the hyperlipidemic pancreatitic animals as compared with the nonhyperlipidemic rats (Table 2).

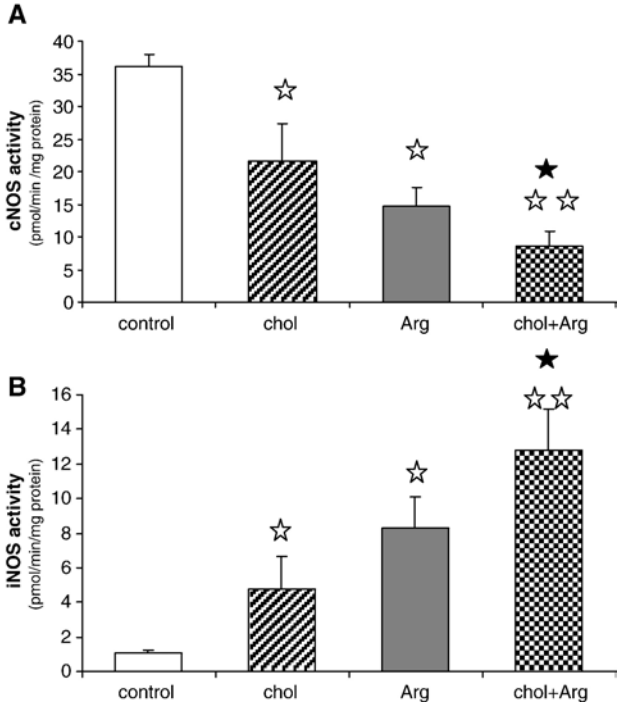

Fig. 2. Pancreatic (A) cNOS and (B) iNOS activity in the control, cholesterol-fed (chol) groups, and in normal and hyperlipidemic rats with necrotizing pancreatitis (Arg and chol+Arg). Results are means±S.E.M. ($n=7$). ☆: significant difference ($P<0.05$) vs. control group. ★: significant difference ($P<0.05$) vs. Arg group. ☆☆: significant difference ($P<0.05$) vs. chol group.

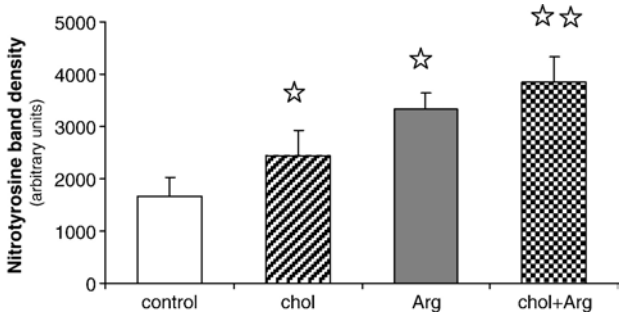

Fig. 3. Pancreatic nirotyrosine level, a marker for peroxynitrite generation. The bar chart show the band densities of all 3-nitrotyrosine-containing proteins. Rats were treated in the same manner as described in the legend to Fig. 2. Results are means±S.E.M. ($n=7$). ☆: significant difference ($P<0.05$) vs. control group. ☆☆: significant difference ($P<0.05$) vs. chol group.

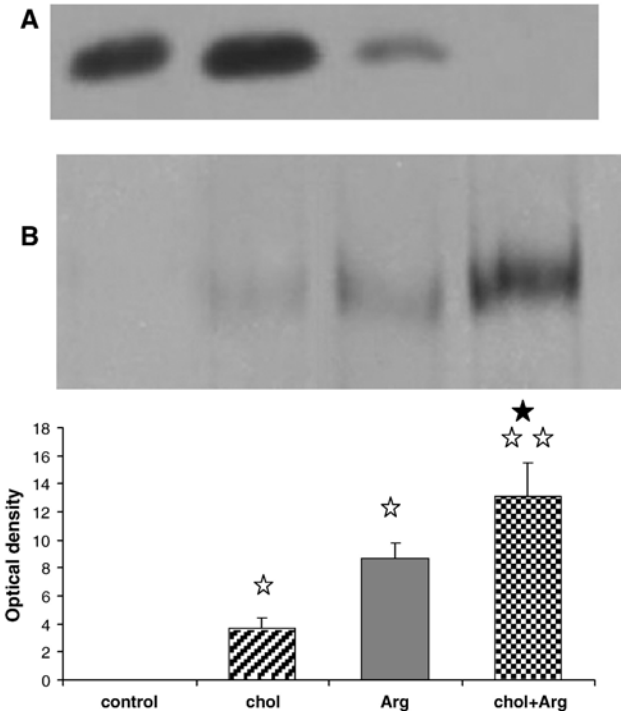

Fig. 4. Pancreatic IκB-α levels and NF-κB DNA-binding activity. (A) Pancreatic cytosolic protein fractions were analyzed by Western blot analysis (40 μg/lane), using a specific IκB-α antibody. (B) Pancreatic NF-κB DNA-binding activity was assessed by EMSA. The bar diagram shows the optical densities of the EMSA bands. Rats were treated in the same manner as described in the legend to Fig. 2. Results are means±S.E.M. ($n=7$). ☆: significant difference ($P<0.05$) vs. control group. ★: significant difference ($P<0.05$) vs. Arg group. ☆☆: significant difference ($P<0.05$) vs. chol group.

Please cite this article as: Czakó, L. et al. Hyperlipidemia induced by a cholesterol-rich diet aggravates necrotizing pancreatitis in rats. Eur. J. Pharmacol. (2007), doi:10.1016/j.ejphar.2007.05.064

3.4. Pancreatic NO synthase

As concerns the activities of the free radical NO-synthesizing enzymes, the cNOS activity in the pancreas was significantly decreased, while that of iNOS was significantly increased as a result of the cholesterol diet. The cNOS activity was significantly further decreased in the animals with pancreatitis. Its level was significantly lower in the animals with pancreatitis on the cholesterol diet as compared with those on the normal diet. The iNOS activity was significantly increased in the animals with pancreatitis as compared with the rats without pancreatitis. The iNOS level was significantly higher in the animals with pancreatitis on the cholesterol diet as compared with those on the normal diet (Fig. 2).

3.5. Pancreatic $ONOO^-$ formation

High-cholesterol diet increased the formation of $ONOO^-$ in the pancreas, as the levels of pancreatic 3-nitrotyrosine (a marker of $ONOO^-$ formation) were found to be significantly increased in the cholesterol-fed rats as compared with the controls. The 3-nitrotyrosine level proved significantly higher in the animals with necrotizing pancreatitis (Fig. 3).

3.6. Pancreatic NF-κB activation

Interestingly, the cholesterol diet in itself led to significantly increased pancreatic NF-κB DNA-binding activity relative to the rats on the normal diet. Pancreatic IκB-α levels were not altered by cholesterol treatment. However, Arg administration significantly decreased IκB-α expression and this was further reduced in pancreatitic rats on a cholesterol diet. Furthermore, the level of NF-κB DNA-binding activity was significantly higher in the rats with necrotizing pancreatitis receiving the cholesterol diet as compared with the pancreatitic animals on the normal diet (Fig. 4).

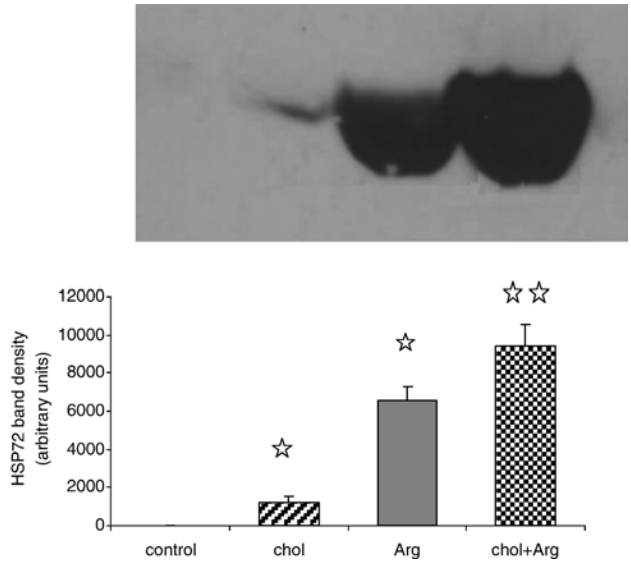

Fig. 5. Pancreatic HSP72 expression as assessed by Western blotting. The densities of the Western blot bands were quantified by using the ImageJ software. Rats were treated in the same manner as described in the legend to Fig. 2. Results are means ± S.E.M. ($n=7$). ☆: significant difference ($P<0.05$) vs. control group. ☆☆: significant difference ($P<0.05$) vs. chol group.

3.7. Pancreatic HSP72 protein expression

We assessed if hyperlipidemia induced by cholesterol-enriched diet affected the production of HSP72 in the pancreas in response to necrotizing pancreatitis. In the pancreas of the control rats, the basal level of HSP72 was very low, but the cholesterol-enriched diet significantly increased its expression. Arg-induced necrotizing pancreatitis resulted in further significant increases in pancreatic HSP72 content both in the animals on the normal diet and also in those on the cholesterol diet as compared with the controls (Fig. 5).

4. Discussion

The present results show that the rats on this cholesterol-enriched diet for 16 weeks exhibited reduced endogenous scavengers and cNOS activities and increased iNOS and NF-κB DNA binding activities, enhanced $ONOO^-$ formation in the pancreas and aggravation of their necrotizing pancreatitis.

A hyperlipidemia prevalence of 12–38% has been reported in acute human pancreatitis in previous studies. This wide range of hyperlipidemia in acute pancreatitis seems to result from the variations in the patient population, since alcohol consumption and diabetes mellitus may themselves cause hyperlipidemia (Dominguez-Munoz et al., 1991; Toskes, 1990; Yadav and Pitchumoni, 2003). Accordingly, we have to rely on animal studies to evaluate hyperlipidemia as a risk factor in acute pancreatitis. Only a few animal studies have been published, but the results are contradictory. In isolated *ex-vivo* perfused dog pancreata, hyperlipidemia was found to induce histological and serological alterations of acute pancreatitis (Saharia et al., 1977). No confirmatory studies have been reported. The contributory effect of hyperlipidemia has also been demonstrated. Endogenous hyperlipidemia was observed to intensify the course of acute edematous and necrotizing pancreatitis in the rat (Hofbauer et al., 1996), while exogenous triglycerides increased the pancreatic damage in acute edematous and necrotizing pancreatitis, initiated via different pathogenetic pathways in the isolated perfused pancreas (Kimura and Mossner, 1996). However, other reports suggest that hyperlipidemia does not aggravate the course of acute edematous pancreatitis in rats (Paye et al., 1995, 1996). The role of hyperlipidemia in acute pancreatitis therefore, seems questionable.

The present study demonstrated that this high-cholesterol diet in itself did not damage the exocrine pancreas, and did not alter the course of acute edematous pancreatitis, but it did aggravate acute necrotizing pancreatitis. The discrepancies between our findings and those in the previous studies may be explained by methodological differences (Saharia et al., 1977; Hofbauer et al., 1996; Kimura and Mossner, 1996). All of the previous animal models involved studies of the effects of acute hyperlipidemia induced by triglyceride infusion or by the injection of an active detergent (Triton WR 1339) leading to

Please cite this article as: Czakó, L. et al. Hyperlipidemia induced by a cholesterol-rich diet aggravates necrotizing pancreatitis in rats. Eur. J. Pharmacol. (2007), doi:10.1016/j.ejphar.2007.05.064

endogenous hyperlipidemia. However, in clinical practice patients usually present with long-standing hyperlipidemia. We therefore, applied hyperlipidemia induced by a cholesterol-enriched diet, which better resembles the human situation.

The catalase and Mn-SOD activities were significantly reduced in the pancreas following the cholesterol diet. Accumulating evidence indicates that oxidative stress in the arterial wall plays a major role in the initiation and progression of the cardiovascular dysfunction associated with hyperlipidemia (Taniyama and Griendling, 2003). This is the first demonstration that a high-cholesterol diet leads to reduced levels of endogenous scavengers in the pancreas. Oxidative stress is a state in which excess ROS overwhelm endogenous antioxidant systems. One of the most important ROS in the vasculature is the superoxide radical anion (O_2^-), formed by the one-electron reduction of the oxygen molecule. SOD transforms O_2^- to the more stable hydrogen peroxide (H_2O_2), which is then converted enzymatically into H_2O by catalase and glutathion peroxidase. Hyperlipidemia reduces Mn-SOD, which may lead to the diminished elimination of O_2^-. Further, the prophylactic administration of a scavenger prior to the induction of acute pancreatitis exerts a beneficial effect on the development of pancreatitis (Czakó et al., 1998; Araki et al., 2003). It is therefore plausible to speculate that the reduced scavenger activity makes the pancreas more vulnerable to further stress, such as that of acute pancreatitis, which may result in more severe damage. Indeed, the activities of GSH, glutathion peroxidase, Mn-SOD and Cu, Zn-SOD were all significantly depleted in the rats with necrotizing pancreatitis receiving the high-cholesterol diet as compared with those on the normal diet.

Besides the reduced endogenous scavenger activities, we observed decreased cNOS and increased iNOS activities in the pancreas following the cholesterol diet. NO appears to have a biphasic (protective and deleterious) effect in acute pancreatitis. A small amount of NO derived from cNOS accounts for the protective action through the regulation of various housekeeping functions, while a large amount of NO derived from iNOS, induced by inflammatory cytokines and endotoxins, mediates the deleterious action through cytotoxic action (Vallance, 2003; Moncada and Higgs, 1993; Werner et al., 1998; Takács et al., 2002). It also emerged that the pancreatic iNOS activity was significantly higher and the cNOS activity was significantly lower in the rats with pancreatitis on the high-cholesterol diet as compared with those in the rats on the normal diet. This imbalance of the NO pathway may be responsible for the more severe pancreatitis seen in the hyperlipidemic rats.

It is well known that NO reacts rapidly with O_2^- to form $ONOO^-$, a potentially deleterious ROS. Hyperlipidemia has been shown to enhance the production of $ONOO^-$ in the vasculature and the heart (Beckman and Koppenol, 1996). The present study demonstrated that the high-cholesterol diet increased the pancreatic level of nitrotyrosine, a marker of $ONOO^-$ generation. The cytotoxic effects of $ONOO^-$ include lipid peroxidation, the nitration of tyrosine residues, the oxidation of sulfhydryl groups, DNA-strand breakage, and the inhibition of mitochondrial respiration, leading to tissue injury (Beckman and Koppenol, 1996). $ONOO^-$ generation in the pancreas of the hyperlipidemic rats may have contributed to the more severe pancreatitis seen in the rats on the high-cholesterol diet.

The NF-κB DNA-binding activity was significantly increased in the pancreas following the cholesterol diet. Unexpectedly, pancreatic IκB-α levels were unaltered by cholesterol treatment. It is possible that the cholesterol-induced NF-κB activation is regulated by IκB-β. NF-κB activation has been related to NO bioavailability and ROS production: while ROS contribute to NF-κB activation, an intact NO pathway system stabilizes it and prevents its activation. Thus, a balance between the oxidative status and the NO-dependent pathways may be one of the regulatory mechanisms of NF-κB activation (Li and Karin, 1999; Peng et al., 1995). In our study, the hyperlipidemia activated both the ROS and the NO pathway systems, and consequently both may contribute to NF-κB activation. The NF-κB DNA-binding activity was significantly higher and IκB-α levels were significantly lower in the rats with necrotizing pancreatitis receiving the high-cholesterol diet as compared with those on the normal diet. The increased activation of NF-κB may be responsible in part for the more severe pancreatitis in the hyperlipidemic rats by activating the many proinflammatory genes in the pancreas.

Hyperlipidemia has been shown to attenuate heat shock protein expression in the heart (Csont et al., 2002). Although, it was not known whether hyperlipidemia leads to a decreased heat shock response in the pancreas, it was tempting to speculate that this mechanism is involved in the increased severity of pancreatitis in hyperlipidemia. Accordingly, we measured the pancreatic HSP72 production. Pancreatic HSP72 was induced by acute necrotizing pancreatitis in animals on the high-cholesterol diet and in others on the normal diet; there was no significant difference in HSP72 expression between the two groups.

The present study involved an *in vivo* model in which the direct effect of plasma triglycerides cannot be excluded. Pancreatic lipase breaks down triglycerides to free fatty acids. Free fatty acids are toxic: they may damage acinar cells directly and injure the vascular endothelium, leading to disturbances of the microcirculation. Moreover, trypsinogen may be activated by acidosis due to the presence of free fatty acids (Saharia et al., 1977; Havel, 1969; Niederau and Grendell, 1998). These mechanisms can also take part in the development of hyperlipidemic pancreatitis.

In summary, the present study revealed that hyperlipidemia decreases the endogenous free radical scavengers and cNOS activities, induces iNOS and NF-κB activation and stimulates $ONOO^-$ generation in the pancreas, which may be responsible for the aggravation of acute necrotizing pancreatitis. Targeting these inflammatory mediators with pharmacological tools could possibly form the basis of a new strategy with which to treat or prevent acute pancreatitis aggravated by hyperlipidemia.

Acknowledgments

This work was supported in part by grants from the Hungarian National Research Fund (OTKA no. T049134), the Hungarian Academy of Sciences (BÖ 5/2003) and the Medical Research Council (ETT 499/2006). The anti-HSP72 antibody was a generous gift from István Kurucz (IVAX Drug Research Institute, Budapest, Hungary).

Please cite this article as: Czakó, L. et al. Hyperlipidemia induced by a cholesterol-rich diet aggravates necrotizing pancreatitis in rats. Eur. J. Pharmacol. (2007), doi:10.1016/j.ejphar.2007.05.064

References

Araki, Y., Andoh, A., Yokono, T., Asano, N., Yoshikawa, K., Bamba, S., Ishizuka, I., Fujiyama, Y., 2003. The free radical scavenger edaravone suppresses experimental closed duodenal loop-induced acute pancreatitis in rats. Int. J. Mol. Med 12, 121–124.

Barnes, P.J., Karin, M., 1997. Nuclear factor-κB: a pivotal transcription factor in chronic inflammatory diseases. N. Engl. J. Med 336, 1066–1071.

Beauchamp, C., Fridovich, I., 1971. Superoxide dismutase: improved assay and an assay applicable to acrylamide gels. Anal. Biochem 44, 276–287.

Beckman, J.S., Koppenol, W.H., 1996. Nitric oxide, superoxide, and peroxynitrite: the good, the bad, and ugly. Am. J. Physiol 271, C1424–C1437.

Beers Jr., R.F., Sizer, I.W., 1951. Spectrophotometric method for measuring the breakdown of hydrogen peroxide by catalase. J. Biol. Chem 195, 133–140.

Bjelik, A., Bereczki, E., Gonda, S., Juhász, A., Rimanóczy, A., Zana, M., Csont, T., Pakaski, M., Boda, K., Ferdinandy, P., Dux, L., Janka, Z., Sántha, M., Kálmán, J., 2006. Human apoB overexpression and a high-cholesterol diet differently modify the brain APP metabolism in the transgenic mouse model of atherosclerosis. Neurochem. Int 49, 393–400.

Chiu, D.T., Stults, F.H., Tappel, A.L., 1976. Purification and properties of rat lung soluble glutathione peroxidase. Biochim. Biophys. Acta 445, 558–566.

Csont, T., Balogh, G., Csonka, C., Boros, I., Horváth, I., Vigh, L., Ferdinandy, P., 2002. Hyperlipidemia induced by high cholesterol diet inhibits heat shock response in rat hearts. Biochem. Biophys. Res. Commun. 290, 1535–1538.

Czakó, L., Takács, T., Varga, I.S., Tiszlavicz, L., Hai, D.Q., Hegyi, P., Matkovics, B., Lonovics, J., 1998. Involvement of oxygen-derived free radicals in L-arginine-induced acute pancreatitis. Dig. Dis. Sci. 43, 1770–1777.

Deliconstantinos, G., Villiotou, V., Stavrides, J.C., 1995. Modulation of particulate nitric oxide synthase activity and peroxynitrite synthesis in cholesterol enriched endothelial cell membranes. Biochem. Pharmacol. 49, 1589–1600.

Dominguez-Munoz, J.E., Malfertheiner, P., Ditschuneit, H.H., Blanco-Chavez, J., Uhl, W., Buchler, M., Ditschuneit, H., 1991. Hyperlipidemia in acute pancreatitis. Relationship with etiology, onset, and severity of the disease. Int. J. Pancreatol. 10, 261–267.

Ferdinandy, P., Szilvássy, Z., Horváth, L.I., Csont, T., Csonka, C., Nagy, E., Szentgyörgyi, E., Nagy, I., Koltai, M., Dux, L., 1997. Loss of pacing-induced preconditioning in rat hearts: role of nitric oxide and cholesterol-enriched diet. J. Mol. Cell Cardiol. 29, 3321–3333.

Giricz, Z., Csonka, C., Onody, A., Csont, T., Ferdinandy, P., 2003. Role of cholesterol-enriched diet and the mevalonate pathway in cardiac nitric oxide synthesis. Basic Res. Cardiol. 98, 304–310.

Goa, J., 1953. A micro biuret method for protein determination; determination of total protein in cerebrospinal fluid. Scand. J. Clin. Lab. Invest. 5, 218–222.

Havel, R.J., 1969. Pathogenesis, differentiation and management of hypertriglyceridemia. Adv. Intern. Med. 15, 117–154.

Hofbauer, B., Friess, H., Weber, A., Baczako, K., Kisling, P., Schilling, M., Uhl, W., Dervenis, C., Buchler, M.W., 1996. Hyperlipaemia intensifies the course of acute oedematous and acute necrotising pancreatitis in the rat. Gut 38, 753–758.

Ignarro, L.J., Cirino, G., Napoli, C., 1999. Nitric oxide as a signaling molecule in the vascular system: an overview. J. Cardiovasc. Pharmacol. 1, 879–886.

Kimura, W., Mossner, J., 1996. Role of hypertriglyceridemia in the pathogenesis of experimental acute pancreatitis in rats. Int. J. Pancreatol. 20, 177–184.

Li, N., Karin, M., 1999. Is NF-kappaB the sensor of oxidative stress? FASEB J. 13, 1137–1143.

Locke, M., Tanguay, R.M., 1996. Diminished heat shock response in the aged myocardium. Cell Stress Chaperones 1, 251–260.

Misra, H.P., Fridovich, I., 1972. The role of superoxide anion in autoxidation of epinephrine and a simple assay for superoxide dismutase. J. Biol. Chem. 247, 3170–3175.

Moncada, S., Higgs, A., 1993. The L-arginine-nitric oxide pathway. N. Engl. J. Med. 329, 2002–2012.

Napoli, C., Witztum, J.L., de Nigris, F., Palumbo, G., D'Armiento, F.P., Palinski, W., 1999. Intracranial arteries of human fetuses are more resistant to hypercholesterolemia-induced fatty streak formation than extracranial arteries. Circulation 99, 2003–2010.

Niederau, C., Grendell, J.H., 1998. Intracellular vacuoles in experimental acute pancreatitis in rats and mice are an acidified compartment. J. Clin. Invest. 81, 229–236.

Parker, R.A., Sabrah, T., Cap, M., Gill, B.T., 1995. Relation of vascular oxidative stress, alpha-tocopherol, and hypercholesterolemia to early atherosclerosis in hamsters. Arterioscler. Thromb. Vasc. Biol. 15, 349–358.

Paye, F., Chariot, J., Molas, G., Benessiano, J., Roze, C., 1995. Nonesterified fatty acids in acute cerulein-induced pancreatitis in the rat. Are they really deleterious in vivo? Dig. Dis. Sci. 40, 540–545.

Paye, F., Chariot, J., Molas, G., Benessiano, J., Roze, C., 1996. Release of nonesterified fatty acids during cerulein-induced pancreatitis in rats. Dig. Dis. Sci. 41, 1959–1965.

Peng, H.B., Libby, P., Liao, J.K., 1995. Induction and stabilisation of IkBalpha by nitric oxide mediates inhibition of NF-κB. J. Biol. Chem. 270, 14214–14219.

Placer, Z.A., Cushman, L., Johnson, B.C., 1966. Estimation of product of lipid peroxidation (malonyl dialdehydes) in biochemical systems. Anal. Biochem. 16, 359–364.

Rakonczay Jr., Z., Jármay, K., Kaszaki, J., Mándi, Y., Duda, E., Hegyi, P., Boros, I., Lonovics, J., Takács, T., 2003a. NF-κB activation is detrimental in arginine-induced acute pancreatitis. Free Radic. Biol. Med. 34, 696–709.

Rakonczay Jr., Z., Takács, T., Boros, I., Lonovics, J., 2003b. Heat shock proteins and the pancreas. J. Cell Physiol 195, 383–391.

Saharia, P., Margolis, S., Zuidema, G.D., Cameron, J.L., 1977. Acute pancreatitis with hyperlipemia: studies with an isolated perfused canine pancreas. Surgery 82, 60–67.

Sedlak, J., Lindsay, R.H., 1968. Estimation of total, protein-bound, and nonprotein sulfhydryls groups in tissue with Ellman's reagent. Anal. Biochem. 25, 192–205.

Tajima, M., Isoyama, S., Nitta, Y., Abe, K., 1997. Attenuation of heat shock protein expression by coronary occlusion in hypertrophied hearts. Am. J. Physiol. 273, H526–H533.

Takács, T., Farkas Jr., Gy., Czakó, L., Jármay, K., Mándi, Y., Lonovics, J., 1996. Time-course changes in serum cytokine levels in two experimental acute pancreatitis models in rats. Res. Exp. Med. 196, 153–161.

Takács, T., Czakó, L., Morschl, É., László, F., Tiszlavicz, L., Rakonczay Jr., Z., Lonovics, J., 2002. The role of nitric oxide in edema formation in L-arginine-induced acute pancreatitis. Pancreas 25, 277–282.

Taniyama, Y., Griendling, K.K., 2003. Reactive oxygen species in the vasculature. Molecular and cellular mechanisms. Hypertension 42, 1075–1081.

Toskes, P.P., 1990. Hyperlipidemic pancreatitis. Gastroenterol. Clin. North. Am. 19, 783–791.

Vallance, P., 2003. Nitric oxide: therapeutic opportunities. Fundam. Clin. Pharmacol. 17, 1–10.

Welch, W.J., 1993. Heat shock proteins functioning as molecular chaperones: their roles in normal and stressed cells. Philos. Trans. R. Soc. Lond. B. Biol. Sci. 339, 327–333.

Werner, J., Fernandez-del Castillo, C., Rivera, J.A., Kollias, N., Lewandrowski, K.B., Rattner, Q.W., Warshaw, A.L., 1998. On the protective mechanisms of NO in acute pancreatitis. Gut 43, 401–407.

White, C.R., Brock, T.A., Chang, L.Y., Crapo, J., Briscoe, P., Ku, D., Bradley, W.A., Gianturco, S.H., Gore, J., Freeman, B.A., Tarpey, M.M., 1994. Superoxide and peroxynitrite in atherosclerosis. Proc. Natl. Acad. Sci. U. S. A. 91, 1044–1048.

Wilson, S.H., Caplice, N.M., Simari, R.D., Holmes Jr., D.R., Carlson, P.J., Lerman, A., 2000. Activated nuclear factor-kappa B is present in the coronary vasculature in experimental hypercholesterolemia. Atherosclerosis 148, 23–30.

Yadav, D., Pitchumoni, C.S., 2003. Issues in hyperlipidemic pancreatitis. J. Clin. Gastroenterol. 36, 54–62.

Zieve, L., 1968. Relationship between acute pancreatitis and hyperlipemia. Med. Clin. North Am. 52, 1493–1501.

Please cite this article as: Czakó, L. et al. Hyperlipidemia induced by a cholesterol-rich diet aggravates necrotizing pancreatitis in rats. Eur. J. Pharmacol. (2007), doi:10.1016/j.ejphar.2007.05.064